THE IMPORTANCE OF THE BACKBONE AND C-TERMINUS TO MASS SPECTROMETRY STUDIES OF PEPTIDES: GAS-PHASE DISSOCIATION AND ACIDITY STUDIES

by

SAMANTHA STARLET BOKATZIAN-JOHNSON

CAROLYN J. CASSADY, COMMITTEE CHAIR
MARGARET JOHNSON
SHANLIN PAN
SHANE C. STREET
STEPHEN A. WOSKI

A DISSERTATION

Submitted in partial fulfillment of the requirements
for the degree of Doctor of Philosophy
in the Department of Chemistry
in the Graduate School of
The University of Alabama

TUSCALOOSA, ALABAMA

2012

ABSTRACT

The work described in this dissertation shows the importance of the C-terminus and the backbone in dissociation and deprotonation of peptides. Characteristic dissociative behavior can be extremely valuable in proteomic applications and for mechanistic interpretation of mass spectra. Identification of the deprotonation site of a peptide is also important to the development of mechanisms for mass spectrometry, as dissociation is often charge-directed.

Collsion-induced dissociation (CID) and electron transfer dissociation (ETD) have been used to discover distinguishing features of peptide dissociation related to the presence of an amidated C-terminus (-$CONH_2$) compared with the standard acid C-terminus (-COOH). Protonated peptide acids and amides are found to produce practically identical spectra, except for increased ammonia loss from the precursor for the peptide amide. ETD of multiply-protonated peptide acids and amides also produce similar spectra, although dissociation trends related to the basic amino acid residues (e.g. Arg, His, Lys) are observed for the peptide pairs. Deprotonated peptide acids and amides produced several unique product ions that differentiated the analogs. In CID experiments, abundant c_{m-2}^- (m = the number of amino acid residues in the peptide) formed for many of the peptide amides and c_{m-3}^- formed for many of the peptide acids. Supporting computational work by Michele Stover of the Dixon Group shows that the process leading to c_{m-2}^- from peptide amides is less endothermic than the same process for peptide acids.

Gas -phase acidities (GA) have been determined for tyrosine, phenylalanine, their amino acid amides and 4-(4-hydroxyphenyl)-2-butanone using bracketing ion/molecule reactions. Two deprotonated species of tyrosine are observed, corresponding to deprotonation at the carboxylic

acid -OH and the phenolic -OH. The two GAs determined for tyrosine are: GA(1) = 332.4 ± 2.2 kcal/mol and GA(2) = 333.5 ± 2.4 kcal/mol. Tyrosine amide has an experimental GA of 336.4 ± 2.7 kcal/mol, phenylalanine has a GA of 332.5 ± 2.2 kcal/mol, phenylalanine amide has a GA of 345.8 ± 3.8 kcal/mol, and 4-(4-hydroxyphenyl)-2-butanone has a GA of 339.6 ± 3.0 kcal/mol.

The GAs of six tripeptides (with alkyl or H- side chains) have been determined. All of the experimental GAs fall within a 1.2 kcal/mol range, which is consistent with the C-terminus being the most acidic site on the peptides. The GAs of three methyl esters have been determined, demonstrating the ability of peptides to deprotonate on the backbone. The peptide methyl ester GAs are all very similar and fall within a 1.4 kcal/mol range. Computational results indicate that these methyl esters are deprotonating at the central amide NH. Three other methyl esters could not be deprotonated by ESI, because of conformation and steric hindrance to the deprotonation site.

LIST OF ABBREVIATIONS AND SYMBOLS

AAA	trialanine
A′	methylalanine
A′A′A′	tri-2-methylalanine
AGA	alanylglycylalanine
AA	amino acid
AC	alternating current
Ala	alanine (A)
Arg	arginine (R)
Asp	aspartic acid (D)
bar	unit of pressure
Cys	cysteine (C)
cal	calorie
CID	collision-induced dissociation
Da	Dalton
DC	direct current
DFT	density functional theory
DIC	1,3-diisopropylcarbodiimide
ΔG	Gibbs free energy change
ΔH	enthalpy change
DMF	N,N-dimethylformamide

ΔS	entropy change
eV	electron volt
ESI	electrospray ionization
ETCaD	electron transfer collisional activation dissociation
ETD	electron transfer dissociation
ETnoD	electron transfer no dissociation
Fmoc	9-fluoroenylmethoxycarbonyl
FT	Fourier transform
FID	free inductance decay
FWHM	full width half maximum
g	grams
GB	gas-phase basicity
GA	gas-phase acidity
GAG	glycylalanylglycine
GGG	triglycine
G′G′G′	trisarcosine
Gln	glutamine (Q)
Glu	glutamic acid (E)
Gly	glycine (G)
HCT	high capacity trap
His	histidine (H)
HPB	4-(4-hydroxyphenyl)-2-butanone
Hz	hertz
HOBt	1-hydroxybenxotriazole
ICR	ion cyclotron resonance

Ile	isoleucine (I)
I/M	ion/molecule
IRMPD	infrared radiation multiphoton dissociation
J	joule
k	kilo (prefix)
KE	kinetic energy
L	liter
LC	liquid chromatography
Leu	leucine (L)
Lys	lysine (K)
MALDI	matrix-assisted laser desorption ionization
Met	methionine (M)
MS	mass spectrometry (or mass spectrometer)
μ	micro (prefix)
m	milli (prefix)
m	meter
M	moles/liter (concentration)
MeOH	methanol
mol	mole(s)
MS/MS	tandem mass spectrometry
MS^n	tandem mass spectrometry
m/z	mass-to-charge ratio
n	nano (prefix)
nCI	negative chemical ionization
NMP	n-methylpyrrolidinone

NMR	nuclear magnetic resonance
-OMe	methyl ester (-OCH_3)
p	pico (prefix)
Phe	phenylalanine (F)
Phe-NH_2	phenylalanine amide
PIP	piperidine
Pro	proline (P)
PSD	post-source decay
PTM	post-translational modification
QIT	quadrupole ion trap
RF	radio frequency
s	second
Sar	sarcosine (G′)
Ser	serine (S)
S/N	signal-to-noise ratio
SORI	sustained off-resonance irradiation
T	tesla
TFA	trifluoroacetic acid
Thr	threonine (T)
TIPS	triisopropyl silane
TOF	time-of-flight
Trp	tryptophan (W)
Tyr	tyrosine (Y)
Tyr-NH_2	tyrosine amide
UW	Utah-Washington

Val	valine (V)
V	volt
ω	angular frequency

ACKNOWLEDGEMENTS

I would like to thank my research advisor Dr. Carolyn J. Cassady for a wonderful graduate school experience. Her passion for chemistry and mass spectrometry is inspiring. I am very thankful that I took her mass spectrometry course during my first semester of graduate school, because it changed my path completely. I hope that one day I can instill the same type of curiosity and determination in students.

Thank you to my dissertation committee members, Drs. Margaret Johnson, Shanlin Pan, Shane Street, and Stephen Woski. I appreciate the encouragement and support each committee member has provided during my graduate years. I would like to thank Dr. David Dixon, Michele Stover, and other Dixon group members for their hard work on the theoretical calculations.

Several funding sources made this dissertation research possible: the National Alumni Association License Tag Fellowship, National Science Foundation American Recovery and Reinvestment Act (NSF ARRA), and National Science Foundation Chemistry Research Instrumentation and Facilities (NSF CRIF) grants. A generous gift of several peptides from Christine Enjalbal from the University of Montpellier made the work in Chapters 3 and 4 possible, and I am very thankful for her contribution.

I would also like to thank the Cassady research group members past and present, especially Dr. Heather Malone Watson. I'm not sure graduate school would have been nearly as much fun without her, and I am really glad we both made it out alive. I would also like to thank Qiaoli Liang for all of her help through the past several years.

I would like to say a special thank you to Dr. Eugene A. Cioffi at the University of South Alabama, for encouraging me to attend graduate school. My undergraduate research experience in his lab gave me confidence in my aptitude as a chemist, and was the catalyst for everything that has followed.

My family has been a tremendous source of support through my entire life, and their faith in me was comforting when I was not sure I could finish. My sister Sunshine and her family deserve a special thank you for housing me for several months at the end of graduate school. It was comforting to have a family to come home to during my most stressful months.

Finally, I would like to thank my husband Paul for his patience and encouragement over the past nine years. This has been an experiment in endurance, and the completion of this dissertation signifies a new beginning for both of us.

TABLE OF CONTENTS

LIST OF TABLES

LIST OF SCHEMES

LIST OF FIGURES

CHAPTER 1: OVERVIEW OF DISSERTATION

The field of proteomics has become the focus of many scientific disciplines that have progressed in the "post-genomic era."[1-3] At the core of proteomics is the proteome, the complete set of proteins expressed by an organism. Studying these proteins is not a trivial task, which explains the existence of databases dedicated solely to protein identification.[4-10] Bioinformatic methods are rapidly being developed to keep up with the demand for accurate protein identifications[11-15] and a more complete understanding of proteins is essential to this venture. Fingerprint characteristics used in bioinformatic models can be determined using classical proteomic analysis methods, which includes techniques such as protein digestions (e.g. trypsin),[16-22] separations (e.g. 2-dimensional gel electrophoresis and capillary separations),[16-19, 21, 23-25] nuclear magnetic resonance (NMR) spectroscopy,[26-30] x-ray crystallography,[27, 28, 31-33] and mass spectrometry (MS).[34-38] These fingerprint characteristics are ultimately responsible for the positive or negative identification of a protein.

Structural proteomics, which deals with all four levels of structural organization within a protein, benefits greatly from developments in fundamental MS studies.[37, 39-45] Protein and peptide sequencing using tandem mass spectrometry techniques has become commonplace in many laboratories. Unfortunately, most biological systems are not fully sequenced using a single technique.[45] Further understanding of all modes of gas-phase behavior is important to improve the sequencing of peptides by mass spectrometry.

Complimentary tandem MS techniques such as collision-induced dissociation (CID) and electron transfer/capture dissociation (ETD/ECD or ExD) have been established as desirable methods for studying biological systems.[38, 46] Both CID and ExD can provide valuable structural information;[38, 45-47] CID traditionally provides fragmentation related to amide bond cleavage in a protein or peptide, whereas ExD usually provides information related to the N−C_α bond.[48, 49] The combination of these two techniques can frequently provide complete sequence information about a protein or peptide.[47, 50]

The capability of most mass spectrometers to easily operate in both positive and negative polarities adds even more depth to what information can be gathered from the CID of a biological compound. Protonated CID of peptides and proteins produces mainly amide bond cleavages and neutral losses, and is well studied.[49, 51-57] Deprotonated CID is underutilized, but equally informative.[58-71] Amide bond cleavages and neutral losses are abundant in both positive and negative ion mode CID, but N−C_α bond cleavage products are also often present. Basic residues tend to direct cleavage in protonated CID whereas acidic residues enhance deprotonated CID fragmentation.[60, 72, 73] Utilizing both polarities in CID can be advantageous in proteomic analysis, since protonated and deprotonated peptides differ in their gas-phase behavior and charge site.

Charge location on a peptide is important to the development of dissociation mechanisms, since most dissociation is charge-directed.[52, 74, 75] Protonation of a peptide typically occurs at basic functional groups such as the N-terminus, backbone amide carbonyl oxygens, or basic amino acid side chains (e.g. arginine, lysine, histidine).[74, 76-79] Deprotonation of a peptide is generally accepted to take place at an acidic functional group such as the C-terminus or a glutamic acid or aspartic acid side chain.[65, 80] Exploration of alternate deprotonation sites for

peptides may enhance the collective understanding of the mechanistic pathways of peptide dissociation in mass spectrometry. Even with the many advantages to using CID and ExD, there are some caveats. For example, in addition to the amide bond cleavages observed in CID, neutral losses (e.g. water, ammonia, side chains) frequently overwhelm the spectra. The presence of arginine, the most basic amino acid residue, in a peptide sequence can limit protonated CID fragmentation due to charge sequestering.[57, 81-83] Neutral losses are not as overwhelming in ExD, but are still prolific. Labile post-translational modifications such as phosphorylation, glycosylation, and disulfide linkages can be identified by the ExD process,[38, 48, 84-86] but are more difficult to locate by CID.

In addition to tandem MS techniques, the mass spectrometer can be used as a medium for conducting controlled reactions in high vacuum. Ion/molecule (I/M) reactions performed in a mass spectrometer can provide important information about a biological system, such as gas-phase basicity[77, 87-93] (for protonated systems) and gas-phase acidity[80, 94-97] (for deprotonated systems). The two aforementioned thermochemical properties offer a better understanding of the location of charge on a protein or peptide, and can validate proposed mechanisms.

Studying the behavior of peptides in the gas phase, by various mass spectrometry methods, can aide in the development of bioinformatic methods for protein identification in proteomics.[98] Linking gas-phase behavior to specific structural characteristics will enhance the possibility of protein identification. One such characteristic is the C-terminal amide, which is abundant in natural peptides.[99, 100] The behavior of a C-terminal amide functional group (rather than the much more common C-terminal carboxylic acid group) has been addressed regarding CID of protonated peptides,[101] but not deprotonated peptides. Protonated behavior of peptides containing C-terminal amides in CID is unremarkable, mainly producing abundant loss of

ammonia. The charge site on a peptide is another attribute that can be valuable to the development of bioinformatic methods.[52] For example, knowing the site of deprotonation on a peptide can assist in determining the most probable mechanistic course of dissociation.

This dissertation investigates the importance of the backbone and C-terminus in mass spectrometry of peptides. Several of the foremost techniques in contemporary mass spectrometry are employed. Dissociation techniques such as CID and ETD are used to probe the behavior of C-terminally modified peptides of varying length and amino acid composition. I/M reactions using the bracketing method[102] are used to acquire valuable thermochemical information (i.e. gas-phase acidity) about smaller systems. Each of the projects discussed herein represent progress in the advancement of MS as a valuable tool for proteomics as well as for fundamental mass spectrometry studies of biomolecules.

Chapter 2 will introduce the experimental procedures used in this research. Each of the mass spectrometers used in this work will be described and each component (i.e. ion source, mass analyzer) will be discussed individually. Then, the dissociation techniques, CID and ETD, are addressed. Experimental procedures related to the ion/molecule reactions are described, as are the related theoretical calculations. Additional consideration is given to synthetic strategies, as many of the peptides in this research were made or modified in-house. Finally, the nomenclature used to describe peptide fragmentation will be discussed briefly.

Chapters 3 and 4 will focus on the dissociation of peptides possessing various C-terminal endgroups. Chapter 3 deals with low-energy CID of various peptides. Both positive and negative mode dissociation patterns are explored, as the two polarities have been shown to produce unique products and fragmentations. Chapter 4 concentrates on using ETD, a novel dissociation technique, to probe the behavior of C-terminally modified peptides. The peptides in

Chapters 3 and 4 were studied in varying lengths and compositions with several different modifications to the C-terminus. C-terminal modifications involved in the study include the standard C-terminal carboxylic acid (-COOH), amide ($-CONH_2$), substituted amides (-CONHEt and $-CONMe_2$), and the methyl ester (-COMe).

Chapters 5 and 6 probe the essential thermochemical properties associated with the deprotonation of amino acids, amino acid amides, small peptides, and other small organic molecules. Gas-phase acidity (GA, the negative of the Gibbs free energy change of the reaction $AH \rightarrow A^- + H^+$ at 298 K) values are determined for the aforementioned types of biomolecules using ion/molecule reactions in a Fourier transform ion cyclotron resonance (FT-ICR) mass spectrometer. High level G3(MP2) calculations have also been performed by David Dixon's group here at the University of Alabama to determine the theoretical GAs in support of the experimental data.

Chapter 5 deals with the deprotonation of amino acids. The site of deprotonation on an amino acid has been debated in recent years. Several groups have investigated deprotonation sites other than the generally accepted site, the C-terminal carboxylic acid group.[95, 103-105] Tyrosine is an interesting case, because it possesses two sites that are capable of deprotonation, the C-terminal carboxylic acid and the phenolic -OH group. Previously, the overall GA of tyrosine has been determined by the equilibrium method and the kinetic and extended kinetic methods.[95, 96, 106, 107] Kass and coworkers[95] addressed the GA of the phenolic and carboxylic acid sites experimentally and computationally. The research shown in this dissertation addresses the GAs tyrosine (Tyr), tyrosine amide (Tyr-NH_2), phenylalanine (Phe), phenylalanine amide (Phe-NH_2), and 4-(4-hydroxyphenyl)-2-butanone (HPB). Each was chosen based on structural similarity to tyrosine: Tyr-NH_2 and HPB both possess a phenolic -OH, and Phe has a carboxylic

acid. Phe-NH_2 does not have the phenolic -OH or a carboxylic acid but does have the aromatic sidechain. The order of experimental acidity is as follows: Phe-NH_2 < HPB < Tyr-NH_2 < Phe < Tyr. Experimental evidence of two ion species was observed for tyrosine, which supports the previously mentioned work of Tian and Kass.[95]

Chapter 6 deals with the deprotonation of peptides and peptide backbones. We have found several cases of peptides that do not possess acidic sites (i.e. C-terminal carboxylic acid or an acidic amino acid residue like glutamic acid or aspartic acid) that are still capable of deprotonation.[64, 108-111] Thus, the backbone must be considered as an alternate site of deprotonation. Several model tripeptides composed of alanine and/or glycine amino acid residues were selected to study using ion/molecule reactions to measure their GAs by the bracketing method. Three of the model peptides were converted to the methyl ester to investigate the possibility of backbone deprotonation. Methyl esterification removes the lone acidic site on a neutral peptide, thus forcing deprotonation to occur on the next most acidic site. Chapter 6 will also address an interesting phenomenon that occurred during the preliminary phase of the project. Several of the model peptide methyl esters that were chosen for the study were incapable of deprotonating in appreciable amounts. These peptides were eliminated from the GA study, but their behavior warrants discussion, as it provided insight to the mechanism for the deprotonation process.

Chapter 7 will review the most important aspects of the research shown in this dissertation. The impact of each project will be discussed with respect to proteomics and fundamental mass spectrometry. This chapter will also address prospective future projects that may further enhance our understanding of the concepts discussed in this dissertation.

References

1. Auerbach, D.; Thaminy, S.; Hottiger, M. O.; Stagljar, I. The post-genomic era of interactive proteomics: Facts and perspectives. *Proteomics* 2002, *2*, 611-623.

2. Pandey, A.; Mann, M. Proteomics to study genes and genomes. *Nature (London)* 2000, *405*, 837-846.

3. Eisenberg, D.; Marcotte, E. M.; Xenarios, I.; Yeates, T. O. Protein function in the post-genomic era. *Nature (London)* 2000, *405*, 823-826.

4. Bateman, A.; Coin, L.; Durbin, R.; Finn, R. D.; Hollich, V.; Griffiths-Jones, S.; Khanna, A.; Marshall, M.; Moxon, S.; Sonnhammer, E. L. L.; Studholme, D. J.; Yeats, C.; Eddy, S. R. The Pfam protein families database. *Nucleic Acids Res.* 2004, *32*, D138-D141.

5. Xenarios, I.; Salwinski, L.; Duan, X. Q. J.; Higney, P.; Kim, S. M.; Eisenberg, D. DIP, the database of interacting proteins: A research tool for studying cellular networks of protein interactions. *Nucleic Acids Res.* 2002, *30*, 303-305.

6. Apweiler, R.; Attwood, T. K.; Bairoch, A.; Bateman, A.; Birney, E.; Biswas, M.; Bucher, P.; Cerutti, T.; Corpet, F.; Croning, M. D. R.; Durbin, R.; Falquet, L.; Fleischmann, W.; Gouzy, J.; Hermjakob, H.; Hulo, N.; Jonassen, I.; Kahn, D.; Kanapin, A.; Karavidopoulou, Y.; Lopez, R.; Marx, B.; Mulder, N. J.; Oinn, T. M.; Pagni, M.; Servant, F.; Sigrist, C. J. A.; Zdobnov, E. M. The InterPro database, an integrated documentation resource for protein families, domains and functional sites. *Nucleic Acids Res.* 2001, *29*, 37-40.

7. Tatusov, R. L.; Natale, D. A.; Garkavtsev, I. V.; Tatusova, T. A.; Shankavaram, U. T.; Rao, B. S.; Kiryutin, B.; Galperin, M. Y.; Fedorova, N. D.; Koonin, E. V. The COG database: new developments in phylogenetic classification of proteins from complete genomes. *Nucleic Acids Res.* 2001, *29*, 22-28.

8. Bairoch, A.; Apweiler, R. The SWISS-PROT protein sequence database and its supplement TrEMBL in 2000. *Nucleic Acids Res.* 2000, *28*, 45-48.

9. Murzin, A. G.; Brenner, S. E.; Hubbard, T.; Chothia, C. Scop - A structural classification of proteins database for the investigation of sequences and structures. *J. Mol. Biol.* 1995, *247*, 536-540.

10. Eng, J. K.; Mccormack, A. L.; Yates, J. R. An approach to correlate tandem mass-spectral data of peptides with amino-acid-sequences in a protein database. *J. Am. Soc. Mass Spectrom.* 1994, *5*, 976-989.

11. Kanehisa, M.; Goto, S.; Kawashima, S.; Okuno, Y.; Hattori, M. The KEGG resource for deciphering the genome. *Nucleic Acids Res.* 2004, *32*, D277-D280.

12. Vazquez, A.; Flammini, A.; Maritan, A.; Vespignani, A. Global protein function prediction from protein-protein interaction networks. *Nat. Biotechnol.* 2003, *21*, 697-700.

13. Paton, N. W.; Khan, S. A.; Hayes, A.; Moussouni, F.; Brass, A.; Eilbeck, K.; Goble, C. A.; Hubbard, S. J.; Oliver, S. G. Conceptual modelling of genomic information. *Bioinformatics* 2000, *16*, 548-557.

14. Thompson, J. D.; Koehl, P.; Ripp, R.; Poch, O. BAliBASE 3.0: Latest developments of the multiple sequence alignment benchmark. *Proteins: Struct., Funct., Bioinf.* 2005, *61*, 127-136.

15. Bordner, A. J.; Abagyan, R. Statistical analysis and prediction of protein-protein interfaces. *Proteins: Struct., Funct., Bioinf.* 2005, *60*, 353-366.

16. Shevchenko, A.; Tomas, H.; Havlis, J.; Olsen, J. V.; Mann, M. In-gel digestion for mass spectrometric characterization of proteins and proteomes. *Nature Protocols* 2006, *1*, 2856-2860.

17. Wang, C.; Oleschuk, R.; Ouchen, F.; Li, J. J.; Thibault, P.; Harrison, D. J. Integration of immobilized trypsin bead beds for protein digestion within a microfluidic chip incorporating capillary electrophoresis separations and an electrospray mass spectrometry interface. *Rapid Commun. Mass Spectrom.* 2000, *14*, 1377-1383.

18. Hellman, U.; Wernstedt, C.; Gonez, J.; Heldin, C. H. Improvement of an in-gel digestion procedure for the micropreparation of internal protein-fragments for amino-acid sequencing. *Anal. Biochem.* 1995, *224*, 451-455.

19. Rosenfeld, J.; Capdevielle, J.; Guillemot, J. C.; Ferrara, P. In-gel digestion of proteins for internal sequence-analysis after 1-dimensional or 2-dimensional gel-electrophoresis. *Anal. Biochem.* 1992, *203*, 173-179.

20. Cobb, K. A.; Novotny, M. High-sensitivity peptide-mapping by capillary zone electrophoresis and microcolumn liquid-chromatography, using immobilized trypsin for protein digestion. *Anal. Chem.* 1989, *61*, 2226-2231.

21. Aebersold, R. H.; Leavitt, J.; Saavedra, R. A.; Hood, L. E.; Kent, S. B. H. Internal amino-acid sequence-analysis of proteins separated by one-dimensional or two-dimensional gel-electrophoresis after in situ protease digestion on nitrocellulose. *Proc. Natl. Acad. Sci. U.S.A.* 1987, *84*, 6970-6974.

22. Mihalyi, E.; Szent-Gyorgyi, A. N. D. R. E. W. G. Trypsin digestion of muscle proteins. I. Ultracentrifugal analysis of the process. *J. Biol. Chem.* 1953, *201*, 189-196.

23. Cooper, J. W.; Wang, Y.; Lee, C. S. Recent advances in capillary separations for proteomics. *Electrophoresis* 2004, *25*, 3913-3926.

24. Braun, P.; LaBaer, J. High throughput protein production for functional proteomics. *Trends Biotechnol.* 2003, *21*, 383-388.

25. Oh-Ishi, M.; Maeda, T. Separation techniques for high-molecular-mass proteins. *J. Chromatogr., B: Anal. Technol. Biomed. Life Sci.* 2002, *771*, 49-66.

26. Rehm, T.; Huber, R.; Holak, T. A. Application of NMR in structural proteomics screening for proteins amenable to structural analysis. *Structure (Cambridge, MA, U.S.A.)* 2002, *10*, 1613-1618.

27. Snyder, D. A.; Chen, Y.; Denissova, N. G.; Acton, T.; Aramini, J. M.; Ciano, M.; Karlin, R.; Liu, J.; Manor, P.; Rajan, P. A.; Rossi, P.; Swapna, G. V. T.; Xiao, R.; Rost, B.; Hunt, J.; Montelione, G. T. Comparisons of NMR spectral quality and success in crystallization demonstrate that NMR and x-ray crystallography are complementary methods for small protein structure determination. *J. Am. Chem. Soc.* 2005, *127*, 16505-16511.

28. Yee, A. A.; Savchenko, A.; Ignachenko, A.; Lukin, J.; Xu, X.; Skarina, T.; Evdokimova, E.; Liu, C. S.; Semesi, A.; Guido, V.; Edwards, A. M.; Arrowsmith, C. H. NMR and x-ray crystallography, complementary tools in structural proteomics of small proteins. *J. Am. Chem. Soc.* 2005, *127*, 16512-16517.

29. Yee, A.; Chang, X.; Pineda-Lucena, A.; Wu, B.; Semesi, A.; Le, B.; Ramelot, T.; Lee, G. M.; Bhattacharyya, S.; Gutierrez, P.; Denisov, A.; Lee, C.; Cort, J. R.; Kozlov, G.; Liao, J.; Finak, G.; Chen, L.; Wishart, D.; Lee, W.; McIntosh, L. P.; Gehring, K.; Kennedy, M. A.; Edwards, A. M.; Arrowsmith, C. H. An NMR approach to structural proteomics. *Proc. Natl. Acad. Sci. U. S. A.* 2002, *99*, 1825-1830.

30. Galvao-Botton, L. M. P.; Katsuyama, A. M.; Guzzo, C. R.; Almeida, F. C. L.; Farah, C. S.; Valente, A. P. High-throughput screening of structural proteomics targets using NMR. *FEBS Lett.* 2003, *552*, 207-213.

31. Chayen, N. E. Turning protein crystallisation from an art into a science. *Curr. Opin. Struct. Biol.* 2004, *14*, 577-583.

32. Kimber, M. S.; Vallee, F.; Houston, S.; Necakov, A.; Skarina, T.; Evdokimova, E.; Beasley, S.; Christendat, D.; Savchenko, A.; Arrowsmith, C. H.; Vedadi, M.; Gerstein, M.; Edwards, A. M. Data mining crystallization databases: Knowledge-based approaches to optimize protein crystal screens. *Proteins: Struct., Funct., Genet.* 2003, *51*, 562-568.

33. Pechkova, E.; Nicolini, C. Protein nanocrystallography: A new approach to structural proteomics. *Trends Biotechnol.* 2004, *22*, 117-122.

34. Bergquist, J.; Palmblad, M.; Wetterhall, M.; Hakansson, P.; Markides, K. E. Peptide mapping of proteins in human body fluids using electrospray ionization fourier transform ion cyclotron resonance mass spectrometry. *Mass Spectrom. Rev.* 2002, *21*, 2-15.

35. Gygi, S. P.; Han, D. K. M.; Gingras, A.; Sonenberg, N.; Aebersold, R. Protein analysis by mass spectrometry and sequence database searching. Tools for cancer research in the post-genomic era. *Electrophoresis* 1999, *20*, 310-319.

36. Jonsson, A. P. Mass spectrometry for protein and peptide characterization. *Cell Mol. Life Sci.* 2001, *58*, 868-884.

37. Kaltashov, I. A.; Eyles, S. J. Studies of biomolecular conformations and conformational dynamics by mass spectrometry. *Mass Spectrom. Rev.* 2002, *21*, 37-71.

38. Kim, M.; Zhong, J.; Kandasamy, K.; Delanghe, B.; Pandey, A. Systematic evaluation of alternating CID and ETD fragmentation for phosphorylated peptides. *Proteomics* 2011, *11*, 2568-2572.

39. Aebersold, R.; Goodlett, D. R. Mass Spectrometry in Proteomics. *Chem. Rev.* 2001, *101*, 269-296.

40. Aebersold, R.; Mann, M. Mass spectrometry-based proteomics. *Nature* 2003, *422*, 198-207.

41. Cooper, H.; Hakansson, K.; Marshall, A. The role of electron capture dissociation in biomolecular analysis. *Mass Spectrom. Rev.* 2005, *24*, 201-222.

42. Guan, J.; Chance, M. Structural proteomics of macromolecular assemblies using oxidative footprinting and mass spectrometry. *Trends Biochem. Sci.* 2005, *30*, 583-592.

43. Maiolica, A.; Cittaro, D.; Borsotti, D.; Sennels, L.; Ciferri, C.; Tarricone, C.; Musacchio, A.; Rappsilber, J. Structural analysis of multiprotein complexes by cross-linking, mass spectrometry, and database searching. *Mol. Cell. Prot.* 2007, *6*, 2200-2211.

44. Becker, J. S.; Jakubowski, N. The synergy of elemental and biomolecular mass spectrometry: new analytical strategies in life sciences. *Chem. Soc. Rev.* 2009, *38*, 1969-1983.

45. Steen, H.; Mann, M. The ABC's (and XYZ's) of peptide sequencing. *Nature Rev. Mol. Cell Biol.* 2004, *5*, 699-711.

46. Sobott, F.; Watt, S. J.; Smith, J.; Edelmann, M. J.; Kramer, H. B.; Kessler, B. M. Comparison of CID versus ETD based MS/MS fragmentation for the analysis of protein ubiquitination. *J. Am. Soc. Mass Spectrom.* 2009, *20*, 1652-1659.

47. Molina, H.; Matthiesen, R.; Kandasamy, K.; Pandey, A. Comprehensive comparison of collision induced dissociation and electron transfer dissociation. *Anal. Chem.* 2008, *80*, 4825-4835.

48. Syka, J. E. P.; Coon, J. J.; Schroeder, M. J.; Shabanowitz, J.; Hunt, D. F. Peptide and protein sequence analysis by electron transfer dissociation mass spectrometry. *Proc. Natl. Acad. Sci. U. S. A.* 2004, *101*, 9528-9533.

49. Papayannopoulos, I. A. The interpretation of collision-induced dissociation tandem mass-spectra of peptides. *Mass Spectrom. Rev.* 1995, *14*, 49-73.

50. Bertsch, A.; Leinenbach, A.; Pervukhin, A.; Lubeck, M.; Hartmer, R.; Baessmann, C.; Elnakady, Y. A.; Mueller, R.; Boecker, S.; Huber, C. G.; Kohlbacher, O. De novo peptide sequencing by tandem MS using complementary CID and electron transfer dissociation. *Electrophoresis* 2009, *30*, 3736-3747.

51. Martin, D.; Eng, J.; Nesvizhskii, A.; Gemmill, A.; Aebersold, R. Investigation of neutral loss during collision-induced dissociation of peptide ions. *Anal. Chem.* 2005, *77*, 4870-4882.

52. Wysocki, V. H.; Tsaprailis, G.; Smith, L. L.; Breci, L. A. Special feature: Commentary - Mobile and localized protons: a framework for understanding peptide dissociation. *J. Mass Spectrom.* 2000, *35*, 1399-1406.

53. Vaisar, T.; Urban, J. Low-energy collision induced dissociation of protonated peptides. Importance of an oxazolone formation for a peptide bond cleavage. *Eur. Mass Spectrom.* 1998, *4*, 359-364.

54. Tang, X. J.; Thibault, P.; Boyd, R. K. Fragmentation reactions of multiply-protonated peptides and implications for sequencing by tandem mass-spectrometry with low-energy collision-induced dissociation. *Anal. Chem.* 1993, *65*, 2824-2834.

55. El Aribi, H.; Rodriquez, C. F.; Almeida, D. R. P.; Ling, Y.; Mak, W. W.; Hopkinson, A. C.; Siu, K. W. M. Elucidation of fragmentation mechanisms of protonated peptide ions and their products: A case study on glycylglycylglycine using density functional theory and threshold collision-induced dissociation. *J. Am. Chem. Soc.* 2003, *125*, 9229-9236.

56. Wells, J.; McLuckey, S. Collision-induced dissociation (CID) of peptides and proteins. *Biol. Mass Spectrom.* 2005, *402*, 148-185.

57. Dongre, A. R.; Jones, J. L.; Somogyi, A.; Wysocki, V. H. Influence of peptide composition, gas-phase basicity, and chemical modification on fragmentation efficiency: Evidence for the mobile proton model. *J. Am. Chem. Soc.* 1996, *118*, 8365-8374.

58. Bilusich, D.; Bowie, J. H. Fragmentations of $(M-H)^-$ anions of underivatised peptides. Part 2: characteristic cleavages of Ser and Cys and of disulfides and other post-translational modifications, together with some unusual internal processes. *Mass Spectrom. Rev.* 2009, *28*, 20-34.

59. Harrison, A. G.; Young, A. B. Fragmentation reactions of deprotonated peptides containing aspartic acid. *Int. J. Mass Spectrom.* 2006, *255-256*, 111-122.

60. Li, Z.; Yalcin, T.; Cassady, C. J. C-terminal amino acid residue loss for deprotonated peptide ions containing glutamic acid, aspartic acid, or serine residues at the C-terminus. *J. Mass Spectrom.* 2006, *41*, 939-949.

61. Eckersley, M.; Bowie, J. H.; Hayes, R. N. Collision-induced dissociations of deprotonated α-amino acids. The occurrence of specific proton transfers preceding fragmentation. *Int. J. Mass Spectrom. Ion Processes* 1989, *93*, 199-213.

62. Harrison, A. G.; Siu, K. W. M.; El Aribi, H. Amide bond cleavage in deprotonated tripeptides: a newly discovered pathway to "b_2 ions. *Rapid Commun. Mass Spectrom.* 2003, *17*, 869-875.

63. Harrison, A. G. Effect of phenylalanine on the fragmentation of deprotonated peptides. *J. Am. Soc. Mass Spectrom.* 2002, *13*, 1242-1249.

64. Harrison, A. G. Sequence-specific fragmentation of deprotonated peptides containing H or alkyl side chains. *J. Am. Soc. Mass Spectrom.* 2001, *12*, 1-13.

65. Marzluff, E. M.; Campbell, S.; Rogers, M. T.; Beauchamp, J. L. Low-energy dissociation pathways of small deprotonated peptides in the gas phase. *J. Am. Chem. Soc.* 1994, *116*, 7787-7796.

66. Waugh, R. J.; Bowie, J. H. A review of the collision-induced dissociations of deprotonated dipeptides and tripeptides. An aid to structure determination. *Rapid Commun. Mass Spectrom.* 1994, *8*, 169-173.

67. Waugh, R. J.; Bowie, J. H.; Gross, M. L.; Vollmer, D. Collision induced dissociations of deprotonated peptides. Dipeptides and tripeptides containing proline. *Int. J. Mass Spectrom. Ion Processes* 1994, *133*, 165-174.

68. Waugh, R. J.; Bowie, J. H.; Gross, M. L. Collision-induced dissociations of deprotonated peptides. Dipeptides containing methionine or cysteine. *Rapid Commun. Mass Spectrom.* 1993, *7*, 623-625.

69. Waugh, R. J.; Bowie, J. H.; Hayes, R. N. Collision induced dissociations of deprotonated peptides : Dipeptides containing phenylalanine, tyrosine, histidine and tryptophan. *Int. J. Mass Spectrom. Ion Processes* 1991, *107*, 333-347.

70. Waugh, R. J.; Eckersley, M.; Bowie, J. H.; Hayes, R. N. Collision induced dissociations of deprotonated peptides: dipeptides containing serine or threonine. *Int. J. Mass Spectrom. Ion Processes* 1990, *98*, 135-145.

71. Eckersley, M.; Bowie, J. H.; Hayes, R. N. Collision-induced dissociations of deprotonated peptides, dipeptides and tripeptides with hydrogen and alkyl a groups. An aid to structure determination. *Org. Mass Spectrom.* 1989, *24*, 597-602.

72. Jai-nhuknan, J.; Cassady, C. J. Negative ion post source decay time-of-flight mass spectrometry of peptides containing acidic amino acid residues. *Anal. Chem.* 1998, *70*, 5122-5128.

73. Steinborner, S. T.; Bowie, J. H. The negative ion mass spectra of $[M-H]^-$ ions derived from caeridin and dynastin peptides. Internal backbone cleavages directed through Asp and Asn residues. *Rapid Commun. Mass Spectrom.* 1997, *11*, 253-258.

74. Cox, K. A.; Gaskell, S. J.; Morris, M.; Whiting, A. Role of the site of protonation in the low-energy decompositions of gas-phase peptide ions. *J. Am. Soc. Mass Spectrom.* 1996, *7*, 522-531.

75. Summerfield, S.; Gaskell, S. Fragmentation efficiencies of peptide ions following low energy collisional activation. *Int. J. Mass Spectrom.* 1997, *165*, 509-521.

76. Zhang, K.; Cassady, C. J.; Chung-Phillips, A. Ab-initio studies of neutral and protonated triglycines - Comparison of calculated and experimental gas-phase basicity. *J. Am. Chem. Soc.* 1994, *116*, 11512-11521.

77. Carr, S. R.; Cassady, C. J. Gas-phase basicities of histidine and lysine and their selected di- and tripeptides. *J. Am. Soc. Mass Spectrom.* 1996, *7*, 1203-1210.

78. Pu, D.; Clipston, N. L.; Cassady, C. J. A comparison of positive and negative ion collision-induced dissociation for model heptapeptides with one basic residue. *J. Mass Spectrom.* 2010, *45*, 297-305.

79. Gaskell, S. J. Electrospray: Principles and practice. *J. Mass Spectrom.* 1997, *32*, 677-688.

80. Li, Z.; Matus, M. M.; Velazquez, H. A.; Dixon, D. A.; Cassady, C. J. Gas-phase acidities of aspartic acid, glutamic acid, and their amino acid amides. *Int. J. Mass Spectrom.* 2007, *265*, 213-223.

81. Gonzalez, J.; Besada, V.; Garay, H.; Reyes, O.; Padron, G.; Tambara, Y.; Takao, T.; Shimonishi, Y. Effect of the position of a basic amino acid on C-terminal rearrangement of protonated peptides upon collision-induced dissociation. *J. Mass Spectrom.* 1996, *31*, 150-158.

82. Farrugia, J. M.; O'Hair, R. A. J. Involvement of salt bridges in a novel gas phase rearrangement of protonated arginine-containing dipeptides which precedes fragmentation. *Int. J. Mass Spectrom.* 2003, *222*, 229-242.

83. Vachet, R.; Asam, M.; Glish, G. Secondary interactions affecting the dissociation patterns of arginine-containing peptide ions. *J. Am. Chem. Soc.* 1996, *118*, 6252-6256.

84. Weisner, J.; Premsler, T.; Sickmann, A. Application of electron transfer dissociation (ETD) for the analysis of posttranslational modifications. *Proteomics* 2008, *8*, 4466-4483.

85. Zhang, Q.; Frolov, A.; Tang, N.; Hoffmann, R.; van de Goor, T.; Metz, T. O.; Smith, R. D. Application of electron transfer dissociation mass spectrometry in analyses of non-enzymatically glycated peptides. *Rapid Commun. Mass Spectrom.* 2007, *21*, 661-666.

86. Zubarev, R. A.; Kruger, N. A.; Fridriksson, E. K.; Lewis, M. A.; Horn, D. M.; Carpenter, B. K.; McLafferty, F. W. Electron capture dissociation of gaseous multiply-charged proteins is favored at disulfide bonds and other sites of high hydrogen atom affinity. *J. Am. Chem. Soc.* 1999, *121*, 2857-2862.

87. Mckiernan, J. W.; Beltrame, C. E. A.; Cassady, C. J. Gas-phase basicities of serine and dipeptides of serine and glycine. *J. Am. Soc. Mass Spectrom.* 1994, *5*, 718-723.

88. Wu, J. Y.; Lebrilla, C. B. Gas-phase basicities and sites of protonation of glycine oligomers (Gly_n, N = 1-5). *J. Am. Chem. Soc.* 1993, *115*, 3270-3275.

89. Zhang, K.; Zimmerman, D. M.; Chung-Phillips, A.; Cassady, C. J. Experimental and ab-initio studies of the gas-phase basicities of polyglycines. *J. Am. Chem. Soc.* 1993, *115*, 10812-10822.

90. Ewing, N. P.; Zhang, X.; Cassady, C. J. Determination of the gas-phase basicities of proline and its di- and tripeptides with glycine: The enhanced basicity of prolylproline. *J. Mass Spectrom.* 1996, *31*, 1345-1350.

91. Harrison, A. G. The gas-phase basicities and proton affinities of amino acids and peptides. *Mass Spectrom. Rev.* 1997, *16*, 201-217.

92. Ewing, N. P.; Pallante, G. A.; Zhang, X.; Cassady, C. J. Gas-phase basicities for ions from bradykinin and its des-arginine analogues. *J. Mass Spectrom.* 2001, *36*, 875-881.

93. Bouchoux, G.; Salpin, J. Y. Gas-phase basicity of glycine, alanine, proline, serine, lysine, histidine and some of their peptides by the thermokinetic method. *Eur. J. Mass Spectrom.* 2003, *9*, 391-402.

94. Eyet, N.; Villano, S. M.; Bierbaum, V. M. Anchoring the gas-phase acidity scale: From formic acid to methanethiol. *Int. J. Mass Spectrom.* 2009, *283*, 26-29.

95. Tian, Z.; Wang, X.; Wang, L.; Kass, S. R. Are carboxyl groups the most acidic sites in amino acids? Gas-phase acidities, photoelectron spectra, and computations on tyrosine, p-hydroxybenzoic acid, and their conjugate bases. *J. Am. Chem. Soc.* 2009, *131*, 1174-1181.

96. Jones, C. M.; Bernier, M.; Carson, E.; Colyer, K. E.; Metz, R.; Pawlow, A.; Wischow, E. D.; Webb, I.; Andriole, E. J.; Poutsma, J. C. Gas-phase acidities of the 20 protein amino acids. *Int. J. Mass Spectrom.* 2007, *267*, 54-62.

97. Carr, S. R.; Cassady, C. J. Reactivity and gas-phase acidity determinations of small peptide ions consisting of 11 to 14 amino acid residues. *J. Mass Spectrom.* 1997, *32*, 959-967.

98. Yakunin, A. F.; Yee, A. A.; Savchenko, A.; Edwards, A. M.; Arrowsmith, C. H. Structural proteomics: a tool for genome annotation. *Curr. Opin. Chem. Biol.* 2004, *8*, 42-48.

99. Glass, J. D.; Schwartz, I. L.; Walter, R. Enzymatic inactivation of peptide hormones possessing a C-terminal amide group. *Proc. Natl. Acad. Sci. U. S. A.* 1969, *63*, 1426-1430.

100. Bradbury, A. F.; Smyth, D. G. Peptide amidation. *Trends Biochem. Sci.* 1991, *16*, 112-115.

101. Mouls, L.; Subra, G.; Aubagnac, J.; Martinez, J.; Enjalbal, C. Tandem mass spectrometry of amidated peptides. *J. Mass. Spectrom.* 2006, *41*, 1470-1483.

102. Gorman, G. S.; Amster, I. J. Kinetic and thermodynamic considerations of the bracketing method: Entropy-driven proton-transfer reactions in a Fourier transform mass spectrometer. *Org. Mass Spectrom.* 1993, *28*, 1602-1607.

103. Steill, J. D.; Oomens, J. Gas-phase deprotonation of p-hydroxybenzoic acid investigated by IR spectroscopy: Solution-phase structure is retained upon ESI. *J. Am. Chem. Soc.* 2009, *131*, 13570-13571.

104. Tian, Z.; Kass, S. R. Gas-phase versus liquid-phase structures by electrospray ionization mass spectrometry. *Angew. Chem. Int. Edit.* 2009, *48*, 1321-1323.

105. Tian, Z.; Kass, S. R. Does electrospray ionization produce gas-phase or liquid-phase structures? *J. Am. Chem. Soc.* 2008, *130*, 10842-10843.

106. Bouchoux, G.; Huang, S.; Inda, B. S. Acid-base thermochemistry of gaseous aliphatic alpha-amino acids. *Phys. Chem. Chem. Phys.* 2011, *13*, 651-668.

107. O'Hair, R. A. J.; Bowie, J. H.; Gronert, S. Gas phase acidities of the alpha amino acids. *Int. J. Mass Spectrom.* 1992, *117*, 23-36.

108. Clipston, N. L.; Jai-nhuknan, J.; Cassady, C. J. A comparison of negative and positive ion time-of-flight post-source decay mass spectrometry for peptides containing basic residues. *Int. J. Mass Spectrom.* 2003, *222*, 363-381.

109. Brinkworth, C. S.; Dua, S.; Bowie, J. H. Backbone cleavages of $[M - H]^-$ anions of peptides. Cyclisation of citropin 1 peptides involving reactions between the C-terminal $[CONH]^-$ residue and backbone amide carbonyl groups. A new type of b cleavage: a joint experimental and theoretical study. *Rapid Commun. Mass Spectrom.* 2002, *16*, 713-721.

110. Gao, J.; Cassady, C. J. Negative ion production from peptides and proteins by matrix-assisted laser desorption/ionization time-of-flight mass spectrometry. *Rapid Commun. Mass Spectrom.* 2008, *22*, 4066-4072.

111. Vasil'ev, Y. V.; Figard, B. J.; Morre, J.; Deinzer, M. L. Fragmentation of peptide negative molecular ions induced by resonance electron capture. *J. Chem. Phys.* 2009, *131*, 044317.

CHAPTER 2: THEORY, INSTRUMENTATION, AND EXPERIMENTAL PROCEDURES

2.1 Overview

The experimental results discussed in this dissertation were acquired by various mass spectrometry techniques. Fragmentation studies (e.g. CID and ETD) were carried out on a Bruker (Billerica, MA, USA) HCTultra PTM Discovery System equipped with ESI. Gas-phase acidity studies were performed on a Bruker BioApex 7e FT-ICR, also equipped with ESI. Since both mass spectrometers utilize ESI as the ionization technique, this is discussed first. Then, each mass spectrometer is detailed with regard to theory and each of the experimental procedures are discussed. This includes CID, ETD, and gas-phase acidity experiments. Finally, the solid-phase synthesis of peptides, solution-phase modification of peptides, and peptide fragmentation nomenclature are described.

2.2 Electrospray ionization

Originating from the early work of Dole and coworkers[1] and largely credited to eventual Nobel laureate John Fenn,[2-6] electrospray ionization (ESI) has become a familiar method of ionizing samples for mass spectral analysis. The ability of ESI to act as an interface for liquid chromatography/mass spectrometry (LC/MS) has made it even more useful.[4, 7] Additionally, the unique ability of ESI to produce multiple charges on ions, $[M + nH]^{n+}$ or $[M - nH]^{n-}$, allows for the study of very large compounds. The multiply charged ions generated by ESI are also ideal

precursor ions for dissociation techniques such as collision-induced dissociation (CID) and electron transfer dissociation (ETD).

The ESI process is well-studied[3, 8-12] and although there are a few different configurations available, the process is principally the same for each. ESI begins with sample preparation. A sample of interest is dissolved in solvent. The solvent can be composed of one or more of the following components: typically methanol, water, or acetonitrile. Depending on the desired ionization polarity, 1-2% (V/V) of additives such as acetic acid, formic acid, or ammonium hydroxide may be added. Acetic and formic acid help to protonate samples prior to ESI, and ammonium hydroxide aids in deprotonating samples. The concentration of the sample solution can vary depending on sample or mass spectrometer, but the sensitivity of ESI can be in the attomole (1×10^{-15} mole) range. For this dissertation research, a typical ESI sample concentration range of 1-5 μM was used for experiments performed on the Bruker HCTultra PTM Discovery System. Concentrations of 50-100 μM were characteristic of experiments performed on the Bruker BioApex 7e FT-ICR.

The prepared sample solution is introduced using a syringe mounted on a syringe pump set to deliver between 50-250 μL/hr. The syringe is connected to a stainless steel needle via polymeric tubing (i.e. PEEK tubing). The needle, which is inside the electrospray chamber, sprays the sample solution. In some ESI configurations, a voltage (~ 3000-4000 V) is applied to this needle. In others, such as the instruments used in this research, a voltage may be applied to an endplate and capillary entrance that follows in the source design. An inert gas, like nitrogen (N_2) or air, may be used in the nebulization process. Often this same inert gas is used as a drying gas, assisting in solvent stripping. The nebulizing gas is typically flowing in the same direction as the needle carrying the sample, whereas the drying gas flows in the opposite direction toward the needle. This spraying and subsequent drying of the sample solution produces ions. In this

dissertation research, gaseous nitrogen (for the HCTultra) or air (for the BioApex) heated to a temperature of about 220°C was used as the drying gas. The drying gas was set to flow at a rate of ~5 L/min. Nitrogen was also used as the nebulizer gas at a pressure of 10-20 psi.

Droplets formed during nebulization possess charges (positive or negative, depending on polarity) that build up on their surface. Eventually the Rayleigh limit is reached, and the droplets are broken down into even smaller droplets by coulombic explosions.[13-15] These droplets can have charges equal to or greater than one ($[M + nH]^{n+}$ or $[M - nH]^{n-}$, where $n \geq 1$), and are called quasi-molecular ions. These ions are then directed through a glass capillary, commonly coated with platinum on both ends for conductivity. Once through the capillary, the ions pass through a skimmer and a hexapole or octapole then travel through at least two stages of vacuum pumping on their way to the mass analyzer. A simplified diagram of an ESI is illustrated in Figure 2.1. Note that the nebulizing needle may be positioned orthogonally to the capillary as well.

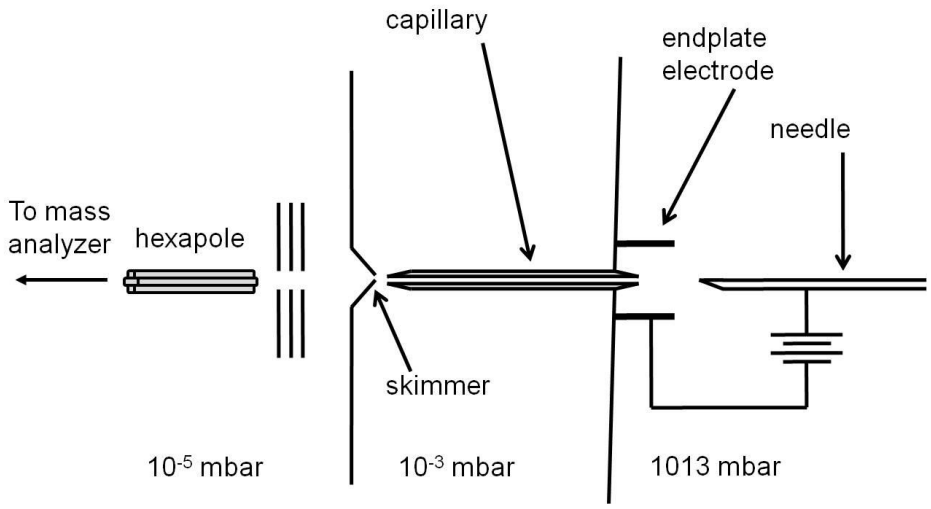

Figure 2.1. Diagram of ESI source.

2.3 Mass analyzers

2.3.1 Quadrupole ion trap

The invention of the quadrupole ion trap (QIT) earned Wolfgang Paul and Hans Dehmelt part of the 1989 Nobel Prize in Physics. Their contributions to the field of mass spectrometry laid the groundwork for the linear and 3-dimensional (3D) QIT mass analyzers used today.[16] The high capacity (HC) 3D QIT used in this dissertation is a component of our HCTUltra PMT Discovery System equipped with ESI. A QIT is a pulsed-type mass analyzer that uses both radio frequency (RF) and direct current (DC) potentials to trap ions in a "pseudopotential well." Figure 2.2 shows a general diagram of the QIT and ion transfer used in this research.

The 3D QIT has a very simple physical design, a ring electrode flanked by two endcaps. Ions are directed to the trap using electrostatic focusing by means of two octopoles and a lens system that connects the ESI source to the mass analyzer. The ions enter (and exit) the trap

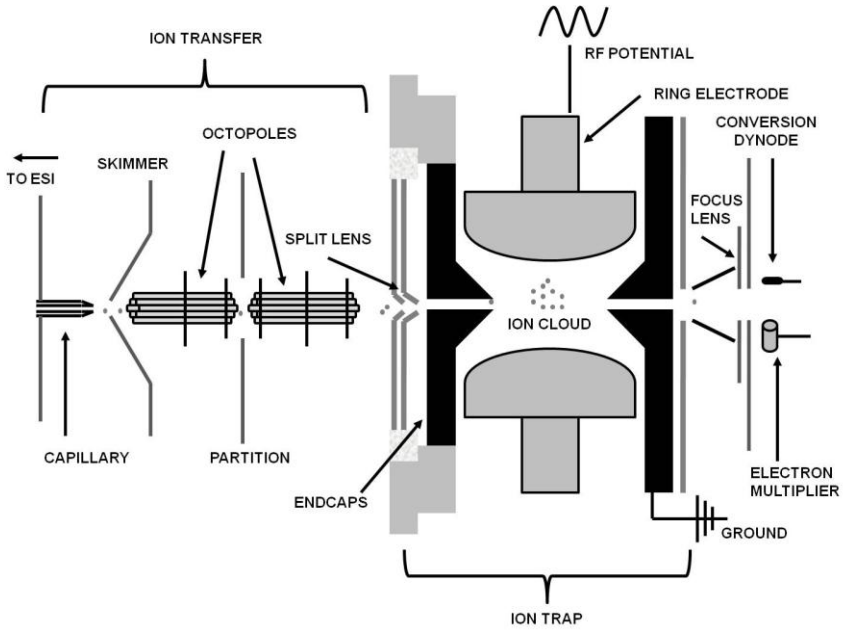

Figure 2.2. QIT and ion transfer diagram.

through small holes in the endcaps. Since ions are produced by a continuous ionization source (i.e. ESI), the ions are stored in the first octapole and allowed into the QIT during a variable accumulation time. Accumulation times can range from 0.01 ms to 200 ms, with the goal of maximum signal and minimizing space charge effects. A high potential is normally applied to the gate lens to keep ions from entering the trap. During the accumulation time, this potential is not applied, thus allowing ions into the trap. To trap ions in the QIT, a DC potential is applied to the endcaps, and an RF potential is applied to the ring electrode. The endcaps are typically at ground and the frequency of the RF potential is held constant at 781 kHz. This forms an oscillating quadrupolar field that excites the ions.

The ions in the trap behave as a cloud, and are being pushed and pulled in a series of complex motions. To focus the ion cloud and minimize motion, a damping gas (*i.e.* helium) is often present in the ion trap at a background pressure of ~10^{-3} Torr. Motion of the ion cloud can be described by solutions of the Mathieu equations:

Canonical Form of Mathieu Equation:

$$\frac{d^2y}{dx^2} + [a - 2q\cos(2x)]y = 0 \qquad 2.1$$

Ion Motion Form of Mathieu Equation:

$$\frac{d^2u}{d\xi^2} + [a_u - 2q_u\cos(2\xi)]u = 0 \qquad 2.2$$

where

$$\xi = \frac{\Omega t}{2} \qquad 2.3$$

In these equations, a_u and q_u are trapping parameters, where *u* describes the direction of motion as axial (z) or radial (xy), ξ is a dimensionless parameter, and Ω is the frequency of the RF potential. As a result of much substitution and rearrangement, several similar expressions arise to describe the motion of the ion cloud in radial (Equations 2.4 and 2.5) and axial (Equations 2.6

and 2.7) directions. The amplitude of the DC voltage is represented by *U*, the amplitude of the AC voltage is *V*, and *r* represents the radius of the ring electrode. The mass of the ion is represented by *m* and the ion's nominal charge is *z* with *e* representing the charge of an electron (*ze* is therefore the charge on the ion in Coulombs).

$$a_x = \frac{8zeU}{mr_0^2\Omega^2} \tag{2.4}$$

$$q_x = -\frac{4zeV}{mr_0^2\Omega^2} \tag{2.5}$$

$$a_z = -\frac{8zeU}{mr_0^2\Omega^2} \tag{2.6}$$

$$q_z = \frac{4zeV}{mr_0^2\Omega^2} \tag{2.7}$$

Axial trapping parameters are most important as they indicate stability in the trap as illustrated in the Mathieu stability diagram (Figure 2.3).[17] The Mathieu diagram also illustrates the mass-to-charge cutoff for the QIT, where $\frac{m}{z} \propto \frac{V}{q_z}$. Thus, the RF potential placed on the ring electrode directly affects the mass-to-charge ratios (*m/z*) of the ions that are successfully trapped. The trapped ions also oscillate at a frequency known as the "secular frequency," which is described by Equations 2.8-2.10. Secular frequency is simply the frequency at which an ion of a particular *m/z* oscillates. Low *m/z* ions oscillate at high frequencies and high *m/z* ions oscillate at low secular frequencies. The *m/z* with secular frequency closest to Ω/2 is the cutoff mass. Typically ions with *m/z* below the cutoff mass will not be effectively trapped in the QIT.

$$\omega_{u,n} = \left(n + \frac{1}{2}\beta_u\right)\Omega \qquad 0 \leq n < \infty \tag{2.8}$$

$$\omega_{u,n} = -(n + \frac{1}{2}\beta_u)\Omega \qquad -\infty < n \leq 0 \tag{2.9}$$

$$\beta_u \approx \sqrt{(a_u + \frac{q_u^2}{2})} \tag{2.10}$$

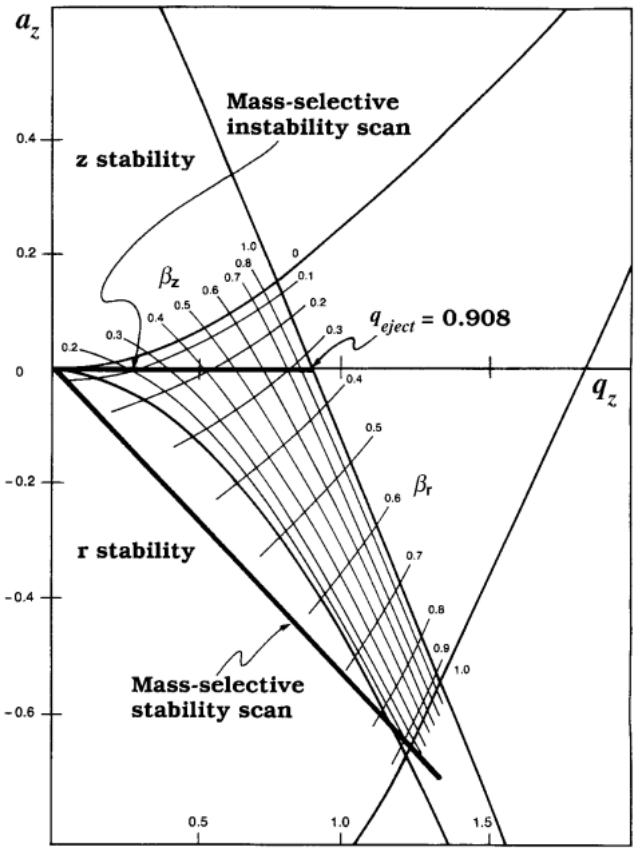

Figure 2.3. Mathieu stability diagram
(used with permission from Reference 17).

Excitation of the trapped ions is a result of placing a supplementary voltage on the endcaps in resonance with the axial secular frequency. This "tickles" the ion cloud, causing the ions to move away from the center of the trap. This movement also causes the ions to increase their kinetic energy due to the increase in the trapping field. Ramping the amplitude of the RF voltage further increases the energy of the ions, ejecting them from the trap for detection by an electron multiplier.

2.3.2 Fourier transform ion cyclotron resonance

Fourier transform ion cyclotron resonance (FT-ICR) mass spectrometry (MS) was introduced in 1974 by Comisarow and Marshall[18] as a potential method for reducing the time

required to scan a wide mass range during spectral acquisition. Their work improved on ICR-MS by applying the Fourier transform technique. Fourier transform increases the speed of spectral acquisition significantly, which allows for analysis over a much wider *m/z* range . Another benefit to FT-ICR is the superior resolution that is not possible with ICR.

The exceptional figures of merit for FT-ICR MS make it one of the most powerful mass spectral techniques available. Figures of merit include: mass resolving power, scan speed, mass range, trapping time, and ion energy. Most notable of these advantages is the capability to routinely measure the *m/z* of a particular system with very high mass resolution and accuracy. The full-width half maximum (FWHM) resolution can be greater than 500,000 for routine measurements, and exceptional resolution can be attained for lower mass compounds since resolution in an FT-ICR is inversely related to mass. Marshall and coworkers[19] demonstrated the resolving power of the FT-ICR by the measurement of two isomeric peptides, RVMRGMR and RSHRGHR. The masses of these peptides differ by 0.00045 Da, and a resolution of 3,300,000 was achieved for this measurement.

In addition to resolution, FT-ICR MS has numerous advantages over other MS techniques. For example, detection of ions is performed inside the cell without the use of a traditional detector (e.g. electron multiplier, microchannel plate). Plates on the FT-ICR are used to excite and detect the ions. All ionization techniques are compatible with FT-ICR MS (e.g. ESI, matrix-assisted laser desorption ionization (MALDI), electron ionization (EI), etc.), which makes it a superior technique for studying almost any compound. Ultra-high vacuum

(~10^{-9} - 10^{-10} mbar) conditions in the FT-ICR cell allow ions to be trapped for an unrestricted amount of time. These low pressures are advantageous for numerous applications; for example, ion/ion and ion/molecule reactions. Tandem mass spectrometry (MS^n) techniques such as CID and ECD are easily performed on an FT-ICR. Tandem MS is performed in time rather than space (as in a sector or multi-stage quadrupole mass spectrometer), allowing for maximum information to be acquired.

The FT-ICR used in this dissertation is a Bruker BioApex 7e FT-ICR MS (Figure 2.4). This instrument is configured with an Apollo API source (Bruker Daltonics, Billerica, MA) as the primary ionization method. A 7 T superconducting magnet is used to produce the magnetic field. A cylindrical analyzer cell is used for ion storage, mass analysis and subsequent detection. An electron ionization (EI) filament is present in the FT-ICR cell, which can also be used for ionization or MS^n experiments (such as electron capture dissociation). Instrumental theory will be discussed as it applies to this instrument using ESI to produce ions. Ions produced by electrospray are transferred to the analyzer cell using electrostatic focusing. A sequence of

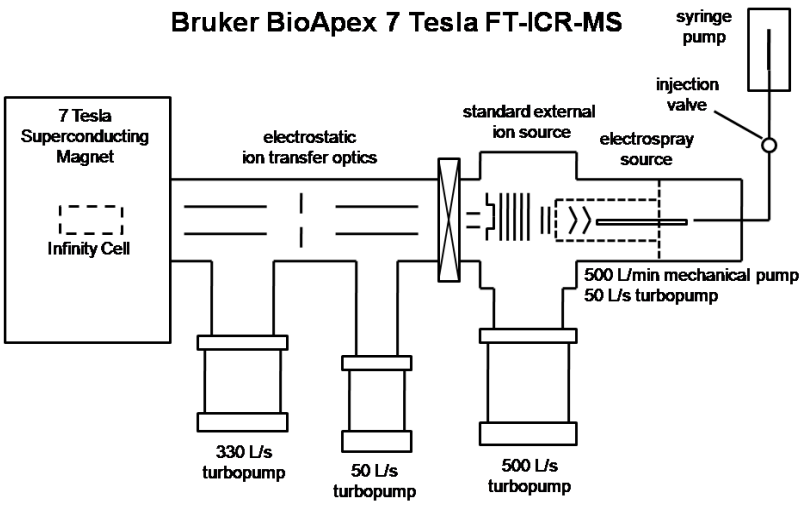

Figure 2.4. Diagram of Bruker BioApex 7 Tesla FT-ICR MS.

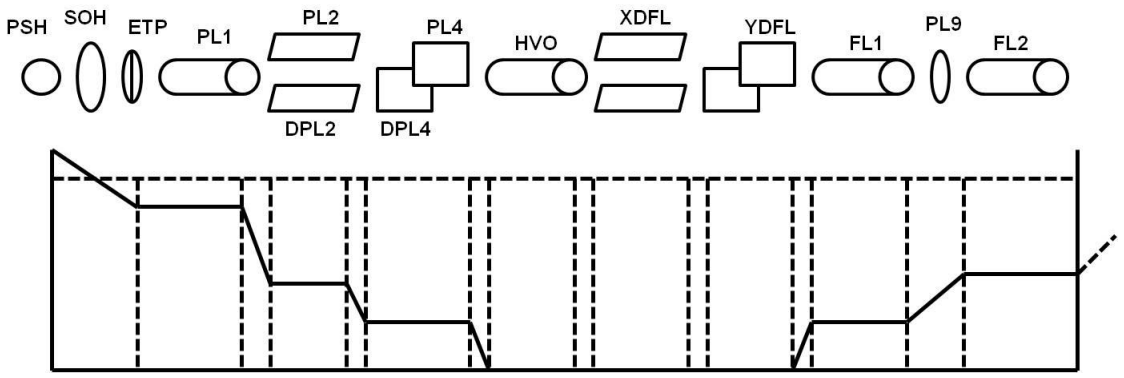

Figure 2.5. Diagram of ion transfer optics in the Bruker BioApex 7 Tesla FT-ICR MS and sample voltage profile for transfer of protonated species.

lenses, plates and tubes are used to provide the necessary voltages for ion transfer. The configuration of the ion transfer optic system used in our FT-ICR can be seen in Figure 2.5. The ion optics serve to increase the velocity of the ions so that they may penetrate the magnetic field to reach the analyzer cell. Prior to entering the cell, the ions must be slowed down so that they may be trapped by the low voltages (1-10 V) used in the analyzer cell. A sample diagram of the voltage profile used may also be seen in Figure 2.5.

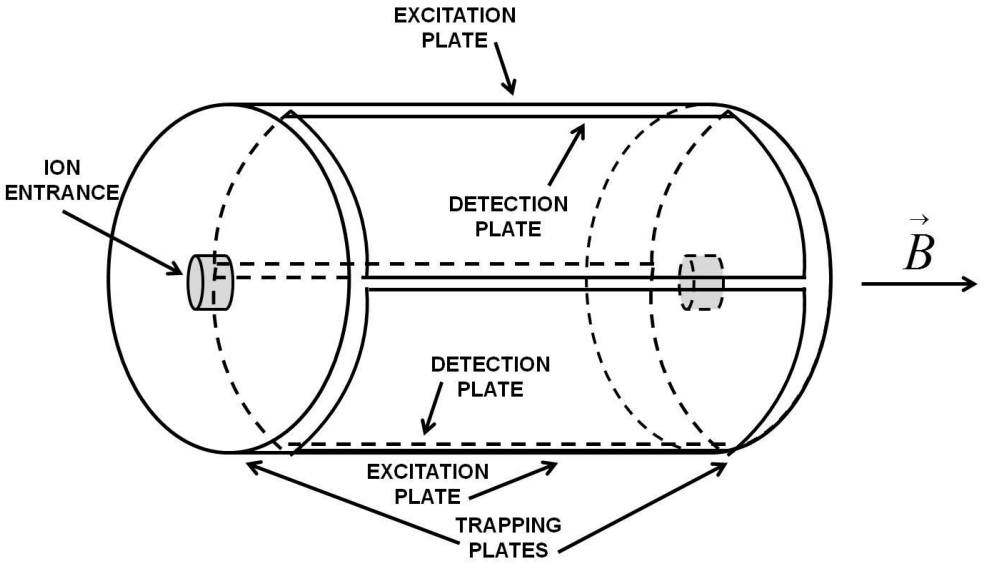

Figure 2.6. Diagram of the cylindrical analyzyer cell.

Figure 2.6 illustrates the "infinity" analyzer cell as originally described by Carvatti and Alleman.[20] The ions enter the analyzer cell through a hole located in the center of the trapping plates nearest the ESI source. The trapping plates are oriented perpendicular to the magnetic field, and voltages between 1-1.5 V are used to trap the ions. Inside the analyzer cell, the ions experience three types of motion: cyclotron motion, trapping motion, and magnetron motion. The most important of these motions is the cyclotron motion, which is used in mass analysis. In cyclotron motion, the ions experience a balance of two forces, magnetic (Lorentz) force and centrifugal force, that causes them to move in circular orbits. Motion occurs in the x-y plane perpendicular to the magnetic field (z-axis). The cyclotron motion of the trapped ions is shown in Figure 2.7: where v represents the velocity of the ion, F_1 is the Lorentz force, F_2 is the centrifugal force, r is the radius of the ion's orbit, and B is the magnetic field (perpendicular to the page). The two forces acting upon the ion are equal, and combining the two equations produces a mathematical relationship to describe the cyclotron motion (Equations 2.11-2.19).

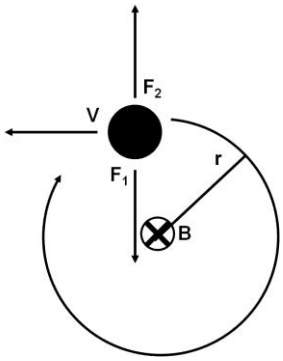

Figure 2.7. Ion cyclotron motion.

$$F_1 = magnetic\ force = Bzv \quad (2.11)$$

$$F_2 = centrifigal\ force = \frac{mv^2}{r} \quad (2.12)$$

$$F_1 = F_2 \quad (2.13)$$

$$Bzv = \frac{mv^2}{r} \quad (2.14)$$

$$\frac{Bz}{m} = \frac{v}{r} \quad (2.15)$$

$$\omega = \frac{v}{r}\ (\omega = orbital\ angular\ frequency) \quad (2.16)$$

$$\text{so, } \frac{m}{z} = \frac{B}{\omega} \quad (2.17)$$

$$and\ \omega = 2\pi f\ (f = ion\ cyclotron\ frequency\ in\ Hz) \quad 2.18$$

$$\text{thus, } \frac{m}{z} = \frac{B}{2\pi f} = (1.537 \times 10^7)\frac{B}{f} \quad 2.19$$

Equation 2.19 directly relates the cyclotron frequency of an ion to the magnetic field strength and its *m/z*. This means that a singly-charged ion with *m/z* 150 in a 7 T magnetic field will have a cyclotron frequency of approximately 717 kHz.

To detect ions in an FT-ICR experiment, a radio frequency (RF) sweep is applied to the excitation plates (as shown in Figure 2.6). The RF sweep excites the ions into larger orbits causing those with identical *m/z* to move coherently as a single packet of charge. Each *m/z* is then detected as an image current on the detect plates (shown in Figure 2.5) producing the transient signal. Fourier transform of the time-domain transient produces a mass frequency spectrum. Figure 2.8 shows a simple illustration of a transient signal produced by an FT-ICR experiment and its consequential transformed mass spectrum.

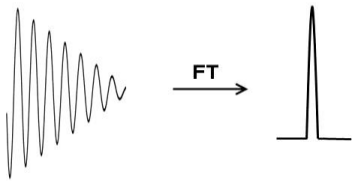

Figure 2.8. FT of transient from an FT-ICR experiment.

An experimental setup for simple mass analysis in an FT-ICR consists of three steps. The first step is typically a quenching pulse that is used to eliminate any ions present in the analyzer cell prior to the experiment. The voltage used for this pulse is opposite in polarity to that of the ions being studied (i.e. negative voltages for positive ions). After quenching, ions are brought into the cell through the hole in the front trapping plate. Finally, the ions are excited and detected. Tandem mass spectrometry techniques would add at least two additional steps to the procedure prior to excitation and detection. For example, a particular ion of interest may be isolated in the cell by an RF sweep over all of the frequencies except that of the ion being isolated. This RF sweep ejects all ions other than the mass selected ion.[21] After isolation, the ion

may be dissociated by CID or perhaps undergo an I/M reaction with a neutral reference compound before excitation and detection.

2.4 Dissociation techniques

2.4.1 Collision-induced dissociation

Collision-induced dissociation (CID) is defined by the International Union of Pure and Applied Chemistry (IUPAC) Gold Book to be "an ion/neutral species process wherein the projectile ion is dissociated as a result of interaction with a target neutral species. This is brought about by conversion of part of the translational energy of the ion to internal energy in the ion during the collision."[22] CID is a common feature on commercial mass spectrometers, and is one of the most widely used members of the tandem MS family. In the CID process, an ion is isolated and then fragmented by collisions with an inert gas such as helium, argon, xenon, or nitrogen (N_2). There are high-energy and low-energy versions of CID; high-energy CID can have keV collision energies whereas low-energy CID typically has collision energies >10 eV. Both protonated and deprotonated species may be studied using CID, and they are often complimentary methods. Coupled with the multiple charging capabilities of ESI, CID can be a powerful tool for fragmenting large compounds. The CID process will be discussed here as performed using peptides in the QIT of the Bruker HCTultra PTM Discovery System used in this research. The CID process on the BioApex 7e is very similar.

Low-energy CID is frequently used to study biomolecules such as proteins and peptides. Structural, kinetic, and energetic information may be obtained from a well-designed CID experiment and such information is valuable to both fundamental studies as well as proteomic studies.[23-28] Fragmentation of protonated peptides by CID has been exhaustively researched, providing the field with such concepts as the "mobile proton model."[29, 30] The mobile proton

model states that the initial protonation site (i.e. N-terminal amino group or basic residue side chain) does not retain the proton and it moves freely along the peptide backbone to sites that are energetically less favorable.[29, 30] This causes destabilization of the amide bond, and produces the commonly observed b/y fragment ions. (The nomenclature of peptide fragmentation is discussed in Section 2.5.) Discovery of fragmentation patterns based on sequence,[31-40] conformation,[41-43] salt bridge formation,[44, 45] identity of N- or C-terminal group,[46] and other structural attributes have developed CID into a powerful tool for proteomic analysis. CID of deprotonated peptides is not as developed as its protonated counterpart, but many advances have been made in recent years.

The CID process begins after the ions have been produced by ESI and transported to the QIT by electrostatic focusing. A peptide ion of interest is isolated by subjecting the trapped ions to a broadband range of frequencies (for the AC voltage) that causes ions moving with these frequencies to increase their kinetic energies and be ejected from the trap. The resonant frequency of the precursor ion is not included; thus it remains in the trap. Once isolated, the fragmentation sequence is as follows: resonant excitation of the precursor ion, collisions with neutral gas (helium in this case) present in trap, fragmentation, and finally detection. The resonant excitation of the precursor ion requires an excitation voltage amplitude of approximately 1 V which increases the kinetic energy of the precursor and results in more energetic collisions with the helium present in the trap. The kinetic energy from the collisions is then distributed along the backbone of the peptide causing fragmentation. The entire CID process takes place over a timescale of approximately 20-60 ms.

For the low-energy CID experiments described in this dissertation, precursor ions were allowed to accumulate in the trap for up to 200 ms and then mass selected using ejection pulses. The isolation window was 4 *m/z* wide in most cases, but was narrowed to 1 *m/z* for situations that

had interfering peaks nearby. Helium was used as the collision gas. A collision energy sweep of 30-200% with amplitude between 0.1 and 1.0 V was used to maximize CID fragmentation.

2.4.2 Electron transfer dissociation

Electron transfer dissociation (ETD) is one of the more contemporary methods of fragmentation in MS. Introduced by Hunt and coworkers[47] in 2004, the ETD experiment is designed for use in ion trap mass spectrometers. A similar technique introduced in 1998, electron capture dissociation (ECD), was designed for use in FT-ICR mass spectrometers.[48] Both ETD and ECD processes involve the transfer of a low energy electron to a multiply-charged ion to induce fragmentation by vibrational excitation of the N–C_α bond. This type of experiment requires positive ions, and an ionic charge greater than one. Transfer of an electron to a singly protonated ion would merely neutralize the ion, which could not be detected without reionization. Recent progress in the field has expanded the ECD and ETD experiments to include negative ions. Although still in infancy, negative electron transfer dissociation (nETD) and electron-detachment dissociation (EDD) are the negative ion analogs of ETD and ECD.[49, 50]

The ETD experiments discussed in this dissertation were performed on a Bruker HCTultra PTM Discovery System. Multiply-charged ions were produced by ESI, transferred to the QIT, and isolated. The transfer of a low-energy electron to the multiply-charged precursor ion requires an ETD reagent with an electron affinity (EA) low enough to release the electron

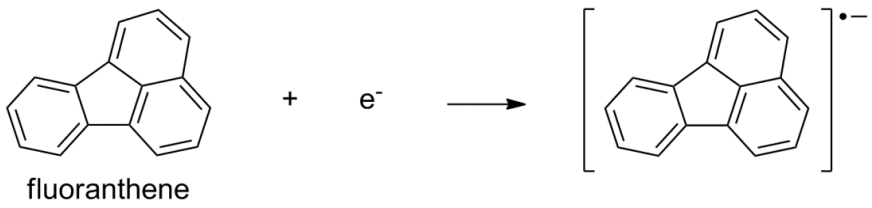

Figure 2.9. Production of fluoranthene anion in NCI source.

(<60-70 kcal/mol). Fluoranthene is used as the standard ETD reagent in the Bruker HCTultra system and in this dissertation research. Other ETD reagents such as azobenzene and anthracene may be used as well with little or no experimental modification.[51] The fluoranthene anion is produced by negative chemical ionization (nCI) as shown in Figure 2.9. As shown in Figure Figure 2.10,[52] the nCI source is located outside of the QIT, so the fluoranthene anions must be transported to the trap using the same ion transfer octopole that is used to transfer the multiply-protonated precursor ions. This is accomplished simply by switching the polarity on the transport octopole. Once the reagent anions are accumulated in the trap, an ion/ion reaction between the multiply-protonated precursor ions and the fluoranthene anions occurs. The ion/ion reaction (i.e. ETD process) occurs on a timescale of 40-100 ms, which is a longer timescale than the 20-60 ms scale observed with CID. Transfer of a low-energy electron from the reagent anion to a multiply-protonated peptide causes excess vibrational energy to be dispersed throughout the peptide backbone, causing primarily N–C_α bond cleavage.

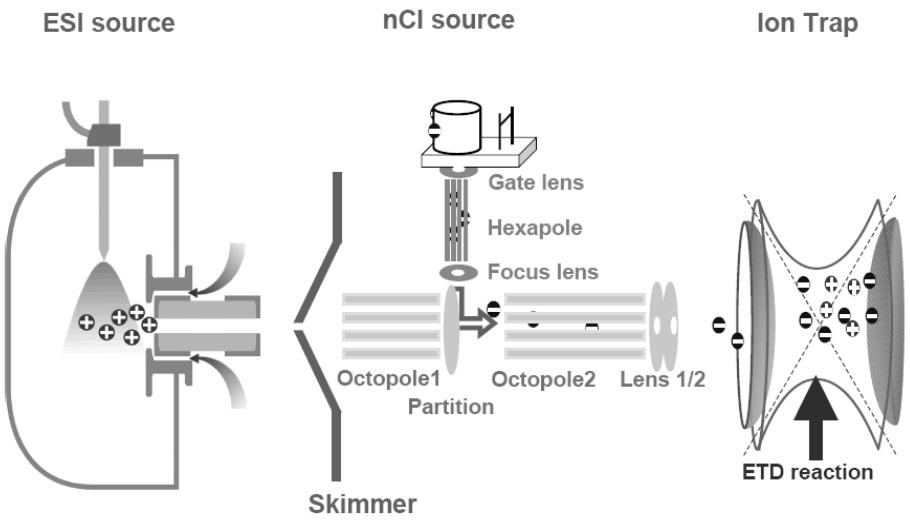

Figure 2.10. ETD in the Bruker HCTultra PMT Discovery System.

For the ETD experiments described in this dissertation, a multiply-charged ion of interest was mass selected for isolation. A low-energy electron was transferred to the multiply-charged ions by a reaction in the trap with the ETD reagent, fluoranthene, on the order of 40-100 ms. Each spectrum is the average of approximately 200 scans.

2.5 Ion/molecule reactions

Thermochemical properties such as gas-phase basicity (GB) and gas-phase acidity (GA) are valuable in the study of biological compounds such as proteins, peptides and amino acids. These properties can be easily extracted from gas-phase proton transfer reactions involving the system of interest. There are several methods have been developed for this purpose and each is based on experimental conditions.

The equilibrium method can be traced back to the early work of Kebarle and coworkers with pulsed electron high pressure mass spectrometry.[53] Since then, equilibrium determinations have been made for numerous systems such as: anilines,[54] phenols,[55] benzoic acids,[55, 56] carboxylic acids,[57] and numerous other organic and inorganic species.[58-64] Equilibrium determination experiments are traditionally performed using pulsed ICR or flowing afterglow techniques. The experiment requires that the ionized compound of interest be in thermal and chemical equilibrium with the neutral reactant. This means that the pressures of both compounds must be known. Conventional ionization methods such as electron ionization are often used, which requires the compound to be sufficiently volatile. Due to these volatility constraints, insufficiently volatile peptides and amino acids are typically not studied using the equilibrium method. The kinetic method (and later extended kinetic method), conceived by R. G. Cooks[65-67], was initially designed to probe the proton affinity of gas-phase bases. This experimental method requires a cluster-type ion (usually a proton-bound dimer) of the compound of interest with a

reference compound. The dissociation of this cluster in the mass spectrometer is monitored to determine thermochemical properties based on the rate constants. Recently the extended kinetic method[68, 69] has been used to determine the GAs of the α-amino acids.[70, 71] The extended kinetic method differs from the kinetic method by consideration of the entropy changes that occur during a reaction.[68]

The bracketing method[72-82] was used for the research described in this dissertation. The Bruker BioApex 7e FT-ICR MS was used to perform bracketing experiments to determine the gas-phase acidity (GA) of several small peptides, amino acids, and amino acid amides. A bracketing experiment involves ionizing and isolating an ion of interest and reacting it with a series of reference compounds that have known GAs. This allows one to determine the experimental GA of the compound being studied based on the efficiency of the proton transfer reaction with the reference compound.

The GA of a species of interest, M, is the negative free energy change ($-\Delta G°$) for the proton transfer reaction:

$$M \rightarrow [M - H]^- + H^+ \qquad -\Delta G° = GA \qquad 2.20$$

The proton transfer reaction of the species of interest, M, with a reference compound, A, is shown in Equation 2.21.

$$[M - H]^- + A \rightarrow M + [A - H]^- \qquad 2.21$$

A fast (exoergic) reaction has a negative Gibbs free energy change whereas a slow reaction or no reaction at all (endoergic) has a positive Gibbs free energy change. Identification of the GA of the species of interest lies at the point where reactions with reference compounds become exoergic. This point is generally established by a comparison of reaction efficiencies. The reaction efficiency (RE, Equation 2.22) relates the experimental rate constant of the proton

transfer reaction (Equation 2.21) to the theoretical rate constant as calculated using collision theory.[83, 84]

$$RE = \frac{k_{exp}}{k_{cap}} \qquad 2.22$$

The experimental rate constant, k_{exp}, is determined experimentally and k_{cap} is calculated by:

$$k_{cap} = k_L K_{cap} \qquad 2.23$$

where,
$$k_L = 2\pi q\sqrt{\frac{\alpha}{\mu}} = 2342\sqrt{\frac{\alpha \times 10^{-24}}{\mu}} \times I \qquad 2.24$$

(q = unit of electron charge, α = polarizability, μ = reduced mass, I = moment of inertia)

$$K_{cap} = K(T_R, I^*) \qquad 2.25$$

where
$$T_R = \frac{2\alpha K_B T}{\mu_D^2} \qquad 2.26$$

and
$$I^* = \frac{\mu_D I}{\alpha e \mu} \qquad 2.27$$

$$K_{cap} = \frac{(x+0.5090)^2}{10.526} + 0.9754 \qquad when\ x \leq 2 \qquad 2.28$$

$$K_{cap} = 0.4767x + 0.6200 \qquad when\ 2 \leq x \leq 3 \qquad 2.29$$

$$K_{cap} = 0.5781x = 0.3165 \qquad when\ 3 \leq x \leq 35 \qquad 2.30$$

$$x = \frac{1}{\sqrt{T_R}} = \sqrt{\frac{{\mu_D}^2}{2\alpha K_B T}} \qquad 2.31$$

(T_R = reduced temperature , μ_D = dipole moment, K_B = Boltzman constant,

T = temperature, e = elementary charge)

This relation of experimental and theoretical rate constants provides a tangible value for the percentage of collisions that produce a reaction. For example, an RE of 0.25 means that 25% of the collisions are resulting in a proton transfer reaction. The GA is established at an RE that is defined to be the point at which the reactions become exoergic, otherwise known as the break point. Using past data published by the Cassady research group,[73] Bouchoux and coworkers

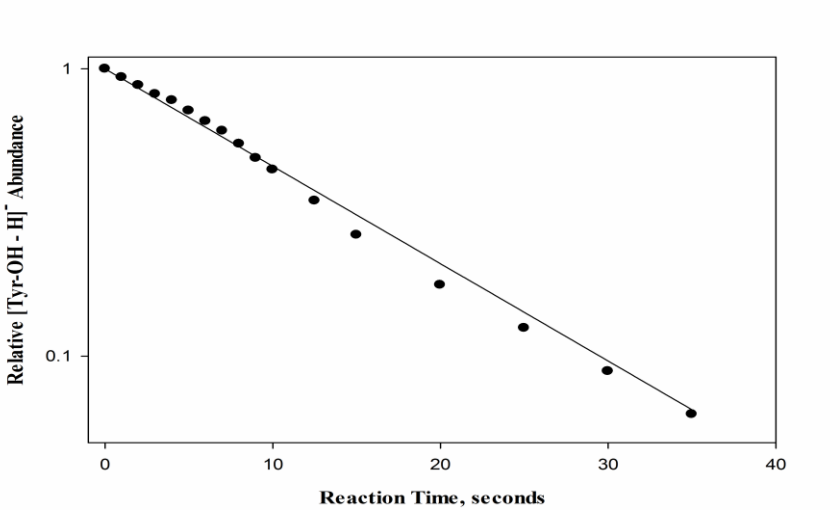

Figure 2.11. Plot of the natural log of the relative precursor ion intensities versus time for the reactions of deprotonated tyrosine with 4-trifluoromethylaniline.

recently showed that establishing the break point at a RE of 0.269 gives the most accurate representation of GA.[69, 70, 85-87] Past work in our group on the GAs of aspartic acid, glutamic acid and their amides used this RE as the break point for assigning numerical GA values with good outcome.[73]

The experimental rate constant, k_{exp}, is found by a relationship of the relative intensity of the precursor ion to reaction time. The pressure of the neutral reactant is held constant in the cell of the FT-ICR MS, therefore the reaction is pseudo-first-order. A plot of the natural log of the relative intensity of the precursor ion versus time produces a straight line (as shown in Figure 2.11). The slope of this line is used to calculate k_{exp} (in $cm^3 \bullet molec^{-1} \bullet s^{-1}$) using Equation 2.32. In this equation, R_x is the relative

$$k_{exp} = \frac{slope(1.333)R_x}{(3.23\times10^{16})P_{exp}IG_{corr}} \qquad 2.32$$

sensitivity of the ion gauge to the specific neutral reactant as described by Bartmess and Georgiadis.[88] The experimental pressure of the neutral (in mbar) as read off of the pressure meter is represented by P_{exp} and the correction factor for the positioning of the Bayard-Alpert

ionization gauge is represented by IG_{corr}. (1.333 is the conversion factor between mbar, which are the units of the ion gauge, and Torr. There are 3.23×10^{16} molec/cm^3 in 1 Torr.)

The ion gauge correction factor (IG_{corr}) is necessary for accurate representation of the experimental pressure. This is because the ion gauge is located outside of the cell (outside of the magnetic field) and away from where the reaction takes place. To account for this, the ion gauge was calibrated with the proton transfer reaction between protonated glycine and N,N-dimethylformamide (DMF)[89] as seen in Equation 2.33:

$$[Gly + H]^+ + DMF \rightarrow Gly + [DMF + H]^+ \qquad 2.33$$

This reaction has an average experimental rate constant (k_{exp}) of 8.19×10^{-10} cm^3/molec•sec, a standard deviation of 1.07×10^{-10} cm^3/molec•sec, and a relative standard deviation of 13%.

Aside from simple proton transfer, other pathways may be present, which requires modification of the method used to calculate the experimental rate constant. For example, a proton-bound dimer of the precursor and reactant, $[M + A - H]^-$, may form. This is especially common when the two reacting species are very close in GA. For these situations, the rate constant is determined by the relationship shown in Equation 2.34 (where $[A - H]^-$ is the relative intensity of the deprotonated reference compound, k_{deprot} is the rate constant for deprotonation only and k_{all} is the rate constant for all pathways).[90]

$$\frac{[A-H]^-}{Total\ Ion\ Intensity} = \frac{k_{deprot}}{k_{all}}(1 - e^{-k_{all}t}) \qquad 2.34$$

There are also cases where two reacting species of the precursor ion are present. This can be observed in the non-linear plot of the natural log of the relative precursor ion intensity versus time. For this type of situation, the experimental rate constants are determined for each species by fitting the data to the sum of two exponential relationships.

2.6 Peptide fragmentation nomenclature

The peptide fragmentation nomenclature introduced by Roepstorff and Fohlman[91] will be used to describe both CID and ETD spectra. Figure 2.12 illustrates the nomenclature as it relates to the dissociation of a peptide. This nomenclature uses letters to describe the sites of C_α–C, amide, and N–C_α bond cleavages. The letters a, b and c relate to these respective cleavages with charge retention on the N-terminal side of the cleavage site. The letters x, y and z relate to these respective bond cleavages with charge retention on the C-terminal side of the cleavage site. The subscript number indicates the position in the amino acid sequence that is involved in the fragmentation relative to the terminus retaining the charge. Prime symbols are used to denote the addition or subtraction of hydrogens. For example, in protonated spectra, c- and y- type ions have two more hydrogens than standard bond cleavages. These ions are represented by $c_n''^+$ and $y_n''^+$, which stands for $[c_n + 2H]^+$ and $[y_n + 2H]^+$ respectively (where n is position of cleavage in the peptide sequence). Another example from fragmentation of protonated peptide species is $z_n'^+$, where one additional hydrogen is present. In the fragmentation of deprotonated peptides, b-type cleavages often produce ions that are two mass units lower than standard bond cleavages. This means that the fragment ion has lost two hydrogens, and is denoted by $''b_n^-$. Note that placing the prime symbol to the left indicates loss of a hydrogen, whereas placement to the right indicates the gain of a hydrogen.

In 2003, Roman Zubarev[92] introduced a modified version of standard nomenclature for use with ETD. His modification of the peptide fragmentation nomenclature accounts for radical location and hydrogen transfer. Two types of ions are described using his nomenclature: radical products, $c_n^{+\bullet}$ and $z_n^{+\bullet}$, and hydrogen-atom transfer products, $z_n'^+$ and $c_n'^+$. Radical product ions are one mass unit higher than standard homolytic bond cleavage, and hydrogen-atom transfer

product ions are two mass units higher. The results described in this dissertation are characterized by the number of hydrogens that are associated with the ETD fragment ions. Tthe standard peptide fragmentation nomenclature is better suited to keeping track of the additional hydrogens and is therefore used here rather than using the modified Zubarev nomenclature.

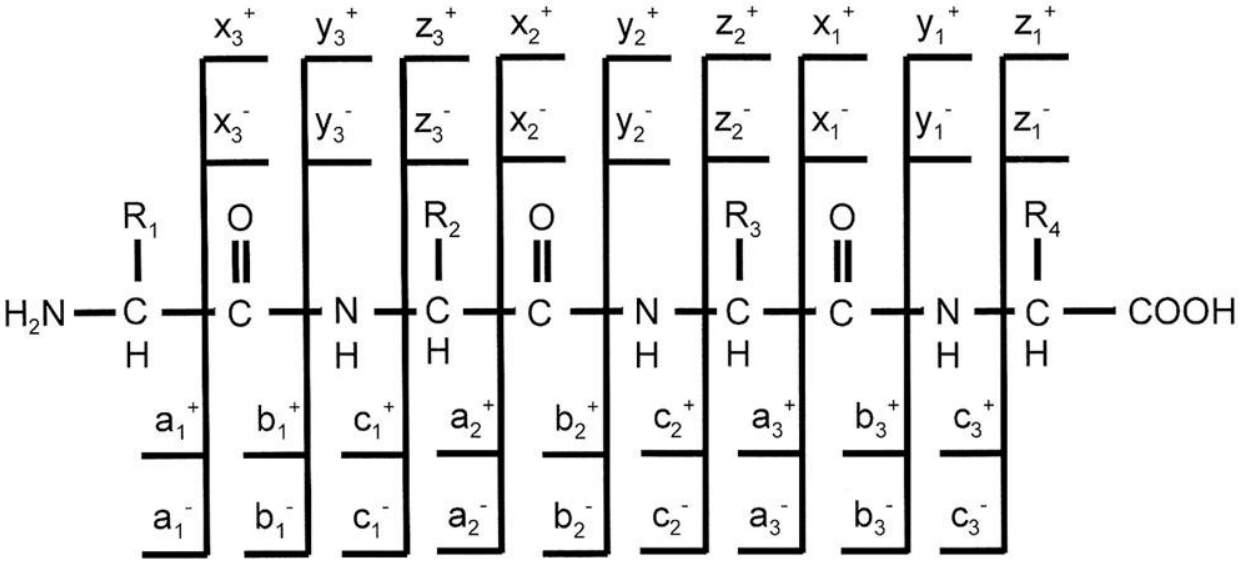

Figure 2.12. Peptide sequencing nomenclature.

2.7 Peptide synthesis

Some of the peptides used in this research were available through commercial sources or were provided by academic contacts. However, there were many peptides needed that are unusual or otherwise commercially unavailable. These peptides were synthesized in house using standard Fmoc-based chemistry. The term *Fmoc* is derived from the protecting group, 9-fluorenylmethoxycarbonyl, used to block the amine group of the amino acid. In cases where a non-standard C-terminus was desired, modification strategies were employed after synthesis or directly to the commercial peptide.

2.7.1 Fmoc solid-phase synthesis

Established by Merrifield[93] in 1963, solid-phase peptide synthesis (SPPS) has allowed the common research laboratory to circumvent the time and effort consumed by classical liquid-phase peptide synthesis techniques. This technique is generally based on attaching the C-terminal residue to a solid support, which is traditionally some sort of porous polystyrene resin bead (although polyacrylamide, polyethylene glycol, surface, and composite-based supports are used as well). The N-terminal amine of the residue is protected by a protecting group such as Fmoc (Figure 2.13.). Synthesis is accomplished by a series of wash-deprotect-couple-wash steps, building the peptide from the C-terminus (which is attached to the solid support) to the N-terminus. The final step of the synthetic strategy is to remove the solid support, leaving the newly formed peptide.

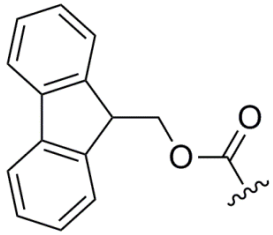

Figure 2.13. Fmoc protecting group.

Several of the peptides studied in this dissertation were synthesized in our laboratory using the standard Fmoc protocol[94] on an Advanced ChemTech Model 90 peptide synthesizer (Louisville, KY, USA). Automated peptide synthesizers such as this greatly decrease the at-bench time required for synthesizing peptides, and can be more cost-effective than commercial custom synthesis for producing small batches of peptides. Solid support resins were chosen based on the desired functionality for the C-terminus. The resins were purchased with the C-terminal amino acid residue in place and an Fmoc protecting group on the free amine of the residue. Wang and Rink amide resins (Advanced ChemTech) were used to produce C-terminal acid (-COOH) and amide functionalities ($-CONH_2$), respectively. The Sieber resin (Anaspec, San Jose, CA, USA) was used to produce a C-terminal secondary amide functionality (-NHEt).

The solid support resin was placed in a reaction vessel that works with the Advanced Chemtech peptide synthesizer. The wash/deprotect/couple/wash(/repeat) sequence is automated

and can be customized to meet the needs of the synthesis. The resin is first washed with N,N-dimethylformamide (DMF), then methanol (MeOH), then again with DMF. Next, the Fmoc protecting group is removed using 20% piperidine (PIP) in DMF (V:V). After deprotection and a DMF/MeOH/DMF wash, an Fmoc-protected amino acid is coupled to the now free amine of the residue that is anchored on the resin. A 0.5 M solution of the Fmoc-protected amino acid in 0.5 M 1-hydroxybenzotriazole hydrate (HOBt) in N-methyl-2-pyrrolidinone (NMP) is introduced to the reaction vessel. A 0.5 M solution of 1,3-diisopropylcarbodiimide (DIC) in NMP is also used in the coupling step to activate the carboxyl group. After the coupling step is completed, another wash cycle of DMF/MeOH/DMF is performed. This entire sequence is repeated until the desired peptide has been built.

Post-synthesis, the peptide is still attached to the resin. Thus, a resin cleavage step must be used to yield free peptide. A cleavage solution of 92% trifluoroacetic acid (TFA), 5% ultrapure water, and 3% trisopropylsilane (TIPS) is used to cleave the peptide from the resin at room temperature. The reaction mixture is then filtered to remove the solid resin, and the peptide is precipitated using diethyl ether that has been cooled to -78°C in a bath of dry ice and acetone. The precipitated peptide is separated by centrifuging and decanting the diethyl ether mixture. The peptide is allowed to dry at room temperature in a dessicator. No further purification steps are used since mass spectrometry is capable of isolating the peptide ion of interest from any contaminants.

2.7.2 Methyl esterification

To eliminate the C-terminal carboxylic acid functional group as a potential site for deprotonation, several of the peptides in this dissertation research were converted to methyl esters. Conventional solution-phase chemistry[95] was applied to the raw peptides. Figure 2.14 shows the reaction procedure to form the methyl esterified peptides. The peptide methyl esters tend to revert to carboxyl form when stored in aqueous or acidic solvent systems, thus working solutions were prepared from solid peptides for each experiment to minimize degradation.

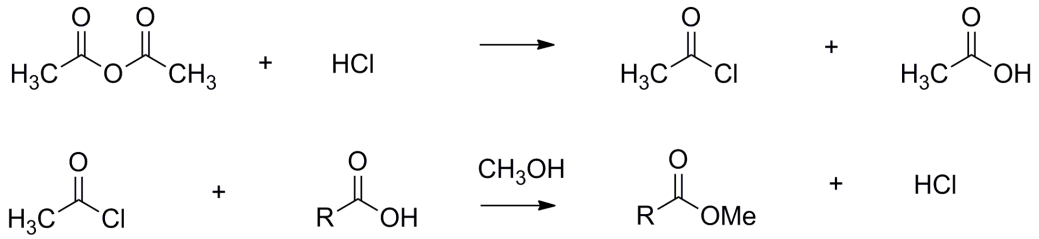

Figure 2.14. Methyl esterification strategy.

2.7.3 Amino acid structures and C-termini

The peptides involved in this dissertation were composed of various amino acids. Many of the peptides were studied in the standard free acid form (C-terminal acid, -COOH) as well as amide form (C-terminal amide, $-CONH_2$). Select peptides were studied with other C-terminal modifications such as methyl esterification (-COOMe) and substituted secondary and tertiary amides (e.g. -CONHEt and $-CONMe_2$). Figures 2.15 through 2.22 illustrate the amino acids whose residues composed peptides in this research. Figure 2.23 illustrates the various C-terminal modifications that were utilized.

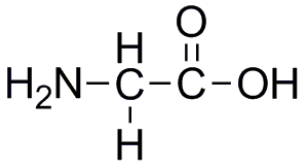

Glycine

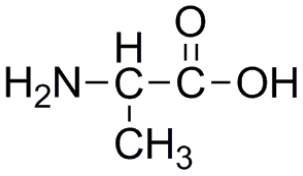

Alanine

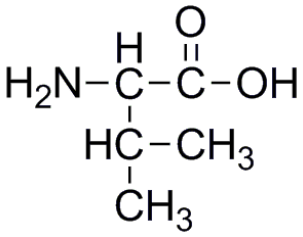

Valine

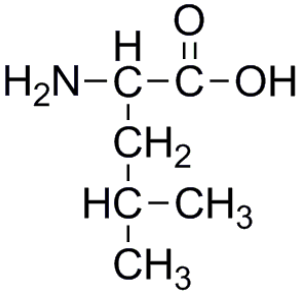

Leucine

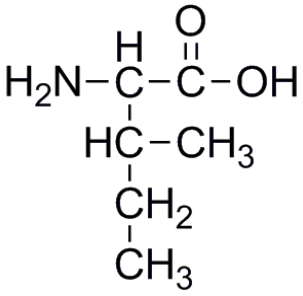

Isoleucine

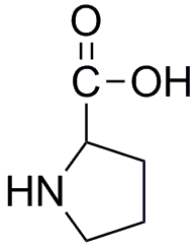

Proline

Figure 2.15. Amino acids with alkyl side chains.

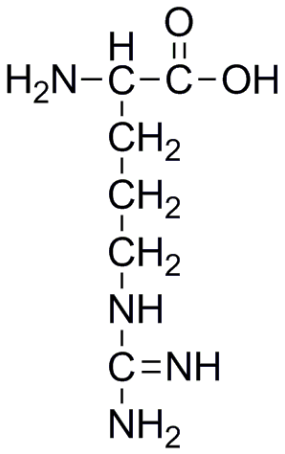

Arginine

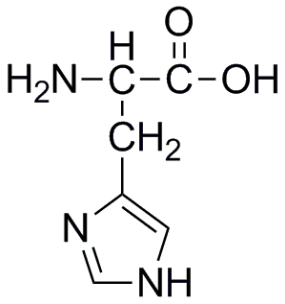

Histidine

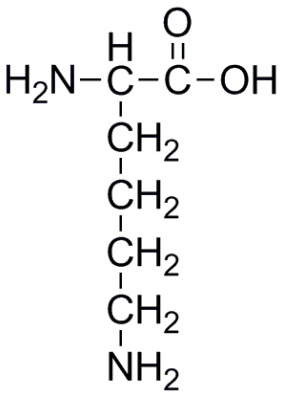

Lysine

Figure 2.16. Amino acids with basic side chains.

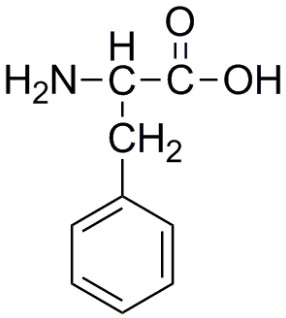

Phenylalanine

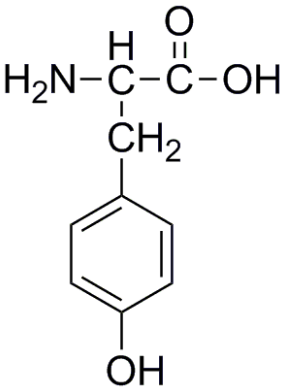

Tyrosine

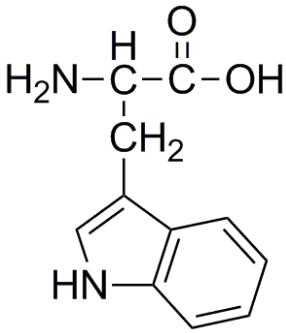

Tryptophan

Figure 2.17. Amino acids with aromatic side chains.

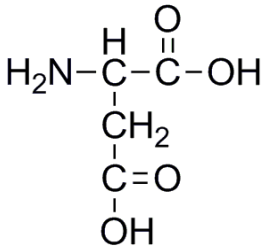

Aspartic Acid

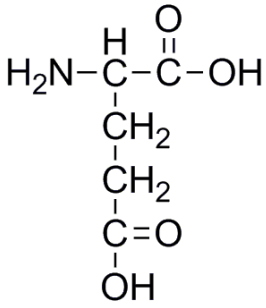

Glutamic Acid

Figure 2.18. Amino acids with acidic side chains.

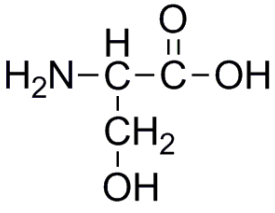

Serine

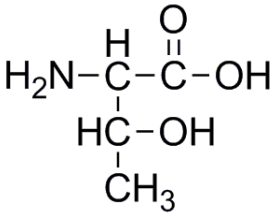

Threonine

Figure 2.19. Amino acids with hydroxylated side chains.

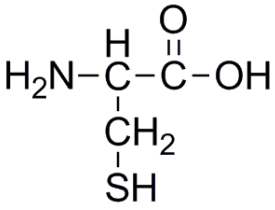

Cysteine

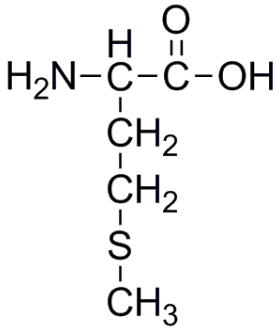

Methionine

Figure 2.20. Amino acids with sulfur-containing side chains.

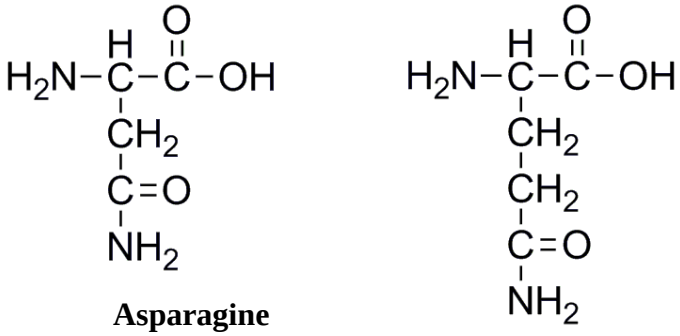

Asparagine **Glutamine**

Figure 2.21. Amino acids with amidated side chains.

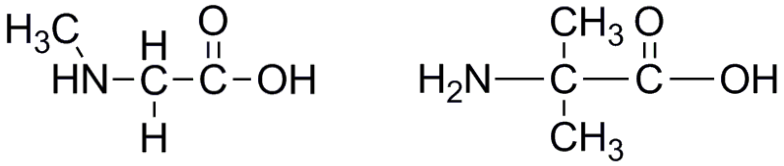

Sarcosine **2-methylalanine**

Figure 2.22. Non-standard, selectively methylated amino acids.

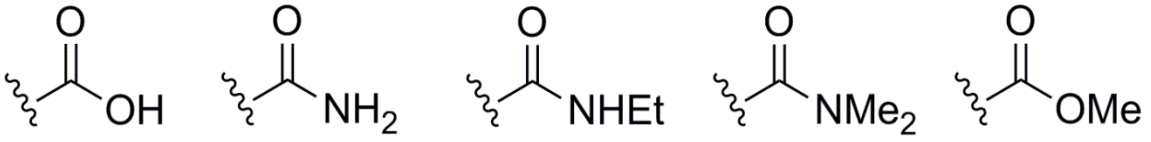

Carboxylic acid **Amide** **Ethylamide** **Dimethylamide** **Methyl ester**

Figure 2.23. Peptide C-terminal endgroups utilized in this dissertation.

References

1. Dole, M.; Mack, L. L.; Hines, R. L. Molecular beams of macroions. *J. Chem. Phys.* **1968,** *49,* 2240.

2. Fenn, J. B.; Mann, M.; Meng, C. K.; Wong, S. F.; Whitehouse, C. M. Electrospray ionization for mass spectrometry of large biomolecules. *Science.* **1989,** *246,* 64-71.

3. Fenn, J. B.; Mann, M.; Meng, C. K.; Wong, S. F.; Whitehouse, C. M. Electrospray ionization - Principles and practice. *Mass Spectrom. Rev.* **1990,** *9,* 37-70.

4. Whitehouse, C. M.; Dreyer, R. N.; Yamashita, M.; Fenn, J. B. Electrospray interface for liquid chromatographs and mass spectrometers. *Anal. Chem.* **1985,** *57,* 675-679.

5. Yamashita, M.; Fenn, J. B. Electrospray ion-source - Another variation on the free-jet theme. *J. Phys. Chem.* **1984,** *88,* 4451-4459.

6. Yamashita, M.; Fenn, J. B. Negative-ion production with the electrospray ion-source. *J. Phys. Chem.* **1984,** *88,* 4671-4675.

7. Ikonomou, M. G.; Blades, A. T.; Kebarle, P. Investigations of the electrospray interface for liquid-chromatography mass-spectrometry. *Anal. Chem.* **1990,** *62,* 957-967.

8. Ikonomou, M. G.; Blades, A. T.; Kebarle, P. Electrospray ion spray - A comparison of mechanisms and performance. *Anal. Chem.* **1991,** *63,* 1989-1998.

9. Kebarle, P. A brief overview of the present status of the mechanisms involved in electrospray mass spectrometry. *J. Mass Spectrom.* **2000,** *35,* 804-817.

10. Kebarle, P.; Peschke, M. On the mechanisms by which the charged droplets produced by electrospray lead to gas phase ions. *Anal. Chim. Acta.* **2000,** *406,* 11-35.

11. Kebarle, P.; Tang, L. From ions in solution to ions in the gas-phase - The mechanism of electrospray mass-spectrometry. *Anal. Chem.* **1993,** *65,* A972-A986.

12. Gaskell, S. J. Electrospray: Principles and practice. *J. Mass Spectrom.* **1997,** *32,* 677-688.

13. Wilm, M. S.; Mann, M. Electrospray and Taylor-cone theory, Doles beam of macromolecules at last. *Int. J. Mass Spectrom.* **1994,** *136,* 167-180.

14. Gomez, A.; Tang, K. Q. Charge and fission of droplets in electrostatic sprays. *Phys. Fluids.* **1994,** *6,* 404-414.

15. Tang, K.; Gomez, A. On the structure of an electrostatic spray of monodisperse droplets. *Phys. Fluids.* **1994,** *6,* 2317-2332.

16. Paul, W. Electromagnetic traps for charged and neutral particles. *Rev. Mod. Phys.* **1990,** *62,* 531-540.

17. Reprinted from *Anal. Biochem.*, *244*, Jonscher, K. R.; Yates III, J. R., The quadrupole ion trap mass spectrometer - A small solution to a big challenge, 1-15, **1997**, with permission from Elsevier.

18. Comisaro, M. B.; Marshall, A. G. Fourier-transform ion-cyclotron resonance spectroscopy. *Chem. Phys. Lett.* **1974,** *25,* 282-283.

19. He, F.; Hendrickson, C. L.; Marshall, A. G. Baseline mass resolution of peptide isobars: A record for molecular mass resolution. *Anal. Chem.* **2001,** *73,* 647-650.

20. Caravatti, P.; Allemann, M. The infinity cell - A new trapped-ion cell with radiofrequency covered trapping electrodes for Fourier-transform ion-cyclotron resonance mass-spectrometry. *Org. Mass Spectrom.* **1991,** *26,* 514-518.

21. de Koning, L. J.; Nibbering, N. M. M.; van Orden, S. L.; Laukien, F. H. Mass selection of ions in a Fourier transform ion cyclotron resonance trap using correlated harmonic excitation fields (CHEF). *Int. J. Mass Spectrom.* **1997,** *165,* 209-219.

22. In *IUPAC. Compendium of Chemical Terminology.* Blackwell Scientific Publications: Oxford, 1997.

23. Aebersold, R.; Mann, M. Mass spectrometry-based proteomics. *Nature.* **2003,** *422,* 198-207.

24. Aebersold, R.; Goodlett, D. R. Mass spectrometry in proteomics. *Chem. Rev.* **2001,** *101,* 269-295.

25. Barlow, C. K.; O'Hair, R. A. J. Gas-phase peptide fragmentation: How understanding the fundamentals provides a springboard to developing new chemistry and novel proteomic tools. *J. Mass Spectrom.* **2008,** *43,* 1301-1319.

26. El Aribi, H.; Rodriquez, C. F.; Almeida, D. R. P.; Ling, Y.; Mak, W. W.; Hopkinson, A. C.; Siu, K. W. M. Elucidation of fragmentation mechanisms of protonated peptide ions and their products: A case study on glycylglycylglycine using density functional theory and threshold collision-induced dissociation. *J. Am. Chem. Soc.* **2003,** *125,* 9229-9236.

27. Harrison, A. Energy-resolved mass spectrometry: A comparison of quadrupole cell and cone-voltage collision-induced dissociation. *Rapid Commun. Mass Spectrom.* **1999,** *13,* 1663-1670.

28. Harrison, A. G.; Young, A. B. Fragmentation of protonated oligoalanines: Amide bond cleavage and beyond. *J. Am. Soc. Mass Spectrom.* **2004,** *15,* 1810-1819.

29. Wysocki, V. H.; Tsaprailis, G.; Smith, L. L.; Breci, L. A. Special feature: Commentary - Mobile and localized protons: A framework for understanding peptide dissociation. *J. Mass Spectrom.* **2000,** *35,* 1399-1406.

30. Dongre, A. R.; Jones, J. L.; Somogyi, A.; Wysocki, V. H. Influence of peptide composition, gas-phase basicity, and chemical modification on fragmentation efficiency: Evidence for the mobile proton model. *J. Am. Chem. Soc.* **1996,** *118,* 8365-8374.

31. Harrison, A. G. Sequence-specific fragmentation of deprotonated peptides containing H or alkyl side chains. *J. Am. Soc. Mass Spectrom.* **2001,** *12,* 1-13.

32. Waugh, R. J.; Bowie, J. H.; Gross, M. L. Collision-induced dissociations of deprotonated peptides. Dipeptides containing methionine or cysteine. *Rapid Commun. Mass Spectrom.* **1993,** *7,* 623-625.

33. Harrison, A. G. Effect of phenylalanine on the fragmentation of deprotonated peptides. *J. Am. Soc. Mass Spectrom.* **2002,** *13,* 1242-1249.

34. Bilusich, D.; Bowie, J. H. Fragmentations of $(M-H)^-$ anions of underivatised peptides. Part 2: Characteristic cleavages of Ser and Cys and of disulfides and other post-translational modifications, together with some unusual internal processes. *Mass Spectrom. Rev.* **2009,** *28,* 20-34.

35. Bowie, J. H.; Brinkworth, C. S.; Dua, S. Collision-induced fragmentations of the $(M-H)^-$ parent anions of underivatized peptides: An aid to structure determination and some unusual negative ion cleavages. *Mass Spectrom. Rev.* **2002,** *21,* 87-107.

36. Waugh, R. J.; Bowie, J. H.; Hayes, R. N. Collision induced dissociations of deprotonated peptides : Dipeptides containing phenylalanine, tyrosine, histidine and tryptophan. *Int. J. Mass Spectrom. Ion Processes.* **1991,** *107,* 333-347.

37. Waugh, R. J.; Eckersley, M.; Bowie, J. H.; Hayes, R. N. Collision induced dissociations of deprotonated peptides: Dipeptides containing serine or threonine. *Int. J. Mass Spectrom. Ion Processes.* **1990,** *98,* 135-145.

38. Harrison, A. G.; Young, A. B. Fragmentation reactions of deprotonated peptides containing proline. The proline effect. *J. Mass. Spectrom.* **2005,** *40,* 1173-1186.

39. Vaisar, T.; Urban, J. Probing proline effect in CID of protonated peptides. *J. Mass Spectrom.* **1996,** *31,* 1185-1187.

40. Li, Z.; Yalcin, T.; Cassady, C. J. C-terminal amino acid residue loss for deprotonated peptide ions containing glutamic acid, aspartic acid, or serine residues at the C-terminus. *J. Mass Spectrom.***2006,** *41,* 939-949.

41. Zhang, Z.; Bordas-Nagy, J. Peptide conformation in gas phase probed by collision-induced dissociation and its correlation to conformation in condensed phases. *J. Am. Soc. Mass Spectrom.* **2006,** *17,* 786-794.

42. Brinkworth, C. S.; Bilusich, D.; Bowie, J. H. The unusual loss of an internal Val residue from the $(M-H)^-$ parent anions of the antimicrobial peptide citropin 1.1 and synthetically modified analogues. Fragmentations which require a specific conformation of the decomposing anion. *Int. J. Mass Spectrom.* **2004,** *236,* 43-53.

43. Kaltashov, I. A.; Eyles, S. J. Studies of biomolecular conformations and conformational dynamics by mass spectrometry. *Mass Spectrom. Rev.* **2002,** *21,* 37-71.

44. Farrugia, J. M.; O'Hair, R. A. J. Involvement of salt bridges in a novel gas phase rearrangement of protonated arginine-containing dipeptides which precedes fragmentation. *Int. J. Mass Spectrom.* **2003,** *222,* 229-242.

45. Paizs, B.; Suhai, S.; Hargittai, B.; Hruby, V. J.; Somogyi, Á. Ab initio and MS/MS studies on protonated peptides containing basic and acidic amino acid residues: I. Solvated proton vs. salt-bridged structures and the cleavage of the terminal amide bond of protonated RD-NH_2. *Int. J. Mass Spectrom.* **2002,** *219,* 203-232.

46. Kim, J.; Kim, K. Identification of the C-terminal amino acid amides by carboxypeptidase Y digestion and fast atom bombardment mass spectrometry. *Biochem. Mol. Biol. Int.* **1994,** *34,* 897-907.

47. Syka, J. E. P.; Coon, J. J.; Schroeder, M. J.; Shabanowitz, J.; Hunt, D. F. Peptide and protein sequence analysis by electron transfer dissociation mass spectrometry. *Proc. Natl. Acad. Sci. U. S. A.* **2004,** *101,* 9528-9533.

48. Zubarev, R. A.; Kellerher, N. L.; McLafferty, F. W. Electron capture dissociation of multiply charged protein cations. A nonergodic process. *J. Am. Chem. Soc.* **1998,** *120,* 3265-3266.

49. Coon, J. J.; Shabanowitz, J.; Hunt, D. F.; Syka, J. E. P. Electron transfer dissociation of peptide anions. *J. Am. Soc. Mass Spectrom.* **2005,** *16,* 880-882.

50. Budnik, B. A.; Haselmann, K. F.; Zubarev, R. A. Electron detachment dissociation of peptide di-anions: An electron-hole recombination phenomenon. *Chem. Phys. Lett.* **2001,** *342,* 299-302.

51. Gunawardena, H. P.; He, M.; Chrisman, P. A.; Pitteri, S. J.; Hogan, J. M.; Hodges, B. D. M.; McLuckey, S. A. Electron transfer versus proton transfer in gas-phase ion/ion reactions of polyprotonated peptides. *J. Am. Chem. Soc.* **2005,** *127,* 12627-12639.

52. Bruker Daltonics, *HCTultra PTM Discovery System User Manual;* Billerica, MA, 2006.

53. Kebarle, P.; Godbole, E. W. Mass-spectrometric study of ions from the α-particle irradiation of gases at near atmospheric pressures. *J. Chem. Phys.* **1963,** *39,* 1131-1132.

54. Lau, Y. K.; Nishizawa, K.; Tse, A.; Brown, R. S.; Kebarle, P. Protonation and site of protonation of anilines. Hydration and site of protonation after hydration. *J. Am. Chem. Soc.* **1981,** *103,* 6291-6295.

55. McMahon, T. B.; Kebarle, P. Intrinsic acidities of substituted phenols and benzoic acids determined by gas-phase proton-transfer equilibriums. *J. Am. Chem. Soc.* **1977,** *99,* 2222-2230.

56. Yamdagni, R.; McMahon, T. B.; Kebarle, P. Substituent effects on the intrinsic acidities of benzoic acids determined by gas phase proton transfer equilibria measurements. *J. Am. Chem. Soc.* **1974,** *96,* 4035-4037.

57. Caldwell, G.; Renneboog, R.; Kebarle, P. Gas phase acidities of aliphatic carboxylic acids, based on measurements of proton transfer equilibria. *Can. J. Chem.* **1989,** *67,* 611-618.

58. Aue, D. H.; Bowers, M. T. In *Stabilities of Positive Ions from Equilibrium Gas-Phase Basicity Measurements;* Academic: 1979; Vol. 2, pp 1-51.

59. Grimsrud, E. P.; Kebarle, P. Gas phase ion equilibriums studies of the hydrogen ion by methanol, dimethyl ether, and water. Effect of hydrogen bonding. *J. Am. Chem. Soc.* **1973,** *95,* 7939-7943.

60. Higgins, P. R.; Bartmess, J. E. The gas-phase acidities of long-chain alcohols. *Int. J. Mass Spectrom. Ion Processes.* **1998,** *175,* 71-79.

61. Kebarle, P. Gas phase ion thermochemistry based on ion-equilibria. From the ionosphere to the reactive centers of enzymes. *Int. J. Mass Spectrom.* **2000,** *200,* 313-330.

62. McMahon, T. B. High pressure mass spectrometry. Instrumentation, techniques and applications. *NATO Sci. Ser., Ser. C.* **1999,** *535,* 259-280.

63. McMahon, T. B.; Kebarle, P. Bridging the gap. A continuous scale of gas-phase basicities from methane to water from pulsed electron beam high pressure mass spectrometric equilibria measurements. *J. Am. Chem. Soc.* **1985,** *107,* 2612-2617.

64. Wolf, J. F.; Staley, R. H.; Koppel, I.; Taagepera, M.; McIver, R. T., Jr.; Beauchamp, J. L.; Taft, R. W. Gas phase basicities and relative proton affinities of compounds between water and ammonia from pulsed ion cyclotron resonance thermal equilibriums measurements. *J. Am. Chem. Soc.* **1977,** *99,* 5417-5429.

65. McLuckey, S. A.; Cameron, D.; Cooks, R. G. Proton affinities from dissociations of proton-bound dimers. *J. Am. Chem. Soc.* **1981,** *103,* 1313-1317.

66. Cooks, R. G.; Patrick, J. S.; Kotiaho, T.; McLuckey, S. A. Thermochemical determinations by the kinetic method. *Mass Spectrom. Rev.* **1994,** *13,* 287-339.

67. Cooks, R. G.; Wong, P. S. H. Kinetic method of making thermochemical determinations: Advances and applications. *Acc. Chem. Res.* **1998,** *31,* 379-386.

68. Bouchoux, G.; Sablier, M.; Berruyer-Penaud, F. Obtaining thermochemical data by the extended kinetic method. *J. Mass Spectrom.* **2004,** *39,* 986-997.

69. Bouchoux, G. Microcanonical modeling of the thermokinetic method. *J. Phys. Chem. A.* **2006,** *110,* 8259-8265.

70. Bouchoux, G.; Huang, S.; Inda, B. S. Acid-base thermochemistry of gaseous aliphatic alpha-amino acids. *Phys. Chem. Chem. Phys.* **2011,** *13,* 651-668.

71. Jones, C. M.; Bernier, M.; Carson, E.; Colyer, K. E.; Metz, R.; Pawlow, A.; Wischow, E. D.; Webb, I.; Andriole, E. J.; Poutsma, J. C. Gas-phase acidities of the 20 protein amino acids. *Int. J. Mass Spectrom.* **2007,** *267,* 54-62.

72. Zhang, K.; Zimmerman, D. M.; Chung-Phillips, A.; Cassady, C. J. Experimental and ab-initio studies of the gas-phase basicities of polyglycines. *J. Am. Chem. Soc.* **1993,** *115,* 10812-10822.

73. Li, Z.; Matus, M. M.; Velazquez, H. A.; Dixon, D. A.; Cassady, C. J. Gas-phase acidities of aspartic acid, glutamic acid, and their amino acid amides. *Int. J. Mass Spectrom.* **2007,** *265,* 213-223.

74. Ewing, N. P.; Pallante, G. A.; Zhang, X.; Cassady, C. J. Gas-phase basicities for ions from bradykinin and its des-arginine analogues. *J. Mass Spectrom.* **2001,** *36,* 875-881.

75. Carr, S. R.; Cassady, C. J. Reactivity and gas-phase acidity determinations of small peptide ions consisting of 11 to 14 amino acid residues. *J. Mass Spectrom.* **1997,** *32,* 959-967.

76. Carr, S. R.; Cassady, C. J. Gas-phase basicities of histidine and lysine and their selected di- and tripeptides. *J. Am. Soc. Mass Spectrom.* **1996,** *7,* 1203-1210.

77. Ewing, N. P.; Zhang, X.; Cassady, C. J. Determination of the gas-phase basicities of proline and its di- and tripeptides with glycine: The enhanced basicity of prolylproline. *J. Mass Spectrom.* **1996,** *31,* 1345-1350.

78. Cassady, C. J.; Carr, S. R.; Zhang, K.; Chung-Phillips, A. Experimental and ab-initio studies on protonations of alanine and small peptides of alanine and glycine. *J. Org. Chem.* **1995,** *60,* 1704-1712.

79. Zhang, X.; Cassady, C. J. Apparent gas-phase acidities of multiply protonated peptide ions: Ubiquitin, insulin B, and renin substrate. *J. Am. Soc. Mass Spectrom.* **1996,** *7,* 1211-1218.

80. Gorman, G. S.; Amster, I. J. Kinetic and thermodynamic considerations of the bracketing method: Entropy-driven proton-transfer reactions in a Fourier transform mass spectrometer. *Org. Mass Spectrom.* **1993,** *28,* 1602-1607.

81. Wu, J. Y.; Lebrilla, C. B. Gas-phase basicities and sites of protonation of glycine oligomers (Gly_n, N = 1-5). *J. Am. Chem. Soc.* **1993,** *115,* 3270-3275.

82. Gorman, G. S.; Speir, J. P.; Turner, C. A.; Amster, I. J. Proton affinities of the 20 common α-amino acids. *J. Am. Chem. Soc.* **1992,** *114,* 3986-8.

83. Su, T. Trajectory calculations of ion-polar molecule capture rate constants at low-temperatures. *J. Chem. Phys.* **1988,** *89,* 5355-5355.

84. Su, T.; Chesnavich, W. J. Parametrization of the ion-polar molecule collision rate-constant by trajectory calculations. *J. Chem. Phys.* **1982,** *76,* 5183-5185.

85. Bouchoux, G.; Salpin, J. Y. Re-evaluated gas phase basicity and proton affinity data from the thermokinetic method. *Rapid Commun. Mass Spectrom.* **1999,** *13,* 932-936.

86. Bouchoux, G.; Salpin, J. Y. Gas-phase basicity of glycine, alanine, proline, serine, lysine, histidine and some of their peptides by the thermokinetic method. *Eur. J. Mass Spectrom.* **2003,** *9,* 391-402.

87. Bouchoux, G.; Salpin, J. Y.; Leblanc, D. A relationship between the kinetics and thermochemistry of proton transfer reactions in the gas phase. *Int. J. Mass Spectrom. Ion Processes.* **1996,** *153,* 37-48.

88. Bartmess, J. E.; Georgiadis, R. M. Empirical-methods for determination of ionization gauge relative sensitivities for different gases. *Vacuum.* **1983,** *33,* 149-153.

89. Zhang, K.; Cassady, C. J.; Chung-Phillips, A. Ab-initio studies of neutral and protonated triglycines - Comparison of calculated and experimental gas-phase basicity. *J. Am. Chem. Soc.* **1994,** *116,* 11512-11521.

90. Espenson, J. H. In *Chemical Kinetics and Reaction Mechanisms;* McGraw-Hill: New York, 1981.

91. Roepstorff, P.; Fohlman, J. Proposal for a common nomenclature for sequence ions in mass spectra of peptides. *Biomed. Mass Spectrom.* **1984,** *11,* 601.

92. Zubarev, R. A. Reactions of polypeptide ions with electrons in the gas phase. *Mass Spectrom. Rev.* **2003,** *22,* 57-77.

93. Merrifield, R. B. Solid phase peptide synthesis. I. The synthesis of a tetrapeptide. *J. Am. Chem. Soc.* **1963,** *85,* 2149-2154.

94. Chan, W. C.; White, P. D. In *Fmoc Solid Phase Peptide Synthesis: A Practical Approach;* Oxford University Press: New York, 2000, pp 345.

95. Greene, T. W.; Wuts, P. G. M., Eds.; In *Protective Groups in Organic Synthesis;* John Wiley & Sons, Inc.: New York, 1991.

CHAPTER 3: A COMPARISON OF THE EFFECTS OF AMIDE AND ACID GROUPS AT THE C-TERMINUS ON THE COLLISION-INDUCED DISSOCIATION OF DEPROTONATED PEPTIDES

3.1 Overview

The dissociative behavior of peptide amides and free acids is explored using low-energy collision-induced dissociation (CID) and high level computational theory. Both positive and negative ion modes were utilized in the study, but the most profound differences were observed for the deprotonated peptide species. Amidation of the C-terminus removes a potential deprotonation site on a peptide. Elimination of this charge site is shown to have consequences on the resulting deprotonated CID spectra, producing amide-specific product ions (i.e. c_{m-2}^-, where m is the number of residues in the peptide) that are either absent or in low abundance for the analogous peptide free acid. It is postulated that the driving force behind c_{m-2}^- in peptide amides is the formation of a diketopiperazine (DKP) neutral. The most notable occurrence of an amide-specific product ion is the presence of c_3^- in the spectrum of laminin amide (YIGSR-NH_2). This case has been thoroughly investigated to determine the cause of c_{m-2}^- formation in amidated peptides due to its convenient size. In support of these experimental findings, G3(MP2) calculations have been performed using model oligoglycines to determine the energetic differences between the peptide amides and free acids. Computational results show that the formation of c_{m-2}^- and the proposed DKP neutral from a peptide amide requires 31.6 kcal/mol, which is 26.1 kcal/mol less than the same process involving the peptide free acid.

These complimentary experimental and computational results indicate that deprotonated amide-specific fragmentation patterns may be useful in bioinformatic methods related to proteomics.

3.2 Introduction

Hydrophobic amide groups at the C-termini of peptides are prolific in nature and generally thought to be one of the key binding sites on biologically active peptides.[1-4] For example, a C-terminal amide group is a post-translational modification found in peptides that have the C-terminus extended by a glycine residue.[5-7] In addition, there are several groups of well-known biologically active peptides that are C-terminal amides; for example, the tachykinins, a family of neurological peptides. Substance P, discovered by Von Euler and Gaddum in 1931, belongs to the broad tachykinin family and is one of the peptides used in our study.[8] There are several groups of peptides with antimicrobial and anticancer properties that possess a C-terminal amide.[9] Additional biologically active C-terminal amide peptides include the adrenomedullins, amylins, calcitonin, cholecystokinins, endokinins, growth hormone releasing factor, and oxytocins.[10-17] Furthermore, C-terminal amide dipeptides are easily converted to 2,5-diketopiperazines, a 6-membered ring species, in the presence of an acid[18] and the formation of diketopiperazines from the N-terminal amino group has been reported.[19, 20] Wang et al.[21] studied endomorphin-1 and endomorphin-2, both C-terminal amides, and their activity when the C-terminus was modified. Their results showed that the functionality of the C-terminus was important and that derivatizing the amide by converting the terminus to an ester had a detrimental effect on the activity of the endomorphin peptide.

There has been a great deal of research comparing the properties of peptide acids and amides by chemical methods other than mass spectrometry. Dennison et al.[9] studied the effects of changing the C-terminus on peptides that exhibit antimicrobial and anticancer activity via

physical and computational methods. Their work demonstrated an unpredictable effect on the efficacy and no effect on the selectivity of the peptides studied. Krstenansky et al.[22] synthesized several C-terminal analogs of hirudin(54-65) to probe the structure-activity relationship. The C-terminal amide was among the modifications studied and its presence lessened the activity of the antithrombin peptide. Chemical means have been used to determine the C-terminal end group of peptides and proteins by converting the C-terminus from a carboxylic acid to an amide via ammonolysis or hydrazinolysis.[23, 24]

There have been few reports comparing acid and amide analogous peptides by mass spectrometry. Kim and Kim[25] employed a carboxypepsidase Y digestion to identify amino acid amides using fast atom bombardment (FAB) mass spectrometry. Brinkworth and Bowie[26] investigated the maculatin family of C-terminal amide peptides by negative ion electrospray ionization (ESI) mass spectrometry. Although their work did not consider the acid versions of the peptides, it did demonstrate the dissociation patterns of deprotonated peptide amides. Enjalbal and coworkers[27] performed an extensive study comparing the differences in positive ion mode collision-induced dissociation (CID) fragmentation patterns of both peptide acids and amides. Their work included 76 pairs of peptide acids and amides with a variety of amino acid compositions. For their study of protonated peptides, the presence of the amide group at the C-terminus had little effect on the resulting CID spectra, apart from an increased loss of ammonia from the protonated peptide amide. This minor difference is likely influenced by the peptide composition and is not solely due to the C-terminal end group. To date, there has been no published report of a comparison of the acid/amide analogous peptides via *negative ion mode* CID.

Conversion of a C-terminal carboxylic acid group to an amide group may remove a possible charge site in negative ion mode. Consequently, absence of this carboxylic acid group

should alter the fragmentation pattern of the deprotonated peptide. Complimentary to the positive ion mode work of Enjalbal and coworkers,[27] our effort focuses on the differences observed in negative ion mode fragmentation. Differing fragmentation patterns between nearly identical deprotonated species will allow for greater identification of unknown peptides.

3.3 Experimental

3.3.1 Peptides

Table 3.11 shows the amino acid sequence of each peptide studied and its monoisotopic mass for the protonated and deprotonated ions. Substance P acid and amide, cholecystokinin acid, and laminin acid and amide were purchased from Anaspec (San Jose, CA). Cholecystokinin amide was purchased from American Peptide (Sunnyvale, CA). Pentaalanine and the laminin analogs were synthesized in our laboratory using standard Fmoc protocol [28] on an Advanced ChemTech Model 90 peptide synthesizer (Louisville, KY). Wang and Rink amide resins (Advanced ChemTech) were used to produce the acid (-COOH) and amide functionalities (-$CONH_2$), respectively. The Sieber resin (Anaspec, San Jose, CA) was used to produce the secondary amide functionality (-NHEt). YIGSR-NMe_2 was custom synthesized by NEO BioScience (Cambridge, MA). YIGSR-OMe was produced in our laboratory via methyl esterification[29] of the commercially available laminin acid. The remaining peptides were provided by Christine Enjalbal's group at the University of Montpellier (Montpellier, France).

3.3.2 Sample preparation

Stock peptide solutions were prepared in ultrapure water from solid peptide at a concentration of 1-2 mg/mL. Peptides that had low solubility in water were prepared in a 50:50

Table 3.1 Peptide sequences, monoisotopic masses, and predominant backbone cleavage ions from CID of $[M - H]^-$.

Peptide Sequence (name)	Monoisotopic mass[a] of $[M - H]^-$		Base peak of spectrum[a]		Observed CID backbone product ions[b,c]	
	amide	acid	amide	acid	amide	acid
AAAAA (pentaalanine)	371.1	372.2	c_3^-/y_3^-	c_2^-	a_3^-, a_4^-, a_5^-, c_2^-, **c_3^-**, y_2^-, **y_3^-**, y_4^-	a_3^-, a_4^-, a_5^-, **c_2^-**, c_3^-, y_2^-, y_3^-, y_4^-
YIGSR (laminin)	592.3	593.3	$[M\text{-H-CH}_2\text{O}]^-$	$[M\text{-H-CH}_2\text{O}]^-$	**c_3^-**	c_2^-, c_3^-
YIGSA	507.2	508.2	$[M\text{-H}]^-$	$[M\text{-H-NH}_3]^-$	c_2^-, **c_3^-**	c_2^-, c_3^-
FPARVGI	756.4	757.4	$[M\text{-H}]^-$	$[M\text{-H-NH}_3]^-$	c_2^-, c_3^-, c_4^-, **c_5^-**, y_3^-, y_4^-, y_5^-, y_6^-	c_2^-, c_3^-, c_4^-, c_5^-, y_3^-, y_4^-, y_5^-, y_6^-
DYMGWMDF (cholecystokinin)	1061.4	1062.4	$[M\text{-H-H}_2\text{O}]^-$	$[M\text{-H-H}_2\text{O}]^-$	c_6^-, y_7^-	c_6^-, y_7^-
LMYVHWVK	1072.6	1073.6	y_6^- and c_6^{-e}	c_5^-	c_3^-, **c_4^-**, c_5^-, **c_6^-**, y_3^-, **y_4^-**, **y_5^-**, **y_6^-**, y_7^-	c_3^-, c_4^-, **c_5^-**, c_6^-, y_3^-, y_4^-, **y_5^-**, **y_6^-**, y_7^-
LMYVHWVR	1100.6	1101.6	c_6^- and $[M\text{-H-HN=C=NH}]^-$	$[M\text{-H-HN=C=NH}]^-$	c_3^-, **c_4^-**, **c_5^-**, **c_6^-**, **c_7^-**, y_4^-, **y_5^-**, **y_6^-**, y_7^-	c_3^-, c_4^-, c_5^-, c_6^-, c_7^-, y_4^-, y_5^-, y_6^-, y_7^-
MLGFRSVGYA	1097.5	1098.5	$[M\text{-H}]^-$	$[M\text{-H-CH}_2\text{O}]^-$	c_3^-, c_4^-, c_5^-, c_6^-, c_7^-, c_8^-, c_9^-, y_3^-, y_4^-, y_5^-, y_6^-, y_7^-, y_8^-, y_9^-, y_{10}^-	c_3^-, c_4^-, c_5^-, c_6^-, c_7^-, c_8^-, c_9^-, c_{10}^-, y_3^-, y_4^-, y_5^-, y_6^-, y_7^-, y_8^-, y_9^-, y_{10}^-
WFAPPRVGYL	1202.6	1203.6	$[M\text{-H}]^-$	$[M\text{-H-NH}_3]^-$	c_2^-, c_5^-, c_6^-, c_7^-, **c_8^-**, y_3^-, y_4^-, y_5^-, y_6^-, y_7^-, y_8^-, y_9^-, y_{10}^-	c_5^-, c_6^-, c_7^-, c_8^-, c_9^-, y_3^-, y_4^-, y_5^-, y_6^-, y_7^-, y_8^-, y_9^-, y_{10}^-
RPKPQQFFGLM (substance P)	1345.7	1346.7	c_9^-	$[M\text{-H-HN=C=NH}]^-$	c_4^-, c_5^-, c_6^-, c_7^-, c_8^-, **c_9^-**, y_4^-, y_5^-, **y_6^-**, y_7^-, **y_8^-**, y_9^-, y_{10}^-	c_8^-, c_9^-, y_4^-, y_5^-, y_6^-, y_7^-, **y_8^-**, y_9^-, y_{10}^-

[a] Units of *m/z* are Thomson.
[b] Neutral loss peaks are excluded.
[c] Ions in **bold red** have an intensity of >40% of base peak.

mixture (by volume) of ultrapure water and methanol. Solutions for mass spectral analysis were obtained by diluting the stock solutions to (1-5) μM in a 50:50 mixture of acetonitrile and ultrapure water. A 0.1-1% volume of either acetic acid or ammonium hydroxide was added to the sample solution (to assist in protonation or deprotonation, respectively).

3.3.3 Mass spectrometry

Low-energy CID experiments were performed using a Bruker HCTultra PTM Discovery System (Billerica, MA) high capacity quadrupole ion trap (QIT) equipped with ESI. Peptide samples were introduced into the ESI source using a KD Scientific syringe pump (Holliston, MA) at a flow rate of 100-250 μL/hr. Ions were produced by ESI using a spray voltage of ±(3000-4000 V). Nitrogen was used as the ESI drying gas and was heated to a temperature of 300°C and set to flow at a rate of 5 L/min. The nebulizer gas, also nitrogen, was set to a pressure of 10 psi.

For low-energy CID experiments, precursor ions were allowed to accumulate in the trap for up to 200 ms and then mass selected using ejection pulses. The isolation window was 4 m/z wide in most cases, but was narrowed to 1 *m/z* for a couple of situations that had interfering peaks nearby. Narrowing the isolation window had a negligible effect on the intensity of the ion of interest, and effectively removed the interfering peak. Helium was the collision gas. A collision energy sweep of 30-200% with amplitude between 0.8 and 1.0 V was used to maximize CID fragmentation. Care was taken to use the same CID conditions for each of the peptide acid and amide pairs. To describe the observed fragmentation of the peptides in the study, nomenclature introduced by Roepstorff and Fohlman[30] is used. (Chapter 2 discusses fragmentation nomenclature in more detail.)

3.3.4 Computations

All calculations were performed by Michele Stover of Dr. David Dixon's group at the University of Alabama. The calculations were performed at the density functional theory (DFT) and correlated molecular orbital (MO) theory levels with the program Gaussian-03.[31] The geometries were initially optimized at the DFT level with the B3LYP exchange-correlation functional[32, 33] and the DZVP2 basis set.[34] Vibrational frequencies were calculated to show that the structures were minima and to provide zero point and thermal corrections to the enthalpy and entropies so that free energies could be calculated for direct comparison to experiment. A range of structures was optimized to determine the most stable conformers. In our previous work on amino acid acidities[35, 36] (and results in Chapters 5 and 6) the Dixon and Cassady groups have shown that the high level G3(MP2) correlated molecular orbital method[37] gave agreement for the acidities with the experimental values to within about ±1 kcal/mol. G3(MP2) has an additional advantage over DFT methods in terms of reliable predictions for these types of compounds because the correlated molecular orbital methods in G3(MP2) perform better in the prediction of hydrogen bond energies as well as steric non-bonded interactions than do most widely-used DFT exchange-correlation functionals.

3.4 Results and discussion

3.4.1 CID of peptide acid/amide pairs

Protonated, $[M + H]^+$, and deprotonated, $[M - H]^-$, peptides were fragmented by low-energy CID. For protonated peptides, loss of NH_3 was more prominent in the amide spectra (data not shown), but few other differences were observed. This is consistent with the C-terminal acid and amide groups not being charge sites in positive ion mode. These results are in

agreement with those of Enjalbal and coworkers for CID on protonated ions from 76 acid/amide pairs.[27]

For the deprotonated peptides, common negative ion mode CID backbone cleavages occur; that is, c_n^- and y_n^-.[38-41] Pentaalanine also produces a_n^- and $''b_n^-$, which is typical of oligoalanine peptides in negative ion mode.[40] Neutral loss peaks common to specific amino acid residues are abundant in the spectra; for example, elimination of H_2O and CH_2O from serine [41-48], the guanidino group (HN=C=NH) from arginine,[39, 48, 49] H_2O from aspartic acid,[50-53] $O=C_6H_4=CH_2$ from tyrosine,[53] and CH_3SH, CH_3SCH_3, and $CH_2CH_2SCH_3$ from methionine.[54]

In negative ion mode, a dominant backbone cleavage product ion forms for most of the peptides studied and is typically several times more abundant than other backbone product ions. The deprotonated peptide amides produce abundant c_{m-2}^-, where m is the number of residues in the peptide sequence. Many of the peptide acids produce c_{m-3}^- in abundance, which was also observed in prior work by Cassady and coworkers.[39]

Data from the deprotonated peptide CID experiments has been compiled in Table 3.1. Three sets of example spectra are given in Figures 3.1, 3.2 and 3.3. The CID spectra for the remaining peptides can be seen in the Supplementary Materials at the end of this chapter. These example spectra illustrate the differences observed between the acid and amide peptides. Laminin amide (Figure 3.1(a)), which is a pentapeptide (m = 5), produces c_3^- as the only backbone cleavage ion in abundance. This c_{m-2}^- type ion is far more pronounced in the amide spectrum than in the acid spectrum. Laminin acid (Figure 3.1(b)), whose sequence is YIGSR, produces a very simple spectrum consisting mainly of neutral loss peaks and c_2^- and c_3^- in low abundance. Another example can be seen in the spectra of FPARVGI (m = 7, Figure 3.2). Dissociation of the FPARVGI amide (Figure 3.2(a)) produces several c_n^- and y_n^-, as well as

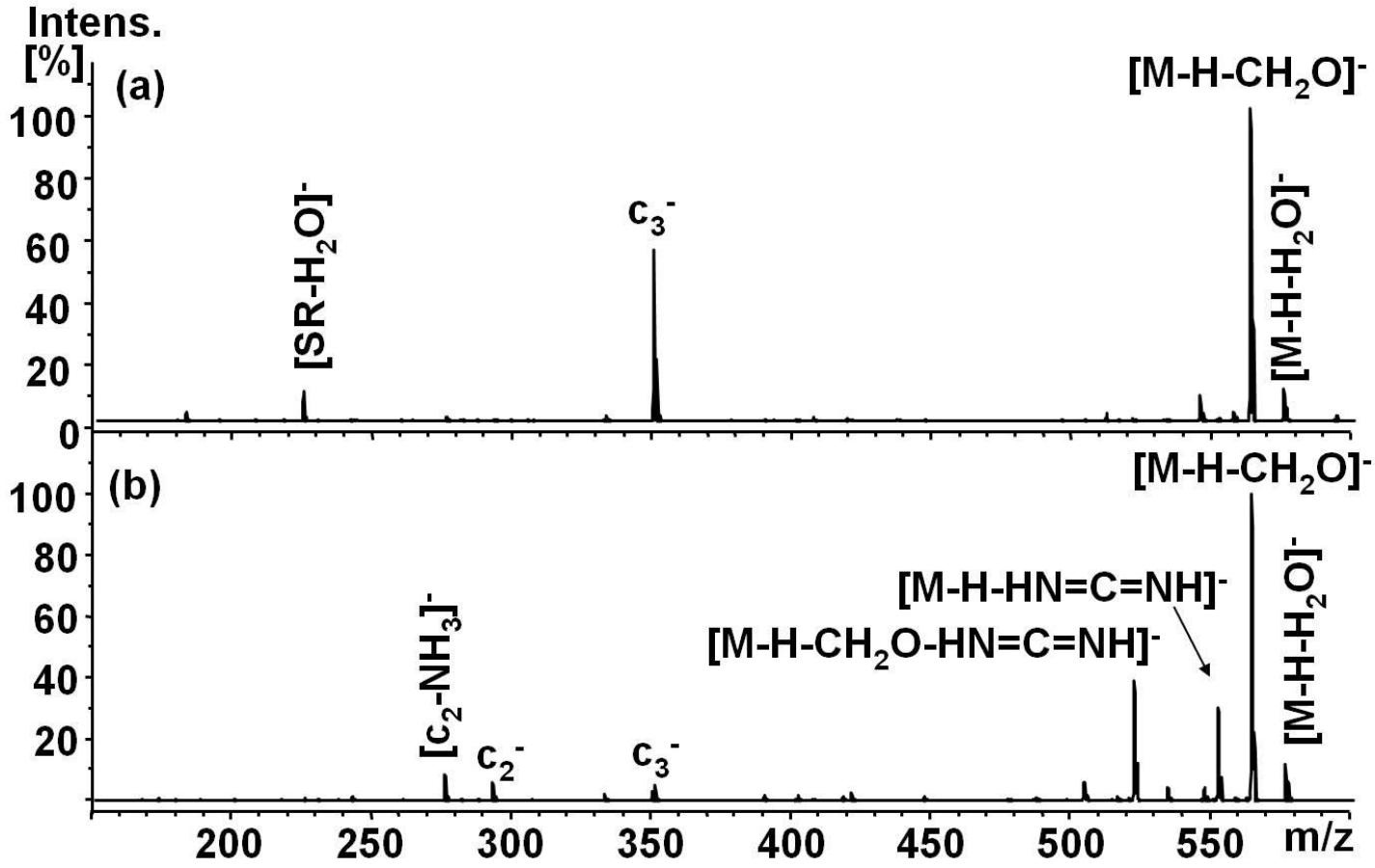

Figure 3.1. CID spectra of $[M - H]^-$ from laminin (YIGSR) (a) amide and (b) acid.

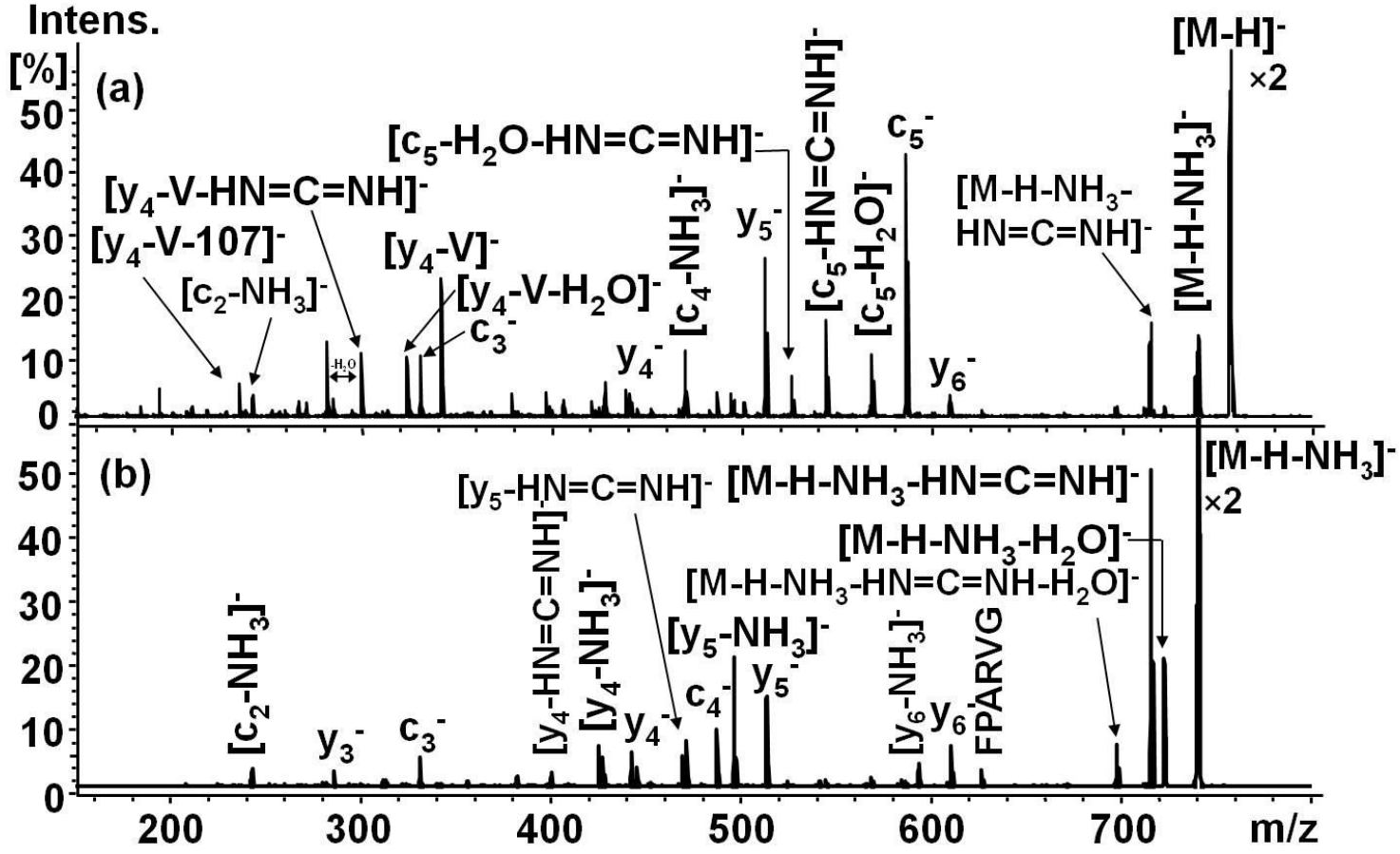

Figure 3.2. CID spectra of [M - H]⁻ from FPARVGI (a) amide and (b) acid.

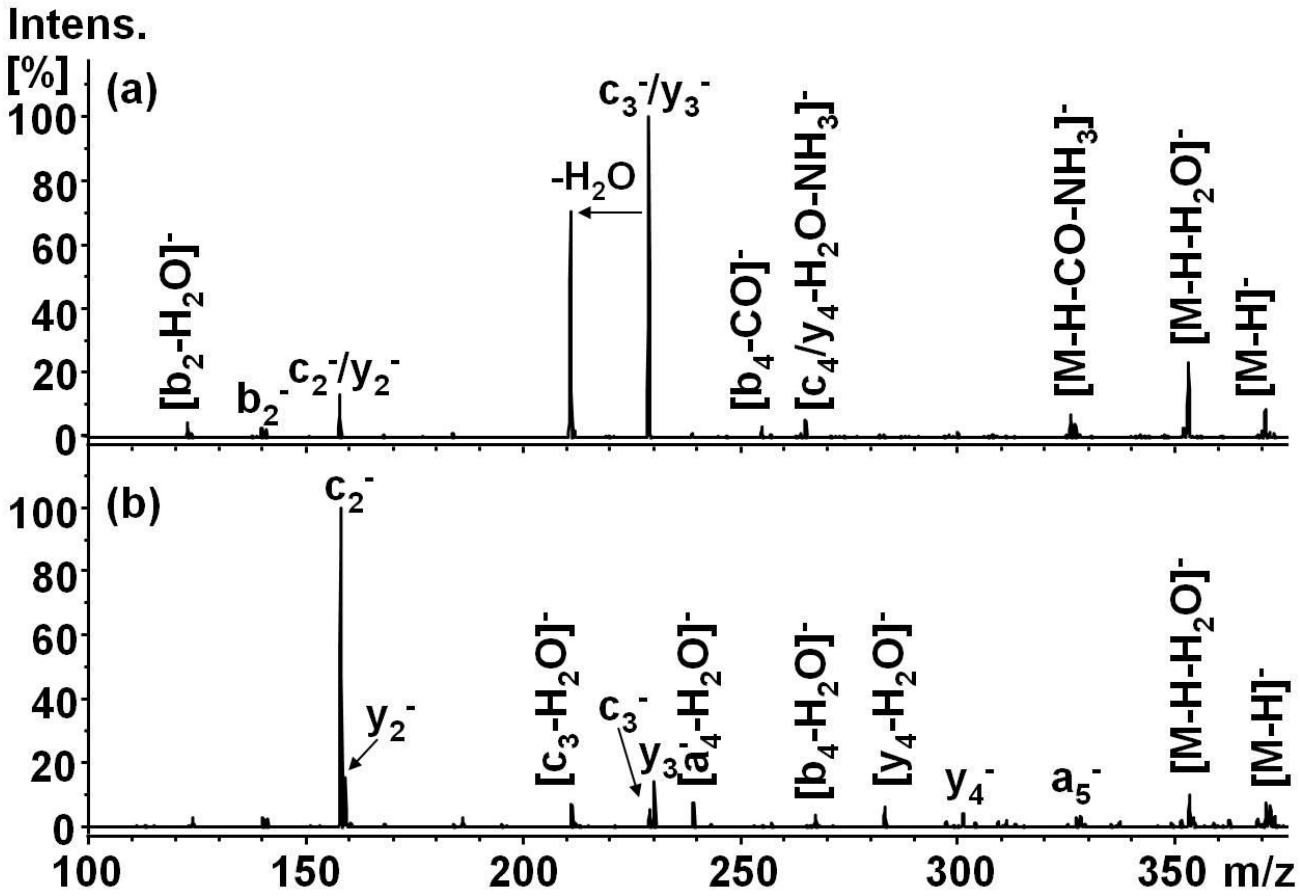

Figure 3.3. CID spectra of $[M - H]^-$ from AAAAA (a) amide and (b) acid.

many neutral loss peaks. A very intense c_5^- (a c_{m-2}^- type ion) and products from internal valine (V) residue elimination (e.g., $[y_4 - V]^-$ and neutral loss products from this ion) are unique to the amide spectrum. The acid form of FPARVGI (Figure 3.2(b)) produces a spectrum similar to the amide, without the intense c_5^- and valine loss. Another significant aspect of the FPARVGI acid spectrum is the appearance of a more abundant c_4^- (a c_{m-3}^- type ion). Pentaalanine (AAAAA, m = 5) is also shown to demonstrate the differences between acids and amides without interaction from side chains. Pentaalanine amide (Figure 3.3(a)) has c_3^-/y_3^- as the base peak of the spectrum (masses are identical due to symmetry) and a very prominent water loss peak associated with this ion. The remaining product ions are less than 20% relative to the base peak. Pentaalanine acid (Figure 3.3(b)) has c_2^- as the base peak of its CID spectrum. Other backbone fragment ions are observed for pentaalanine, but they are all less than 20% relative to the base peak.

These selected spectra demonstrate the differences in dissociative behavior of deprotonated peptide acids and their amide analogs. Formation of c_{m-3}^- in the CID of the peptide acids has been observed previously.[39, 55] However, the production of c_{m-2}^- in the CID spectra of the peptide amides has not been addressed. There are several factors that must be considered in this case. Since conversion of the C-terminus to an amide removes an acidic site on a peptide, the site of deprotonation may be a factor in c_{m-2}^- formation. Another factor is the reaction enthalpy which accounts for the difference in energies between the deprotonated peptide precursor ion and the product neutral leaving group and the product c-ion.

3.4.2 Peptide composition effects on c_{m-2}^- formation

To elucidate the involvement of a C-terminal amide group in formation of c_{m-2}^-, we chose to modify laminin and study these peptides by CID. Several laminin analogs were synthesized with altered C-termini to explore the involvement of the C-terminus. Other analogs were studied

Table 3.2. Comparison of CID fragmentation observed for laminin (YIGSR) and related derivatives.

Peptide	C-terminus	Relative intensity[a] of c_3^-	Absolute intensity of c_3^-
YIGSR-NH_2	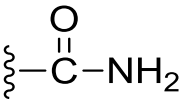	60%	73108
YIGSR-OH	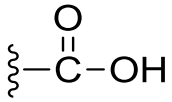	<5%	7218
YIGSR-NHEt	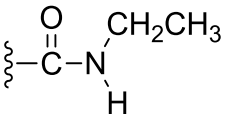	30%	2770
YIGSR-NMe_2	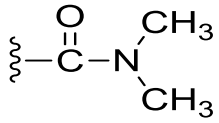	40%	38710
YIGSR-OMe	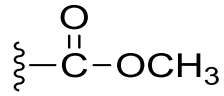	<6%[b]	252
YIGSA-NH_2	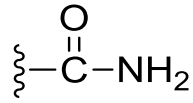	80%	371294
YIGSA-OH	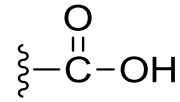	8%	50060
YIGA′R-NH_2	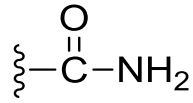	100%[c]	103225
YIGG′R-NH_2	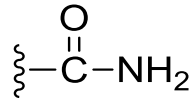	100%[c]	75374

[a] Relative to the base peak, $[M - H - CH_2O]^-$.

[b] Base peak is $[M - H - MeOH - HN{=}C{=}NH]^-$.

[c] Because this peptide does not contain a serine residue, the c_3^- ion is the base peak.

to test amino acid residue and backbone site interactions. Table 3.2 shows the C-terminal modifications as well as the absolute and relative (to $[M - H - CH_2O]^-$) intensities of c_3.

The first modification is replacement of one of the hydrogens on the C-terminal amide moiety with an ethyl group, producing YIGSR-NHEt. Dissociation of deprotonated YIGSR-NHEt produces a CID spectrum (Figure 3.4(a)) nearly identical to that of the original laminin amide (Figure 3.1(b)), with the exception of product ions related to the C-terminal ethyl group. The intensity of c_3^- is reduced in half when one amide hydrogen is substituted by an ethyl group, from ~60% of the base peak for laminin amide to ~30% of base peak for the -NHEt analog.

The second modification was to completely remove the both C-terminal amide hydrogen and replace them with methyl groups, producing YIGSR-NMe_2. Although its intensity has dropped by about a third relative to unmodified laminin amide, c_3^- is still present at ~40% of the base peak (Figure 3.4(b)). This suggests that a precursor ion structure involving deprotonation at the C-terminal amide group is responsible for some, but not all, of the c_{m-2}^- formation.

A third C-terminal modification was to produce the methyl ester of laminin acid. The CID spectrum of YIGSR-OMe (Figure 3.5) is dominated by products formed from elimination of CH_3OH from the methyl ester functional group. There have been previous reports of CH_3OH loss in CID of peptide methyl esters [56, 57]. Laminin acid (Figure 3.1(a)) produces $[c_2 - NH_3]^-$ and c_2^-; these ions do not form for the laminin methyl ester. However, the laminin methyl ester does produce small amounts of $y_3'^-$, c_3^-, and $c_3'^-$. The $c_3'^-$ ion (i.e., $[c_3 + H]^-$) appears adjacent to c_3^- and is not observed in other spectra, which suggests that this product ion stems from the presence of the C-terminal methyl ester group.

Laminin was also modified internally by replacing specific residues in the sequence to test their involvement in the formation of c_{m-2}^-. The first of these modifications was replacement of arginine with a neutral alanine residue, to form YIGSA. This was done to rule out the

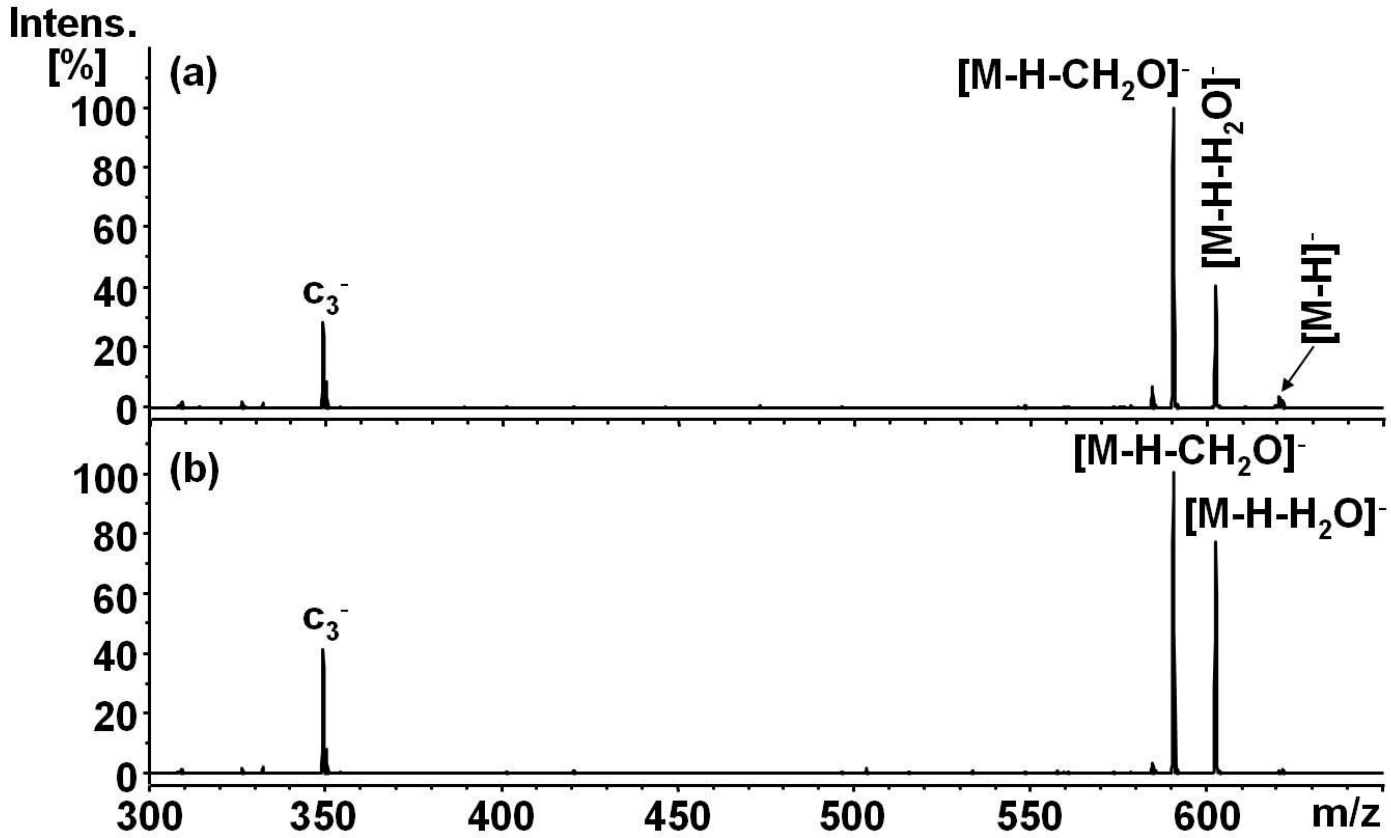

Figure 3.4: CID spectra of $[M - H]^-$ from (a) YIGSR-NHEt and (b) YIGSR-NMe_2.

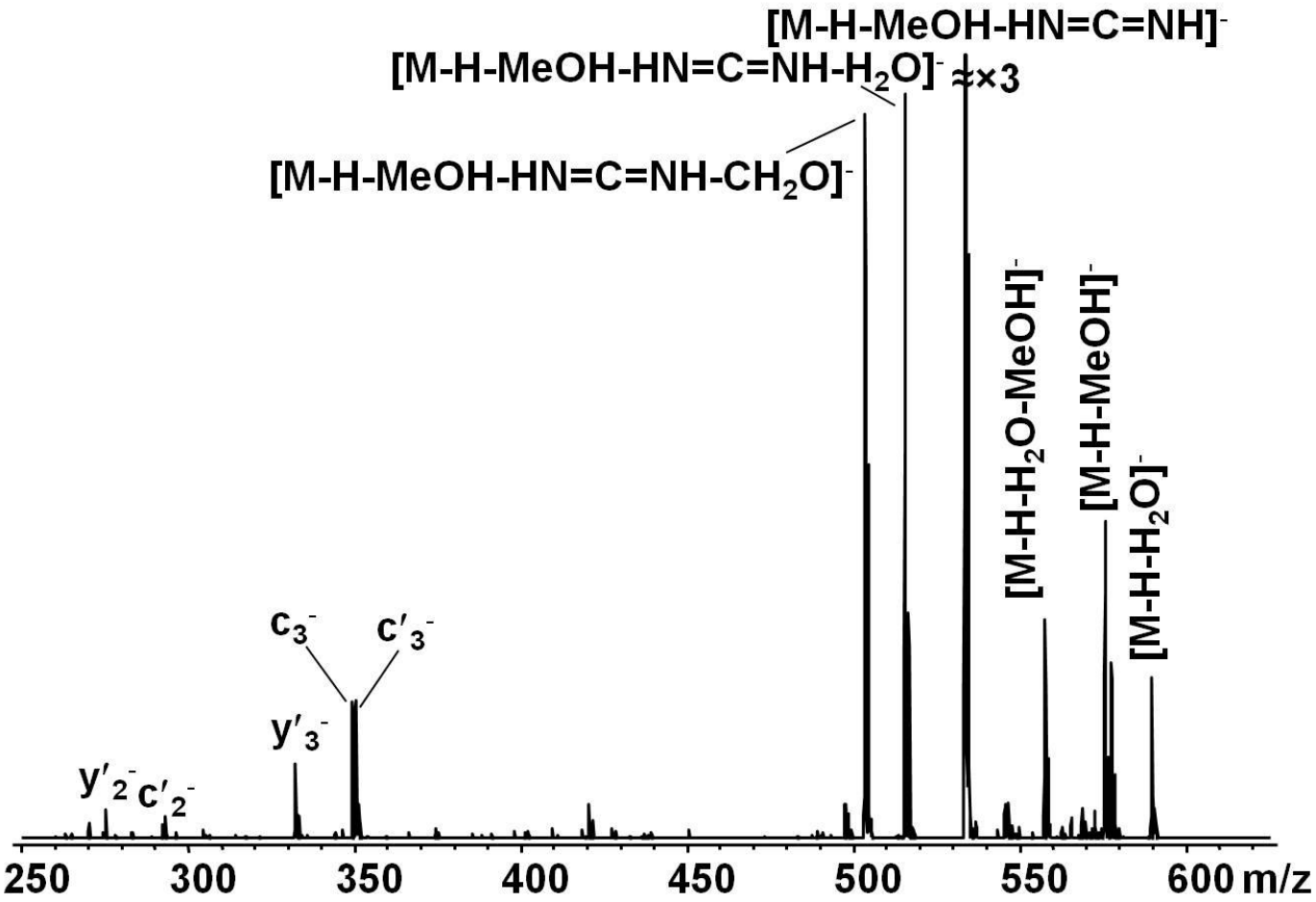

Figure 3.5: CID spectrum of $[M - H]^-$ from YIGSR-OMe.

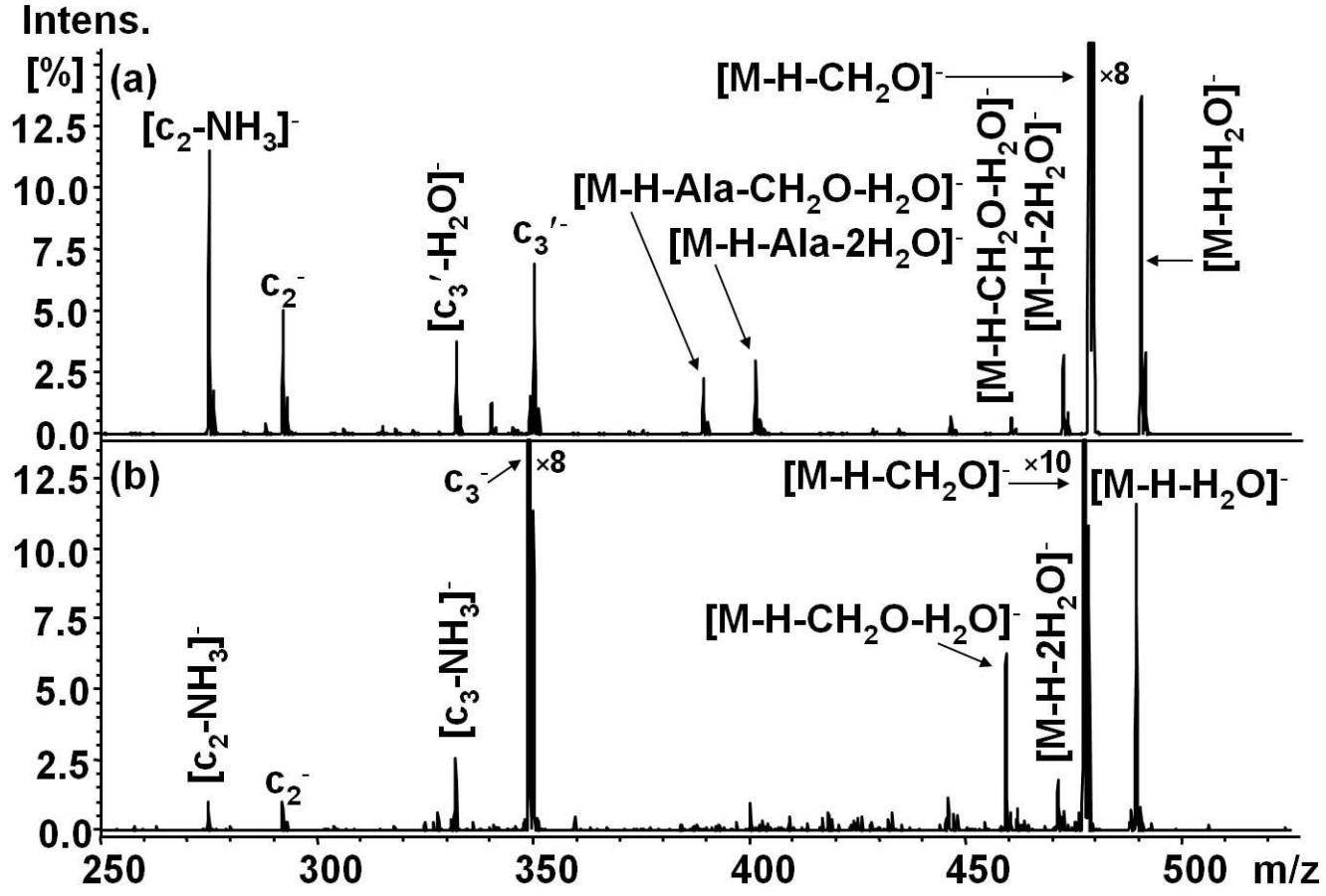

Figure 3.6: CID spectra of $[M - H]^-$ from YIGSA (a) acid and (b) amide.

possibility of a salt bridge interaction involving the highly basic arginine residue.[49, 58] Both acid and amide analogs were synthesized and fragmented by CID (Figure3.6). The acid and amide analogs of YIGSA yield spectra nearly identical to the acid and amide analogs of laminin (YIGSR) except without the neutral loss peaks related to the side chain of arginine. These spectra indicate that arginine is not participating in the mechanism that leads to production of c_{m-2}^- or c_{m-3}^-.

Additional internally modified peptides, YIGA′R-NH_2 and YIGG′R-NH_2, were studied to test the involvement of the backbone alpha carbon and the amide nitrogen on formation of c_{m-2}^-. The penultimate residue of these laminin amide analogs is either 2-amino-2-methylpropanoic acid (2-methylalanine or aminoisobutyric acid, A′), which is essentially alanine with an additional methyl group on the alpha carbon (i.e., 2 methyl groups on the alpha carbon), or sarcosine (G′), which is glycine substituted with a methyl group on the amide nitrogen. Both of these laminin analogs (Figures 3.7 and 3.8, respectively) produce abundant c_3^- as the base peak in the CID spectra. These results indicate that at least one mechanism of c_{m-2}^- formation does not require hydrogen substitution on the methylene carbon or amide nitrogen of the penultimate residue. Thus, c_{m-2}^- can form even when it is not possible to deprotonate the backbone amide site at the penultimate residue.

3.4.3 Peptide deprotonation site

In general, gas-phase deprotonation of a peptide occurs at an acidic site like the carboxylic acid groups of the glutamic acid (E) and aspartic acid (D) side chains and the C-terminus.[45] In the peptide amides, the carboxylic acid group at the C-terminus is replaced with a less acidic terminal amide group. A comparison of the gas-phase acidities (GAs) of simple compounds like acetic acid and acetamide reveals a distinct difference in the energy required for

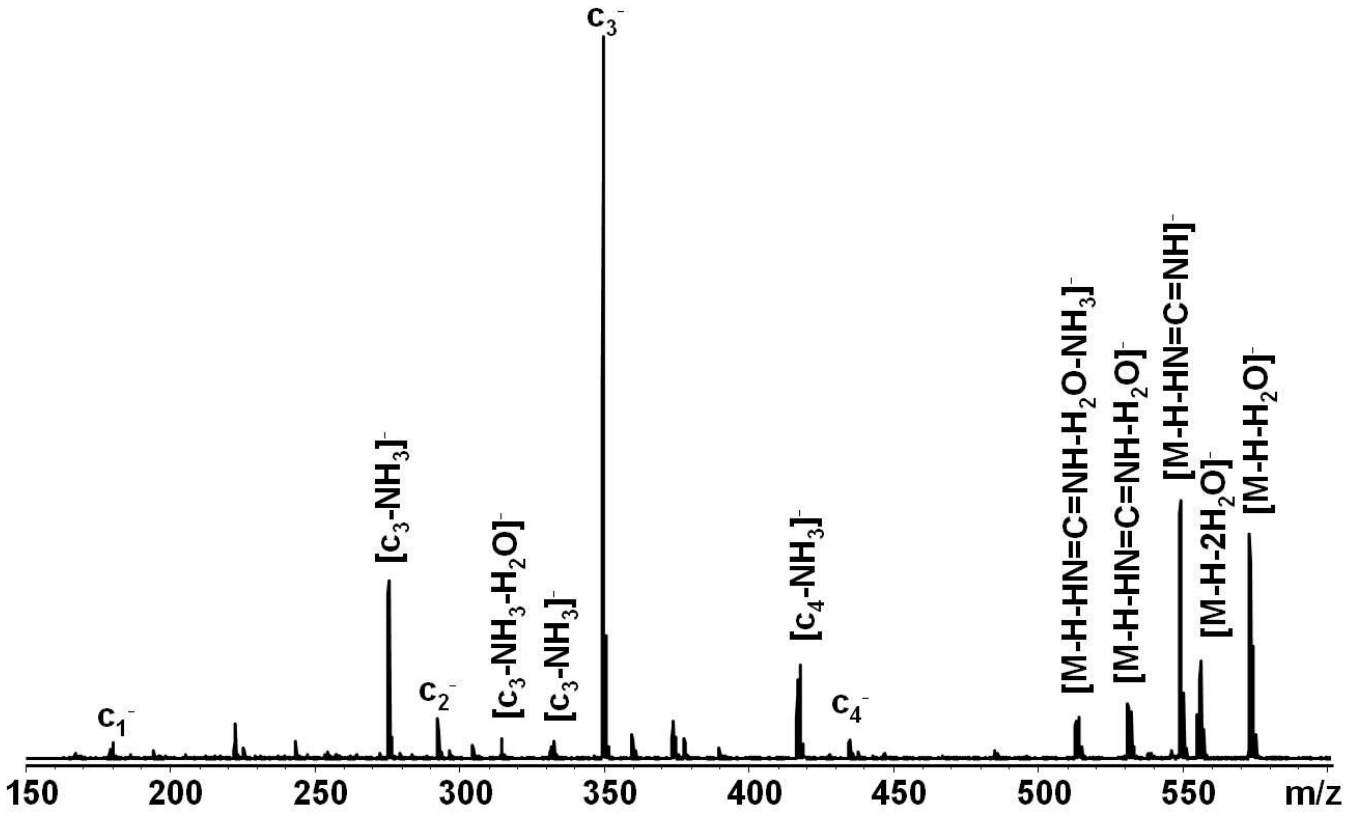

Figure 3.7: CID spectrum of $[M - H]^-$ from YIGA′R-NH_2.

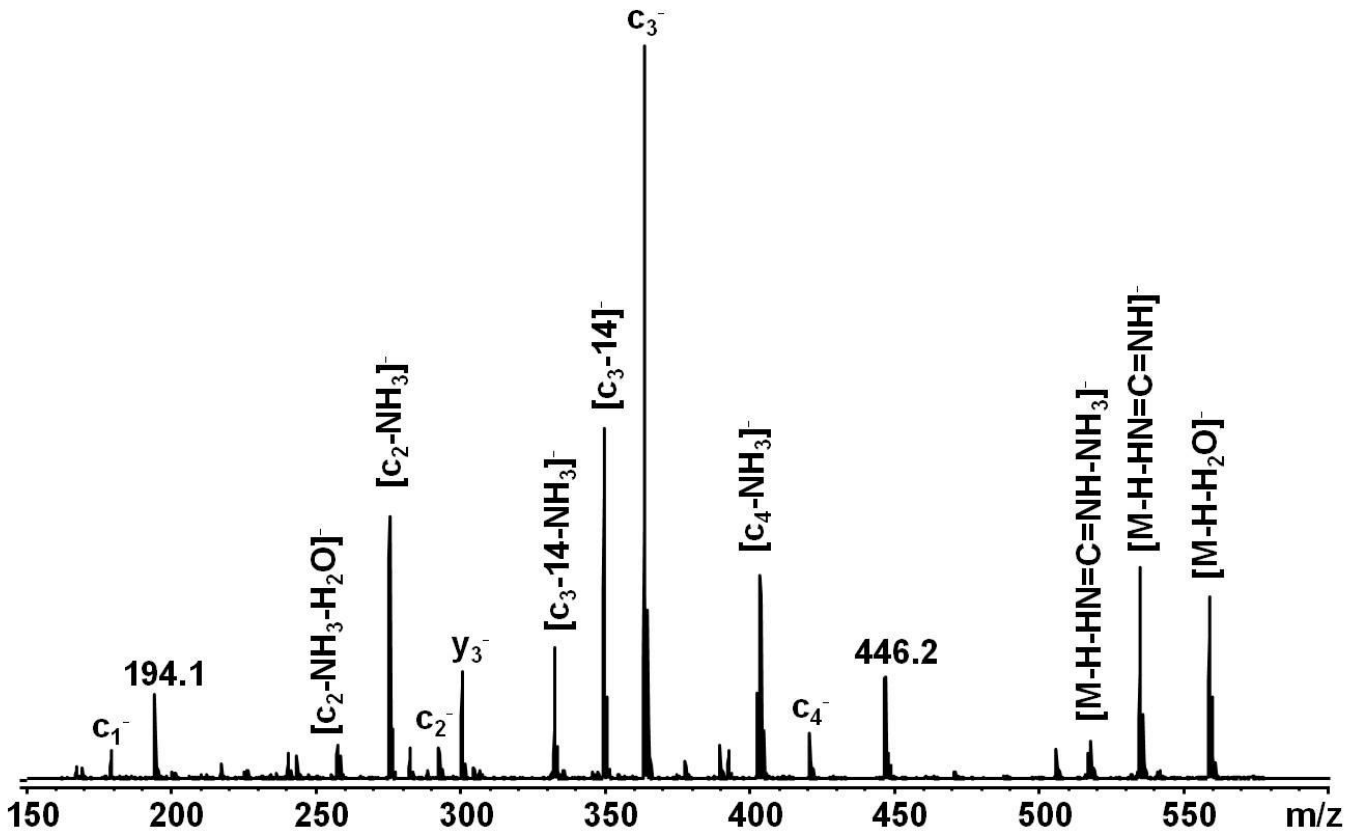

Figure 3.8: CID spectrum of $[M - H]^-$ from YIGG′R-NH_2.

the reaction of carboxylic acid versus amide functional groups. Acetic acid has a GA of 341.1 ± 2.0 kcal/mol whereas acetamide has a GA of 355.0 ± 2.0 kcal/mol,[59] an energy difference of 13.9 kcal/mol with acetic acid being more acidic (i.e. lower GA). Yet, the peptide amides studied here produce abundant $[M - H]^-$ by ESI. These peptide amides deprotonate even though (with the exception of cholecystokinin, CCK) they are composed of amino acid residues without acidic side chains. This is consistent with past work by Gao and Cassady[60] where peptides with no carboxylic acid groups deprotonate readily by matrix-assisted laser desorption ionization (MALDI) mass spectrometry. In addition, Bowie and coworkers[41, 45, 61] have reported instances of deprotonation occurring at the amide nitrogen for peptide and organic amides. Their experimental results are supported by lower level theoretical calculations (HF/6-31G*//AM1) using model systems.[61] Thus, amide nitrogens and alpha carbons of the peptide backbone must be considered as alternative deprotonation sites.

We have also undertaken a comprehensive experimental and high level G3(MP2) computational study of the GAs for all possible deprotonation sites of numerous small peptides. This is the subject of Chapter 6. We have found that the amide nitrogens are the most energetically favorable peptide backbone deprotonation sites due to their ability to form a $–(O^-)C=N–$ resonance structure. Therefore, these sites need to be considered in the present study.

Table 3.3 includes the calculated G3(MP2) heats of formation (ΔH_f) for several deprotonated peptide ions produced from acid and amide analogs of tri- to pentaglycine. The lowest energy structure for each deprotonated peptide has been calculated by sampling a variety of conformers. For the peptide amides, the ΔH_f values indicate that there is only a few kcal/mol difference between deprotonation at the C-terminal amide nitrogen and deprotonation at a backbone amide nitrogen. For example, consider pentaglycine amide: ΔH_f of the anion is -261.8

Table 3.3 G3(MP2) calculated heats of formation.

	ΔH_f (kcal/mol)		
	Deprotonation Site		
	C-terminus	**Backbone for 6-membered ring formation[a]**	**Backbone for 9-membered ring formation[b]**
Precursor Ions			
$[GGG\text{-}NH_2 - H]^-$	-156.5	-164.6	NA[c]
$[GGG\text{-}OH - H]^-$	-220.4	-210.4	NA
$[GGG\text{-}NHEt - H]^-$	-166.9	-172.7	NA
$[GGGG\text{-}NH_2 - H]^-$	-209.5	-213.9	-216.4
$[GGGG\text{-}OH - H]^-$	-271.5	-258.7	-254.2
$[GGGG\text{-}NHEt - H]^-$	-214.2	-221.6	-224.4
$[GGGGG\text{-}NH_2 - H]^-$	-261.8	-263.7	-265.7
$[GGGGG\text{-}OH - H]^-$	-325.2	-298.7	-312.8
$[GGGGG\text{-}NHEt - H]^-$	-264.5	-271.5	-271.0
$[AAAAA\text{-}OH - H]^-$	-369.4	-341.4	-353.2
Product Ions[d]			
c_{m-2}^- from GGG peptides	-55.4		
c_{m-2}^- from GGGG peptides	-108.6		
c_{m-3}^- from GGGG peptides	-55.4		
c_{m-2}^- from GGGGG peptides	-156.5		
c_{m-3}^- from GGGGG peptides	-108.6		
c_{m-2}^- from AAAAA peptides	-182.4		
c_{m-3}^- from AAAAA peptides	-125.7		
Neutral Products[e]			
Diketopiperazine (DKP)	-73.7		
1-ethylpiperazine-2,5-dione (DKP-Et)[f]	-83.6		
1,4,7-triazonane-2,5,8-trione (TAT)	-105.1		
1-ethyl-1,4,7-triazonane-2,5,8-trione (TAT-Et)[g]	-114.6		
Diketomorpholine (DKM)	-111.0		

1,4,7-oxadiazonane-2,5,8-trione (ODAT)	-147.1
1,4-dimethyl-2,5-diketomorpholine ($DKM(Me_2)$)[h]	-130.5
3,5,9-trimethyl-1,4,7-oxadiazone-2,5,8-trione ($ODAT(Me_3)$)[i]	-175.1

[a] Deprotonation is at the backbone amide nitrogen adjacent to the N-C bond cleavage site for formation of c_{m-2}^- and the 6-membered ring DKP and DKM species.
[b] Deprotonation is at the backbone amide nitrogen adjacent to the N-C bond cleavage site for formation of c_{m-3}^- and the 9-membered ring TAT and ODAT species.
[c] NA = not applicable. For triglycine (GGG), loss of a neutral incorporating a 9-membered ring containing all three residues would not leave sufficient atoms to form a c-ion.
[d] Changing the C-terminal end group (-OH, $-NH_2$, -NHEt) does not change ΔH_f of the product ions. All of the calculations involve c-ions with linear structures where the negative charge is on the amide nitrogen at the C-terminal side.
[e] Neutral structures are shown in Schemes 1 and 2. The neutral products do not possess a deprotonation site.
[f] Structure is equivalent to DKP with an ethyl group on a ring nitrogen.
[g] Structure is equivalent to TAT with an ethyl group on a ring nitrogen.
[h] Structure is equivalent to DKM with a methyl group on each ring carbon.
[i] Structure is equivalent to ODAT with a methyl group on each ring carbon.

kcal/mol when deprotonated at the carboxylic acid group of the C-terminus, -265.7 kca/mol when deprotonated at the amide nitrogen of the central residue, and -263.7 kcal/mol when deprotonated at the amide nitrogen of the penultimate residue. Given this relatively small difference in energies, the ESI process in the mass spectrometer should be capable of deprotonation at all three sites. The fact that multiple precursor ion structures are potentially involved explains why removal of both C-terminal amide hydrogens in the YIGSR-NMe_2 experiments lessens, but does not eliminate, c_{m-2}^- formation by CID and why removing both backbone amide hydrogens in the YIGA′R-NH_2 experiments also does not eliminate c_{m-2}^- formation.

For the peptide acids, the ΔH_f values of Table 3.3 indicate that C-terminal deprotonation is more favorable than backbone deprotonation by 10-30 kcal/mol. For example, with pentaglycine acid, ΔH_f for the peptide ion deprotonated at the C-terminal carboxylic acid group is -325.2 kcal/mol, which is more favorable than ΔH_f's for the ions deprotonated at the central amide nitrogen (-312.8 kcal/mol) and at the penultimate amide nitrogen (-298.7 kcal/mol). ESI is a very soft ionization technique that produces ions will little excess energy and, therefore, preferentially generates ions with the lowest energy structure.[62-66] As a result, the majority of the precursor ions produced by ESI on the peptide acids should be deprotonated at the C-terminal carboxylic acid group. However, the presence of some peptide acid anions with backbone amide deprotonation cannot be ruled out. In particular, after ion activation by CID, the location of negative charge on the ion may move in an analogous manner to the "mobile proton model"[67] that occurs during CID on protonated peptides in the positive ion mode.

3.4.4 Proposed dissociation mechanisms

We propose a substituted 2,5-piperazinedione (or diketopiperazine, DKP) as the stable, heterocyclic leaving group for the formation of c_{m-2}^- by deprotonated peptide amides. The general DKP structure is shown in Structure 1 of Scheme 3.1 for X = NH. DKP analogs frequently form as a by-product in solid-phase peptide synthesis.[68-70] These 6-membered ring dipeptides are often biologically active and commonly present in nature as secondary metabolites.[71, 72] DKP analogs have been the subject of much debate in the formation of b_2^+ from protonated peptides,[73-76] but there have been few reports of the role of this structure in deprotonated peptide spectra. Harrison and co-workers[77] proposed involvement of a DKP neutral in the formation of $''b_2^-$ from a_3^- in low-energy CID of tripeptides, but their theoretical calculations suggested this was not a key pathway.[78] Harrison and Young[79] mentioned the possible formation of DKPs in their study involving formation of oxazolones in CID of deprotonated N-benzoylpeptides. Bowie and coworkers[56] proposed the formation of a deprotonated DKP from diglycine methyl ester in high-energy CID. There have also been reports of CID fragmentation of deprotonated DKPs, as well as theoretical calculations of fragmentation pathways.[80, 81] A diketomorpholine (DKM) is the analogous leaving group for a deprotonated peptide acid. This compound is identical to DKP, except that DKM has an oxygen in place of one ring nitrogen (Structure 1 with X = O). Diketomorpholines are frequently used in synthetic applications and are occasionally biologically active.[82, 83]

Scheme 3.1 illustrates our proposed mechanism to form c_{m-2}^- from either the acid or amide form of a pentapeptide with involvement of the C-terminus. The process proceeds by a nucleophilic attack of the deprotonated C-terminus on the alpha carbon of the penultimate residue. When the C-terminus is a carboxylic acid, the neutral leaving group is a DKM. In instances where the C-terminus is an amide, the leaving group is a DKP. A factor of importance

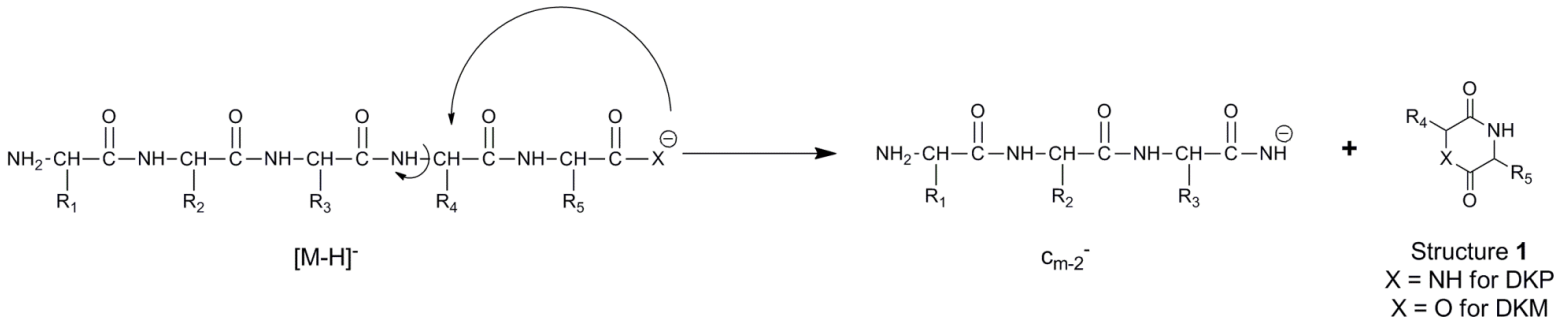

Scheme 3.1: Mechanism for the formation of DKP/DKM and c_{m-2}^- from $[M - H]^-$.

to the proposed mechanism is the nucleophilicity of the deprotonated functional group on the C-terminus of the peptide. As neutrals, both groups are weakly nucleophilic, with the carboxylic acid being a somewhat better nucleophile.[84] However, deprotonation renders the amide, NH^-, to be a much stronger nucleophile than the deprotonated acid, COO^-.

Reaction enthalpies (ΔH_{rxn}) give a more complete energetic explanation for the processes occurring here, especially as they are endothermic processes. G3(MP2) calculations have been performed for the thermodynamics of a variety of dissociation processes of deprotonated peptides. The calculated structures and the respective processes for GGGG are shown in Figure 3.9, the G3(MP2) heats of formation are given in Table 3.3, and the reaction enthalpies are given in Table 3.4. For each peptide, deprotonation has been considered at the C-terminus and also at the backbone amide nitrogen adjacent to the cleavage site. Heats of formation have been calculated for the backbone fragment ions, c_{m-2}^- and c_{m-3}^-, as these are two prominent features of the peptide amide and acid spectra, respectively. Heats of formation have also been calculated for the neutral leaving groups resulting from the CID processes. When c_{m-2}^- forms, the proposed neutral leaving groups are the 6-membered ring species DKP (Figure 3.9(a) and Scheme I) for the peptide amide and DKM for the peptide acid (Figure 3.9(b) and Scheme 3.1). As shown in Scheme 3.2, formation of c_{m-3}^- is proposed to involve elimination of a 9-membered ring neutral, which is 1,4,7-triazonane-2,5,8-trione (TAT, Structure 2 with X = NH) for peptide amides, and 1,4,7-oxadiazonane-2,5,8-trione (ODAT, Structure 2 with X = O) for peptide acids. For comparison, G3(MP2) calculations for the C-terminal ethyl amide (-NHEt) analogs of the oligoglycines are also included in Tables 3.3 and 3.4.

The reaction enthalpies shown in Table 3.4 are in most cases substantially endothermic, which explains the need for collisional activation and dissociation to form the fragmentation products. Several noteworthy trends can be obtained from these values. Many of the examples

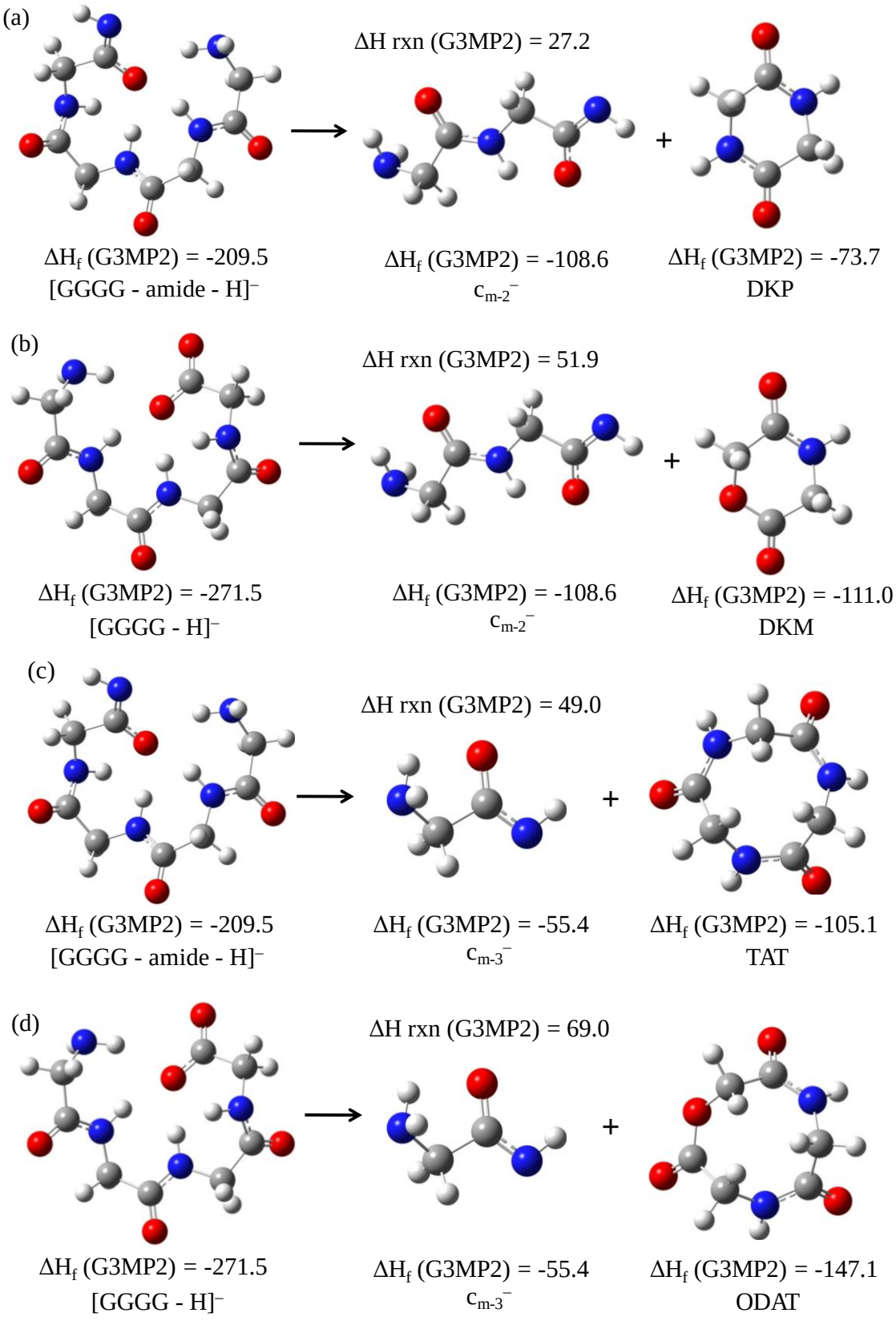

Figure 3.9: G3(MP2) calculations of enthalpies of formation (ΔH_f) and of reaction enthalpies (ΔH_{rxn}) in kcal/mol for (a) GGGG-CONH$^-$ forming c_{m-2}^- and DKP (b) GGGG-COO$^-$ forming c_{m-2}^- and DKM (c) GGGG-CONH$^-$ forming c_{m-3}^- and 1,4,7-triazonane-2,5,8-trione (d) GGGG-COO$^-$ forming c_{m-3}^- and 1,4,7-oxadiazonane-2,5,8-trione.

Table 3.4. G3(MP2) calculated reaction enthalpies.

Reaction	ΔH_{rxn} (kcal/mol)			
	GGG m =3	**GGGG m =4**	**GGGGG m = 5**	**AAAAA m = 5**
C-terminus deprotonation of precursor ion				
[Peptide Amide - H]$^-$ → c_{m-2}^- + DKP	27.4	27.2	31.6	–[d]
[Peptide Ethyl Amide - H]$^-$ → c_{m-2}^- + DKP-Et	27.9	22.0	24.4	–
[Peptide Acid - H]$^-$ → c_{m-2}^- + DKM	54.0	51.9	57.7	56.5[e]
[Peptide Amide - H]$^-$ → c_{m-3}^- + TAT	NA[a]	49.0	48.1	–
[Peptide Ethyl Amide - H]$^-$ → c_{m-3}^- + TAT-Et	NA	44.2	41.3	–
[Peptide Acid - H]$^-$ → c_{m-3}^- + ODAT	NA	69.0	69.5	68.6[f]
Backbone deprotonation of precursor ion				
[Peptide Amide - H]$^-$ → c_{m-2}^- + DKP[b]	35.5	31.6	33.5	–
[Peptide Ethyl Amide - H]$^-$ → c_{m-2}^- + DKP-Et[b]	33.7	29.4	31.4	–
[Peptide Acid - H]$^-$ → c_{m-2}^- + DKM[b]	44.0	39.1	31.2	28.5[e]
[Peptide Amide - H]$^-$ → c_{m-3}^- + TAT[c]	NA	55.9	52.0	–
[Peptide Ethyl Amide - H]$^-$ → c_{m-3}^- + TAT-Et[c]	NA	54.4	47.8	–
[Peptide Acid - H]$^-$ → c_{m-3}^- + ODAT[c]	NA	51.7	57.1	52.4[f]

[a] NA = not applicable. Due to the small size of triglycine (GGG), c-ions can not form with a 9-membered ring neutral.
[b] Backbone deprotonation for the precursor ion is at the amide nitrogen adjacent to the N-C bond cleavage site for formation of c_{m-2}^- and the 6-membered ring neutrals.
[c] Backbone deprotonation for the precursor ion is at the amide nitrogen adjacent to the N-C bond cleavage site for formation of c_{m-3}^- and the 6-membered ring neutrals.
[d] Not calculated for this species.
[e] The DKM species formed in this case is $DKM(Me)_2$.
[f] The ODAT species formed in this case is $ODAT(Me)_3$.

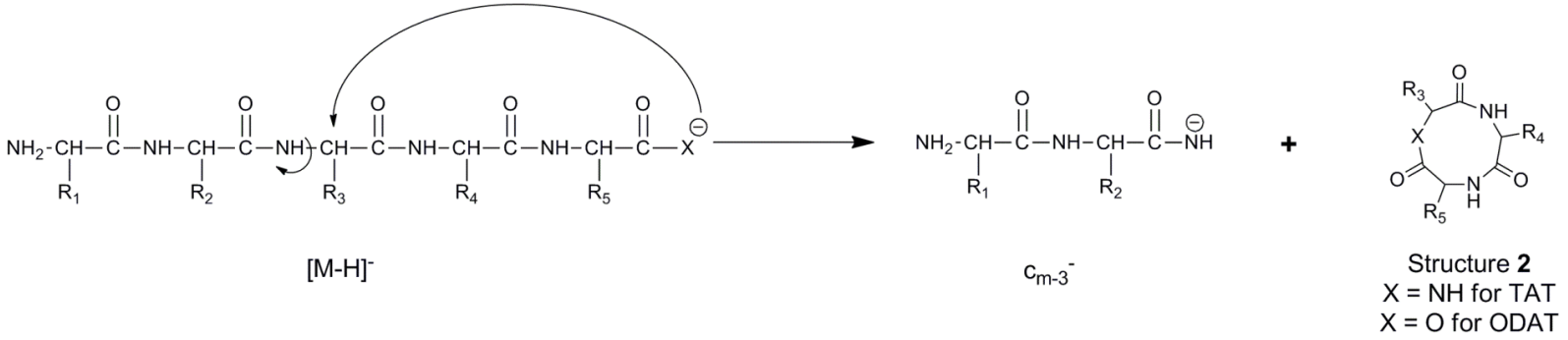

Scheme 3.2: Mechanism for the formation of TAT/ODAT and c_{m-3}^- from $[M - H]^-$.

discussed below will involve the pentaglycine analogs because all of the peptides studied experimentally by CID had five or more residues.

For the mechanism shown in Scheme 3.1 with deprotonation at the C-terminus, formation of DKP from a peptide amide is considerably less endothermic than production of DKM from a peptide acid, regardless of peptide length. For example, with C-terminal deprotonation and dissociation to yield c_{m-2}^- and a 6-membered ring neutral, pentaglycine amide requires greater than 31.6 kcal/mol, whereas pentaglycine acid requires greater than 57.7 kcal/mol. This is consistent with the CID results where c_{m-2}^- forms in much greater abundance for peptide amides than for peptide acids. When the peptide amides are deprotonated at the backbone nitrogen adjacent to the site of N-C_α bond cleavage, the process is 2-8 kcal/mol more endothermic than for C-terminal deprotonation. Also, as the size of the peptide increases, the energy difference between processes involving C-terminus deprotonation and backbone deprotonation decreases. The process to form c_{m-2}^- and DKP with C-terminus deprotonation of the dissociating ion is less endothermic than the analogous process with backbone deprotonation by 8.1 kcal/mol for triglycine amide, 4.4 kcal/mol for tetraglycine amide, and 1.9 kcal/mol for pentaglycine amide. This suggests that for larger peptide amides both C-terminal and backbone deprotonation sites may contribute to c_{m-2}^- formation.

For the mechanism shown in Scheme 3.2, formation of a 9-membered ring neutral from a peptide amide is ~20 kcal/mol less endothermic than from a peptide acid. This is true for both tetraglycine and pentaglycine. (Triglycine analogs, m = 3, cannot form c_{m-3}^- because of their short sequences.) For example, pentaglycine amide requires greater than 48.1 kcal/mol to form c_{m-3}^- and TAT when the precursor ion has C-terminal deprotonation and greater than 52.0 kcal/mol with backbone deprotonation. The analogous process to produce ODAT from

pentaglycine acid requires greater than 69.5 kcal/mol with C-terminal deprotonation and greater than 57.1 kcal/mol with backbone amide deprotonation.

The reaction enthalpies indicate that processes leading to the formation of 6-membered ring neutrals are always lower in energy (less endothermic) than those that produce 9-membered rings, regardless of peptide length or deprotonation site of the precursor ion. With pentaglycine amide, formation of c_{m-2}^- and DKP is less endothermic than production of c_{m-3}^- and TAT by 16.5 kcal/mol for C-terminal deprotonation and 18.5 kcal/mol for backbone amide deprotonation. For pentaglycine acid deprotonated at the C-terminus, formation of c_{m-2}^- and DKM is less endothermic than production of c_{m-3}^- and ODAT by 11.8 kcal/mol. The predicted reaction enthalpy trend is interesting because it is the opposite of the trend in our CID experiments where peptide acids generally produce more c_{m-3}^- than c_{m-2}^-. The difference between the predicted thermodynamic trend and experiment may relate to the ability of ESI to generate the deprotonated peptide precursor ion and to the contribution of backbone deprotonation in these fragmentation pathways. As the ΔH_f values in Table 3.3 indicate for pentaglycine acid anions, $[GGGGG\text{-}OH - H]^-$, deprotonation at the amide nitrogen of the central residue (which is a precursor for c_{m-3}^-) requires 12.4 kcal/mol more energy than deprotonation at the carboxylic acid group of the C-terminus; however, deprotonation at the penultimate residue (which is a precursor for c_{m-2}^-) requires a significantly larger amount of energy, 26.5 kcal/mol more than C-terminal deprotonation. Therefore, for peptide acids with five residues or more, the ESI process may preferentially generate the deprotonated backbone precursor for the c_{m-3}^- pathway, resulting in a more intense c_{m-3}^- in the CID spectra. We note that the calculated energy differences for dissociation processes starting from the same anion are much larger than the estimated ± 1 to ± 2 kcal/mol errors for such calculated energy differences.

The above discussion assumes that the reactions are under thermodynamic control. It is of course possible that the reactions that are under kinetic control. For the highly endoergic dissociations, this seems to be unlikely as the location of the barrier will be displaced towards the products and the barrier will be small.[85] The Dixon group searched for transition states for [GGGG-OH - H]$^-$ to form the 6-member and 9-member rings. Initially, they used a semi-empirical molecular orbital method with the PM6 parameterization scheme[86] to search for the transition states with the AMPAC version 9 program (http://www.semichem.com/). This gave PM6 barrier heights of 76.5 and 78.9 kcal/mol for the dissociation to the 6-member and 9-member rings respectively. Using these geometries, single point calculations at the DFT/B3LP/DZVP2 level gave respective barriers of 85 and 100 kcal/mol for the 6- and for the 9-member rings. These energy differences are in the order of the dissociation energies and the differences in the barriers to the dissociated products is almost the same for both rings (31 - 33 kcal/mol). Numerous subsequent optimizations of these transition states at the DFT level always led back to the low energy chain structure so it is likely that there is no or only a small barrier to dissociation at the higher computational level. Thus, no evidence exists for why there could be a kinetic preference for the 9-member ring unless there are dynamic effects that would not be found by the calculation of specific points on the potential energy surface.

The G3(MP2) calculations show that production of c_{m-2}^- and DKP from C-terminally deprotonated peptide ions requires only 27.4 kcal/mol, 27.2 kcal/mol, and 31.6 kcal/mol, respectively, for the amides of tri-, tetra-, and pentaglycine. Calculations were also performed for oligoglycine amides where one hydrogen on the amide C-terminus was replaced with an ethyl group. When comparing the processes that led to DKP and DKP-Et, the reactions involving triglycine are very close in energy (27.4 kcal/mol versus 27.9 kcal/mol). However, for tetra-and pentaglycine analogs, the processes that led to DKP-Et are less endothermic by 5-7 kcal/mol than

that of DKP. These same trends can be seen in the reactions that produce TAT-Et and TAT; TAT-Et production is less endothermic by 5-7 kcal/mol. Steric hindrance from the relatively bulky ethyl group apparently lowers the reaction energy for the tetraglycine and pentaglycine ethyl amides; however, in triglycine ethyl amide the ethyl group causes the reaction to be more endothermic and comparable to that for the triglycine amide. Steric hindrance may also be a factor in the CID experiments where replacement of the $-NH_2$ group on the laminin with a -NHEt group decreased the intensity of c_3^- by approximately half.

The Dixon group used the same G3(MP2) computational approach to study the thermodynamics of the pentaalanine anion decomposition. For C-terminus deprotonation, the effect of the 5 methyl groups is small, on the order of 1 kcal/mol decreasing both reaction energies (ΔH_{rxn} = 68.6 kcal/mol for [AAAAA-Peptide Acid - H]$^-$ → c_{m-3}^- + ODAT(Me_3) and ΔH_{rxn} = 56.5 kcal/mol for [AAAAA-Peptide Acid - H]$^-$ → c_{m-2}^- + DKM(Me_2)). Backbone deprotonation at the third nitrogen from the C-terminus of pentaalanine is 11.8 kcal/mol more probable than deprotonation of the second nitrogen from the C-terminus for AAAAA. Deprotonation from the third nitrogen leads to the formation of the nine-member ring ODAT(Me_3) (see Supporting Information for a molecular drawing) and from the second nitrogen to the six-member ring DKM(Me_2). The effect of the methyl groups are to lower the endothermicity of the nine-member ring formation by 4.7 kcal/mol (ΔH_{rxn} = 52.4 kcal/mol for AAAAA-Peptide Acid - H]$^-$ → c_{m-3}^- + ODAT(Me_3) and that of the six-member ring by 2.7 kcal/mol (ΔH_{rxn} = 28.5 kcal/mol for AAAAA-Peptide Acid - H]$^-$ → c_{m-2}^- + DKM(Me_2) as compared to the unsubstituted reactions. These effects are larger than for the C-terminus deprotonation as the methyl groups have more of an impact on the anion site in the main chain deprotonated pentaalanine.

3.4.5 Internal valine residue loss

An interesting aspect of the CID spectrum for FPARVGI amide (Figure 3.2(a)) is the incidence of $[y_4 - V]^-$ and related products such as $[y_4 - V - H_2O]^-$ and $[y_4 - V - HN{=}C{=}NH]^-$. This is not observed in the CID of FPARVGI acid (Figure 3.2(b)). Loss of an internal valine residue was originally reported by Bowie and coworkers when studying CID of deprotonated citropin 1.1 and its synthetic analogs; these peptides all have C-terminal amide groups.[87, 88] They proposed that the helical structure of the peptide allows a conformational rearrangement to take place. They found that the ESI solvent can affect the process. Elimination of valine has also been observed by Jai-nhuknan[89] in a study of protonated transform growth factor (TGF) α (34-43) using sustained off-resonance irradiation (SORI) CID in a Fourier transform ion cyclotron resonance (FT-ICR) mass spectrometer. The valine loss appears as $[M + 2H - V]^{2+}$ in the SORI-CID spectrum of $[M + 3H]^{3+}$ from TGF α (34–43), which has a C-terminal carboxylic acid group and a disulfide bond.[89] Jai-nhuknan also studied the reduced form of TGF α (34-43), where the disulfide bond is cleaved; this ion did not eliminate the valine residue. This suggests that the intact disulfide bond in TGF α (34-43) facilitates a peptide ion conformation that contributes to a unique loss of an internal valine.[89]

3.4.6 Peptides with no difference in CID spectra between acid and amide analogs

Although most of the peptide amides in this study produced abundant c_{m-2}^-, there were a few that did not follow this trend. The peptide amides of SWAMVR, MLGFRSVGYA, and cholecystokinin produce only a small amount of c_{m-2}^-. (These spectra can be found in the Supplemental Materials.) In these cases, backbone fragmentation is overshadowed by neutral loss products from specific amino acid side chains. Each of the peptides contains at least one methionine residue, which is known for its abundant side chain loss in negative ion mode [54].

Cholecystokinin also has two aspartic acid residues in its sequence; acidic amino acid residues yield significant H_2O loss.[50, 53] In addition, serine is responsible for the production of abundant CH_2O loss in the spectra of deprotonated SWAMVR and MLGFRSVGYA.[42, 52, 57, 88]

3.5 Conclusions

The effects of differing C-termini were studied using positive and negative ion mode CID on a group of peptides. Key differences were observed in the fragmentation of deprotonated substance P, laminin, pentaalanine, WFAPPRVGYL, LMYVHWVR, LMYVHWVK, and FPARVGI peptide acids and amides. G3(MP2) calculations show that formation of c_{m-2}^- and a diketopiperazine neutral leaving group from a deprotonated peptide amide requires significantly less energy than the analogous process of a deprotonated peptide acid leading to the formation of a diketomorpholine. The presence of a prominent c_{m-2}^- in a negative ion mode CID spectrum is a strong indicator that a peptide has an amide group at the C-terminus. However, in some cases, side chain eliminations can suppress this distinctive fragmentation.

3.6 Supplementary figures

The CID spectra for the peptides in Table 3.1 that were not shown in the body of the chapter appear on the following pages.

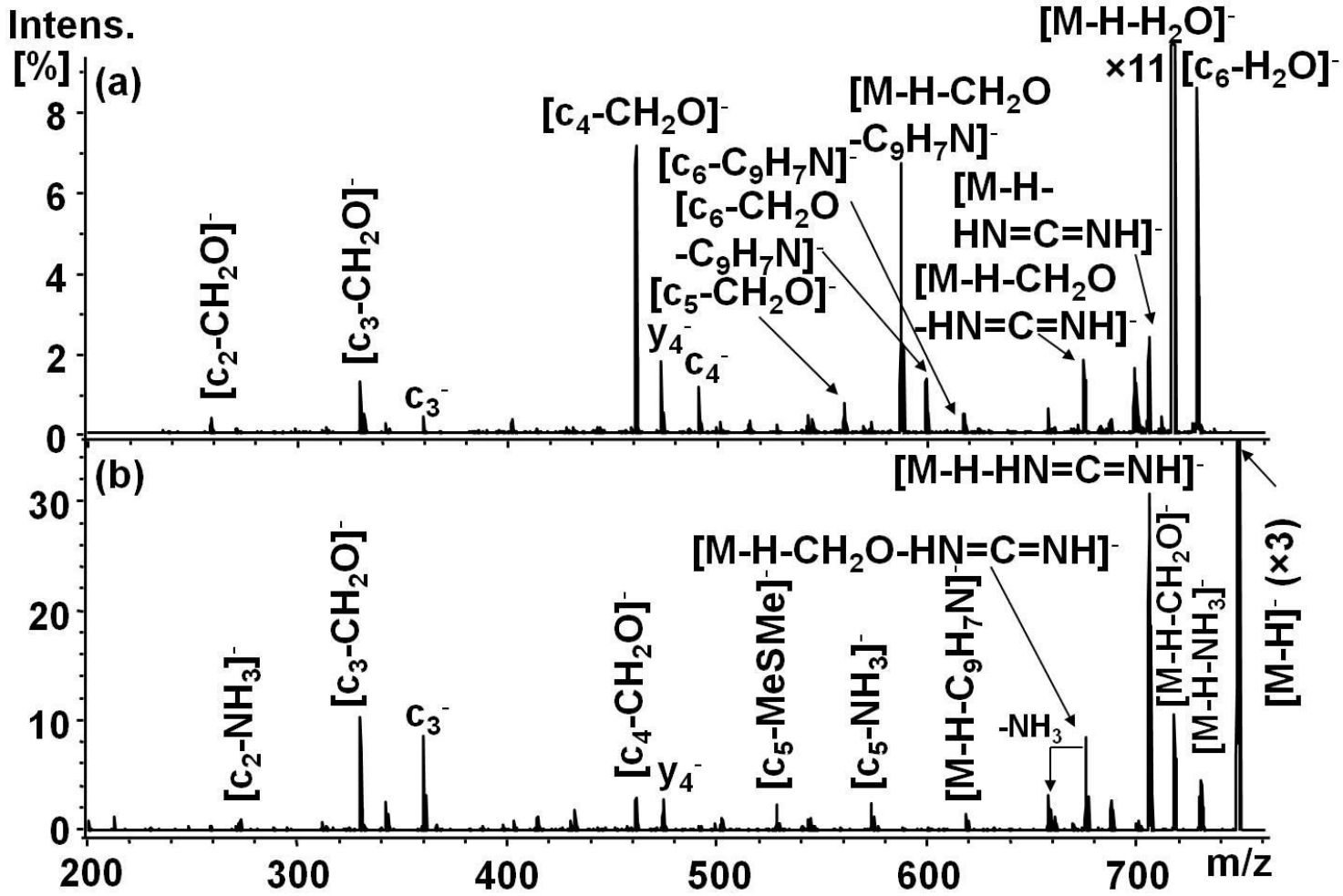

Figure 3.10. CID spectra of $[M - H]^-$ from SWAMVR (a) acid and (b) amide..

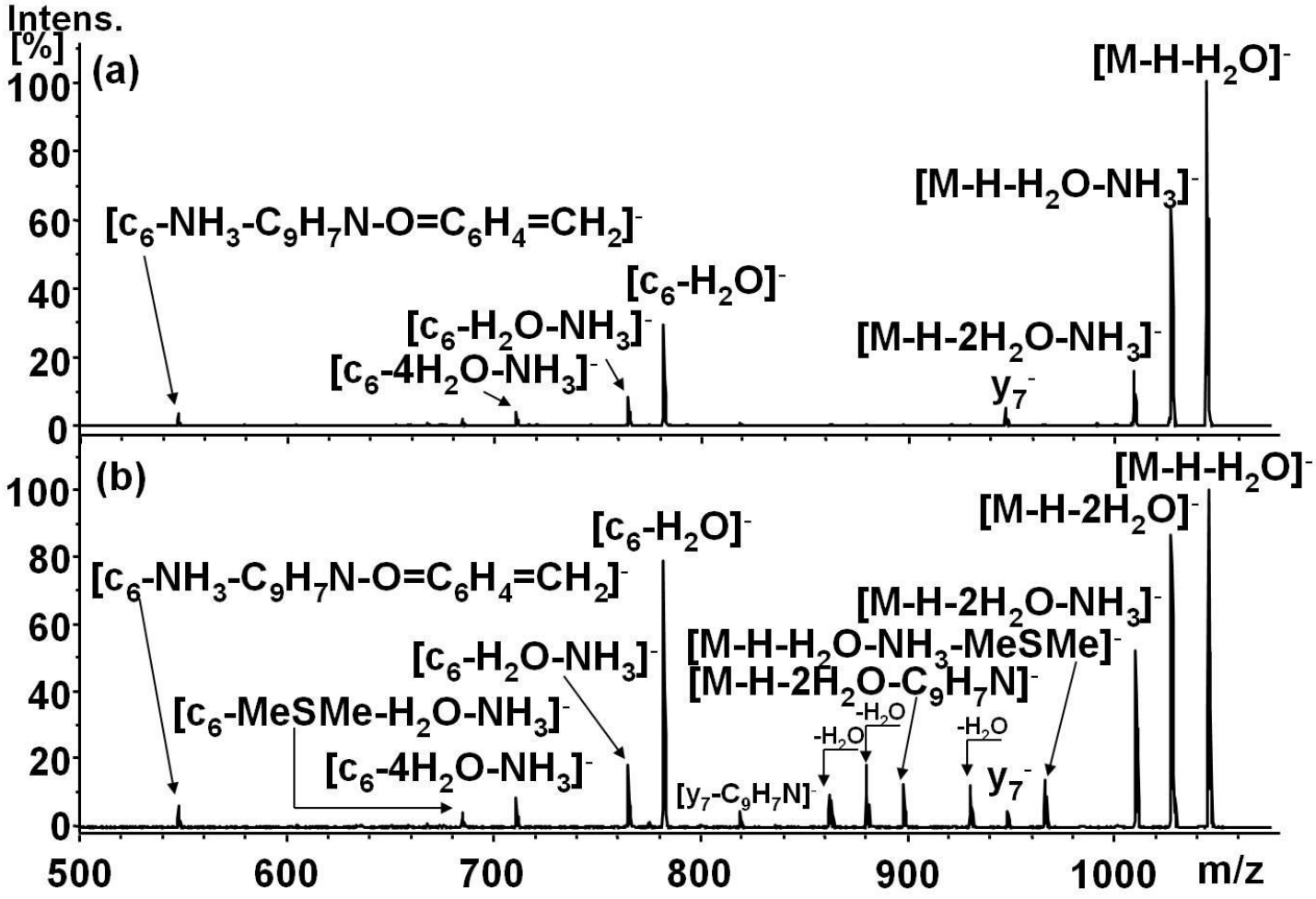

Figure 3.11. CID spectra of $[M - H]^-$ from CCK (a) acid and (b) amide.

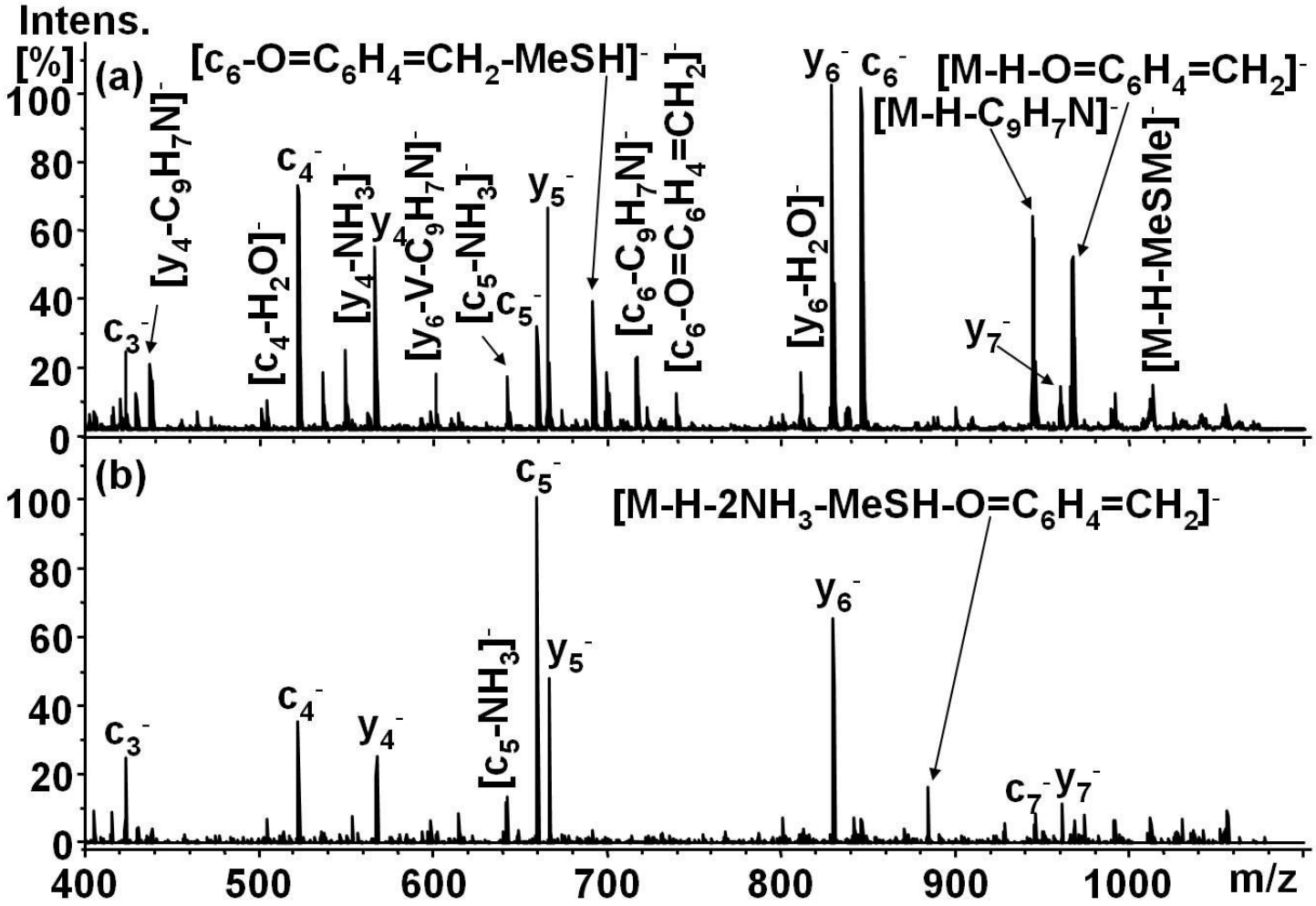

Figure 3.12. CID spectra of $[M - H]^-$ from LMYVHWVK (a) amide and (b) acid.

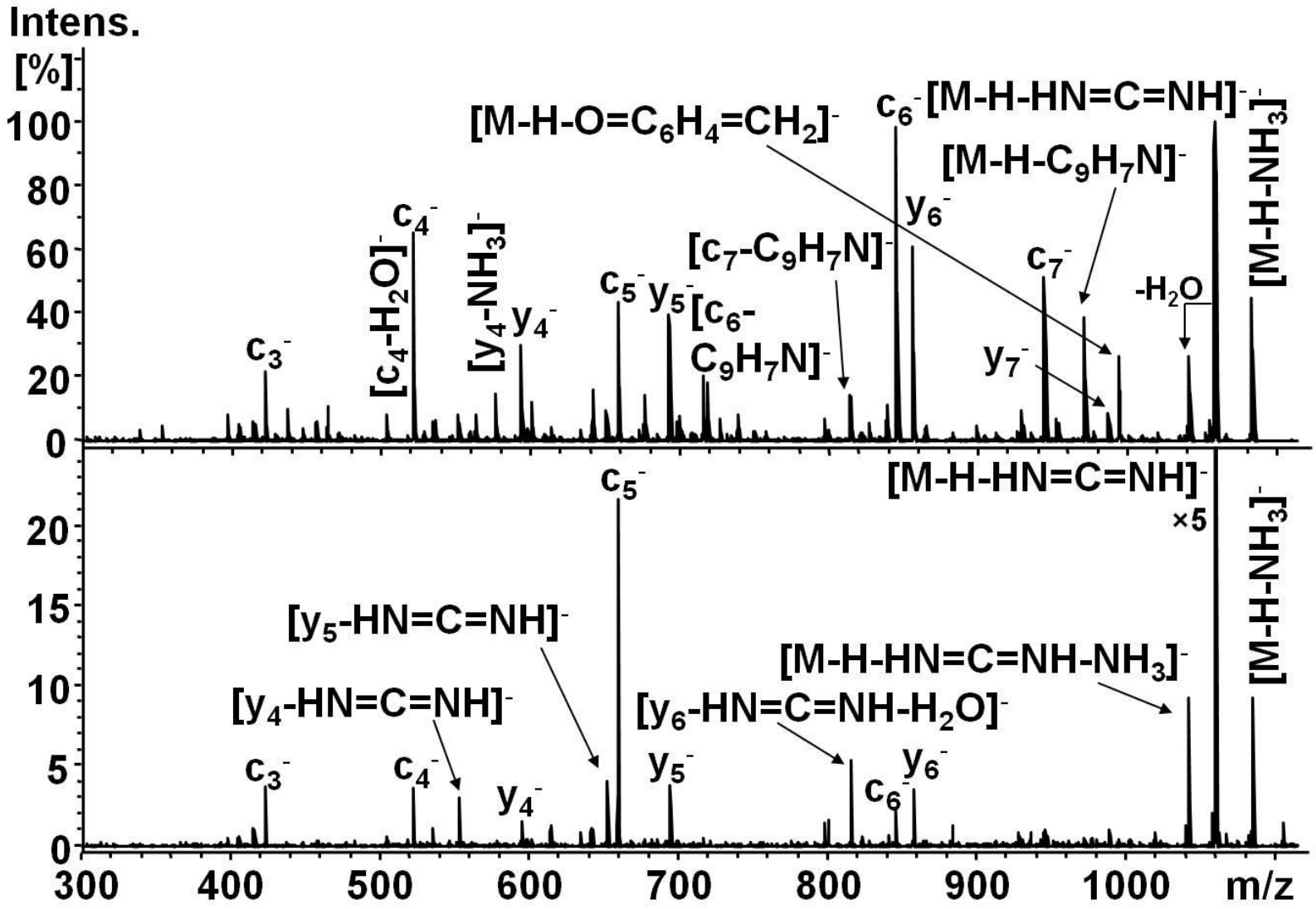

Figure 3.13. CID spectra of $[M - H]^-$ from LMYVHWVR (a) amide and (b) acid.

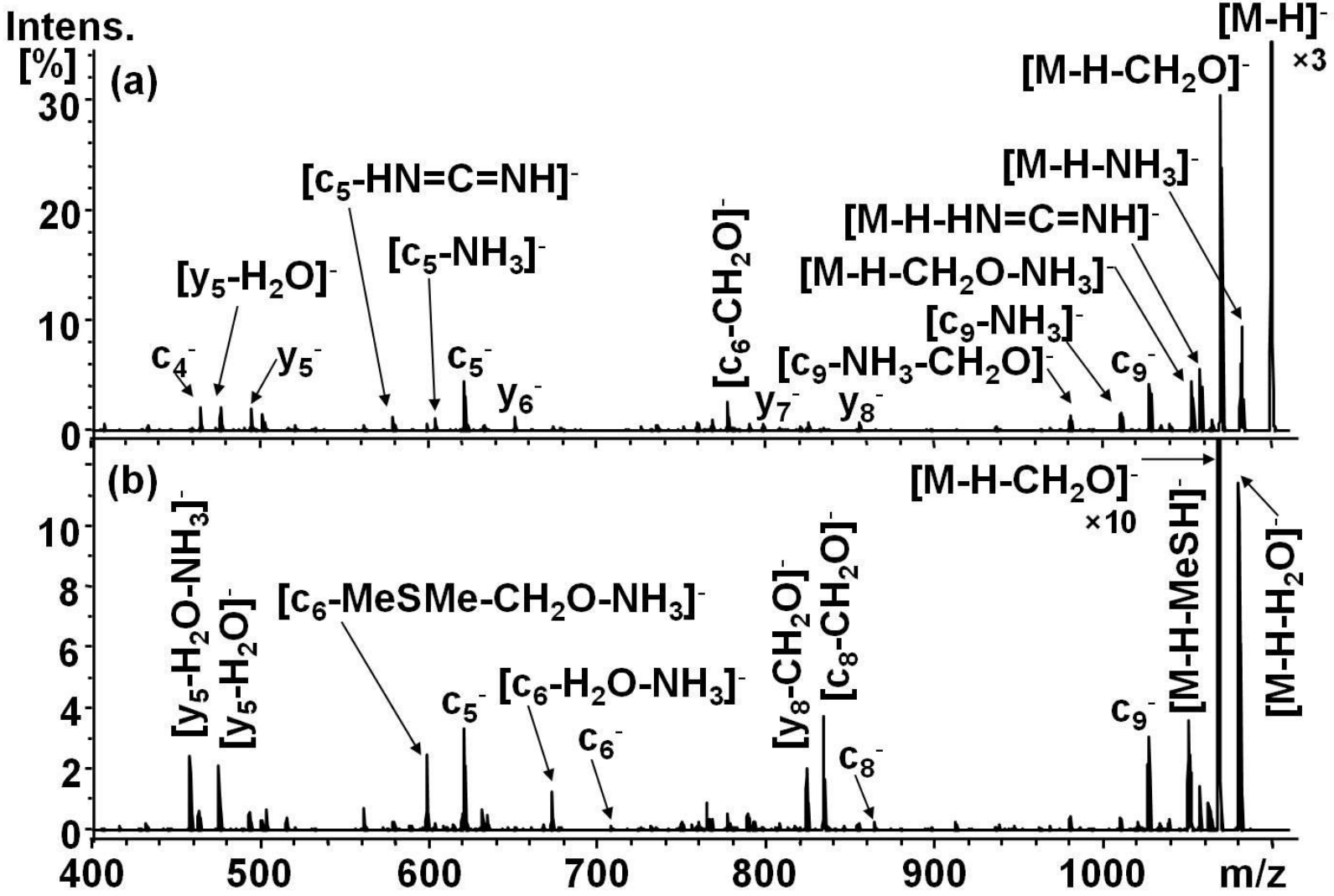

Figure 3.14. CID spectra of $[M - H]^-$ from MLGFRSVGYA (a) amide and (b) acid.

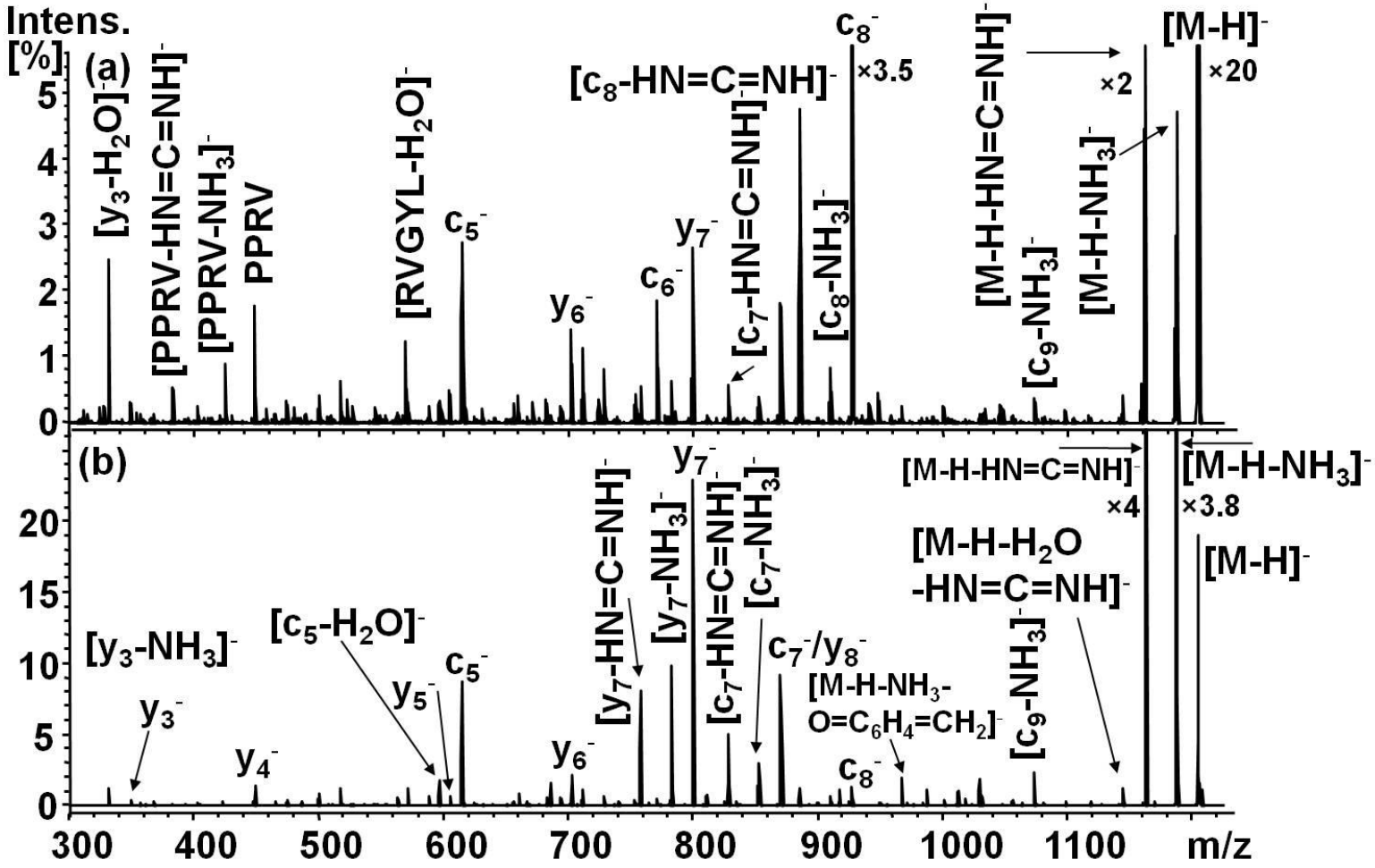

Figure 3.15. CID spectra of $[M - H]^-$ from WFAPPRVGYL (a) amide and (b) acid.

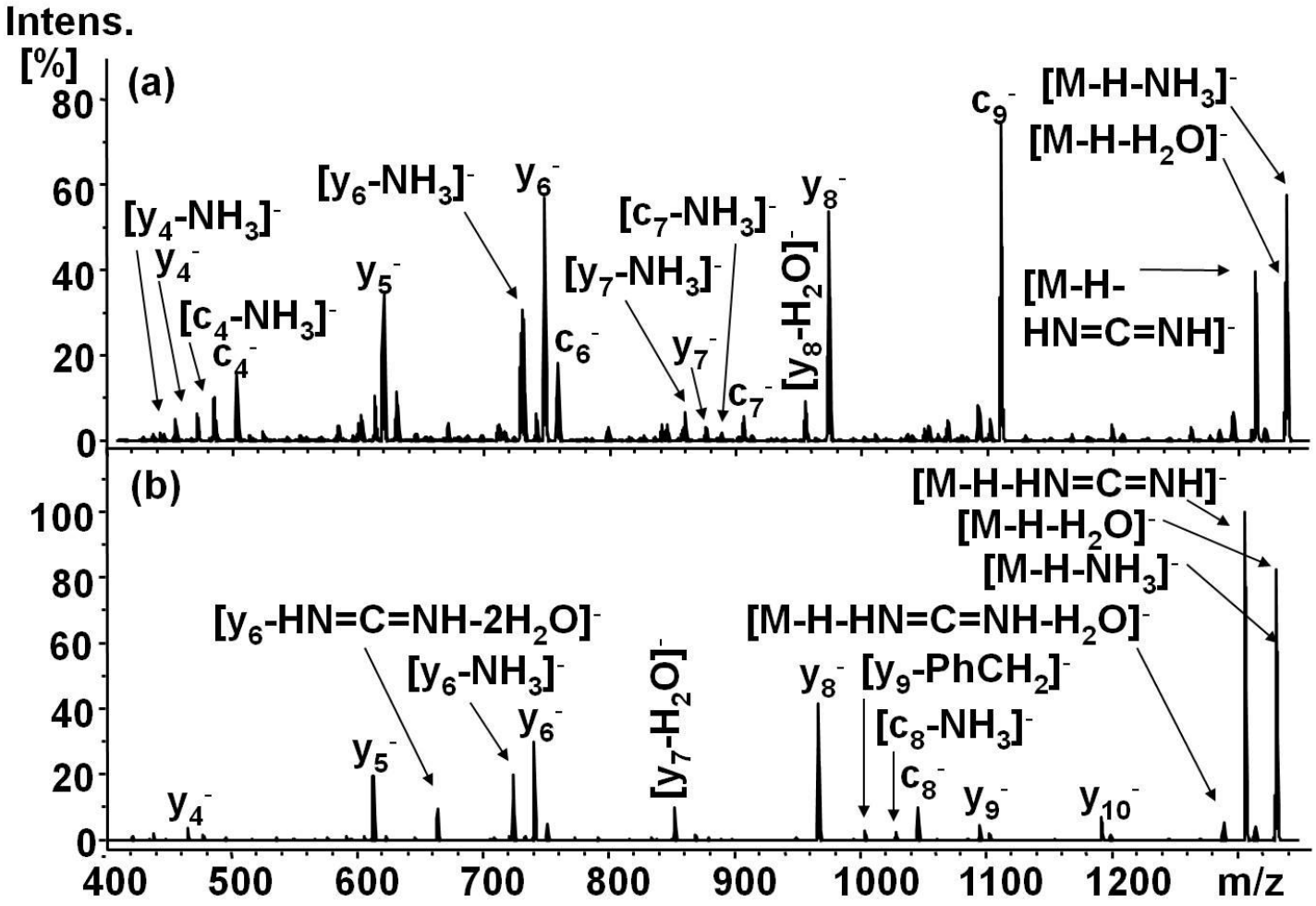

Figure 3.16. CID spectra of $[M - H]^-$ from Substance P (a) amide and (b) acid.

References

1. Ferrier, B. M.; du Vigneaud, V. 9-Deamidooxytocin, an analog of the hormone containing a glycine residue in place of the glycinamide residue. *J. Med. Chem.* **1966**, *9*, 55-57.

2. Rittel, W.; Maier, R.; Brugger, M.; Kamber, B.; Riniker, B.; and Sieber, P. Structure-activity relationship of calcitonin. III. Biological activity of synthetic analogues with shortened or terminally modified peptide chains. *Experientia* **1976**, *32*, 246-248.

3. Morley, J. S. Structure-function relationships in gastrin-like peptides. *Proc. R. Soc. London, B* **1968**, *170*, 97-111.

4. Glass, J. D.; Schwartz, I. L.; Walter, R. Enzymatic inactivation of peptide hormones possessing a C-terminal amide group. *Proc. Natl. Acad. Sci. U. S. A.* **1969**, *63*, 1426-1430.

5. Bradbury, A. F.; Smyth, D. G. Biosynthesis of the C-terminal amide in peptide hormones. *Biosci. Rep.* **1987**, *7*, 907-916.

6. Bradbury, A. F.; Smyth, D. G. Peptide amidation. *Trends Biochem. Sci.* **1991**, *16*, 112-115.

7. Merkler, D. J. C-Terminal amidated peptides: Production by the in vitro enzymatic amidation of glycine-extended peptides and the importance of the amide to bioactivity. *Enzyme Microb. Technol.* **1994**, *16*, 450-456.

8. Von Euler, U. S.; Gaddum, J. H. An unidentified depressor substance in certain tissue extracts. *J. Physiol.* **1931**, *72*, 74-87.

9. Dennison, S. R.; Harris, F.; Bhatt, T.; Singh, J.; Phoenix, D. A. The effect of C-terminal amidation on the efficacy and selectivity of antimicrobial and anticancer peptides. *Mol. Cell. Biochem.* **2009**, *332*, 43-50.

10. du Vigneaud, V.; Ressler, C.; Trippett, S. The sequence of amino acids in oxytocin, with a proposal for the structure of oxytocin. *J. Biol. Chem.* **1953**, *205*, 949-957.

11. Neher, R.; Riniker, B.; Rittel, W. Menschliches calcitonin. III. Struktur von calcitonin M und D. *Helv. Chim. Acta* **1968**, *51*, 1900-1905.

12. Guillemin, R.; Brazeau, P.; Bohlen, P.; Esch, F.; Ling, N.; Wehrenberg, W. Growth hormone-releasing factor from a human pancreatic tumor that caused acromegaly. *Science* **1982**, *218*, 585-587.

13. Ling, N.; Esch, F.; Bohlen, P.; Brazeau, P.; Wehrenberg, W. B.; Guillemin, R. Isolation, primary structure, and synthesis of human hypothalamic somatocrinin: Growth hormone-releasing factor. *Proc. Natl. Acad. Sci. U. S. A.* **1984**, *81*, 4302-4306.

14. Kitamura, K.; Kangawa, K.; Kawamoto, M.; Ichiki, Y.; Nakamura, S.; Matsuo, H.; Eto, T. Adrenomedullin: A novel hypotensive peptide isolated from human pheochromocytoma. *Biochem. Biophys. Res. Commun.* **1993**, *192*, 553-560.

15. Cooper, G. J. S. Amylin compared with calcitonin gene-related peptide: structure, biology, and relevance to metabolic disease. *Endocrinol.* **1994**, *15*, 154-160.

16. Schell, D. A.; Vari, R. C.; Samson, W. K. Adrenomedullin: A newly discovered hormone controlling fluid and electrolyte homeostasis. *Trends Endocrin. Met.* **1996**, *7*, 7-13.

17. Page, N. M.; Bell, N. J.; Gardiner, S. M.; Manyonda, I. T.; Brayley, K. J.; Strange, P. G.; Lowry, P. J. Characterization of the endokinins: Human tachykinins with cardiovascular activity. *Proc. Natl. Acad. Sci. U. S. A.* **2003**, *100*, 6245-6250.

18. Yamazaki, Y.; Mori, Y.; Oda, A.; Okuno, Y.; Kiso, Y.; Hayashi, Y. Acid catalyzed monodehydro-2,5-diketopiperazine formation from N-α-ketoacyl amino acid amides. *Tetrahedron* **2009**, *65*, 3688-3694.

19. Battersby, J. E.; Hancock, W. S.; Canova-Davis, E.; Oeswein, J.; O'Connor, B. Diketopiperazine formation and N-terminal degradation in recombinant human growth hormone. *Int. J. Pept. Protein Res.* **1994**, *44*, 215-222.

20. Goolcharran, C.; Borchardt, R. T. Kinetics of diketopiperazine formation using model peptides. *J. Pharm. Sci.* **1998**, *87*, 283-288.

21. Wang, C.; Yao, J.; Yu, Y.; Shao, X.; Cui, Y.; Liu, H.; Lai, L.; Wang, R. Structure–activity study of endomorphin-2 analogs with C-terminal modifications by NMR spectroscopy and molecular modeling. *Bioorg. Med. Chem.* **2008**, *16*, 6415-6422.

22. Krstenansky, J. L.; Payne, M. H.; Owen, T. J.; Yates, M. T.; Mao, S. J. C-terminal peptide alcohol, acid and amide analogs of desulfato hirudin54-65 as antithrombin agents. *Thromb. Res.* **1989**, *54*, 319-325.

23. Chambers, R. W.; Carpenter, F. H. Ammonolysis of peptides: A method of determining C-terminal amino acids. *J. Am. Chem. Soc.* **1955**, *77*, 1527-1531.

24. Akabori, S.; Ohno, K.; and Narita, K. On the hydrazinolysis of proteins and peptides: A method for the characterization of carboxy-terminal amino acids in proteins. *Bull. Chem. Soc. Jpn.* **1952**, *25*, 214-218.

25. Kim, J.; Kim, K. Identification of the C-terminal amino acid amides by carboxypeptidase Y digestion and fast atom bombardment mass spectrometry. *Biochem. Mol. Biol. Int.* **1994**, *34*, 897-907.

26. Brinkworth, C. S.; Bowie, J. H. Negative ion electrospray mass spectra of the maculatin peptides from the tree frogs *Litoria genimaculata* and *Litoria eucnemis*. *Rapid Commun. Mass Spectrom.* **2003**, *17*, 2215-2225.

27. Mouls, L.; Subra, G.; Aubagnac, J.; Martinez, J.; Enjalbal, C. Tandem mass spectrometry of amidated peptides. *J. Mass. Spectrom.* **2006**, *41*, 1470-1483.

28. Chan, W. C.; White, P. D. In *Fmoc Solid Phase Peptide Synthesis: A Practical Approach;* Oxford University Press: New York, 2000, pp 345.

29. Greene, T. W.; Wuts, P. G. M., Eds.; In *Protective Groups in Organic Synthesis;* John Wiley & Sons, Inc.: New York, 1991.

30. Roepstorff, P.; Fohlman, J. Proposal for a common nomenclature for sequence ions in mass spectra of peptides. *Biomed. Mass Spectrom.* **1984**, *11*, 601.

31. Frisch, M. J.; Trucks, G. W.; Schlegel, H. B.; Scuseria, G. E.; Robb, M. A.; Cheeseman, J. R.; Scalmani, G.; Barone, V.; Mennucci, B.; Petersson, G. A.; Nakatsuji, H.; Caricato, M.; Li, X.; Hratchian, H. P.; Izmaylov, A. F.; Bloino, J.; Zheng, G.; Sonnenberg, J. L.; Hada, M.; Ehara, M.; Toyota, K.; Fukuda, R.; Hasegawa, J.; Ishida, M.; Nakajima, T.; Honda, Y.; Kitao, O.; Nakai, H.; Vreven, T.; Montgomery, J. A. J.; Peralta, J. E.; Ogliaro, F.; Bearpark, M.; Heyd, J. J.; Brothers, E.; Kudin, K. N.; Staroverov, V. N.; Keith, T.; Kobayshi, R.; Normand, J.; Raghavachari, K.; Rendell, A.; Burant, J. C.; Iyengar, S. S.; Tomasi, J.; Cossi, M.; Rega, N.; Millam, J. M.; Klene, M.; Knox, J. E.; Cross, J. B.; Bakken, V.; Adamo, C.; Jaramillo, J.; Gomperts, R.; Stratmann, R. E.; Yazyev, O.; Austin, A. J.; Cammi, R.; Pomelli, C.; Ochterski, J. W.; Martin, R. L.; Morokuna, K.; Zakrzewski, V. G.; Voth, G. A.; Salvador, P.; Dannenberg, J. J.; Dapprich, S.; Daniels, A. D.; Farkas, O.; Foresman, J. B.; Ortiz, J. V.; Cioslowshi, J.; Fox, D. J. Gaussian 09, Revision B.0. **2010**.

32. Becke, A. D. Density-functional thermochemistry. III. The role of exact exchange. *J. Chem. Phys.* **1993**, *98*, 5648-5652.

33. Lee, C.; Yang, W.; Parr, R. G. Development of the Colle-Salvetti correllation energy formula into a functional of the electron density. *Phys. Rev. B* **1988**, *37*, 785-789.

34. Godbout, N.; Salahub, D. R.; Andzelm, J.; Wimmer, E. Optimization of Gaussian-type basis sets for local spin density functional calculations. Part I. Boron through neon, optimization technique and validation. *Can. J. Chem.* **92**, *70*, 560-571.

35. Gutowski, K. E.; Dixon, D. A. Ab initio prediction of the gas- and solution-phase acidities of strong Brønsted acids: The calculation of pK_a values less than -10. *J. Phys. Chem. A* **2006**, *110*, 12044-12054.

36. Stover, M. L.; Jackson, V.; Matus, M.; Adams, M.; Cassady, C. J.; Dixon, D. A. Fundamental thermochemical properties of amino acids: Gas-phase and aqueous acidities and gas-phase heats of formation. *J. Phys. Chem. B.* **2012**, *116*, 2905-2916.

37. Curtiss, L. A.; Redfern, P. C.; Raghavachari, K.; Rassolov, V.; Pople, J. A. Gaussian-3 theory using reduced Moller-Plesset order. *J. Chem. Phys.* **1999**, *110*, 4703-4709.

38. Papayannopoulos, I. A. The interpretation of collision-induced dissociation tandem mass-spectra of peptides. *Mass Spectrom. Rev.* **1995**, *14*, 49-73.

39. Pu, D.; Clipston, N. L.; Cassady, C. J. A comparison of positive and negative ion collision-induced dissociation for model heptapeptides with one basic residue. *J. Mass Spectrom.* **2010**, *45*, 297-305.

40. Harrison, A. G. Sequence-specific fragmentation of deprotonated peptides containing H or alkyl side chains. *J. Am. Soc. Mass Spectrom.* **2001**, *12*, 1-13.

41. Bowie, J. H.; Brinkworth, C. S.; Dua, S. Collision-induced fragmentations of the $(M-H)^-$ parent anions of underivatized peptides: An aid to structure determination and some unusual negative ion cleavages. *Mass Spectrom. Rev.* **2002**, *21*, 87-107.

42. Waugh, R. J.; Eckersley, M.; Bowie, J. H.; Hayes, R. N. Collision induced dissociations of deprotonated peptides: Dipeptides containing serine or threonine. *Int. J. Mass Spectrom. Ion Processes* **1990**, *98*, 135-145.

43. Pu, D.; Cassady, C. J. Negative ion dissociation of peptides containing hydroxyl side chains. *Rapid Commun. Mass Spectrom.* **2008**, *22*, 91-100.

44. Ewing, N. P.; Cassady, C. J. Dissociation of multiply charged negative ions for hirudin (54–65), fibrinopeptide B, and insulin A (oxidized). *J. Am. Soc. Mass Spectrom.* **2001**, *12*, 105-116.

45. Marzluff, E. M.; Campbell, S.; Rogers, M. T.; Beauchamp, J. L. Low-energy dissociation pathways of small deprotonated peptides in the gas phase. *J. Am. Chem. Soc.* **1994**, *116*, 7787-7796.

46. Bradford, A. M.; Waugh, R. J.; Bowie, J. H. Characterization of underivatized tetrapeptides by negative-ion fast-atom bombardment mass spectrometry. *Rapid Commun. Mass Spectrom.* **1995**, *9*, 677-685.

47. Reiter, A.; Teesch, L. M.; Zhao, H.; Adams, J. Gas-phase fragmentations of anionic complexes of serine- and threonine-containing peptides. *Int. J. Mass Spectrom. Ion Processes* **1993**, *127*, 17-26.

48. Waugh, R. J.; Bowie, J. H. A review of the collision-induced dissociations of deprotonated dipeptides and tripeptides. An aid to structure determination. *Rapid Commun. Mass Spectrom.* **1994**, *8*, 169-173.

49. Farrugia, J. M.; O'Hair, R. A. J. Involvement of salt bridges in a novel gas phase rearrangement of protonated arginine-containing dipeptides which precedes fragmentation. *Int. J. Mass Spectrom.* **2003**, *222*, 229-242.

50. Harrison, A. G.; Young, A. B. Fragmentation reactions of deprotonated peptides containing aspartic acid. *Int. J. Mass Spectrom.* **2006**, *255-256*, 111-122.

51. Steinborner, S. T.; Bowie, J. H. The negative ion mass spectra of $[M-H]^-$ ions derived from caeridin and dynastin peptides. Internal backbone cleavages directed through Asp and Asn residues. *Rapid Commun. Mass Spectrom.* **1997**, *11*, 253-258.

52. Li, Z.; Yalcin, T.; Cassady, C. J. C-terminal amino acid residue loss for deprotonated peptide ions containing glutamic acid, aspartic acid, or serine residues at the C-terminus. *J. Mass Spectrom.* **2006**, *41*, 939-949.

53. Waugh, R. J.; Bowie, J. H.; Hayes, R. N. Collision induced dissociations of deprotonated peptides : Dipeptides containing phenylalanine, tyrosine, histidine and tryptophan. *Int. J. Mass Spectrom. Ion Processes* **1991**, *107*, 333-347.

54. Waugh, R. J.; Bowie, J. H.; Gross, M. L. Collision-induced dissociations of deprotonated peptides. Dipeptides containing methionine or cysteine. *Rapid Commun. Mass Spectrom.* **1993**, *7*, 623-625.

55. Pu, D. Mass spectrometric studies of peptide fragmentation and complexes of chromium (III) with acidic peptides. Ph.D. Dissertation, University of Alabama, Tuscaloosa, AL, 2007.

56. Bradford, A. M.; Waugh, R. J.; Bowie, J. H.; Vollmer, D. L.; Gross, M. L. Collision-induced dissociations of deprotonated dipeptide methyl esters containing H, alkyl or benzyl α side-chains. *Int. J. Mass Spectrom. Ion Processes* **1994**, *136*, 143-153.

57. Steinborner, S. T.; Bradford, A. M.; Waugh, R. J.; Bowie, J. H.; Vollmer, D. L.; Gross, M. L. Collision-induced dissociations of deprotonated dipeptide methyl esters containing serine or threonine. *Aust. J. Chem.* **1994**, *47*, 1851-1857.

58. Paizs, B.; Suhai, S.; Hargittai, B.; Hruby, V. J.; Somogyi, Á. Ab initio and MS/MS studies on protonated peptides containing basic and acidic amino acid residues: I. Solvated proton vs. salt-bridged structures and the cleavage of the terminal amide bond of protonated RD-NH_2. *Int. J. Mass Spectrom.* **2002**, *219*, 203-232.

59. Bartmess, J. E. In *Negative Ion Energetics Data;* Linstrom, P. J., Mallard, W. G., Eds.; NIST Chemistry WebBook, NIST Standard Reference Database Number 69; National

Institute of Standards and Technology: Gaithersburg MD, 20899, http://webbook.nist.gov, (retrieved August 2, 2011).

60. Gao, J.; Cassady, C. J. Negative ion production from peptides and proteins by matrix-assisted laser desorption/ionization time-of-flight mass spectrometry. *Rapid Commun. Mass Spectrom.* **2008**, *22*, 4066-4072.

61. Brinkworth, C. S.; Dua, S.; Bowie, J. H. Backbone cleavages of $[M - H]^-$ anions of peptides. Cyclisation of citropin 1 peptides involving reactions between the C-terminal $[CONH]^-$ residue and backbone amide carbonyl groups. A new type of b cleavage: A joint experimental and theoretical study. *Rapid Commun. Mass Spectrom.* **2002**, *16*, 713-721.

62. Tian, Z.; Kass, S. R. Does Electrospray ionization produce gas-phase or liquid-phase structures? *J. Am. Chem. Soc.* **2008**, *130*, 10842.

63. Tian, Z.; Kass, S. R. Gas-Phase versus Liquid-Phase Structures by Electrospray Ionization Mass Spectrometry. *Angew. Chem. Int. Edit.* **2009**, *48*, 1321-1323.

64. Joyce, J.; Richards, D. Kinetic Control of Protonation in Electrospray Ionization. *J. Am. Soc. Mass Spectrom.* **2011**, *22*, 360-368.

65. Cole, R. B. Some tenets pertaining to electrospray ionization mass spectrometry. *J. Mass Spectrom.* **2000**, *35*, 763-772.

66. Fenn, J. B.; Mann, M.; Meng, C. K.; Wong, S. F.; Whitehouse, C. M. Electrospray ionization for mass spectrometry of large biomolecules. *Science* **1989**, *246*, pp. 64-71.

67. Dongre, A. R.; Jones, J. L.; Somogyi, A.; Wysocki, V. H. Influence of peptide composition, gas-phase basicity, and chemical modification on fragmentation efficiency: Evidence for the mobile proton model. *J. Am. Chem. Soc.* **1996**, *118*, 8365-8374.

68. Lunkenheimer, W.; Zahn, H. Peptide, LXXIX1) Merrifield-synthese symmetrischer Cystinpeptide2). *Justus Liebigs Ann. Chem.* **1970**, *740*, 1-17.

69. Gisin, B. F.; Merrifield, R. B. Carboxyl-catalyzed intramolecular aminolysis. Side reaction in solid-phase peptide synthesis. *J. Am. Chem. Soc.* **1972**, *94*, 3102-3106.

70. Khosla, M. C.; Smeby, R. R.; Bumpus, F. M. Failure sequence in solid-phase peptide synthesis due to the presence of an N-alkylamino acid. *J. Am. Chem. Soc.* **1972**, *94*, 4721.

71. Morley, J. E.; Levine, A. S.; Prasad, C. Histidyl-proline diketopiperazine decreases food intake in rats. *Brain Res.* **1981**, *210*, 475-478.

72. Martins, M. B.; Carvalho, I. Diketopiperazines: Biological activity and synthesis. *Tetrahedron* **2007**, *63*, 9923-9932.

73. Bythell, B. J.; Somogyi, A.; Paizs, B. What is the structure of b_2 ions generated from doubly protonated tryptic peptides? *J. Am. Soc. Mass Spectrom.* **2009**, *20*, 618-624.

74. Eckart, K.; Holthausen, M. C.; Koch, W.; Spiess, J. Mass spectrometric and quantum mechanical analysis of gas-phase formation, structure, and decomposition of various b_2 ions and their specifically deuterated analogs. *J. Am. Soc. Mass Spectrom.* **1998**, *9*, 1002-1011.

75. Knapp-Mohammady, M.; Young, A. B.; Paizs, B.; Harrison, A. G. Fragmentation of doubly-protonated Pro-His-Xaa tripeptides: Formation of b_2^{2+} ions. *J. Am. Soc. Mass Spectrom.* **2009**, *20*, 2135-2143.

76. Oomens, J.; Young, S.; Molesworth, S.; van Stipdonk, M. Spectroscopic evidence for an oxazolone structure of the b_2 fragment ion from protonated tri-alanine. *J. Am. Soc. Mass Spectrom.* **2009**, *20*, 334-339.

77. Harrison, A. G.; Siu, K. W. M.; El Aribi, H. Amide bond cleavage in deprotonated tripeptides: a newly discovered pathway to "b_2 ions. *Rapid Commun. Mass Spectrom.* **2003**, *17*, 869-875.

78. Chass, G. A.; Marai, C. N. J.; Setiadi, D. H.; Csizmadia, I. G.; Harrison, A. G. A Hartree-Fock, MP2 and DFT computational study of the structures and energies of "b_2 ions derived from deprotonated peptides. A comparison of method and basis set used on relative product stabilities. *J. Mol. Struc.* **2004**, *675*, 149-162.

79. Harrison, A. G.; Young, A. B. Fragmentation of deprotonated N-benzoylpeptides: formation of deprotonated oxazolones. *J. Am. Soc. Mass Spectrom.* **2004**, *15*, 446-456.

80. Guo, Y.; Cao, S.; Wei, D.; Zong, X.; Yuan, X.; Tang, M.; Zhao, Y. Fragmentation of deprotonated cyclic dipeptides by electrospray ionization mass spectrometry. *J. Mass Spectrom.* **2009**, *44*, 1188-1194.

81. Wabnitz, P. A.; Waugh, R. J.; Eckersley, M. A.; Dua, S.; Blumenthal, T.; Bowie, J. H. The negative ion mass spectra of deprotonated 2,5-diketopiperazines. *Int. J. Mass Spectrom. Ion Processes* **1996**, *154*, 193-201.

82. Hasumi, K.; Shinohara, C.; Iwanaga, T.; Endo, A. Lateritin, a new inhibitor of acyl-CoA:cholesterol acyltransferase produced by Gibberella lateritium IFO 7188. *J. Antibiot.* **1993**, *46*, 1782-1787.

83. Szardenings, A. K.; Burkoth, T. S.; Lu, H. H.; Tien, D. W.; Campbell, D. A. A simple procedure for the solid phase synthesis of diketopiperazine and diketomorpholine derivatives. *Tetrahedron* **1997**, *53*, 6573-6593.

84. Bailey, P. D.; Morgan, K. M. In *Organonitrogen Chemistry;* Oxford Chemistry Primers; Oxford University Press: New York, 1996.

85. Hammond, G. S. A correlation of reaction rates. *J. Am. Chem. Soc.* **1955**, *77*, 334-338.

86. Stewart, J. J. P. Optimization of parameters for semi-empirical methods V: Modification of NDDO approximations and application to 70 elements. *J. Mol. Model.* **2007**, *13*, 1173-1213.

87. Brinkworth, C. S.; Bilusich, D.; Bowie, J. H. The unusual loss of an internal Val residue from the $(M-H)^-$ parent anions of the antimicrobial peptide citropin 1.1 and synthetically modified analogues. Fragmentations which require a specific conformation of the decomposing anion. *Int. J. Mass Spectrom.* **2004**, *236*, 43-53.

88. Bilusich, D.; Bowie, J. H. Fragmentations of $(M-H)^-$ anions of underivatised peptides. Part 2: characteristic cleavages of Ser and Cys and of disulfides and other post-translational modifications, together with some unusual internal processes. *Mass Spectrom. Rev.* **2009**, *28*, 20-34.

89. Jai-nhuknan, J. Post-source decay of negative peptide ions in a matrix-assisted laser desorption/ionization time-of-flight mass spectrometer. Ph.D Dissertation, Miami University, Oxford, OH, 1998.

CHAPTER 4: HYDROGEN RECRUITING IN ELECTRON TRANSFER DISSOCIATION OF PEPTIDES WITH DIFFERENT C-TERMINI

4.1 Overview

Electron transfer dissociation (ETD) was used to study the differences in dissociation between peptides that have identical sequences but different C-termini. Peptides were studied in C-terminal carboxylic acid (-COOH) and amide ($-CONH_2$) forms. No major differences were observed between the analogous peptide pairs; however, several sequence-specific trends were observed. All ETD product ions included either a basic residue (i.e. arginine, histidine, or lysine) or a pseudo-basic residue (e.g. tryptophan). Several instances of an N-terminal product ion with an additional associated hydrogen atom were observed when a basic amino acid residue was adjacent to the cleavage site, suggesting that gas-phase conformation of the precursor ion may promote the addition of a hydrogen atom to these product ions.

4.2 Introduction

Electron-based disscociation techniques such as electron transfer dissociation (ETD) and electron capture dissociation (ECD) are rapidly becoming powerful tools in mass spectrometry. For peptides, ETD and ECD (often collectively referred to as ExD) employ low energy electrons to initiate dissociation, producing primarily $N-C_\alpha$ bond cleavage (i.e. c/z cleavage ions) and S−S bond cleavage with cysteine.[1-5] Fragmentation of this sort is complimentary to that of collision-induced dissociation (CID), which typically produces amide bond cleavage (i.e. b/y cleavage

ions) and numerous types of neutral losses. A recent advance has been to combine ETD and CID, producing what is referred to as ETcaD.[2, 6] In ETcaD, supplemental collisional activation is used to fragment non-dissociated ETD products, increasing the amount of information that can be extracted from an ETD experiment.

Ion formation in ExD is thought to follow one of two mechanistic pathways: the Utah-Washington (UW) mechanism[7-14] or the Cornell mechanism[15] (each named for the developing institutions). Both pathways involve the capture of a low energy electron and subsequent dissociation of the N–C_α bond. The UW mechanism maintains that electron capture is occurring in the π^* orbital of a backbone amide and is stabilized by Coulombic interaction with charged side chains, which results in N–C_α bond dissociation.[7, 12] The low-energy electron may also be captured in one of the high Rydberg states, and then intramolecular transfer of the electron to the π^* orbital results in N–C_α bond cleavages.[7, 12] The Cornell mechanism states that the low-energy electron is captured by a positively-charged side chain of a basic amino acid residue to form a hypervalent species with an odd number of electrons, which results in N–C_α bond cleavage.[15] Both mechanisms tyrpically lead to the formation of c and z• ions (called c″ and z′ using Roepstorff and Fohlman nomenclature), but c• and z ions (c′ and z″) have been reported.[5, 16-19]

Although the ExD techniques are fairly young, numerous performance characteristics have already been established. For example, just as in CID of protonated peptides, basic amino acid residues (i.e. arginine, histidine, and lysine) have been identified as influential participants in ExD behavior. Phosphate groups are retained in the ExD process, allowing for facile determination of the site of phosphorylation.[20, 21] Tureček and coworkers[13, 22, 23] discovered the "arginine anomaly" while studying electron transfer to arginine radicals and small arginine-containing peptide radicals. The presence of an arginine residue tends to sequester hydrogen

atoms, or even promote migration of hydrogen atoms from the alpha carbon to the guanidino group of the arginine side chain. This can limit the observed fragmentation by ExD to side chain losses and arginine-containing fragments. The Tureček group[24-27] also reported the "histidine effect," which is characterized by the presence of two populations of radical cations where a hydrogen atom is transferred from the N-terminus or the C-terminus to the side chain of histidine to form a zwitterionic species. As reported by Tureček and coworkers, the histidine effect is not observed when the C-terminus is an amide group, which indicates that hydrogen bonding is a major factor in the occurrence of unusual zwitterionic conformers. Unpublished work in our group[28] has studied the effect of basic residues (in various positions within a model peptide sequence) on ETD, showing that product ions will almost always contain the basic residue.

C-terminal amide groups are common features of many peptides and proteins, and amide functionalities are present on numerous small organic molecules. As discussed in Chapter 3, these amide-containing species have been included in numerous mass spectrometry studies. However, few studies have focused on the effect of this characteristic on mass spectra. Enjalbal and coworkers[29] reported a comprehensive study of numerous analogous C-terminal acid and amide peptide pairs using CID of protonated species. They observed increased occurrence of ammonia loss in the CID spectra of the C-terminal amides, but this was the only major feature that differentiated the two analogous species. Tureček and coworkers[24-26] found that the identity of the C-terminus (carboxylic acid versus amide) has an effect on ETD fragmentation along the peptide backbone. Specifically, they observed an isomerization that is initiated by H-migration from a free carboxyl group to the imidazole ring of a histidine. Conversion of the C-terminus to an amide eliminated the isomerization.

Backbone amide groups are potential charge sites for protonated peptides. (In particular, experimental and computational work by Cassady and coworkers[30, 31] has shown that, aside from the N-terminal amino group, the amide carbonyl oxygen is the most basic site on a peptide backbone.) Amide protonation is a basis for the "mobile proton model" of Wysocki and coworkers,[32, 33] in which protonated peptides undergo charge-directed cleavage alone the backbone after ion activation causes movement of an ionizing proton to backbone amide sites. Prior work by McLuckey and coworkers[34] addressed the effect of methylation of backbone amide sites in ETD. They reported that the backbone amide-methylated peptides behaved identically to the non-methylated peptides in ETD.

The work discussed in this chapter specifically targets the effect that changing the C-terminus has on the resulting ETD spectrum. Though ExD techniques are radical driven in nature (due to the electron transfer/capture process), it is plausible that the amide groups play a similar role as in the mobile proton model, allowing the hydrogen atom to move freely along the backbone. Presence of an amide site on the C-terminus could behave as a basic site, increasing the occurrence of C-terminal ETD fragments (i.e. z-type product ions). C-terminal amides can also affect the hydrogen bonding motifs within a peptide structure, which has been reported[35, 36] to affect dissociation.

4.3 Experimental

4.3.1 Peptides

Substance P, cholecystokinin free acid, and laminin were purchased from Anaspec (San Jose, CA). Cholecystokinin amide was purchased from American Peptide (Sunnyvale, CA). The remaining peptides (FPARVGI, MLGFRSVGYA, WFAPPRGYL, SWAMVR,

LMYVHWVR, and LMYVHWVK) were a generous gift from Christine Enjalbal at the University of Montpellier (Montpellier, France). Peptides were used without further purification. Stock solutions were prepared for each peptide at ~1 mg/mL in ultrapure water. Samples were prepared for analysis by diluting the stock solutions to 2 μM in 50:50 (V:V) acetonitrile and ultrapure water, with a 1% spike of acetic acid to aid in ion formation.

4.3.2 Mass spectrometry

Electron-transfer dissociation experiments were performed using a Bruker HCTUltra PMT Discovery System (Billerica, MA, USA) high capacity quadrupole ion trap equipped with electrospray ionization (ESI). Peptide samples were introduced to the ESI source using a KD Scientific (Holliston, MA) syringe pump with a flow rate of 100-150 μL/min. Ions were produced by ESI using a spray voltage of ~ -4000 V. The nitrogen drying gas was held at a temperature of ~220°C and a flow rate of 5 L/min. Nitrogen was also used as the ESI nebulizer gas at 10 psi. Ions were transferred to the QIT using an octopole ion guide, and the multiply-charged ions of interest were m/z-selected for isolation.

Fluoranthene, which was used as the ETD reagent to transfer a low-energy electron to the multiply-charged ions, was produced using a negative chemical ionization (nCI) source. Fluoranthene was then transferred to the QIT and allowed to react with the isolated precursor ion. Each spectrum is the average of ~200 scans.

4.3.3 Nomenclature

Standard peptide fragmentation nomenclature introduced by Roepstorff and Fohlman[37] is used. The ETD nomenclature introduced in 2003 by Zubarev[17] is not used to describe this work.

The Zubarev modification of the peptide fragmentation nomenclature accounts for radical location and hydrogen transfer. Two types of ions are described using the Zubarev nomenclature: radical products, $c_n^{+\bullet}$ and $z_n^{+\bullet}$, and hydrogen-atom transfer products, $z_n'^{+}$ and $c_n'^{+}$. These ions are called $c_n'^{+}$ and $z_n'^{+}$, and $c_n''^{+}$ and $z_n''^{+}$ (respectively) using the Roepstorff and Fohlman nomenclature. Radical product ions are one mass unit higher than standard homolytic bond cleavage, and hydrogen-atom transfer product ions are two mass units higher. The results described here are characterized by the number of hydrogens that are associated with the ETD fragment ions, thus the standard peptide fragmentation nomenclature is more suitable for keeping track of the additional hydrogens rather than using the aforementioned Zubarev nomenclature. Use of the standard nomenclature also allows the ETD studies discussed in this chapter to be more directly comparable to the results of the CID studies on many of these same peptides, which are discussed in Chapter 3.

4.4 Results and discussion

ETD was performed for each of the peptides listed in Table 4.1. The $[M+2H]^{2+}$ ion was selected for isolation from the profile spectrum and subsequently allowed to react with the fluoranthene ETD reagent for 40-100 ms, producing predominantly $N-C_\alpha$ bond cleavage products. Upon comparing the spectra produced from the ETD experiments, there were few variations observed between the free acid and amide peptides. Table 6.1 shows c- and z- ions observed for each of the peptides in the ETD spectra of $[M + 2H]^+$ as well as *m/z* of the precursor ion. Not all of the peptides undergo triple protonation by ESI. For the peptides that do, ETD of $[M + 3H]^+$ are discussed individually. The peptides are grouped below with respect to presence and location of a basic residue in the peptide's amino acid sequence.

Table 4.1. Peptide sequences, *m/z* of $[M+2H]^{2+}$, and observed c/z cleavages.

	m/z[1] of $[M+2H]^{2+}$		Observed ETD fragment ions	
	amide	free acid	amide	free acid
No Basic Residues				
Cholecystokinin, CCK (DYMGWMDF)	532.2	532.7	$c_4'^{+}$, $c_n''^{+}$ (n = 5 - 7) $z_n'^{+}$ (n = 4 - 7)	$c_4'^{+}$, $c_n''^{+}$ (n = 5 - 7) $z_n'^{+}$ (n = 4 - 7)
N-terminal Basic Residue				
Substance P (RPKPQQFFGLM)	674.4	674.9	$c_n''^{+}$ (n = 2, 4 - 10) $z_n'^{+}$ (n = 9)	$c_n''^{+}$ (n = 2, 4 - 10) $z_n'^{+}$ (n = 9)
Central Basic Residue				
FPARVGI	379.7	380.2	$c_n''^{+}$ (n = 4 - 6) $z_n'^{+}$ (n = 4 - 5)	$c_n''^{+}$ (n = 4 - 6) $z_n'^{+}$ (n = 4 - 5)
MLGFRSVGYA	550.3	550.8	$c_n'^{+}$ (n = 5 - 7), $c_n''^{+}$ (n = 5 - 9) $z_n'^{+}$ (n = 6 - 10), $z_n''^{+}$(n = 6 - 10)	$c_n'^{+}$ (n = 5 - 7), $c_n''^{+}$ (n = 5 - 9) $z_n'^{+}$ (n = 6 - 10), $z_n''^{+}$(n = 6 - 10)
WFAPPRVGYL	602.8	603.3	$c_n'^{+}$ (n = 6 - 7), $c_n''^{+}$ (n = 6 - 9) $z_n'^{+}$(n = 5, 8 - 9), $z_n''^{+}$,(n = 5, 8 - 9)	$c_n'^{+}$ (n = 6 - 7), $c_n''^{+}$ (n = 6 - 9) $z_n''^{+}$(n = 5, 8 - 9), $z_n''^{+}$(n = 5, 8 - 9)
C-terminal Basic Residue				
Laminin (YIGSR)	297.7	298.2	$z_n'^{+}$ (n = 2 - 5)	$z_n'^{+}$ (n = 2 - 5)
SWAMVR	374.7	375.2	$z_n'^{+}$ (n = 2 - 6), $z_1''^{+}$	$z_n'^{+}$ (n = 2 - 6), $z_1''^{+}$
C-terminal and Central Basic Residues				
LMYVHWVR	551.8	552.3	$c_7'^{+}$ $z_n'^{+}$ (n = 5 - 7), $z_n''^{+}$(n = 3 - 4)	$c_7'^{+}$ $z_n'^{+}$ (n = 5 - 7), $z_n''^{+}$(n = 3 - 4)
LMYVHWVK	537.8	538.3	$c_5'^{+}$, $c_n''^{+}$ (n = 5 − 7) $z_n'^{+}$(n = 4 - 7), $z_n''^{+}$ (n = 4 - 7)	$c_5'^{+}$, $c_n''^{+}$ (n = 5 - 7) $z_n'^{+}$(n = 4 - 7), $z_n''^{+}$ (n = 4 - 7)

[1] Units of *m/z* are Thomson.

4.4.1 Peptides without a basic residue

4.4.1.1 Cholecystokinin (CCK) peptides (DYMGWMDF)

The ETD spectra for the $[M+2H]^{2+}$ C-terminal amide and acid forms of CCK can be seen in Figure 4.1. CCK is the only peptide in this study that does not contain a basic residue. ETD of both species produces C-terminal and N-terminal backbone fragmentation. All of the observed C-terminal fragments include the tryptophan residue (W, residue 5) and are $z_n'^{+}$ type ions. The observed N-terminal product ions begin with cleavages N-terminal to tryptophan residue and extend to the C-terminus. The $c_4'^{+}$ ion is the only product ion that does not contain the tryptophan residue. Interestingly, this ion also has only one added hydrogen whereas the other c-ions are of the $c_n''^{+}$ variety. In the ETD spectrum of CCK amide, $c_5''^{+}$ is the most abundant product ion in the spectrum and $c_7''^{+}$ is very close in intensity. The $c_5''^{+}$ cleavage is C-terminal to tryptophan. The $c_7''^{+}$ ion is the most abundant product ion in the ETD spectrum of the peptide acid of CCK, but $c_5''^{+}$ is more abundant than the remainder of product ions in the spectrum. Both spectra contain *m/z* 653, and could be attributed to loss of NH_3 from $c_5''^{+}$ or formation of b_5^{+}. The ETD spectrum of the peptide amide also contains an abundant $a_8'^{+}$ ion. This ion is not nearly as abundant in the peptide acid spectrum.

McLafferty and coworkers[38] reported that ECD cleavage C-terminal to a tryptophan residue is five times more abundant than other observed cleavages due to the high hydrogen-atom ($H^{\bullet}$) affinity of the 9-methylindole functionality on tryptophan. The $c_4'^{+}$ ion from CCK does not incorporate the tryptophan residue, and has one less hydrogen than the other c-type ions. In this case, the lack of the high hydrogen ($H^{\bullet}$) affinity from the tryptophan side chain results in an N-terminal product ion with one less hydrogen. In effect, the tryptophan behaves as a pseudo-basic residue in CCK (there are no "real" basic residues (e.g. Arg, His, Lys) in the

peptide sequence). Tryptophan is the fourth most basic amino acid residue (GB = 219.0 kcal/mol),[39] thus it will be referred to as a pseudo-basic residue. The abundant $c_7''^+$ in both ETD spectra of the CCK peptides is a $c_{m-1}''^+$ type ion (m is the number of residues in the peptide sequence), where the neutral product incorporates the C-terminal residue. Wysocki and coworkers[40] recently reported a statistical analysis of the ETD spectra of thousands of peptides, where loss of the C-terminal residue to produce c_{n-1} (where n = number of residues in the peptide sequence) is very abundant in all of the spectra of lower-charged peptides (charge of $\leq$+3), regardless of the C-terminal residue identity. These researchers concluded that the secondary structure of the precursor ion is the main reason for the formation of c_{n-1}. The c_{n-1}^- ion was not nearly as abundant in ETD of peptides with higher charge states ($\geq$+4). Wysocki and coworkers also observed increased cleavage C-terminal to several amino acids that are present in peptide sequences related to this chapter (i.e. histidine, arginine, glutamine, and tryptophan).

Minor production of *m/z* 653 is observed in both CCK spectra (not labeled), and is considered to be loss of NH_3 from $c_5''^+$ or formation of b_5^+. Liu and Hakansson[41] included CCK amide in a study on ECD of peptides that do not possess amino acids. They observed a very different ECD spectrum for CCK amide than the ETD spectrum discussed here; b_5^+ was observed as the most abundant product ion. Other spectral differences included presence of several moderately abundant b- and y- ions in the ECD spectrum. This suggests that the ECD and ETD processes may differ for peptides that do not possess typical basic residues (e.g. Arg, His, Lys). The $a_8'^+$ ion produced in the ETD spectrum of CCK amide is a 44 Da loss from $[M + H]^+$. This ion could result from elimination of CO_2 from the side chain of aspartic acid and/or elimination of $CONH_2$ from the C-terminus.

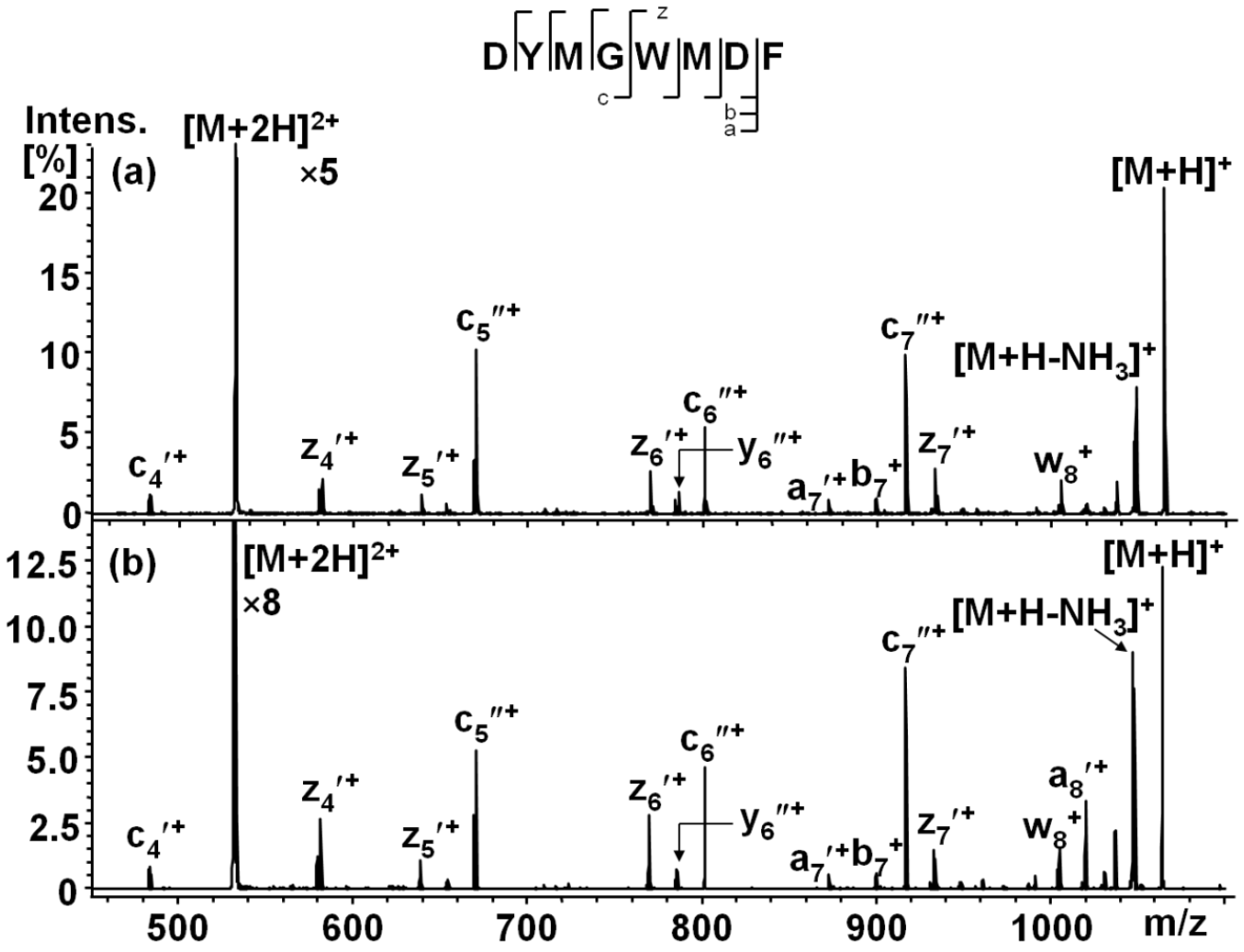

Figure 4.1 ETD spectra of $[M + 2H]^{2+}$ from CCK (a) acid and (b) amide.

4.4.2 Peptides with an N-terminal basic residue

4.4.2.1 Substance P peptides (RPKPQQFFGLM)

Substance P contains a basic arginine (R) residue at the N-terminus and a basic lysine residue (K) at position 3. The ETD spectra of $[M+2H]^{2+}$ and $[M+3H]^{3+}$ from substance P can be seen in Figures 4.2 and 4.3, respectively. The ETD spectra of $[M+2H]^{2+}$ for the substance P analogs both contain 8 of 8 possible c-ions. Both c_2 and c_3 would require cleavage of two bonds (due to the presence of proline), which is typically considered unfeasible[42]; therefore, only 8 c-ions are possible even though the peptide has 11 residues. All are $c_n''^{+}$ type ions (rather than $c_n'^{+}$ ions), which is likely due to the charge-sequestering arginine at the N-terminus and the basic N-terminal amino group. This means that the high basicity of arginine and the N-terminus promote the addition of two additional hydrogens to the c- cleavage site. (Formation of $c_n'^{+}$ will be discussed later.) The ECD spectrum of $[M + 2H]^{2+}$ from substance P amide has been previously reported, and the same backbone cleavages were observed.[19, 43]

The C-terminal backbone fragment $z_9'^{+}$ is present as the only C-terminal product ion in the ETD spectra of the substance P analogs that contains a basic residue (residue 3, K). Loss of the C-terminal residue (as previously discussed in the CCK section), to produce $c_{10}''^{+}$, is also observed for both substance P analogs. Two differentiating features are observed for substance P acid and amide related to $c_9''^{+}$ and $a_{10}'^{+}$.

The $c_9''^{+}$ ion is approximately 50% relative to the base peak in the peptide acid spectrum, whereas the same ion is only 25% relative to the base peak in the peptide amide spectrum. A potential explanation is that the gas-phase conformation of the peptide acid is more amenable to cleavage of this bond. Substance P is composed mainly of amino acid residues that have rather bulky side chains. The glycine residue (residue 9, G) is the smallest, possessing a hydrogen side

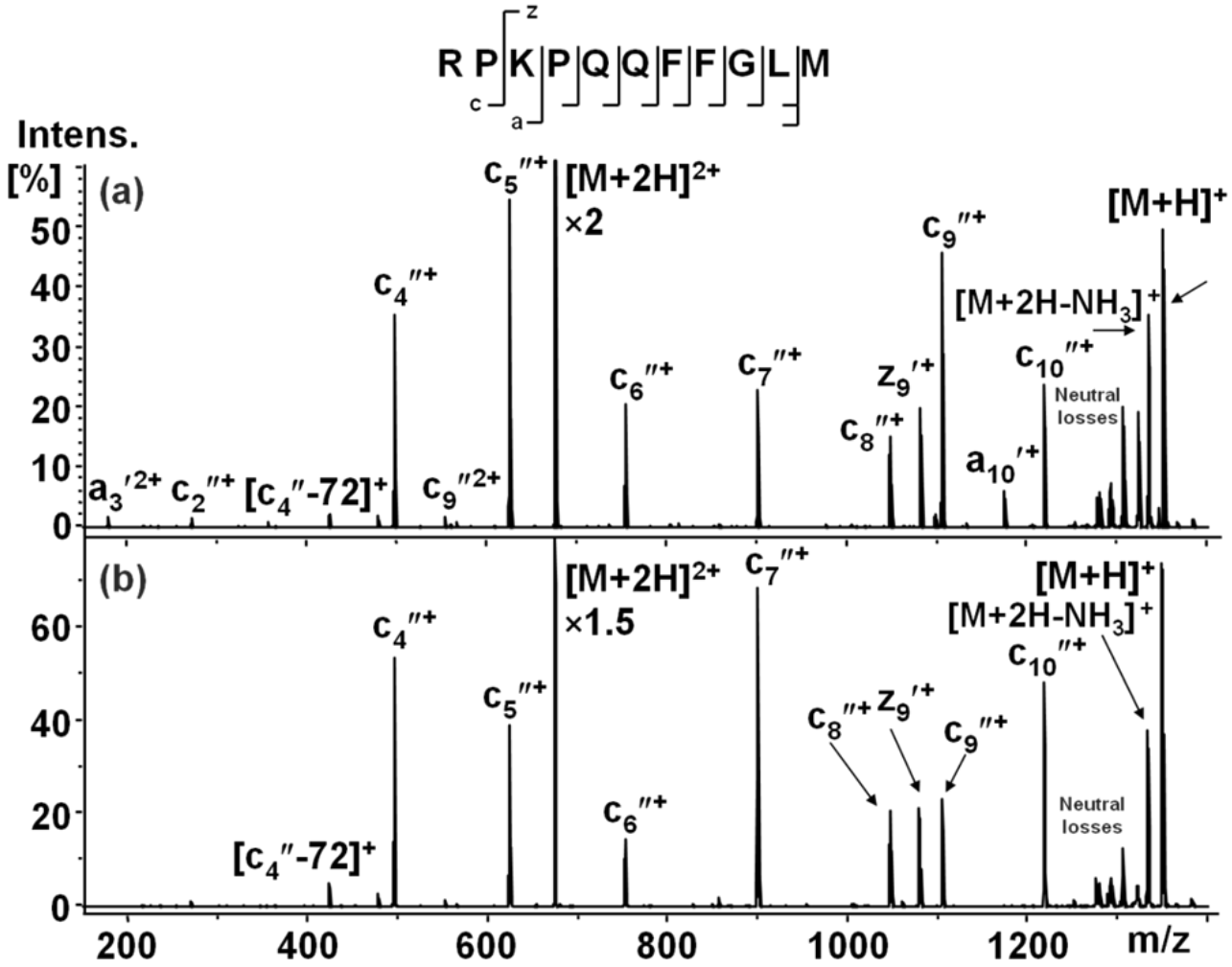

Figure 4.2. ETD spectra of $[M + 2H]^{2+}$ from substance P (a) acid and (b) amide. The label "neutral losses" refers to typical side chain losses like those from arginine, as well as other neutral losses such as water.

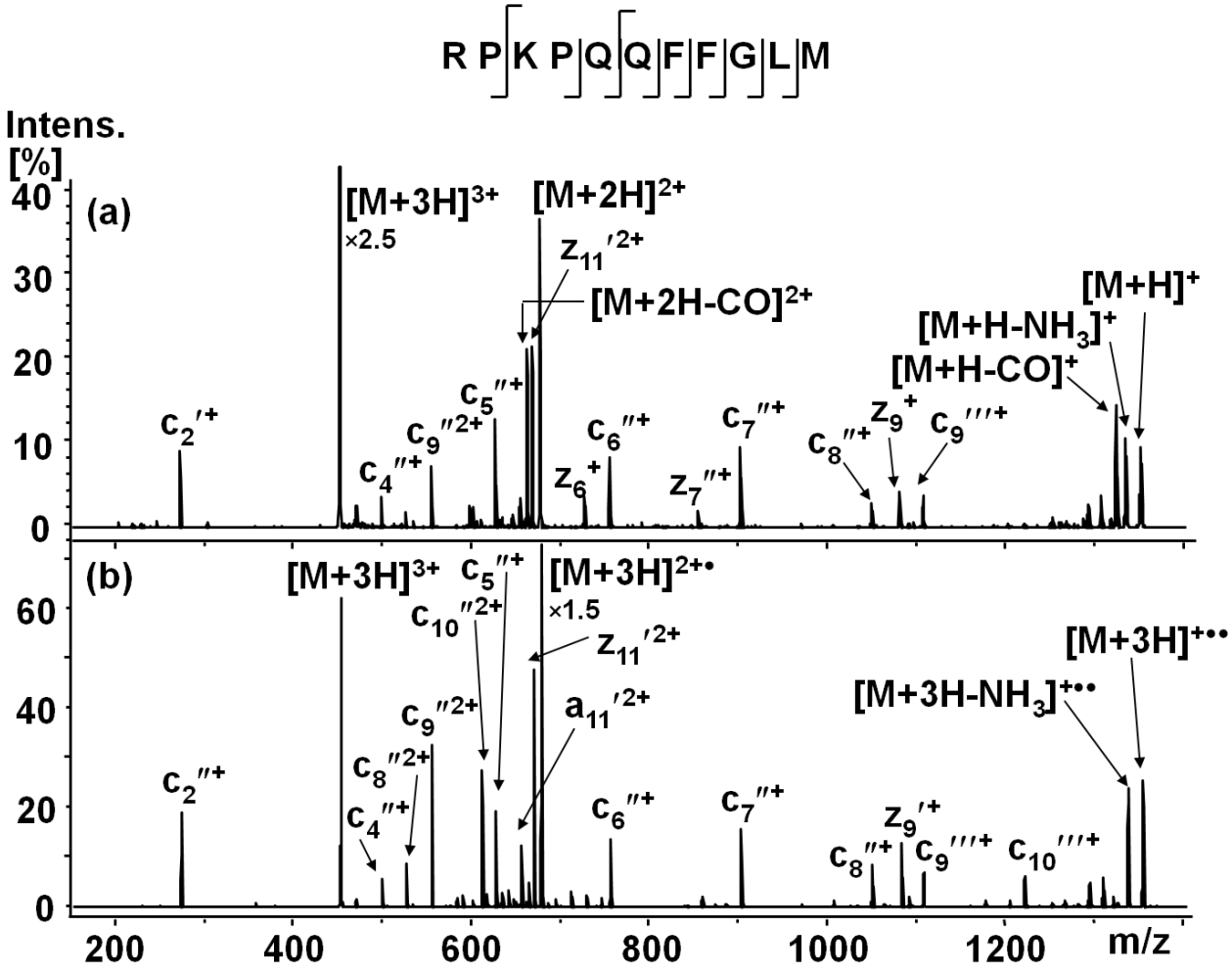

Figure 4.3. ETD spectra of $[M + 3H]^{3+}$ from substance P (a) amide and (b) acid.

chain. Hydrogen bonding involving the C-terminal carboxylic acid group could weaken the N–C_α bond between Gly_9 and Leu_{10}, increasing the probability of forming enhanced $c_9''^+$. Both carboxylic acid and amide functional groups can behave as the proton donor and acceptor in hydrogen bonding.[44] The carbonyl oxygen of an amide, however, has increased basicity since an additional oxygen is not present as it is in the carboxylic acid.[45] This slight difference in carbonyl oxygen basicity can alter the hydrogen-bonding pattern between carboxylic acid- and amide-containing peptides considerably.

The second feature that distinguishes the ETD of the peptide acid from the peptide amide is presence of $a_{10}'^+$ produced by cleavage of the C_α–C bond between Leu_{10} and Met_{11}. Production of this product ion likely stems from loss of $CONH_2$ from $c_{10}''^+$. Formation of $c_{10}''^+$ cleaves the N–C_α bond between Leu_{10} and Met_{11}. Thus, $CONH_2$ can be easily eliminated from the product ion. Production of $c_{10}''^+$ is also observed for substance P amide, yet $a_{10}'^+$ is not produced, so there must be another unexplored pathway for enhanced $a_{10}'^+$ formation in substance P amide.

Substance P contains three highly basic sites (i.e., the N-terminal amino group and the side chains of the arginine, R, and lysine, K, residues) and can therefore be triply protonated by ESI. The ETD spectra of $[M+3H]^{3+}$ for the substance P peptides can be seen in Figure 4.3. Singly- and doubly-charged product ions form. All of the product ions observed in ETD of $[M+2H]^{2+}$ are in these spectra as well, with the exception of c_{10} in the peptide amide. It is interesting to note that c_9 from both peptides is 3 Da higher in mass than the species resulting from cleavage of the N–C_α bond of Gly_8–Leu_9, which indicates that this singly-charged product ion has three added hydrogens. The c_{10} ion observed in the peptide acid spectrum also seems to have three added hydrogens. This type of product ion has not been previously reported, so

another pathway must be considered. A potential explanation is that the peak ($c_{10}'''^{+}$) results from elimination of leucine from the singly-charged peptide, $[M + H - Leu]^{+}$, which has the same nominal mass as $c_{10}'''^{+}$. Loss of a leucine residue (113 Da) was previously reported in the ECD of cyclic peptides.[46] Loss of an internal valine residue in CID of deprotonated peptides has also been reported[47, 48] and was previously discussed in Chapter 3. Loss of the C-terminal residue to produce c_{n-1} is observed in both ExD and CID techniques.[40, 49]

4.4.3 Peptides with a centrally located basic residue

4.4.3.1 FPARVGI peptides

FPARVGI contains a highly basic arginine (R) amino acid residue in position 4. The ETD spectra of the $[M+2H]^{2+}$ species for FPARVGI can be seen in Figure 4.4. The spectra for the peptide acid and peptide amide are essentially identical. All of the observed product ions contain the highly basic arginine residue. Each of the c-ions ($c_n''^{+}$, n = 4-6) have two additional hydrogens. These ions are likely protonated on the N-terminus and the arginine residue. The N-terminal ions $a_4'^{+}$ and $a_6'^{+}$ are also present. These ions represent cleavage of the C_α–C bonds between Arg_4–Val_5 and Gly_6–Ile_7. The C-terminal ions $z_4'^{+}$ and $z_5'^{+}$ have only one additional hydrogen; this is consistent with the second site of protonation being the N-terminal amino group. The presence of proline in the peptide sequence also explains why $z_6'^{+}$ is not observed because production of this ion would require breaking two bonds along the peptide backbone. C-terminal residue loss is abundant in both spectra. However, $c_4''^{+}$ is the most abundant product ion in the ETD of the peptide amide, resulting from cleavage of the N–C_α bond of Arg_4–Val_5.

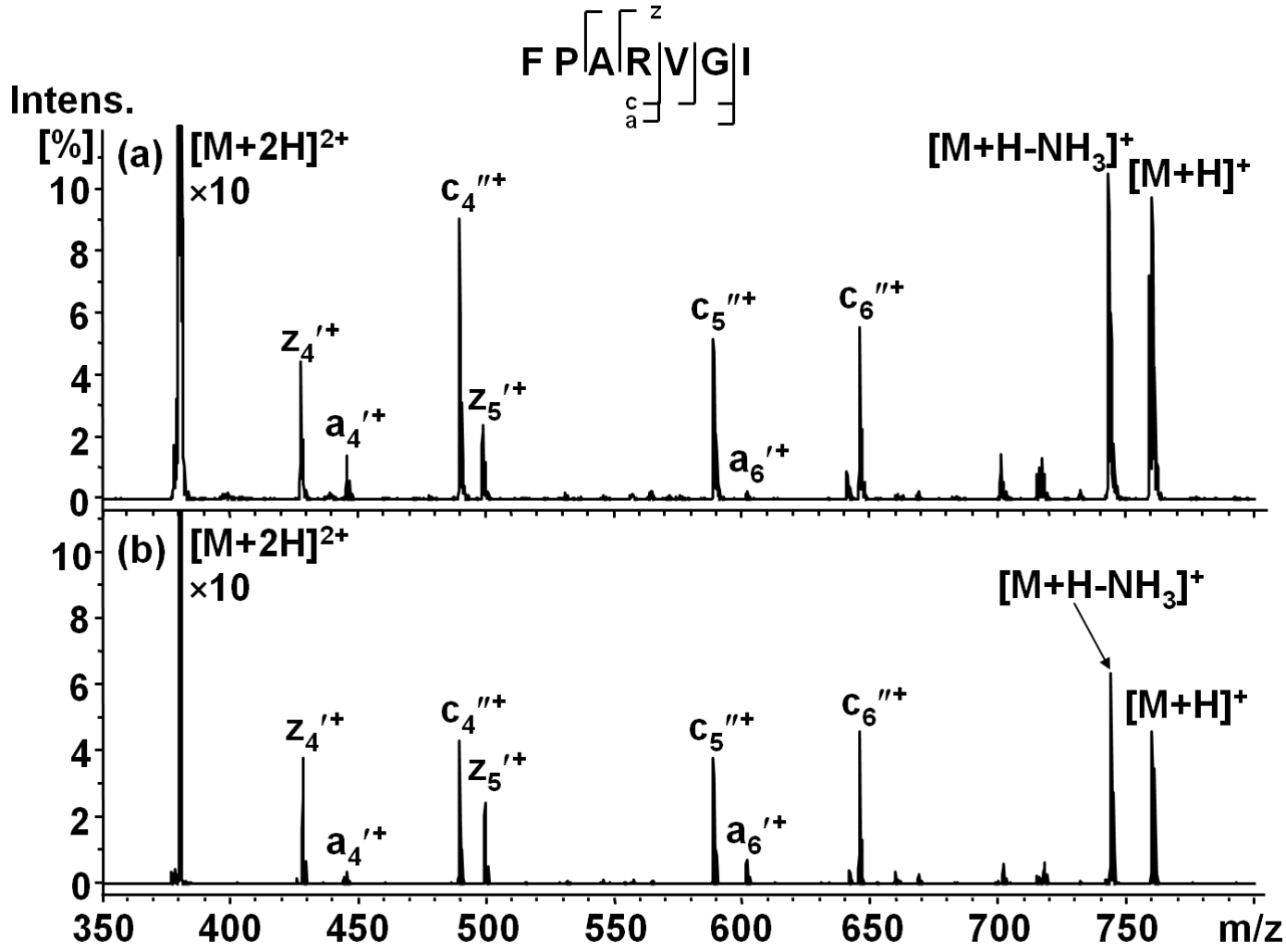

Figure 4.4. ETD spectra of $[M + 2H]^{2+}$ from FPARVGI (a) amide and (b) acid.

4.4.3.2 MLGFRSVGYA peptides

MLGFRSVGYA contains one basic residue, arginine (R) in position 5. The ETD spectra for $[M+2H]^{2+}$ of the two peptide analogs can be seen in Figure 4.5. All of the observed product ions contain the highly-basic arginine residue. The C- and N-terminal product ions provide complete sequence coverage of N–C_α bond cleavage. Loss of the C-terminal residue to produce $c_9''^{+}$ is abundant for both peptides. Cleavage C-terminal to the arginine residue is also very abundant. The peptide acid and amide ETD spectra are very similar.

4.4.3.3 WFAPPRVGYL peptides

WFAPPRVGYL contains an arginine (R) residue in position 6. The ETD spectra of the two $[M+2H]^{2+}$ species can be seen in Figure 4.6. The peptide amide and acid produce nearly identical ETD spectra. All of the observed product ions contain the arginine residue, and 7 out of 9 N–C_α bonds are cleaved. Cleaving the remaining two N–C_α bonds is unlikely since they involve proline and would require cleavage of two bonds along the peptide backbone. Loss of the C-terminal residue to form $c_9''^{+}$ is the most abundant fragment. The $z_5''^{+}$ ion is the only z-type ion that has two additional hydrogens. This ion is a result of cleaving the N–C_α bond of Pro_5–Arg_6. An interesting feature of the ETD spectrum of the peptide acid is the presence of abundant $c_9'''^{+}$ in addition to the equally abundant $c_9''^{+}$. The $c_9'''^{+}$ ion is also present in the ETD spectrum of the peptide amide, but is much less abundant than $c_9''^{+}$. The charge-reduced precursor, $[M + 2H]^{+\bullet}$, is present in the peptide amide spectrum, but observation of the charge-reduced species varies from experiment to experiment and is not consistent. Charge reduction (also called ET no D) is a common occurrence in ExD techniques where the transfer/capture of

the low-energy electron to the multiply-charged precursor does not always result in dissociation.[50] Often, the result is a charge-reduced version of the precursor ion, $[M + nH]^{(n-1)+\bullet}$.

The peaks at *m/z* 1189 and 1190 in the ETD spectra of the peptide amide and acid, respectively, do not correspond to a typical neutral loss. For the peptide amide, this peak corresponds to $[M + 2H - 16]^{+\bullet}$. A 16 Da loss is not likely, so this peak is postulated to be $[M + 3H - NH_3]^{3+\bullet\bullet}$. For the peptide acid, this peak corresponds to $[M + H - 16]^{+}$, and is proposed to be $[M + 2H - NH_3]^{+\bullet}$, with NH_3 originating from the N-terminus.

4.4.4 Peptides with a C-terminal basic residue

4.4.4.1 Laminin peptides (YIGSR)

Laminin pentapeptide contains one basic residue, arginine (R) at the C-terminus. The ETD spectra for the $[M+2H]^{2+}$ species of laminin can be seen in Figure 4.7. Both laminin peptides produce exclusively C-terminal backbone fragments of primarily the z-type. This is consistent with the fact that the only basic residue (R) is at the C-terminus. In a study of peptides containing basic residues, Feng and Cassady[14] have recently found that virtually all ETD product ions contain the basic residue.

For both laminin peptides, complete sequence coverage is observed, yielding $z_1''^{+}$ and $z_n'^{+}$ (n = 2-4) from both versions of laminin ($z_1''^{+}$ not shown in Figure 4.7). Cleavage of the amide bond of Ile_2–Gly_3 produces $y_3''^{+}$, an ion not typical of ETD (c/z-type ions typically dominate ETD spectra). There are also a small amount of neutral loss peaks present in both ETD spectra; for example, $[M + H - HN{=}C{=}NH]^{+}$ and $[M + H - HN{=}C{=}NH - CH_2O]^{+}$.

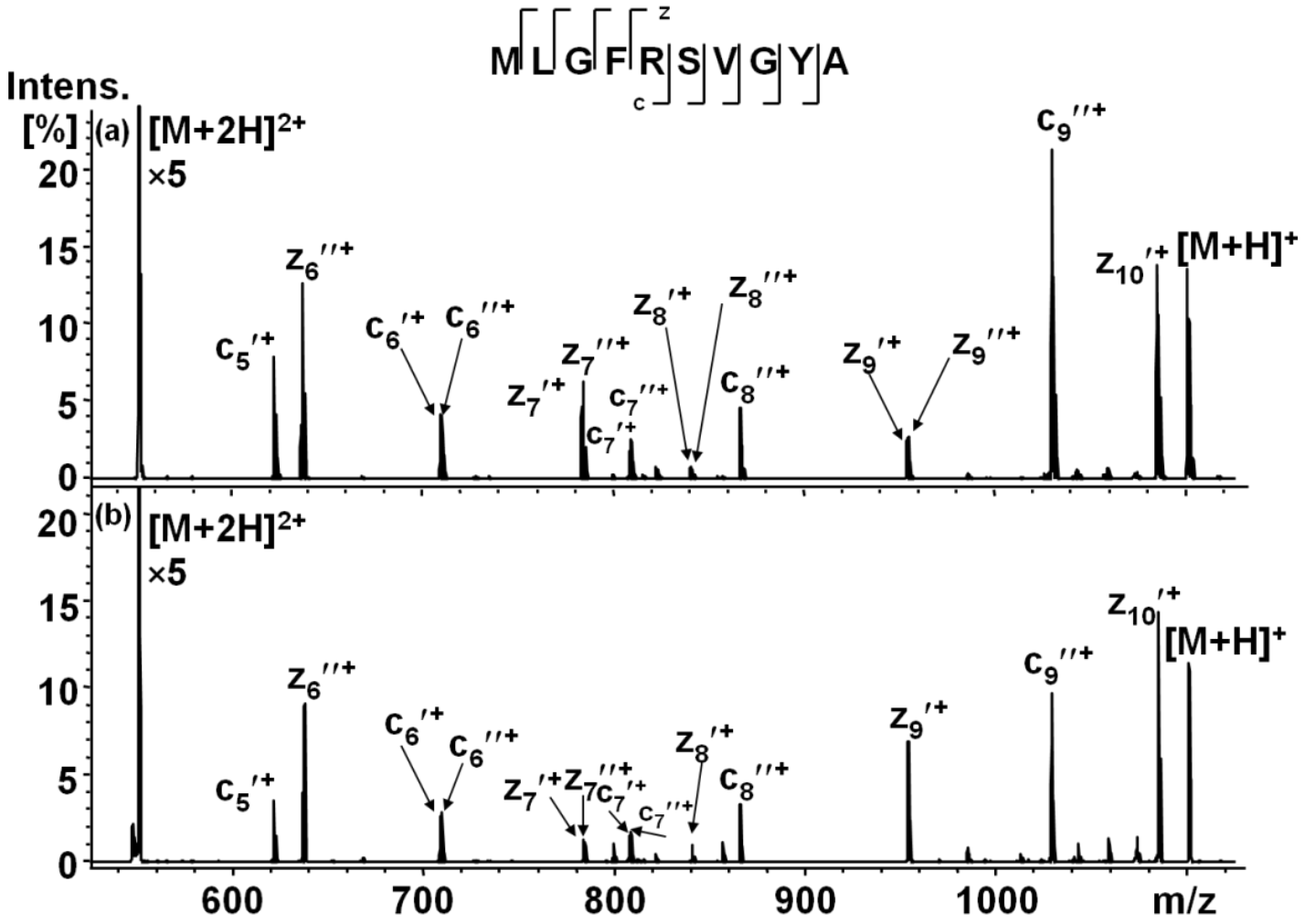

Figure 4.5 ETD spectra of $[M + 2H]^{2+}$ from MLGFRSVGYA (a) amide and (b) acid.

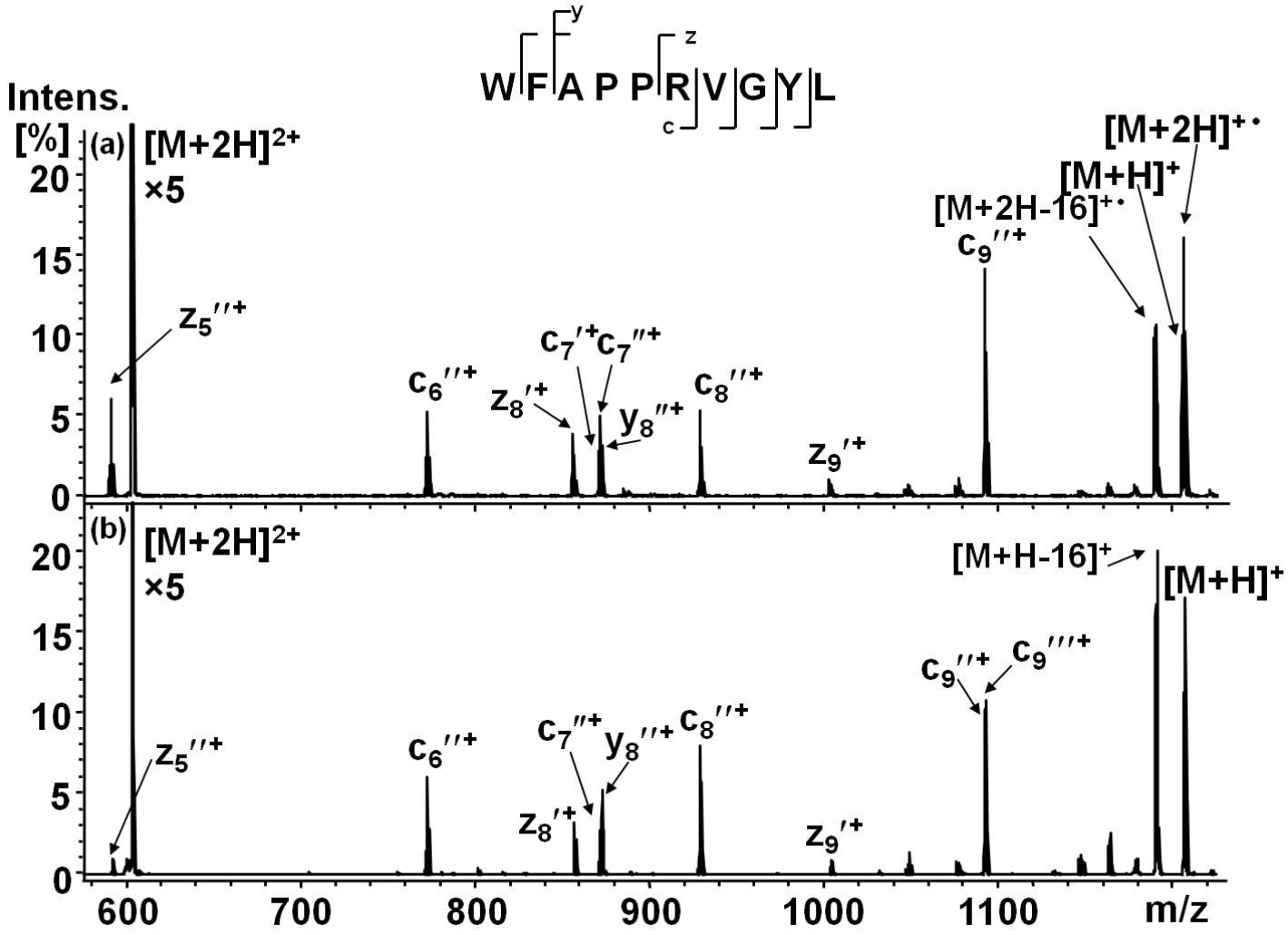

Figure 4.6. ETD spectra of $[M + 2H]^{2+}$ from WFAPPRVGYL (a) amide and (b) acid.

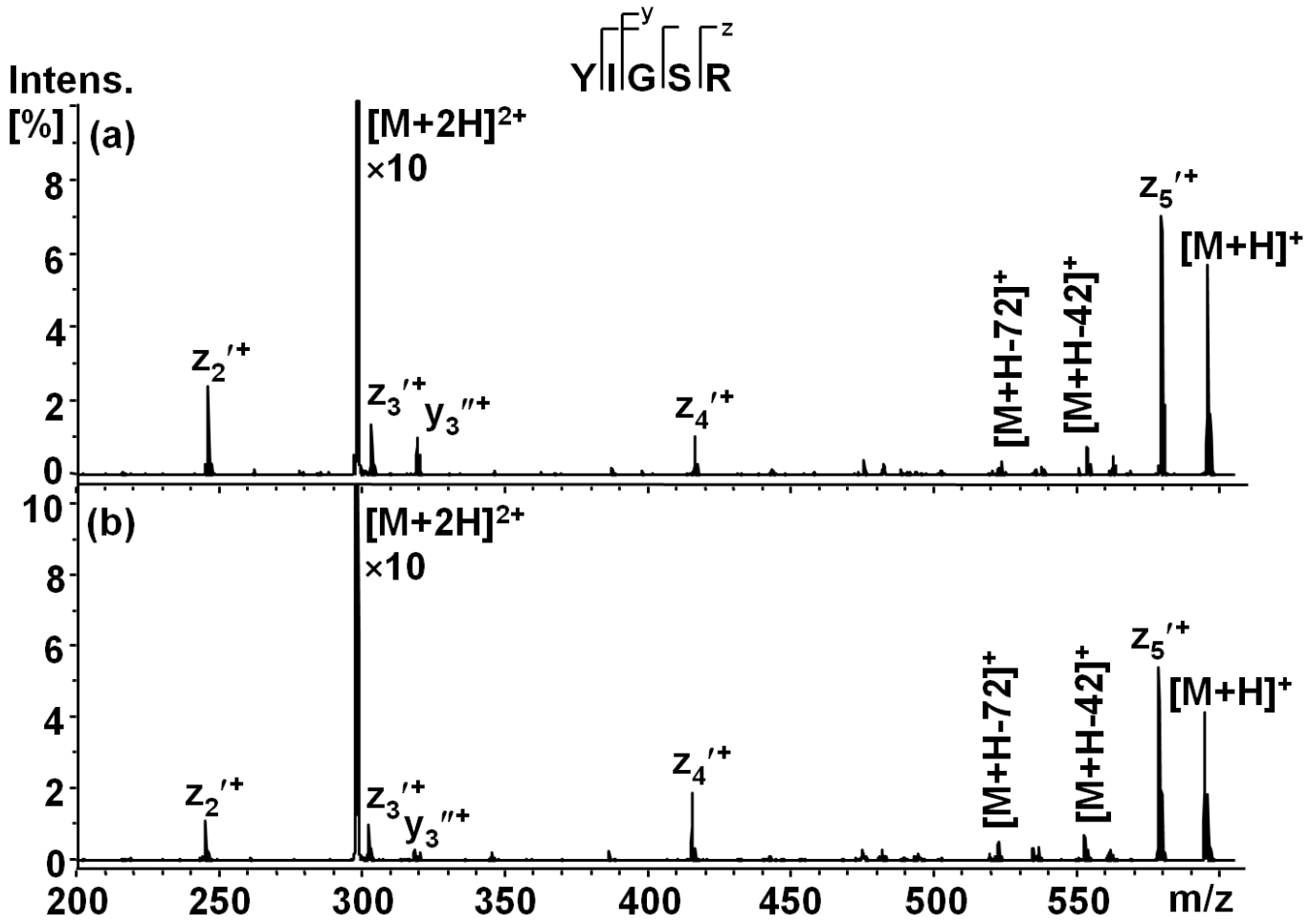

Figure 4.7 ETD spectra of $[M + 2H]^{2+}$ from laminin (YIGSR) (a) amide and (b) acid.

4.4.4.2 SWAMVR peptides

SWAMVR contains the basic arginine (R) residue at the C-terminus. The ETD spectra for the $[M+2H]^{2+}$ species can be seen in Figure 4.8. As expected based on the position of the arginine at the C-terminus, the backbone fragments observed for the free acid and amide versions of the peptide arise solely from the C-terminus. Complete sequence coverage is observed for both the peptides with formation of $z_1''^{+}$ and $z_n'^{+}$ (n = 2-5). There are also several small peaks associated with neutral losses. The peptide acid and amide analogs both produced $z_1''^{+}$, the only C-terminal ion with two additional hydrogens. Both peptides produced this ion, indicating that the C-terminal end group is not involved in formation of the product ion. The $z_1''^{+}$ ion was also formed in the ETD spectra of the laminin peptides. Both laminin and SWAMVR have the highly basic arginine residue at the C-terminus. The conformation of the doubly-charged precursor could be facilitating hydrogen transfer from serine (or elsewhere) to arginine.

4.4.4.3 LMYVHWVR peptides

LMYVHWVR contains two basic residues; histidine (H) in position 5 and arginine (R) at the C-terminus. The ETD spectra for the $[M+2H]^{2+}$ species of the two peptide analogs can be seen in Figures 4.9. ETD of $[M+2H]^{2+}$ produces 5 out of 7 possible C-terminal backbone fragments for both the peptide acid and the peptide amide. Product ions $z_3''^{+}$ and $z_4''^{+}$ result from cleavage of the N–C_α bonds of His_5–Trp_6 and Val_4–His_5, respectively. These two ions are 2 Da higher than standard z-type cleavage, and the remaining z-ions ($z_n'^{+}$, n = 5-7) are only 1 Da higher. Also present in the spectrum is the solitary N-terminal backbone fragment, $c_7'^{+}$. This fragment corresponds to the cleavage of the N-C_α bond of Val_7–Arg_8 and is thus a fragmentation adjacent to a charged residue.

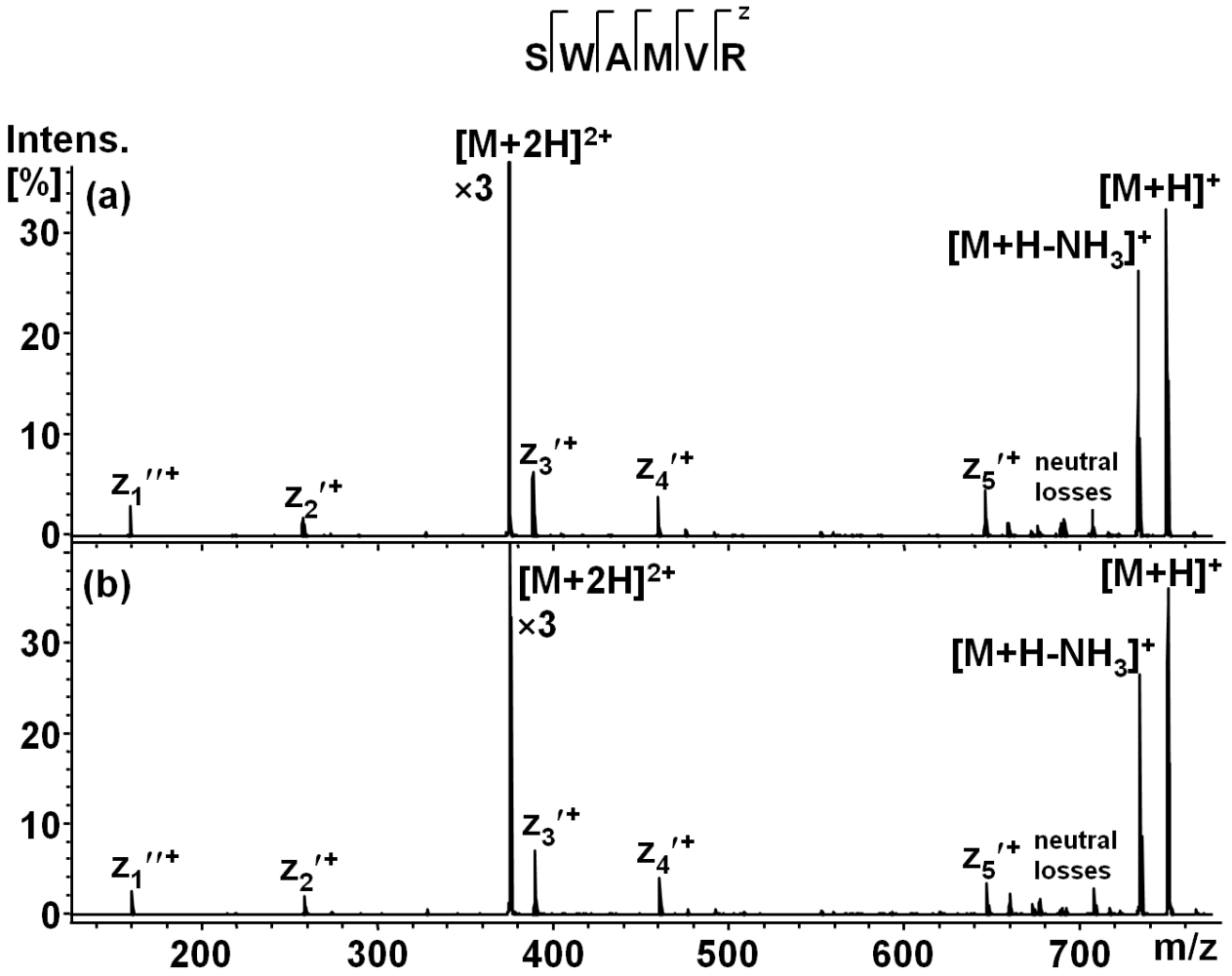

Figure 4.8. ETD spectra of $[M + 2H]^{2+}$ from SWAMVR (a) amide and (b) acid.

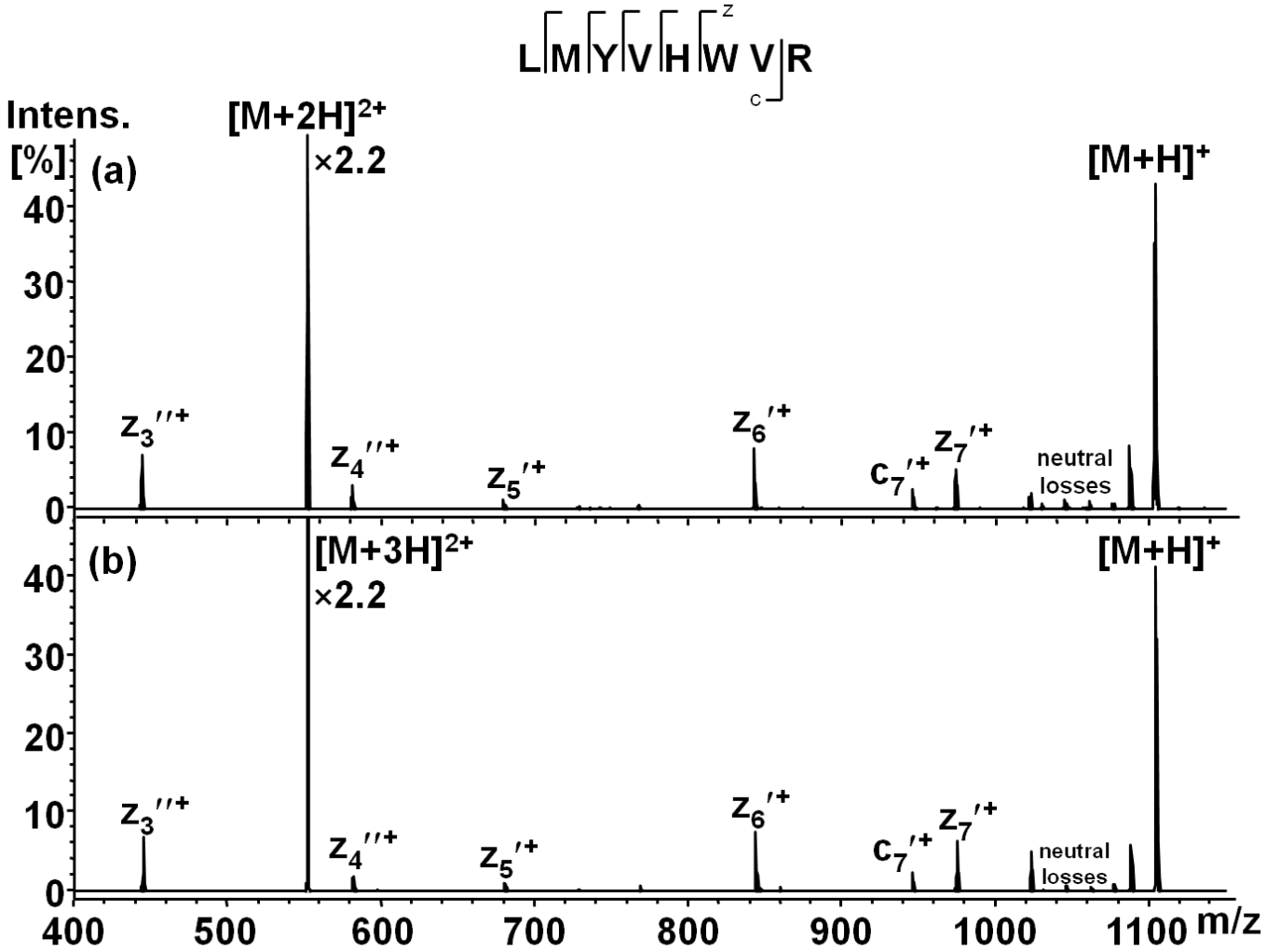

Figure 4.10 ETD spectra of $[M + 3H]^{3+}$ from LMYVHWVR (a) amide and (b) acid.

The basic character of the histidine residue and the hydrogen atom affinity of the tryptophan residue[38] are likely the reason that $z_3''^+$ and $z_4''^+$ have an additional hydrogen. Tryptophan has a reported gas-phase basicity (GB) of 219.0 kcal/mol and histidine has a reported GB of 227.1 kcal/mol.[51] Tryptophan's GB makes it the fourth most basic of the 20 common amino acids, after arginine, lysine, and histidine. The $z_3''^+$ ion likely has hydrogen atoms associated with the arginine and tryptophan side chains. The tryptophan residue is behaving as a pseudo-basic residue (as mentioned in the discussion of CCK results) in this case. The $z_4''^+$ ion likely has hydrogen atoms associated with the arginine and histidine residues. In this case, the high hydrogen ($H^{\bullet}$) affinity of the tryptophan residue is overshadowed by the much more basic histidine residue, and the proximity of the histidine and tryptophan residues makes it unlikely that a third hydrogen would be added to make $z_4'''^+$. It is unusual, however, that the remaining C-terminal product ions ($z_n'^+$, n = 5-7) do not have an additional hydrogen, given that they also contain the histidine, tryptophan, and arginine residues. The gas-phase conformation of $z_n'^+$ (n = 5-7) could have hydrogen bonding patterns that prevent the additional hydrogen from transferring. Spatial orientation of these ions could inhibit the accessibility of the tryptophan and histidine residues, thus preventing the addition of a hydrogen to make $z_n''^+$ type ions.

The ETD spectra of $[M+3H]^{3+}$ for the LMYVHWVR analogs can be seen in Figure 4.10. Six of the possible seven C-terminal product ions are observed, though this time, $z_3'^+$ and $z_4'^+$ have only one additional hydrogen. All of the z-type ions have the species with one additional hydrogen as the predominant form. However, z_7 produces the $z_n'^+$ and $z_n''^+$ forms in nearly equal abundance. Another feature of these spectra is the appearance of more N-terminal ions. A nearly complete $c_n''^+$ (n = 2-7) series is observed for the ETD of the $[M + 3H]^{3+}$ species, whereas only $c_7''^+$ was observed in ETD of the $[M + 2H]^{2+}$ species. Two a-ions, $a_5'^+$ and $a_7'^+$, are present

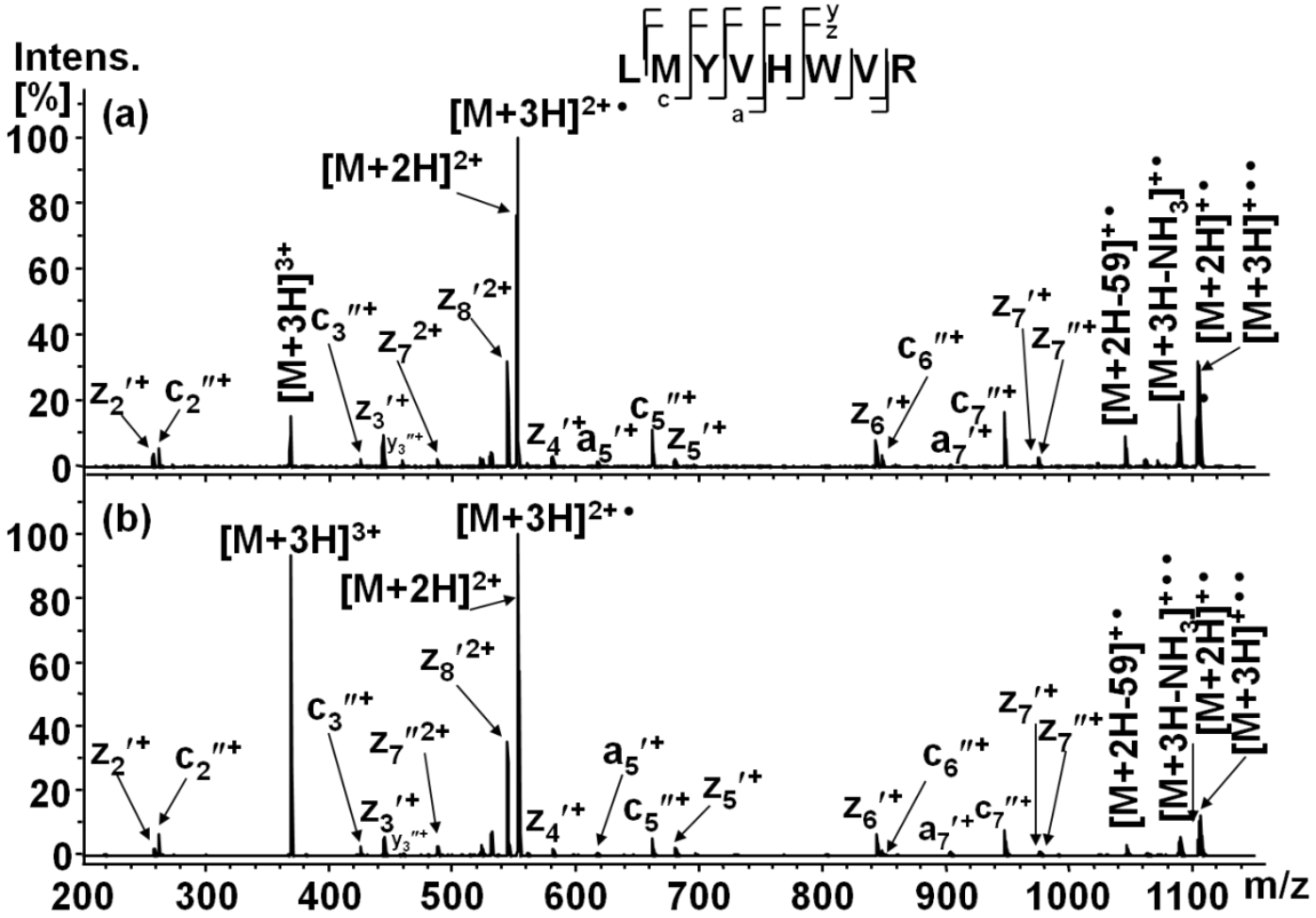

Figure 4.10 ETD spectra of $[M + 3H]^{3+}$ from LMYVHWVR (a) amide and (b) acid.

in the spectra. These ions are the result of cleaving the C_α–C bonds of Val_4 and Val_7 and both of these valine residues are adjacent to a basic residue (i.e. His_5 and Arg_8). The neutral loss of 59 Da observed in both spectra corresponds to the neutral loss of HN=C=NH and NH_3 from $[M + H]^+$.

4.4.4.4 LMYVHWVK peptides

LMYVHWVK possesses two basic residues; histidine (H) is in position 5 of the peptide sequence and lysine (K) is located at the C-terminus. The ETD spectra for the $[M+2H]^{2+}$ species can be seen in Figure 4.11. All of the product ions observed for the peptides include the histidine residue (z_n, n = 4-7). Lysine is present at the C-terminus and is thus only capable of appearing in these C-terminal ions. Histidine and lysine have very similar gas-phase basicities; according to the NIST Webbook,[39] histidine has a GB of 227.7 kcal/mol and lysine has a GB of 227.3, making histidine slightly more basic. This, however, is contradictory to what is observed for small peptides containing either of these amino acids. Carr and Cassady[52] investigated the GBs of di- and tripeptides containing histidine and lysine. They reported that peptides containing lysine were more basic, presumably because the greater flexibility of the lysine side chain allows for more participation in hydrogen bonding. Cleavage adjacent to histidine produces the only C-terminal product ion with two additional hydrogens, $z_4''^+$. Another cleavage adjacent to histidine produces both forms of c_5, $c_5'^+$ and $c_5''^+$.

The ETD spectra for the $[M+3H]^{3+}$ species of LMYVHWVK can be seen in Figure 4.12. All of the product ions that were observed in the ETD spectra of $[M+2H]^{2+}$ are present. An interesting aspect of the $[M+3H]^{3+}$ spectra is the presence of several product ions that do not contain at least one of the basic residues. Nearly complete c- and z-series are observed, with the

exception of the c_1 and z_1 species. The absence of these lower mass product ions are due to the low *m/z* cutoff of the quadrupole ion trap (QIT), which was discussed in Chapter 2. It is also interesting to note that $c_5''^+$ is the only c_5 species present in these spectra, whereas both $c_5'^+$ and $c_5''^+$ were present in the $[M+2H]^{2+}$ ETD spectra. Several a-, b-, and y-type ions appeared in these spectra in low abundance. All of the observed a-ions contain the histidine residue and have an additional hydrogen.

4.4.5 C-terminal residue loss to produce c-ions

Elimination of the C-terminal residue to form abundant $c_{n-1}''^+$ was observed for CCK, substance P, FPARVGI, MLGFRSVGYA, WFAPPRVGYL, LMYVHWVR, and LMYVHWVK. This is in agreement with the extensive study by Wysocki and coworkers,[40] which found that elimination of the C-terminal residue to form c-type ions was largely due to the position of the C-terminal residue as determined by precursor ion structure. The peptides in this dissertation research have basic residues in various positions (except CCK, which does not contain a residue with a basic side chain). Neither laminin nor SWAMVR exhibit C-terminal residue loss. Both peptides have an arginine residue at the C-terminus, however, LMYVHWVR also has an arginine residue at the C-terminus yet it produced $c_7'^+$ (indicating loss of the C-terminal residue). Peptide length may be a factor in C-terminal residue loss (laminin has 5 residues and SWAMVR has 6 residues, whereas LMYVHWVR has 8 residues). Wysocki and coworkers[40] reported average peptide lengths of 13.6 or greater (only averages were reported due to the massive size of the data set). Polfer and coworkers[18] reported that the C-terminal arginine of bradykinin participates in backbone solvation (which means the positively-charged arginine side chain is hydrogen bonded to a backbone carbonyl), which resulted in a preference for

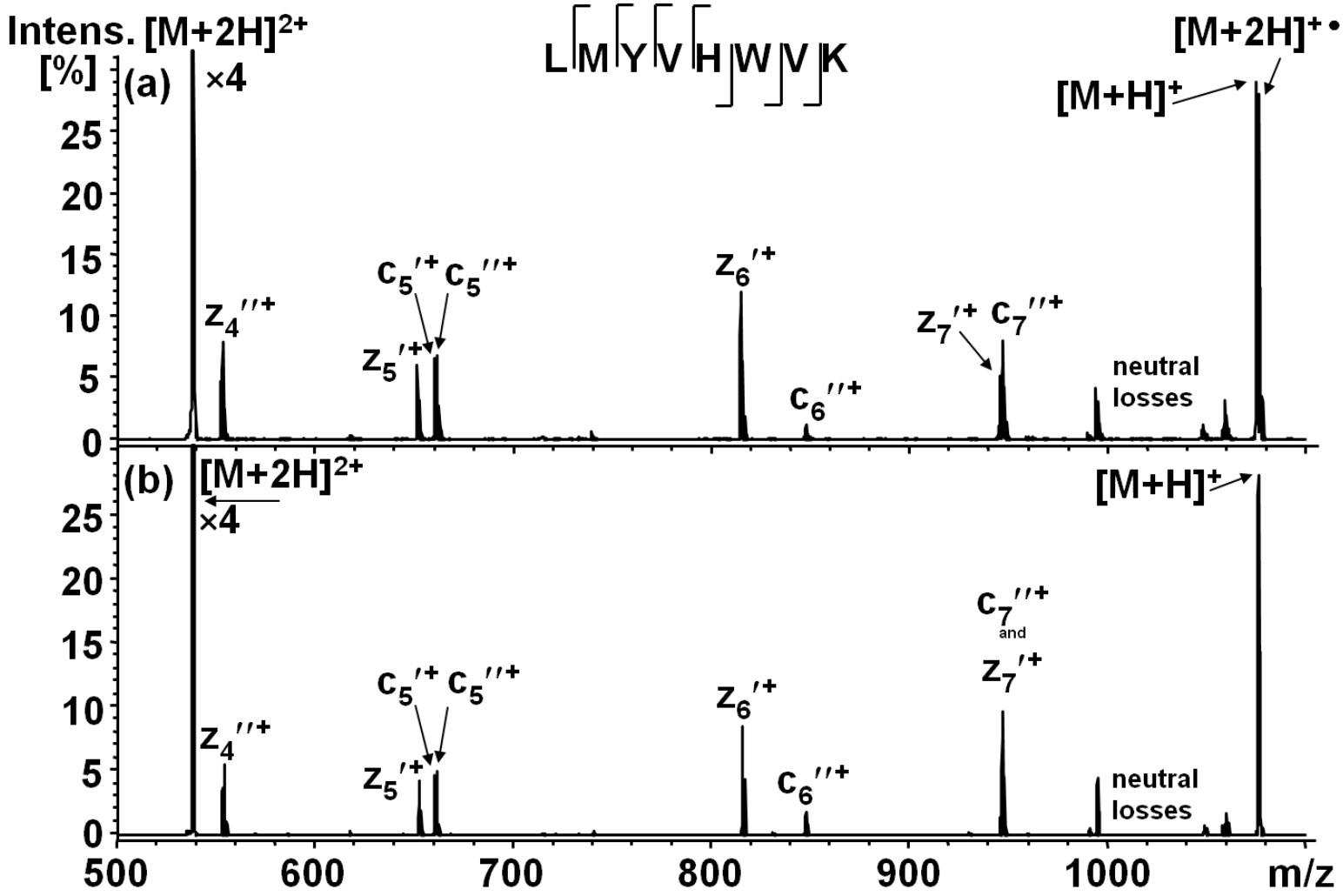

Figure 4.11. ETD spectra of $[M + 2H]^{2+}$ from LMYVHWVK (a) amide and (b) acid.

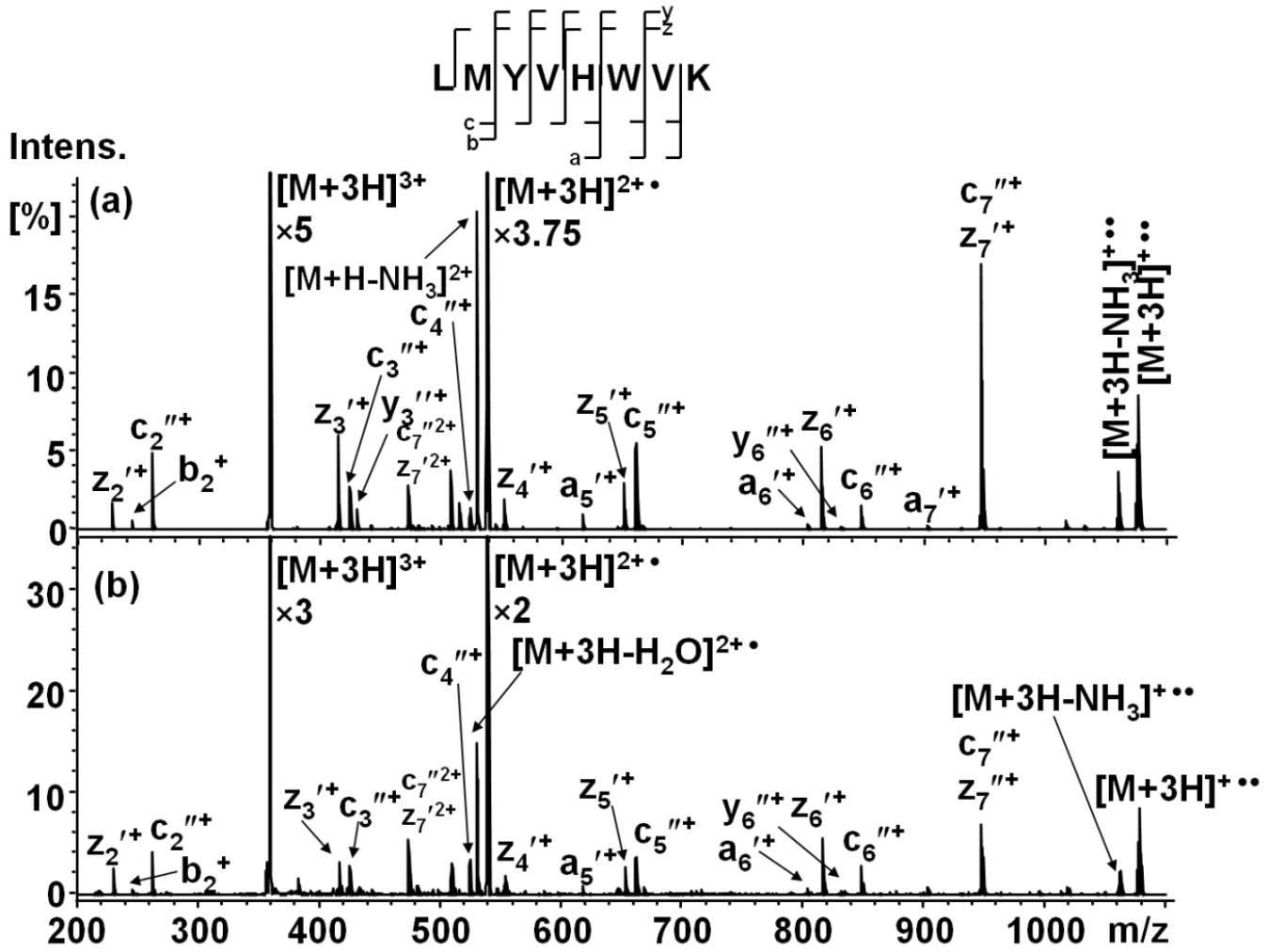

Figure 4.12. ETD spectra of $[M + 3H]^{3+}$ from LMYVHWVK (a) amide and (b) acid.

forming N-terminal ions that contain the N-terminal arginine. Shorter peptide sequences likely have very different $[M+2H]^{2+}$ structures than those from longer peptide sequences. If the C-terminal arginine of SWAMVR or laminin is solvated to the backbone, elimination of the C-terminal residue may not occur. If two basic residues are present in the peptide sequence, c_{n-1}^{+} may form as long as these ions incorporate at least one of the basic residues.

4.4.6 Recruiting hydrogens

Protonation of carboxylic acid and amide functional groups differ greatly in the gas phase. For example, formamide has a GB of 189.1 kcal/mol[39] and formic acid has a GB of 169.8 kcal/mol.[39] Formamide is nearly 20 kcal/mol more basic than its carboxylic acid counterpart. The same trend is observed for acetamide (GB = 199.0 kcal/mol) and acetic acid (GB = 179.9 kcal/mol).[26] Given this difference in basicity, a C-terminal amide on a peptide could behave as a charge site in mass spectrometry studies of protonated ions and, consequentially, may exhibit different dissociative behavior in tandem MS techniques.

C-terminal amide peptides and C-terminal acid peptides behave similarly in CID of protonated peptides. (This was also addressed in Chapter 3.) In ETD, C-terminal amide and acid peptides also exhibit very similar dissociative behavior. The peptide acids and amides discussed here produced nearly identical spectra except for one minor situation. CCK amide produced an $a_8'^{+}$ ion that was not very abundant in the CCK acid spectrum. This is attributed to the loss of the C-terminal $CONH_2$ and/or CO_2 from one of the two aspartic acid residues, located at the N-terminus or in position 4 of the peptide sequence. Since aspartic acid is common to both peptides, the $a_8'^{+}$ is likely an additive feature attributed to *both* aforementioned neutral losses.

This means that $CONH_2$ and CO_2 are being lost from the amide, to produce a peak more abundant than what was observed for the peptide amide.

There are, however, several features of the acid and amide peptide ETD spectra that indicate an interesting occurrence of hydrogen recruiting. Laminin and SWAMVR produce $z_1''^+$, which is cleavage N-terminal to arginine. LMYVHWVR and LMYVHWVK both produce abundant $z_4''^+$, which is cleavage N-terminal to histidine. LMYVHWVR also produces abundant $z_3''^+$, which is cleavage N-terminal to tryptophan. These product ions all result from cleavage of the N–C_α bond N-terminal to a basic residue (e.g. Arg, His) or a pseudo-basic residue (e.g. Trp) and have one more hydrogen than other N-terminal product ions in the spectra. Hydrogens are being "recruited" to these C-terminal product ions based on the basicity and position of these amino acid residues.

The recruitment of hydrogens to C-terminal product ions is not always observed. Formation of $z_4''^+$ from ETD of CCK is not observed, rather $z_4'^+$ occurs (when considering Trp as a pseudo-basic residue). Cleavage of the N–C_α bond N-terminal to lysine in the ETD of substance P produces $z_9'^+$ rather than the z'' species. Arginine is present in the peptide sequence of FPARVGI, yet z_4 and z_5 have only one additional hydrogen (making them $z_n'^+$). The inconsistency of hydrogen recruiting to N-terminal ions (that have basic residues at the cleavage site) indicate that the structure of the dissociating ion is crucial to the transfer of a hydrogen atom.

Polfer and coworkers[18] reported on the formation of c- and z-ions with differing numbers of hydrogens in an ECD study on naturally occurring peptides. For z_n^+ with $n \leq 4$, the z' type ion was preferred, and for z_n^+ with $n>4$, the $z^{+\bullet}$ type ion was preferred. (They used the Zubarev nomenclature mentioned earlier in the in the chapter, thus translated, $z_n''^+$ is preferred for $n \leq 4$

and $z_n'^+$ is preferred for n>4). Formation of both c• and c′ type ions (c′ and c″, respectively) was also reported.[18] The c′/z• ions observed by Polfer and coworkers[18] and earlier reports [19, 38] are considered to be atypical of ExD and the result of hydrogen rearrangement.[5]

4.4.7 Comparison of $[M + 2H]^{2+}$ versus $[M + 3H]^{3+}$ ETD

Only three of the peptides studied, substance P, LMYVHWVR, and LMYVHWVK, produced $[M + 3H]^{3+}$ for study by ETD. Each of these aforementioned peptides have two basic amino acid residues present in the peptide sequence, and these residues are separated by at least one residue. The spacing of the basic amino acid residues and the N-terminal free amine (for each peptide) minimizes potential Coulombic repulsion between multiple charges.[53, 54]

The ETD experiments of the $[M + 3H]^{3+}$ from the aforementioned peptides provided equivalent information when compared to the ETD of the $[M + 2H]^{2+}$ species. Similar cleavages were observed when comparing the $[M + 2H]^{2+}$ and $[M + 3H]^{3+}$ dissociations. Additional higher charge state product ions were observed in the $[M + 3H]^{3+}$ spectra. These ions were not the result of additional cleavages, but just higher charge state versions of the same ions observed in the $[M + 2H]^{2+}$ ETD spectra. Wysocki and coworkers[40] reported the less selective nature of ETD on higher charge state peptides, thus the result of the research in this chapter is not unexpected. The unusual observance of $c_9'''^+$ and $c_{10}'''^+$ from the ETD of $[M + 3H]^{3+}$ from substance P is attributed to the loss of an internal leucine residue.

4.5 Conclusions

Gas-phase basicity differences between amide and carboxylic acid sites suggest that C-terminal peptide amides and acids could behave differently under ETD conditions. However, all

of the peptides in this study produced c/z-type cleavages that are typically observed in ETD. The peptide acids and amides produced nearly identical spectra in all cases, with only a few notable differences. The most remarkable observations were those involving basic residues (i.e. arginine, histidine, and lysine) and amino acid residues with high hydrogen atom ($H^{\bullet}$) affinity (i.e. tryptophan). Cleavage adjacent to either type of amino acid residue produces fragment ions that have at least one additional hydrogen compared to other fragmentation in the ETD spectrum. There is ongoing research in the Cassady group that is studying the direct effect of basic residues on ETD spectra. The study consists of several model peptides (C-terminal acids only) composed mainly of polyalanines with one basic residue (e.g. AAAAAR, AAAKAA, etc.). This will clarify the behavior of basic residues in ETD without the interaction of other non-inert amino acid residues.

The results shown here indicate that a peptide C-terminal amide group behaves similarly to a C-terminal acid group in ETD. This is consistent with the results from studies of CID of protonated ions involving the same peptides (discussed briefly in Chapter 3) and the work of Enjalbal and coworkers in a similar study on CID of protonated peptides.[29] This means that the C-terminal amide is not a distinguishing factor for use in bioinformatic methods for identification of peptides using ETD in the positive ion mode. Nonetheless, it is important to understand the contribution of all chemical functionalities under tandem MS conditions to further develop identification methods.

References

1. Syka, J. E. P.; Coon, J. J.; Schroeder, M. J.; Shabanowitz, J.; Hunt, D. F. Peptide and protein sequence analysis by electron transfer dissociation mass spectrometry. *Proc. Natl. Acad. Sci. U. S. A.* **2004**, *101*, 9528-9533.

2. Good, D. M.; Wirtala, M.; McAlister, G. C.; Coon, J. J. Performance characteristics of electron transfer dissociation mass spectrometry. *Mol. Cell. Proteomics* **2007**, *6*, 1942-1951.

3. McLafferty, F. W.; Horn, D. M.; Breuker, K.; Ge, Y.; Lewis, M. A.; Cerda, B.; Zubarev, R. A.; Carpenter, B. K. Electron capture dissociation of gaseous multiply charged ions by Fourier-transform ion cyclotron resonance. *J. Am. Soc. Mass Spectrom.* **2001**, *12*, 245-249.

4. Kruger, N. A.; Zubarev, R. A.; Horn, D. M.; McLafferty, F. W. Electron capture dissociation of multiply charged peptide cations. *Int. J. Mass Spectrom.* **1999**, *187*, 787-793.

5. Zubarev, R. A.; Horn, D. M.; Fridriksson, E. K.; Kellerher, N. L.; Kruger, N. A.; Lewis, M. A.; Carpenter, B. K.; McLafferty, F. W. Electron capture dissociation for structural characterization of multiply charged protein cations. *Anal. Chem.* **2000**, *72*, 573.

6. Han, H.; Xia, Y.; McLuckey, S. A. Ion trap collisional activation of c and z(center dot) ions formed via gas-phase ion/ion electron-transfer dissociation. *J. Prot. Res.* **2007**, *6*, 3062-3069.

7. Simons, J. Mechanisms for S-S and N-C(alpha) bond cleavage in peptide ECD and ETD mass spectrometry. *Chem. Phys. Lett.* **2010**, *484*, 81-95.

8. Neff, D.; Sobczyk, M.; Simons, J. Through-space and through-bond electron transfer within positively charged peptides in the gas phase. *Int. J. Mass Spectrom.* **2008**, *276*, 91-101.

9. Simons, J. Analytical model for rates of electron attachment and intramolecular electron transfer in electron transfer dissociation mass spectrometry. *J. Am. Chem. Soc.* **2010**, *132*, 7074-7085.

10. Neff, D.; Simons, J. Analytical and computational studies of intramolecular electron transfer pertinent to electron transfer and electron capture dissociation mass spectrometry. *J. Phys. Chem. A* **2010**, *114*, 1309-1323.

11. Anusiewicz, I.; Berdys-Kochanska, J.; Simons, J. Electron attachment step in electron capture dissociation (ECD) and electron transfer dissociation (ETD). *J. Phys. Chem. A* **2005**, *109*, 5801-5813.

12. Turecek, F.; Chen, X.; Hao, C. Where does the electron go? Electron distribution and reactivity of peptide cation radicals formed by electron transfer in the gas phase. *J. Am. Chem. Soc.* **2008**, *130*, 8818-8833.

13. Chen, X.; Turecek, F. The arginine anomaly: Arginine radicals are poor hydrogen atom donors in electron transfer induced dissociations. *J. Am. Chem. Soc.* **2006**, *128*, 12520-12530.

14. Syrstad, E. A.; Turecek, F. Toward a general mechanism of electron capture dissociation. *J. Am. Soc. Mass Spectrom.* **2005**, *16*, 208-224.

15. Zubarev, R. A.; Haselmann, K. F.; Budnik, B.; Kjeldsen, F.; Jensen, F. Towards an understanding of the mechanism of electron-capture dissociation: a historical perspective and modern ideas. *Eur. J. Mass Spectrom.* **2002**, *8*, 337-349.

16. Rand, K. D.; Adams, C. M.; Zubarev, R. A.; Jorgensen, T. J. D. Electron capture dissociation proceeds with a low degree of intramolecular migration of peptide amide hydrogens. *J. Am. Chem. Soc.* **2008**, *130*, 1341-1349.

17. Zubarev, R. A. Reactions of polypeptide ions with electrons in the gas phase. *Mass Spectrom. Rev.* **2003**, *22*, 57-77.

18. Polfer, N.; Haselmann, K.; Langridge-Smith, P.; Barran, P. Structural investigation of naturally occurring peptides by electron capture dissociation and AMBER force field modelling. *Mol. Phys.* **2005**, *103*, 1481-1489.

19. Hakansson, K.; Emmett, M.; Hendrickson, C.; Marshall, A. High-sensitivity electron capture dissociation tandem FTICR mass spectrometry of microelectrosprayed peptides. *Anal. Chem.* **2001**, *73*, 3605-3610.

20. Cooper, H.; Hakansson, K.; Marshall, A. The role of electron capture dissociation in biomolecular analysis. *Mass Spectrom. Rev.* **2005**, *24*, 201-222.

21. Molina, H.; Matthiesen, R.; Kandasamy, K.; Pandey, A. Comprehensive comparison of collision induced dissociation and electron transfer dissociation. *Anal. Chem.* **2008**, *80*, 4825-4835.

22. Hayakawa, S.; Matsubara, H.; Panja, S.; Hvelplund, P.; Nielsen, S. B.; Chen, X.; Turecek, F. Experimental evidence for an inverse hydrogen migration in arginine radicals. *J. Am. Chem. Soc.* **2008**, *130*, 7645-7654.

23. Panja, S.; Nielsen, S. B.; Hvelplund, P.; Turecek, F. Inverse hydrogen migration in arginine-containing peptide ions upon electron transfer. *J. Am. Soc. Mass Spectrom.* **2008**, *19*, 1726-1742.

24. Turecek, F.; Chung, T. W.; Moss, C. L.; Wyer, J. A.; Ehlerding, A.; Holm, A. I. S.; Zettergren, H.; Nielsen, S. B.; Hvelplund, P.; Chamot-Rooke, J.; Bythell, B.; Paizs, B. The histidine effect. Electron transfer and capture cause different dissociations and rearrangements of histidine peptide cation-radicals. *J. Am. Chem. Soc.* **2010**, *132*, 10728-10740.

25. Turecek, F.; Panja, S.; Wyer, J. A.; Ehlerding, A.; Zettergren, H.; Nielsen, S. B.; Hvelplund, P.; Bythell, B.; Paizs, B. Carboxyl-catalyzed prototropic rearrangements in histidine peptide radicals upon electron transfer: Effects of peptide sequence and conformation. *J. Am. Chem. Soc.* **2009**, *131*, 16472-16487.

26. Turecek, F.; Yao, C.; Fung, Y. M. E.; Hayakawa, S.; Hashimoto, M.; Matsubara, H. Histidine-containing radicals in the gas phase. *J Phys Chem B* **2009**, *113*, 7347-7366.

27. Turecek, F.; Jones, J. W.; Towle, T.; Panja, S.; Nielsen, S. B.; Hvelplund, P.; Paizs, B. Hidden histidine radical rearrangements upon electron transfer to gas-phase peptide ions. Experimental evidence and theoretical analysis. *J. Am. Chem. Soc.* **2008**, *130*, 14584-14596.

28. Feng, C.; Cassady, C. J. Unpublished results. **2012**.

29. Mouls, L.; Subra, G.; Aubagnac, J.; Martinez, J.; Enjalbal, C. Tandem mass spectrometry of amidated peptides. *J. Mass. Spectrom.* **2006**, *41*, 1470-1483.

30. Zhang, K.; Cassady, C. J.; Chung-Phillips, A. Ab-initio studies of neutral and protonated triglycines - Comparison of calculated and experimental gas-phase basicity. *J. Am. Chem. Soc.* **1994**, *116*, 11512-11521.

31. Zhang, K.; Zimmerman, D. M.; Chung-Phillips, A.; Cassady, C. J. Experimental and ab-initio studies of the gas-phase basicities of polyglycines. *J. Am. Chem. Soc.* **1993**, *115*, 10812-10822.

32. Dongre, A. R.; Jones, J. L.; Somogyi, A.; Wysocki, V. H. Influence of peptide composition, gas-phase basicity, and chemical modification on fragmentation efficiency: Evidence for the mobile proton model. *J. Am. Chem. Soc.* **1996**, *118*, 8365-8374.

33. Wysocki, V. H.; Tsaprailis, G.; Smith, L. L.; Breci, L. A. Special feature: Commentary - Mobile and localized protons: a framework for understanding peptide dissociation. *J. Mass Spectrom.* **2000**, *35*, 1399-1406.

34. Crizer, D. M.; McLuckey, S. A. Electron Transfer Dissociation of Amide Nitrogen Methylated Polypeptide Cations. *J. Am. Soc. Mass Spectrom.* **2009**, *20*, 1349-1354.

35. Lioe, H.; O'Hair, R. A. J.; Gronert, S.; Austin, A.; Reid, G. E. Experimental and theoretical proton affinities of methionine, methionine sulfoxide and their N- and C-terminal derivatives. *Int. J. Mass Spectrom.* **2007**, *267*, 220-232.

36. Lioe, H.; O'Hair, R. A. J. Comparison of collision-induced dissociation and electron-induced dissociation of singly protonated aromatic amino acids, cystine and related simple peptides using a hybrid linear ion trap–FT-ICR mass spectrometer. *Anal. Bioanal. Chem.* **2007**, *389*, 1429-1437.

37. Roepstorff, P.; Fohlman, J. Proposal for a common nomenclature for sequence ions in mass spectra of peptides. *Biomed. Mass Spectrom.* **1984**, *11*, 601.

38. Zubarev, R. A.; Kruger, N. A.; Fridriksson, E. K.; Lewis, M. A.; Horn, D. M.; Carpenter, B. K.; McLafferty, F. W. Electron capture dissociation of gaseous multiply-charged proteins is favored at disulfide bonds and other sites of high hydrogen atom affinity. *J. Am. Chem. Soc.* **1999**, *121*, 2857-2862.

39. Linstrom, P. J.; Mallard, W. G., Eds.; In *NIST Chemistry WebBook, NIST Standard Reference Database Number 69;* National Institute of Standards and Technology: Gaithersburg MD, 20899.

40. Li, W.; Song, C.; Bailey, D. J.; Tseng, G. C.; Coon, J. J.; Wysocki, V. H. Statistical analysis of electron transfer dissociation pairwise fragmentation patterns. *Anal. Chem.* **2011**, *83*, 9540-9545.

41. Liu, H.; Hakansson, K. Abundant b-type ions produced in electron capture dissociation of peptides without basic amino acid residues. *J. Am. Soc. Mass Spectrom.* **2007**, *18*, 2007-2013.

42. Hayakawa, S.; Hashimoto, M.; Matsubara, H.; Turecek, F. Dissecting the proline effect: Dissociations of proline radicals formed by electron transfer to protonated Pro-Gly and Gly-Pro dipeptides in the gas phase. *J. Am. Chem. Soc.* **2007**, *129*, 7936-7949.

43. Axelsson, J.; Palmblad, M.; Hakansson, K.; Hakansson, P. Electron capture dissociation of substance P using a commercially available Fourier transform ion cyclotron resonance mass spectrometer. *Rapid Commun. Mass Spectrom.* **1999**, *13*, 474-477.

44. Wash, P.; Maverick, E.; Chiefari, J.; Lightner, D. Acid-amide intermolecular hydrogen bonding. *J. Am. Chem. Soc.* **1997**, *119*, 3802-3806.

45. Wu, J. Y.; Lebrilla, C. B. Gas-phase basicities and sites of protonation of glycine oligomers (Gly_n, N = 1-5). *J. Am. Chem. Soc.* **1993**, *115*, 3270-3275.

46. Kuzma, M.; Jegorov, A.; Hesso, A.; Tornaeus, J.; Sedmera, P.; Havlicek, V. Role of amino acid N-methylation in cyclosporins on ring opening and fragmentation mechanisms during collisionally induced dissociation in an ion trap. *J. Mass Spectrom.* **2002**, *37*, 292-298.

47. Jai-nhuknan, J. Post-source decay of negative peptide ions in a matrix-assisted laser desorption/ionization time-of-flight mass spectrometer. Ph.D. Dissertation, Miami University, Oxford, OH, 1998.

48. Brinkworth, C. S.; Bilusich, D.; Bowie, J. H. The unusual loss of an internal Val residue from the $(M-H)^-$ parent anions of the antimicrobial peptide citropin 1.1 and synthetically modified analogues. Fragmentations which require a specific conformation of the decomposing anion. *Int. J. Mass Spectrom.* **2004**, *236*, 43-53.

49. Li, Z.; Yalcin, T.; Cassady, C. J. C-terminal amino acid residue loss for deprotonated peptide ions containing glutamic acid, aspartic acid, or serine residues at the C-terminus. *J. Mass Spectrom.* **2006**, *41*, 939-949.

50. Xia, Y.; Gunawardena, H. P.; Erickson, D. E.; McLuckey, S. A. Effects of cation charge-site identity and position on electron-transfer dissociation of polypeptide cations. *J. Am. Chem. Soc.* **2007**, *129*, 12232-12243.

51. Hunter, E. P. L.; Lias, S. G. Evaluated gas phase basicities and proton affinities of molecules: An update. *J. Phys. Chem. Ref. Data* **1998**, *27*, 413-656.

52. Carr, S. R.; Cassady, C. J. Gas-phase basicities of histidine and lysine and their selected di- and tripeptides. *J. Am. Soc. Mass Spectrom.* **1996**, *7*, 1203-1210.

53. Downard, K. M.; Biemann, K. The effect of charge-state and the localization of charge on the collision-induced dissociation of peptide ions. *J. Am. Soc. Mass Spectrom.* **1994**, *5*, 966-975.

54. Tang, X. J.; Thibault, P.; Boyd, R. K. Fragmentation reactions of multiply-protonated peptides and implications for sequencing by tandem mass-spectrometry with low-energy collision-induced dissociation. *Anal. Chem.* **1993**, *65*, 2824-2834.

CHAPTER 5: DEPROTONATION OF AMINO ACIDS AND AMINO ACID AMIDES: AN EXPERIMENTAL AND COMPUTATIONAL INVESTIGATION INTO THE GAS-PHASE ACIDITIES OF TYROSINE AND PHENYLALANINE

5.1 Overview

The gas-phase acidities (GAs) of tyrosine (Tyr), tyrosine amide (Tyr-NH_2), phenylalanine (Phe), phenylalanine amide (Phe-NH_2), and 4-(4-hydroxyphenyl)-2-butanone (HPB) were determined using proton transfer reactions in a Fourier transform ion cyclotron resonance mass spectrometer (FT-ICR MS). The order of acidity is as follows: Phe-NH_2 < HPB < Tyr-NH_2 < Phe < Tyr. Two ion structures were observed for Tyr-OH and GAs were assigned for each deprotonated structure. The GAs values of the amino acid amides are a valuable tool for understanding fragmentation of deprotonated peptides, as amino acid amides are a better representation of the residues in a peptide backbone than are amino acids. In collaboration with Professor David Dixon's research group at the University of Alabama, high-level G3(MP2) calculations have been performed and are in agreement with the observed experimental acidity trend.

5.2 Introduction

Tyrosine and phenylalanine are among the twenty standard amino acids found in nature. They often have similar properties because both possess aromatic, hydrophobic side chains. Their structures, which are shown in Figure 5.1, are similar with tyrosine having a 4-

hydroxylbenzyl group at the side chain and phenylalanine having a benzyl side chain. Tyrosine plays an important role in signal transduction processes, where phosphorylation of the tyrosine side chain can affect protein function.[1-5]

Tyrosine kinase, in particular, is responsible for the enzymatic transfer of a phosphate group from adenosine triphosphate (ATP) to a target protein.[6, 7] Another enzyme, tyrosine hydroxylase, is responsible for the catalytic conversion of phenylalanine to tyrosine in mammalian liver cells.[5] Tyrosine even participates in photosynthesis, where D1-Tyr161 in photosystem II donates an electron in the reduction of P680.[8, 9] Phenylalanine is responsible for the disorder phenylketonuria, where individuals are unable to metabolize ingested phenylalanine due to reduced function of the phenylalanine hydroxylase enzyme.[10, 11]

The tyrosine and phenylalanine residues of peptides are known to exhibit unique behavior in tandem mass spectrometry techniques such as collision-induced dissociation (CID), and electron transfer dissociation (ETD).[12-16] Bowie and coworkers have detailed the side-chain fragmentation and backbone fragmentation of deprotonated peptides containing tyrosine and phenylalanine in high-energy CID studies.[13, 14, 16] Cleavage adjacent to the tyrosine residue and loss of neutral $O{=}C_6H_4{-}CH_2$ from the side chain of tyrosine are common characteristics of the CID spectra. Harrison[17] reported the fragmentation behavior of phenylalanine residues in the C-terminal, central, and N-terminal positions in low-energy CID of deprotonated dipeptides and tripeptides. Cleavage N-terminal to the phenylalanine residue is reported a major pathway for low- and high-energy CID of deprotonated peptides, as well as abundant loss of C_7H_8 (probably as toluene) when phenylalanine is at the N-terminus. The neutral loss of C_7H_6O from tyrosine was reported by Pu and Cassady[12] in a sustained off-resonance irradiation (SORI) CID study of

deprotonated peptides that possess hydroxyl-containing amino acid residues. Their work agrees with high-energy CID results from Bowie and coworkers.[13]

Proton transfer reactions in the gas phase are important tools for obtaining thermochemical information regarding a compound of interest. Whereas acid and base dissociation constants (pK_a and pK_b, respectively) are important to solution-phase studies, gas-phase acidity (GA) and gas-phase basicity (GB) are particularly valuable for the study of gas-phase biomolecules such as amino acids, peptides, and proteins. Each represents the energetics associated with the deprotonation and protonation of a compound of interest, respectively. Knowledge of the lowest energy site of deprotonation (or protonation) can help explain behavior observed under electrospray ionization (ESI), CID, and ETD conditions and may further assist in the development of fragmentation mechanisms.

Gas-phase acidities have been determined for the standard amino acids by O'Hair and coworkers[18] and Poutsma and coworkers[19] using the kinetic and extended kinetic methods, respectively. The GA values obtained from the two studies are in excellent agreement. Cassady and coworkers[20] recently determined the GAs of glutamic acid, aspartic acid, and their amino acid amides. Recently, Kass and coworkers[21] determined the GA of tyrosine to be 332.5 ± 1.5 kcal/mol using equilibrium gas-phase acidity measurements in a dual cell Fourier transform ioncyclotron resonance mass spectrometer (FT-ICR MS).

In the gas phase, most amino acids and peptides are thought to deprotonate at the C-terminal carboxylic acid group (if such a group is present). Exceptions to this assumption include aspartic acid and glutamic acid residues, which have carboxylic acid groups located on the side chain and can deprotonate readily on either the C-terminus or side chain.[20] Another exception is the cysteine residue, which has been shown to deprotonate on the side chain.[22]

Tyrosine is also unique in that it possesses two acidic functionalities capable of deprotonation, the carboxylic acid group and the phenolic -OH. In the context of a peptide backbone, the carboxylic acid functionality becomes part of the amide linkage, thus removing a likely deprotonation site thath is present in the amino acid but not the amino acid residue. However, deprotonation of peptides lacking acidic sites (such as substance P amide, which part of the MS/MS research of Chapters 3 and 4) has been observed experimentally.[23] Thus, alternative deprotonation sites must be equally accessible using common mass spectrometry ionization techniques such as ESI and matrix-assisted laser desorption ionization (MALDI).

There have been several studies that explore deprotonation of amino acids at the C-terminal carboxylic acid group or elsewhere on the molecule.[20-22, 24 -27] These works demonstrate that the side chain can also be an energetically accessible location for deprotonation. Several studies have addressed the propensity for ESI to produce solution-phase or gas-phase structures.[24, 25, 28] In particular, Kass and coworkers[21, 22] investigated the deprotonation sites of cysteine and tyrosine, as well as several isomeric structures.

Tian and Kass[21, 24] addressed the gas-phase deprotonation (by ESI) of tyrosine and p-hydroxybenzoic acid experimentally and theoretically. They thoroughly investigated whether the compounds were deprotonating on the carboxylic acid group or phenolic -OH. Several different solvent systems were employed, consisting of acetonitrile, water, methanol, or a combination of two of the previously mentioned solvents. Methanol was shown to affect the ratio of phenoxide to carboxylate by increasing the amount of phenoxide substantially. Tian and Kass[21] also developed an elegant reaction involving trimethylsilyl azide ($TMSN_3$) to probe whether the carboxylate anion or the phenolic anion was being produced. Their experimental results indicate that the phenoxide structure is the favored gas-phase deprotonation site when

methanol is used in the solvent system, whereas the carboxylate structure dominates when acetonitrile and/or water are used. Disparate results from photoelectron spectroscopy (PES) experiments indicate the carboxylate structure is dominant. The inconsistency between the $TMSN_3$ and PES experiments is attributed to ESI source differences, where the time ions are trapped in the hexapole differs. These researchers speculated that hexapole accumulation times are thought to affect whether solution-phase or gas-phase structures are produced. The hexapole (see Figure 2.1 in Chapter 2) is present in some mass spectrometer configurations as part of the ESI source where ions are stored and allowed to accumulate prior to transfer to the mass analyzer. Longer accumulation times (1-5 seconds, used in $TMSN_3$ experiments) produce gas-phase structures (e.g. phenoxide), whereas shorter accumulation times (100 milliseconds, used in PES experiments) produce liquid-phase structures (e.g. carboxylate). Computational results from Kass and coworkers (at the B3LYP/aug-cc-pvdz level) show that the carboxylate structure (i.e., deprotonation on the C-terminal carboxylic acid functional group) is the most energetically accessible structure of deprotonated tyrosine by 0.2 kcal/mol over the phenoxide.[21, 25]

Oomens and coworkers[26] performed infrared multiphoton dissociation (IRMPD) on a set of deprotonated amino acids (which included tyrosine) to investigate their gas-phase anionic structures. These spectra were compared to calculated spectra at the B3LYP/6-31++G** level of theory. The amino acid solutions were prepared in 80:20 methanol and water, which is similar to the solvent conditions with which Kass and coworkers[21, 24] observed increased phenoxide production. The ESI source used by Oomens and coworkers[26] was a Micromass Z-spray source with hexapole (and with hexapole accumulation times of several seconds), which is the same commercial source used by Kass and coworkers for the $TMSN_3$ reactions.[21] However, the

experimental IRMPD results show that tyrosine is undoubtedly a carboxylate in the gas-phase under their conditions, with no evidence of a phenoxide structure.

The present study focuses on the GAs of Tyr-OH, Tyr-NH_2, Phe-OH, Phe-NH_2, and HPB (see Figure 5.1 for structures). Tyrosine possesses two possible sites for deprotonation, the carboxylic acid and phenolic functional groups. Phenylalanine has a structure similar to that of tyrosine, but lacking the phenolic -OH group. HPB was chosen for comparison to tyrosine and tyrosine amide because it contains a phenolic side chain, but does not have a carboxy or amino terminus. The amino acid amides, Tyr-NH_2 and Phe-NH_2, are of particular importance because they better represent the behavior of an amino acid residue in the context of a peptide backbone. With the exception of the C-terminal residue, the carboxylic acid moiety is not present along a peptide backbone. The tyrosine amide is expected to provide valuable insight to the ongoing debate over deprotonation site.

5.3 Experimental

5.3.1. Mass spectrometry methods

Ion/molecule reactions were performed in a Bruker BioApex 7e FT-ICR mass spectrometer (Billerica, MA). Samples were prepared at 60 μM (~ 1 mg/mL) in a solvent of 50:50 methanol and ultrapure water (with a 1% spike of ammonium hydroxide to promote deprotonation), then introduced to the Apollo API source (Bruker Daltonics, Billerica, MA) using a syringe pump (Cole Parmer, Vernon Hills, IL) set to deliver ~90 μL/hr. Ions were produced by ESI with a 3.5-4.0 kV potential. The source pressure was ~10^{-7} mbar. Unless noted otherwise in the text, ions produced by ESI were allowed to accumulate in the hexapole for

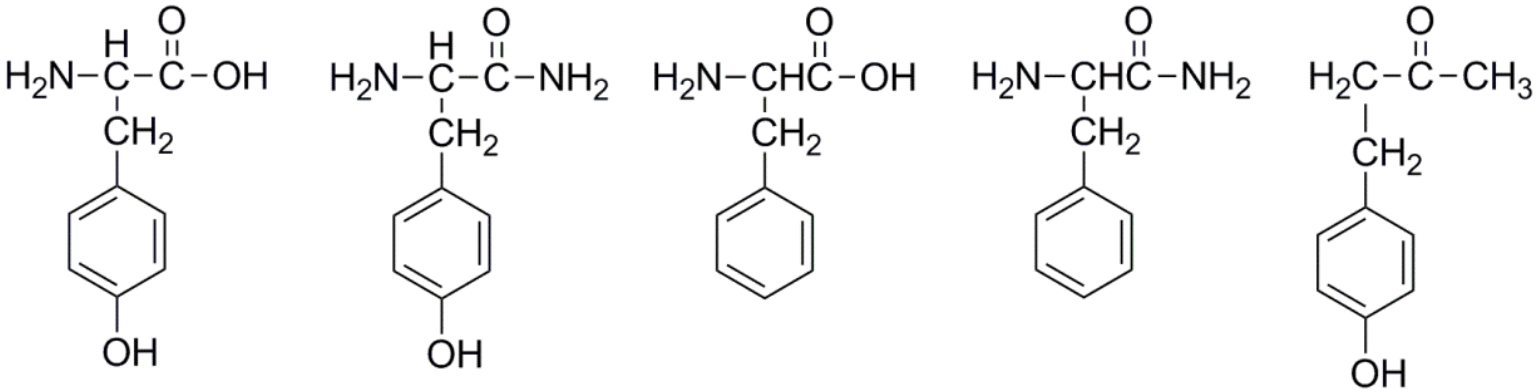

(a) Tyrosine **(b) Tyrosine amide** **(c) Phenylalanine** **(d) Phenylalanine amide** **(e) 4-(4-Hydroxyphenyl)-2-butanone (HPB)**

Figure 5.1 Structures of compounds studied.

700 ms before being transported to the ICR cell by electrostatic focusing. Deprotonated ions, $[M - H]^-$, were mass selected for isolation using correlated frequency ion ejection techniques[29] and then allowed to react with a reference compound that is introduced to the ICR cell through a leak valve at constant pressure. A pumping delay was set to allow the ion/molecule reactions to proceed before detection.

Each of the ions selected for study were reacted with a series of reference compounds that have well-known gas-phase acidities.[30] The reference compound pressures were measured using an ion gauge that has been calibrated as discussed in Chapter 2.[31]

Performing several sets of reactions using reference compounds with varying acidities allows for accurate bracketing to determine the experimental GAs of the amino acid analogs. These pseudo-first order reactions allow for determination of the experimental rate constant (k_{exp}) from a semi-logarithmetic plot of the decreasing precursor ion intensity as a function of time. In cases where deprotonation was in competition with proton-bound dimer formation, k_{exp} was determined from the kinetic relationship (as discussed in Chapter 2) of the relative intensity of the deprotonated reference compound intensity as a function of time. The reactions of Tyr-OH with ethyl cyanoacetate and 4-amino-2,3,5,6-tetrafluoropyridine exhibited non-linear kinetics, indicating the presence of two ion structures reacting at slightly different rates. Experimental rate constants for the non-linear cases were determined from fitting the data to the sum of two exponential decays. A reaction efficiency of 0.27 is used as the break point establish the experimental GA (as detailed in Chapter 2).

5.3.2. Computational methods

The calculations were performed by Michele Stover of Professor David Dixon's research group at the University of Alabama. Calculations were performed at the density functional theory (DFT) and correlated molecular orbital (MO) theory levels with the program Gaussian-03.[32] The geometries were initially optimized at the DFT level with the B3LYP exchange-correlation functional[33, 34] and the DZVP2 basis set.[35] Vibrational frequencies were calculated to show that the structures were minima and to provide zero point and thermal corrections to the enthalpy and entropies so that free energies could be calculated for direct comparison to experiment. The Dixon group optimized a range of structures to determine the most stable conformers. In previous work on the GAs of amino acids[20, 36, 37] and organic acids,[36] the Dixon group showed that the high level G3(MP2) correlated molecular orbital method[38] gave agreement for the acidities with the experimental values to within about ±1 kcal/mol. G3(MP2) has an additional advantage over DFT methods in terms of reliable predictions for these types of compounds because the correlated molecular orbital methods in G3(MP2) perform better in the prediction of hydrogen bond energies as well as steric non-bonded interactions than do most widely-used DFT exchange-correlation functionals.

5.4 Results and discussion

5.4.1 Experimental gas-phase acidities

Structures for each of the studied compounds can be found in Figure 5.1. Tyrosine and phenylalanine (Figures 5.1(a) and 5.1(c), respectively) are standard L-amino acids. Tyrosine amide and phenylalanine amide (Figures 5.1(b) and 5.1(d), respectively) are amino acids that possess a C-terminal amide (-$CONH_2$) rather than a carboxylic acid group (-COOH); they were

also studied in their L-forms. HPB (Figure 5.1(e)) is an organic molecule with a structure similarity to tyrosine, but lacking the N-terminal amine and C-terminal carboxylic acid groups.

Table 5.1 shows the reference compounds that were used in this study, the corresponding gas-phase acidities (GA, ΔG_{acid}), and the reaction efficiencies for proton transfer reactions with each of the reference compounds. Figure 5.2 shows sample mass spectra illustrating the way the proton transfer reactions progress over time. Several reference compounds were attempted that were insufficiently volatile to use in this study; a constant pressure in the 10^{-8} - 10^{-7} mbar range could not be achieved and thus they could not be used. The following compounds were not sufficiently volatile for study in our FT-ICR: 2-chloropropanoic acid (GA = 330.4 ± 2.0 kcal/mol, boiling Point (BP) = 78°C (351 K)), 4-oxo-pentanoic acid (333.7 ± 2.8 kcal/mol, BP = 245-246°C (518-519 K)), methoxyacetic acid (335.3 ± 2.0 kcal/mol, BP = 202-204°C (275-277 K)), 4-chlorophenol (336.2 ± 2.0 kcal/mol, BP = 220°C (493 K)), and butanoic acid (339.5 ± 1.5 kcal/mol, BP = 163.5° (437 K)).

Using the deprotonation reaction efficiency results summarized in Table 5.1, the experimental GAs were assigned at a reaction efficiency of 0.27. Experimental GA values are summarized in Table 5.2. Note that lower numerical GA values correspond to higher acidity. Phenylalanine amide, the least acidic of the compounds studied, has an experimental GA of 345.8 ± 2.4 kcal/mol. HPB has a GA of 339.6 ± 2.7 kcal/mol. Tyrosine amide has an experimental GA of 336.4 ± 2.4 kcal/mol. Phenylalanine has an experimental GA of 332.5 ± 2.2 kcal/mol. This value for phenylalanine is slightly higher than the 329.6 ± 3.0 kcal/mol previously reported by O'Hair and coworkers,[18] but is within experimental error. Poutsma and coworkers[19] reported acidity as ΔH_{acid} = 338.9 ± 4.3 kcal/mol. A comparison of literature values for phenylalanine with this dissertation research may be seen in Table 5.3.

Tyrosine is a special case, since there are two potential sites of deprotonation. Two ion populations were observed in the reactions of $[Tyr\text{-}OH - H]^-$ with ethyl cyanoacetate and 4-amino-2,3,5,6-tetrafluoropyridine (the two ion populations will be discussed later), thus two experimental GAs have been determined. Tyrosine is the most acidic of the compounds studied, with an experimental GA of 332.4 ± 2.4 kcal/mol for deprotonation at the carboxylic acid site, and a GA of 333.5 ± 2.1 kcal/mol for deprotonation at the phenolic -OH site. This is the first report of identification of the distinct GAs for deprotonation of both the phenolic and carboxylic acid sites. This experimental GA of tyrosine is in accord with previously reported values.[18, 19, 21] Table 5.3 shows the literature values for the GA of tyrosine compared with the experimental GA determined in this work.

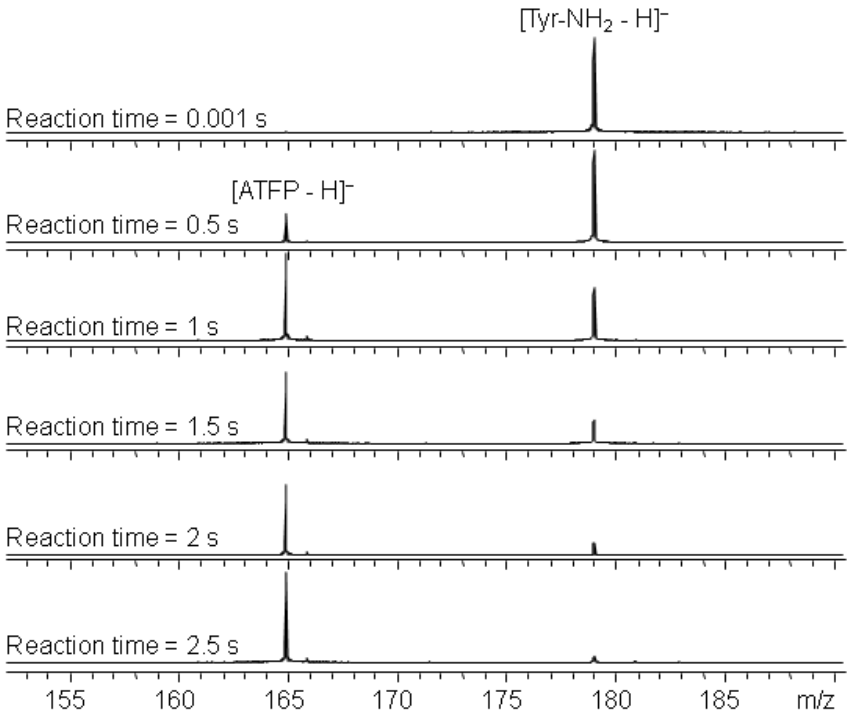

Figure 5.2. Mass spectra for the proton transfer reactions of deprotonated tyrosine amide ($Tyr\text{-}NH_2$) reacting with 4-amino-2,3,5,6-tetrafluoropyridine (ATFP). ATFP is present in the ICR cell at a pressure of 5.2×10^{-8} mbar.

Table 5.1. Reaction efficiencies from the proton transfer reactions of deprotonated tyrosine, phenylalanine, their amino acid amides, and HPB with reference compounds.

Reference Compound	GA[30] (kcal/mol)	Average Reaction Efficiency				
		Phe-NH_2	HPB[b]	Tyr-NH_2	Tyr-OH	Phe-OH
chloroform	349.9 ± 2	0.04 ± 0.01	0.01 ± 0.004	–[b]	–	–
4-trifluoromethyl aniline	346.0 ± 2	0.24 ± 0.05	–	–	–	–
		BREAK				
phenol	342.3 ± 2	0.70 ± 0.05	–	–	–	–
acetic acid	341.1 ± 2	0.29 ± 0.01	0.07± 0.005	0.005 ± 0.004	–	–
			BREAK[c]			
formic acid	339.1 ± 2	0.49 ± 0.06	0.34 ± 0.01	0.12 ± 0.01	–	–
isovaleric acid	338.5 ± 2	0.56 ± 0.04	0.41 ± 0.11	0.09 ± 0.03	–	–
trimethylacetic acid	337.6 ± 2	0.54 ± 0.05	0.41 ± 0.06	0.10 ± 0.02	NR[d]	NR
				BREAK		
p-chlorophenol	336.2 ± 2	–	0.55 ± 0.04	0.33 ± 0.12	NR	NR
ethyl cyanoacetate	333.6 ± 2	–	–	0.20 ± 0.05	0.23 ± 0.06 (24 ± 9%) 0.03 ± 0.04 (76 ± 9%)	0.007 ± 0.001
					BREAK	
4-amino-2,3,5,6-tetrafluoropyridine	332.8 ± 2	–	–	0.33 ± 0.001	0.53 ± 0.25 (30 ± 8%) 0.07 ± 0.01 (70 ± 8%)	0.02 ± 0.003
					BREAK	**BREAK**
3-trifluoromethyl phenol	332.4 ± 2	–	–	1.09 ± 0.04	0.29 ± 0.02	0.36 ± 0.02
3,3,3-trifluoropropionic acid	326.9 ± 2	–	–	–	0.75 ± 0.09	0.79 ± 0.08

[a] HPB stands for 4-(4-hydroxyphenyl)-2-butanone, which is not an amino acid.

[b] "–" indicates that no reaction was performed.

[c] "BREAK" indicates the point where experimental GA was assigned.

[d] "NR" indicates that no reaction was observed.

Table 5.2. Experimental and G3(MP2) calculated GAs (in kcal/mol).

Compound	Deprotonation Site[a]	GA	
		Experimental	G3(MP2)
Phenylalanine	carboxylic acid	332.5 ± 2.2	330.7
Phenylalanine amide	amide	345.8 ± 3.8	347.8
Tyrosine	carboxylic acid	332.4 ± 2.2	330.4
	phenolic -OH	333.5 ± 2.4	332.9
Tyrosine amide	phenolic -OH	336.4 ± 2.7	336.9
HPB	phenolic -OH	339.6 ± 3.0	–[c]

[a] Based on calculations.
[c] Not calculated.

5.4.2 Theoretical gas-phase acidities

Figure 5.3 shows the geometry optimized structures of the amino acids and amino acid amides, as well as their corresponding lowest energy conformer(s) for the deprotonated species. Tyrosine (Figure 5.3(a)) has two low energy structures related to differences in protonation site, the carboxylate and phenoxide, that correspond to calculated GA values of 330.4 and 332.9 kcal/mol, respectively. These two species are nearly isoenergetic, so both are shown. Tyrosine amide (Figure 5.3(b)) does not possess the carboxylic acid functionality; thus its lowest energy structure is the phenoxide, which has a calculated GA of 336.9 kcal/mol. The phenoxide forms of tyrosine and tyrosine amide have calculated GA values that differ by 4 kcal/mol. Hydrogen bonding between the carboxylic acid and amine functionalities on tyrosine has a stabilizing effect on the deprotonated structure. Tyrosine amide does not experience the same hydrogen bonding due to the presence of the amide functionality rather than the carboxylic acid. Previous work by Cassady and coworkers[18] has shown that hydrogen bonding between the carboxylic acid and amine groups of an amino acid has a stabilizing effect on gas-phase conformation. Deprotonation of phenylalanine (Figure 5.3(c)) to form the carboxylate

Table 5.3. Reported experimental and theoretical ΔG_{acid} values for tyrosine and phenylalanine (in kcal/mol).

	Experimental Method	Deprotonation Site	Experimental ΔG_{acid}	Experimental ΔH_{acid}	Computation Level	Theoretical ΔG_{acid}	Theoretical ΔH_{acid}
Tyr-OH:							
Present Work	Bracketing	carboxylic acid	332.4 ± 2.2	–[a]	G3(MP2)	330.4	338.3
		phenolic -OH	333.5 ± 2.4	–		332.9	340.5
Kass and coworkers	Equilibrium	carboxylic acid	332.5 ± 1.5	340.7 ± 1.5	B3LYP	–	339.5
		phenolic -OH	–	–		–	338.3
		carboxylic acid	–	–	G3B3	–	339.9
		phenolic -OH	–	–		–	339.0
Poutsma and coworkers	Extended Kinetic	–	–	337.7 ± 2.6	B3LYP/6-31+G*	–	339.2
O'Hair and coworkers	Kinetic	–	329.5 ± 3.0	337.6 ± 3.1	–	–	–
Phe-OH:							
Present Work	Bracketing	–	332.5 ± 2.2	–	G3(MP2)	330.7	338.5
Poutsma and coworkers	Extended Kinetic	–	–	338.9 ± 4.3	B3LYP/6-31+G*	–	338.7
O'Hair and coworkers	Kinetic	–	329.6 ± 3.0	336.5 ± 3.1	–	–	–

[a] Not reported/available.

[b] Reported theoretical ΔH values include a correction for acetic acid and phenol.

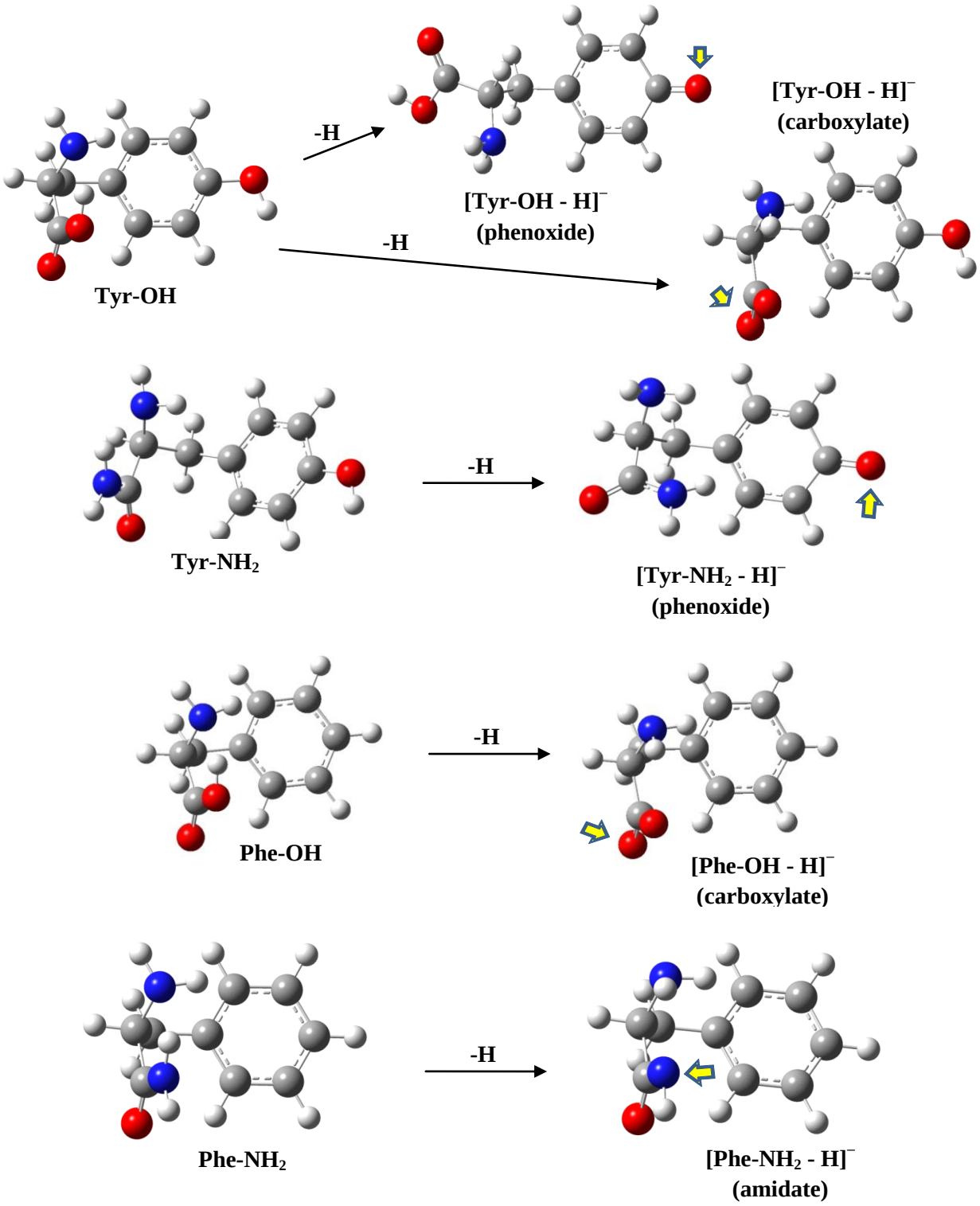

Figure 5.3. Geometry optimized lowest energy structures of neutral and deprotonated forms of tyrosine, phenylalanine, their amino acid amides and HPB. The lowest energy neutral structure is shown for each compound with the corresponding low-energy anion. Arrows indicate the site of deprotonation. Two low-energy anions are shown for tyrosine.

corresponds to a G3(MP2) calculated ΔG_{298}(gas) of 330.7 kcal/mol. Phenylalanine amide (Figure 5.3(d)) deprotonates to form an amidate structure that corresponds to a calculated GA of 347.8 kcal/mol. Table 5.4 shows the G3(MP2) calculated ΔH_{298} and GA (ΔG_{298}) values for all of the explored deprotonation sites of the amino acids and amino acid amides. In all cases, the lowest energy structures of the deprotonated species are more acidic than deprotonation at other sites by at least 8 kcal/mol.

Table 5.4. G3(MP2) calculated thermochemical data at 298 K for tyrosine, phenylalanine, and their amino acid amides.

	Deprotonation Site	ΔH_{298} gas G3(MP2)	ΔH_{298} gas (literature)[19]	ΔG_{298} gas[a] G3(MP2)	pK_a (298) G3(MP2)	pK_a (298) (literature)[39]
Phenylalanine	carboxylic acid	338.5	338.9 ± 4.3	330.7	5.96	1.83
	amine	384.4		376.4	38.01	
	amine	390.3		382.5	46.92	
Phenylalanine amide	amide	355.0		347.8	15.44	
	amide	362.6		355.5	12.94	
	alpha carbon	371.9		364.2	25.43	
Tyrosine	carboxylic acid	338.3	337.7 ± 2.6	330.4	6.50	2.20
	phenolic -OH	340.5		332.9	8.89	
	aromatic ring	358.6		352.9	24.87	
Tyrosine amide	phenolic -OH	344.3		336.9	8.39	
	amide	354.7		347.4	15.50	
	amide	361.3		353.8	15.06	

[a] ΔG_{298} gas = GA.

5.4.3 Isomeric tyrosine species

The reactions of Tyr-OH with ethyl cyanoacetate (ECA) and 4-amino-2,3,5,6-tetrafluoropyridine (ATFP) indicate that there are two ion structures for deprotonated tyrosine. This can be seen in the non-linear nature of the pseudo-first order kinetics plot for the natural log of the relative precursor ion intensity versus reaction time. An example of this from the reaction of deprotonated Tyr-OH with ethyl cyanoacetate is shown in Figure 5.4. Two deprotonated Tyr-OH species are present, a fast reacting species and a slow reacting species. The results of ion/molecule reactions does not provide definitive proof which species is the the fast or slow reacting species, but GAs can be determined for each species. Compared with the theoretical results (see Table 5.2), however, the fast reacting species appears to be the phenolate species. The slow reacting species appears to be the carboxylate species.

When two reacting populations of ions are present, as is the case with the reactions of deprotonated Tyr-OH with ECA and ATFP, the resulting kinetics plot is distinctively non-linear. To obtain the relative abundances of each reacting species and the associated experimental rate constants, the reaction data is fit to the sum of two exponentials.[40] However, many of the data sets from reactions of deprotonated Tyr-OH with ATFP were ill-fitted using this method. Figure 5.5 shows a sample plot of reaction data from the reactions of Tyr-OH with ATFP. The data is clearly non-linear, however, the plot is very different than Figure 5.4. It is possible that the slow reacting population of deprotonated Tyr-OH is converting to the faster reacting population during the reaction with ATFP. However, the GA of ATFP is 332.8 ± 2 kcal/mol[30] and very close to the experimental and theoretical acidities of tyrosine (at either site). Both phenolate and carboxylate species of Tyr-OH are likely reacting with ATFP at such similar rates that they cannot be distinguished.

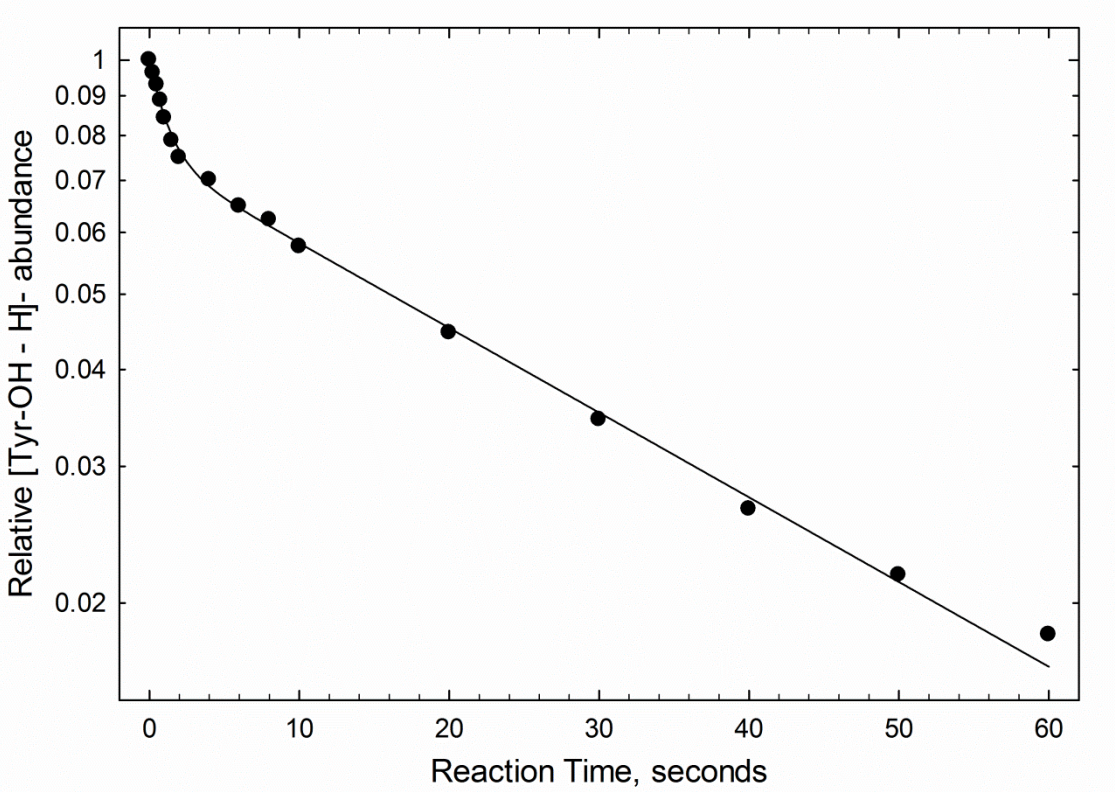

Figure 5.4. Non-linear plot of $[Tyr\text{-}OH - H]^-$ versus reaction time, indicating two isomeric deprotonated species. Data comes from the reactions of deprotonated Tyr-OH with ethyl cyanoacetate at a constant pressure of 8.91×10^{-8} mbar.

Tian and Kass[25] also reported two species of deprotonated Tyr-OH in a previous study of deprotonation site in the gas phase. They designed an elegant method for determining whether the deprotonated tyrosine species was the carboxylate or the phenoxide by a series of reactions of deprotonated Tyr-OH with trimethylsilylazide ($TMSN_3$). Relative ratios of each deprotonated species could be determined from mass spectral product peak intensities. Multiple solvent systems were used in the study[25] and an interesting phenomenon was observed. The phenoxide form of Tyr-OH was predominant, forming in a ratio of 70:30 with the carboxylate, when the solvent system was 3:1 (V:V) methanol to water. Similar ratios of phenoxide were obtained with 1:1 methanol and water. Using a solvent system composed largely of acetonitrile and a small quantity of methanol, ranging from 96:4 to 99:1 acetonitrile to water, the ratio of phenoxide to

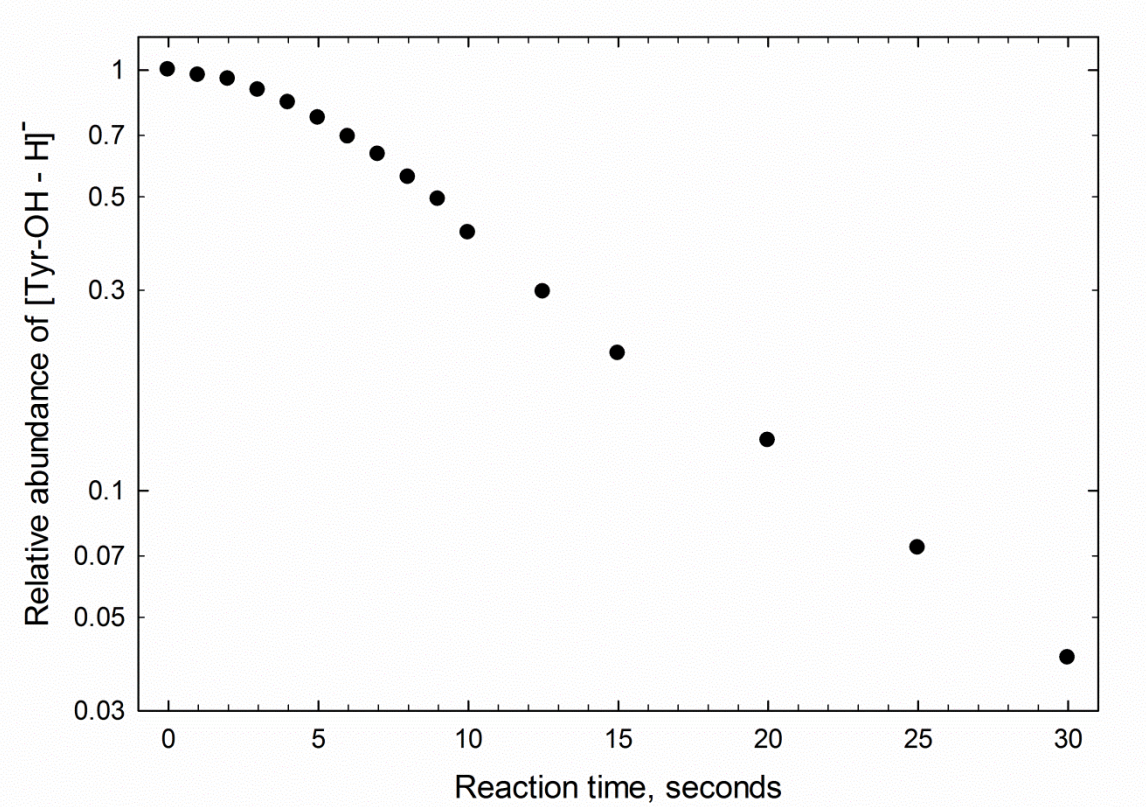

Figure 5.5. Non-linear plot of $[Tyr\text{-}OH - H]^-$ versus reaction time, indicating two isomeric deprotonated species. Data comes from the reactions of deprotonated Tyr-OH with 4-amino-2,3,5,6-tetrafluoropyridine at a constant pressure of 2.8×10^{-8} mbar using a hexapole accumulation time of 1 millisecond.

carboxylate decreased slightly. When methanol was absent from the solvent system (meaning solvent was either pure acetonitrile, or some combination of acetonitrile and water), the carboxylate was dominant and very little phenoxide formed.

Photoelectron spectroscopy (PES) results also previously reported by Kass and coworkers[21] indicate a more dominant carboxylate structure regardless of solvent system. This was attributed to the differences in instrumentation between the PES experiments and $TMSN_3$ reactions. The ESI sources used in the experiments had very different hexapole accumulation times (as discussed in section 6.1 of this chapter). The differing sources were a homebuilt ESI source (used in PES experiments) that had an accumulation time of 100 ms and a commercial

ESI source (used for $TMSN_3$ experiments) that had accumulation times between 1-5 s.[21] As mentioned earlier in the chapter, Oomens and coworkers[26] reported a hexapole accumulation times of several seconds for IRMPD experiments with deprotonated Tyr-OH. These accumulation times match what was used in Kass'[21] $TMSN_3$ experiments, yet conflicting results were reported.

To investigate the effect of hexapole accumulation time and solvent, we performed reactions of deprotonated tyrosine with ethyl cyanoacetate and 4-amino-2,3,5,6-tetrafluoropyridine using varied hexapole accumulation times and solvent systems. The hexapole accumulation time is easily manipulated in the Apollo API source on our Bruker BioApex 7e FT-ICR. Thus, accumulation times similar to the two ESI sources used in Kass' PES and $TMSN_3$ experiments could be used. A short hexapole accumulation time of 1 ms was used to mimic the conditions of the homebuilt ESI and a long hexapole accumulation time of 5 s was used to mimic the conditions in the commercial ESI source. Tyr-OH was prepared in three different solvent systems: 50:50 methanol and ultrapure water, 75:25 methanol and ultrapure water, and 50:50 acetonitrile and ultrapure water (each with an added 1% spike of ammonium hydroxide to assist in ion formation).

The reactions of deprotonated Tyr-OH with ECA produce two interesting results: solvent system does not appear to greatly affect the abundances of each ion population, and hexapole accumulation time greatly affects the relative ion abundances. The three solvent systems utilized in these experiments mirrored those used in both Kass' and Oomens' reported experiments (although the ionization aide (e.g. NaOH, NH_4OH) differed).

The kinetics plots for each of the different solvent systems produced comparable relative ion abundances. This, however, cannot be definitive proof that the solvent system does not

affect the deprotonation of Tyr-OH. Other solvent systems such as pure water, pure acetonitrile, and other varied solvent systems with or without the addition of an ionization aide would be interesting to investigate.

Different hexapole accumulation times produced very different results for the reactions of deprotonated Tyr-OH with ECA. The results of these experiments are compiled in Table 4. At very long accumulation times of 5 seconds, the two deprotonated Tyr-OH species were produced in a 24:76 ratio of fast reacting to slow reacting species. At very short hexapole accumulation times of 1 millisecond, the fast reacting species nearly disappears. The fast reacting to slow reacting ratio for short accumulation times is 7:93. Observation of such different ratios of fast reacting to slow reacting ion species from drastically different accumulation times is indicative that hexapole accumulation time has a considerable effect on ion production. The longer accumulation times allow the deprotonated Tyr-OH to isomerize, forming primarily the lowest energy gas-phase structure. The pressure inside the hexapole is $\sim 1 \times 10^{-3}$ mbar, and isomerization of the deprotonated Tyr-OH may be a result of solvent interactions or heating that occurs while ions are accumulating in the hexapole. This is due to a radial stratification effect of the ion cloud.[41]

Using the reaction data from the 5 second accumulation time reactions of deprotonated Tyr-OH and ECA allowed for determination of the GAs of both the phenoxide and carboxylate species. The 5 second data had much more of the fast reacting species present, thus it was used to determine the reaction efficiencies for the two deprotonated species.

Reactions of deprotonated Tyr-OH and ATFP were also performed using the same three solvent systems and hexapole accumulation times that were used in the ECA reactions. Once again, the solvent systems did not affect the ion populations, and the hexapole accumulation

times did affect the ion populations. In this case, however, the result is not quite as definitive of the relative abundances of the two ion populations. A long hexapole accumulation time of 5 seconds resulted in pseudo-first order kinetics plots that were linear, indicating only one reacting ion species. Short accumulation times of 1 millisecond produce non-linear pseudo-first order kinetics plots. The results of the short accumulation time experiments indicate that there are two reacting ion species.

The sample kinetics plot shown earlier in Figure 5.5 shows the result of a 1 ms accumulation time data set. Figure 5.6 shows a sample kinetics plot from the reaction of deprotonated Tyr-OH with ATFP using a 5 second hexapole accumulation time. The shape of the kinetics plot in Figure 5.5 is different than what was observed previously in the reactions of Tyr-OH with ECA (Figure 5.4). The slow reacting species seems to isomerize to the fast reacting species. Both species are reacting with similar rates, and the acidity of Tyr-OH is very close to that of the ATFP (332.8 ± 2 kcal/mol[30]). Thus, the reactions with ATFP are not a good, reproducible approach to determine relative abundances of the two Tyr-OH anion populations.

Two data sets from the reactions of deprotonated Tyr-OH with ATFP were fit to the sum of two exponentials, and ion populations were observed that were similar to what was observed for the reactions of Tyr-OH with ECA. Thus, the experimental GAs of the two species of anionic Tyr-OH could be assigned using some of the ATFP data.

5.4.4 Comparison of tyrosine and tyrosine amide with HPB

The amino acids and amino acid amides in this study all have structural similarities to each other, and more importantly, to Tyr-OH. HPB, in particular, was chosen because it possesses a phenolic -OH like Tyr-OH, but does not have the carboxylic acid or amine

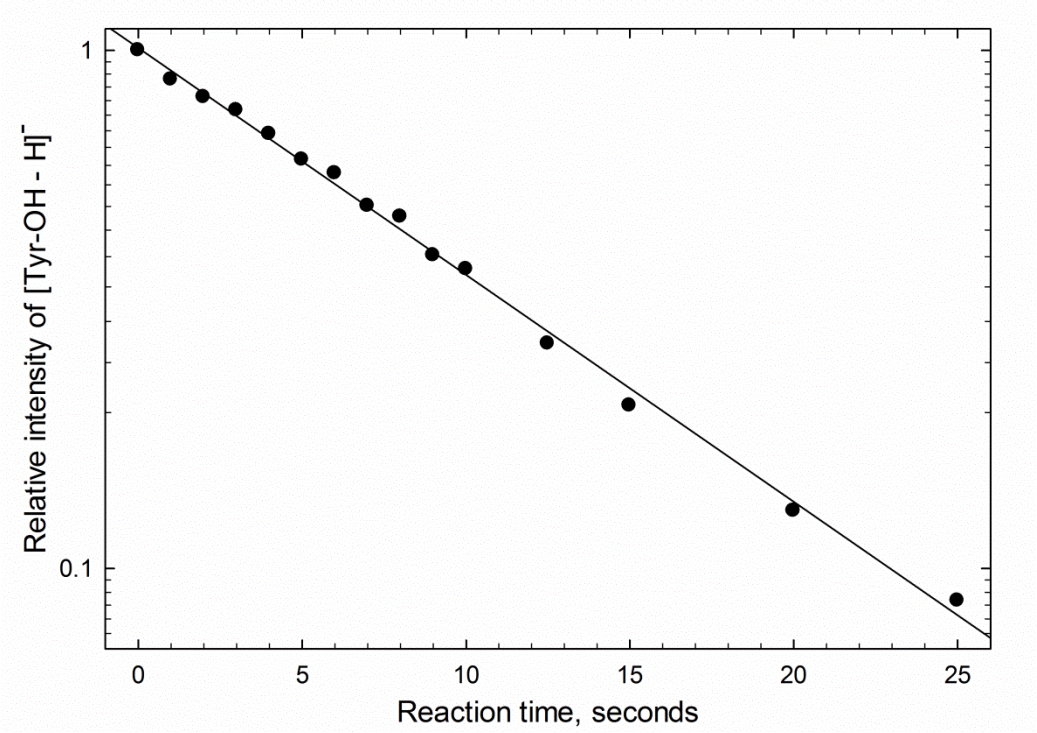

Figure 5.6. Linear plot of $[Tyr\text{-}OH - H]^-$ versus reaction time. Obtained from the reactions of deprotonated Tyr-OH with 4-amino-2,3,5,6-tetrafluoropyridine at a constant pressure of 2.8×10^{-8} mbar using a hexapole accumulation time of 5 seconds.

functionalities. The structure of HPB is also similar to tyrosine amide, but without the amine functionality.

HPB has a GA of 339.6 kcal/mol, which corresponds to deprotonation at the phenolic -OH. This is ~6 kcal/mol less acidic than deprotonation of Tyr-OH at the phenolic -OH and ~7 kcal/mol less acidic than deprotonation of Tyr-OH at the carboxylic acid group. The energy difference between deprotonation at the phenolic -OH for HPB and Tyr-OH show the effect that hydrogen bonding motifs can have on acidity. Tyr-OH can have stabilizing hydrogen bonds between the carboxylic acid and amine groups. Tyrosine amide is ~3 kcal/mol more acidic (lower GA) than HPB. Replacing the carboxylic acid group with an amide group lessens the acidity of the phenolic -OH, but hydrogen bonding between the amide and amine groups can still

occur. HPB cannot experience the same stabilizing effects of hydrogen bonding due to the lack of additional electronegative atoms in the molecular structure. Thus, the GA value of HPB is fairly high (low acidity).

5.5 Conclusions

The GAs of Phe-NH_2, Tyr-NH_2, and HPB have been determined for the first time. The GAs of Phe-OH and Tyr-OH have been determined using the bracketing method, and results are in agreement with previously reported values.[18, 19, 21] Two experimental GAs were obtained for Tyr-OH, corresponding to deprotonation at the phenolic and carboxylic acid -OHs. All of the experimentally determined GAs agree with G3(MP2) calculated GA values within experimental error. The two ion structures observed for Tyr-OH in the reactions with ethyl cyanoacetate and 4-amino-2,3,5,6-tetrafluoropyridine were used to distinguish their individual GAs. These structures correspond to the phenoxide and carboxylate anions of Tyr-OH; however ion/molecule reactions cannot distinguish the ions but can only determine the relative abundances of each. Ion population abundances of fast reacting:slow reacting were 24:76 in reactions with ethylcyanoacetate and 30:70 in reactions with 4-amino-2,3,5,6-tetrafluoropyridine. Very short hexapole accumulation times decreased the amount of the fast reacting species observed in the reactions of Tyr-OH with ethyl cyanoacetate to 7:93. Performing the $TMSN_3$ reactions described by Kass and coworkers[21] using other varied solvent systems and hexapole accumulation times may elucidate the identity of the fast and slow reacting species of deprotonated Tyr-OH.

References

1. Wen, Z. L.; Zhong, Z.; Darnell, J. E. Maximal activation of transcription by Stat1 and Stat3 requires both tyrosine and serine phosphorylation. *Cell* **1995**, *82*, 241-250.

2. Margolis, B.; Rhee, S. G.; Felder, S.; Mervic, M.; Lyall, R.; Levitzki, A.; Ullrich, A.; Zilberstein, A.; Schlessinger, J. Egf induces tyrosine phosphorylation of phospholipase C-Ii - A potential mechanism for Egf receptor signaling. *Cell* **1989**, *57*, 1101-1107.

3. Burridge, K.; Turner, C. E.; Romer, L. H. Tyrosine phosphorylation of Paxillin and Pp125(fak) accompanies cell-adhesion to extracellular-matrix - A role in cytoskeletal sssembly. *J. Cell Biol.* **1992**, *119*, 893-903.

4. Auger, K. R.; Serunian, L. A.; Soltoff, S. P.; Libby, P.; Cantley, L. C. Pdgf-dependent tyrosine phosphorylation stimulates production of novel polyphosphoinositides in intact-cells. *Cell* **1989**, *57*, 167-175.

5. Fitzpatrick, P. Tetrahydropterin-dependent amino acid hydroxylases. *Annu. Rev. Biochem.* **1999**, *68*, 355-381.

6. Ullrich, A.; Schlessinger, J. Signal transduction by receptors with tyrosine kinase-activity. *Cell* **1990**, *61*, 203-212.

7. Marshall, C. J. Specificity of receptor tyrosine kinase signaling - Transient versus sustained extracellular signal-regulated kinase activation. *Cell* **1995**, *80*, 179-185.

8. Debus, R. J.; Barry, B. A.; Sithole, I.; Babcock, G. T.; McIntosh, L. Directed mutagenesis indicates that the donor to P-680+ in photosystem-II is tyrosine-161 of the D1 polypeptide. *Biochemistry* **1988**, *27*, 9071-9074.

9. O'Malley, P. Hybrid density functional studies of the oxidation of phenol-imidazole hydrogen-bonded complexes: A model for tyrosine oxidation in oxygenic photosynthesis. *J. Am. Chem. Soc.* **1998**, *120*, 11732-11737.

10. Kaufman, S.; Holtzman, N. A.; Milstein, S.; Butler, I.; Krumholz, A. Phenylketonuria due to a deficiency of dihydropteridine reductase. *N. Engl. J. Med.* **1975**, *293*, 785-790.

11. Scriver, C.; Waters, P. Monogenic traits are not simple - Lessons from phenylketonuria. *Trends Genet.* **1999**, *15*, 267-272.

12. Pu, D.; Cassady, C. J. Negative ion dissociation of peptides containing hydroxyl side chains. *Rapid Commun. Mass Spectrom.* **2008**, *22*, 91-100.

13. Waugh, R. J.; Bowie, J. H.; Hayes, R. N. Collision induced dissociations of deprotonated peptides : Dipeptides containing phenylalanine, tyrosine, histidine and tryptophan. *Int. J. Mass Spectrom. Ion Processes* **1991**, *107*, 333-347.

14. Bowie, J. H.; Brinkworth, C. S.; Dua, S. Collision-induced fragmentations of the $(M-H)^-$ parent anions of underivatized peptides: An aid to structure determination and some unusual negative ion cleavages. *Mass Spectrom. Rev.* **2002**, *21*, 87-107.

15. Bradbury, A. F.; Smyth, D. G. Biosynthesis of the C-terminal amide in peptide hormones. *Biosci. Rep.* **1987**, *7*, 907-916.

16. Bradford, A. M.; Waugh, R. J.; Bowie, J. H. Characterization of underivatized tetrapeptides by negative-ion fast-atom bombardment mass spectrometry. *Rapid Commun. Mass Spectrom.* **1995**, *9*, 677-685.

17. Harrison, A. G. Effect of phenylalanine on the fragmentation of deprotonated peptides. *J. Am. Soc. Mass Spectrom.* **2002**, *13*, 1242-1249.

18. O'Hair, R. A. J.; Bowie, J. H.; Gronert, S. Gas phase acidities of the alpha amino acids. *Int. J. Mass Spectrom.* **1992**, *117*, 23-36.

19. Jones, C. M.; Bernier, M.; Carson, E.; Colyer, K. E.; Metz, R.; Pawlow, A.; Wischow, E. D.; Webb, I.; Andriole, E. J.; Poutsma, J. C. Gas-phase acidities of the 20 protein amino acids. *Int. J. Mass Spectrom.* **2007**, *267*, 54-62.

20. Li, Z.; Matus, M. M.; Velazquez, H. A.; Dixon, D. A.; Cassady, C. J. Gas-phase acidities of aspartic acid, glutamic acid, and their amino acid amides. *Int. J. Mass Spectrom.* **2007**, *265*, 213-223.

21. Tian, Z.; Wang, X.; Wang, L.; Kass, S. R. Are carboxyl groups the most acidic sites in amino acids? gas-phase acidities, photoelectron spectra, and computations on tyrosine, p-hydroxybenzoic acid, and their conjugate bases. *J. Am. Chem. Soc.* **2009**, *131*, 1174-1181.

22. Tian, Z.; Pawlow, A.; Poutsma, J. C.; Kass, S. R. Are carboxyl groups the most acidic sites in amino acids? Gas-phase acidity, H/D exchange experiments, and computations on cysteine and its conjugate base. *J. Am. Chem. Soc.* **2007**, *129*, 5403-5407.

23. Gao, J.; Cassady, C. J. Negative ion production from peptides and proteins by matrix-assisted laser desorption/ionization time-of-flight mass spectrometry. *Rapid Commun. Mass Spectrom.* **2008**, *22*, 4066-4072.

24. Tian, Z.; Kass, S. R. Gas-phase versus liquid-phase structures by electrospray ionization mass spectrometry. *Angew. Chem. Int. Edit.* **2009**, *48*, 1321-1323.

25. Tian, Z.; Kass, S. R. Does electrospray ionization produce gas-phase or liquid-phase structures? *J. Am. Chem. Soc.* **2008**, *130*, 10842-10843.

26. Oomens, J.; Steill, J. D.; Redlich, B. Gas-phase IR spectroscopy of deprotonated amino acids. *J. Am. Chem. Soc.* **2009**, *131*, 4310-4319.

27. Li, Z.; Yalcin, T.; Cassady, C. J. C-terminal amino acid residue loss for deprotonated peptide ions containing glutamic acid, aspartic acid, or serine residues at the C-terminus. *J. Mass Spectrom.* **2006**, *41*, 939-949.

28. Steill, J. D.; Oomens, J. Gas-phase deprotonation of p-hydroxybenzoic acid investigated by IR spectroscopy: Solution-phase structure is retained upon ESI. *J. Am. Chem. Soc.* **2009**, *131*, 13570-13571.

29. de Koning, L. J.; Nibbering, N. M. M.; van Orden, S. L.; Laukien, F. H. Mass selection of ions in a Fourier transform ion cyclotron resonance trap using correlated harmonic excitation fields (CHEF). *Int. J. Mass Spectrom.* **1997**, *165*, 209-219.

30. Bartmess, J. E. In *Negative Ion Energetics Data;* Linstrom, P. J., Mallard, W. G., Eds.; NIST Chemistry WebBook, NIST Standard Reference Database Number 69; National Institute of Standards and Technology: Gaithersburg MD, 20899, http://webbook.nist.gov, (retrieved August 2, 2011).

31. Zhang, K.; Cassady, C. J.; Chung-Phillips, A. Ab-initio studies of neutral and protonated triglycines - Comparison of calculated and experimental gas-phase basicity. *J. Am. Chem. Soc.* **1994**, *116*, 11512-11521.

32. Frisch, M. J.; Trucks, G. W.; Schlegel, H. B.; Scuseria, G. E.; Robb, M. A.; Cheeseman, J. R.; Scalmani, G.; Barone, V.; Mennucci, B.; Petersson, G. A.; Nakatsuji, H.; Caricato, M.; Li, X.; Hratchian, H. P.; Izmaylov, A. F.; Bloino, J.; Zheng, G.; Sonnenberg, J. L.; Hada, M.; Ehara, M.; Toyota, K.; Fukuda, R.; Hasegawa, J.; Ishida, M.; Nakajima, T.; Honda, Y.; Kitao, O.; Nakai, H.; Vreven, T.; Montgomery, J. A. J.; Peralta, J. E.; Ogliaro, F.; Bearpark, M.; Heyd, J. J.; Brothers, E.; Kudin, K. N.; Staroverov, V. N.; Keith, T.; Kobayshi, R.; Normand, J.; Raghavachari, K.; Rendell, A.; Burant, J. C.; Iyengar, S. S.; Tomasi, J.; Cossi, M.; Rega, N.; Millam, J. M.; Klene, M.; Knox, J. E.; Cross, J. B.; Bakken, V.; Adamo, C.; Jaramillo, J.; Gomperts, R.; Stratmann, R. E.; Yazyev, O.; Austin, A. J.; Cammi, R.; Pomelli, C.; Ochterski, J. W.; Martin, R. L.; Morokuna, K.; Zakrzewski, V. G.; Voth, G. A.; Salvador, P.; Dannenberg, J. J.; Dapprich, S.; Daniels, A. D.; Farkas, O.; Foresman, J. B.; Ortiz, J. V.; Cioslowshi, J.; Fox, D. J. Gaussian 09, Revision B.0. **2010**.

33. Becke, A. D. Density-functional thermochemistry. III. The role of exact exchange. *J. Chem. Phys.* **1993**, *98*, 5648-5652.

34. Lee, C.; Yang, W.; Parr, R. G. Development of the Colle-Salvetti correllation energy formula into a functional of the electron density. *Phys. Rev. B* **1988**, *37*, 785-789.

35. Godbout, N.; Salahub, D. R.; Andzelm, J.; Wimmer, E. Optimization of Gaussian-type basis sets for local spin density functional calculations. Part I. Boron through neon, optimization technique and validation. *Can. J. Chem.* **92**, *70*, 560-571.

36. Gutowski, K. E.; Dixon, D. A. Ab initio prediction of the gas- and solution-phase acidities of strong Brønsted acids: The calculation of pK_a values less than -10. *J. Phys. Chem. A* **2006**, *110*, 12044-12054.

37. Stover, M. L.; Jackson, V.; Matus, M.; Adams, M.; Cassady, C. J.; Dixon, D. A. fundamental thermochemical properties of amino acids: Gas-phase and aqueous acidities and gas-phase heats of formation. *J. Phys. Chem. B* **2012**, *116*, 2905-2916.

38. Curtiss, L. A.; Redfern, P. C.; Raghavachari, K.; Rassolov, V.; Pople, J. A. Gaussian-3 theory using reduced Moller-Plesset order. *J. Chem. Phys.* **1999**, *110*, 4703-4709.

39. *IUPAC. Compendium of Chemical Terminology.* Blackwell Scientific Publications: Oxford, 1997.

40. Espenson, J. H. In *Chemical Kinetics and Reaction Mechanisms;* McGraw-Hill: New York, 1981.

41. Easterling, M. L.; Bruker Daltonics (private communication, March 28, 2012).

CHAPTER 6: DEPROTONATION OF THE PEPTIDE BACKBONE: A GAS-PHASE ACIDITY STUDY OF TRIPEPTIDES

6.1 Overview

The gas-phase acidities (GAs) of several tripeptides were determined for the first time. Gas-phase deprotonation reactions are performed using the bracketing method to determine GAs experimentally. High-level G3(MP2) calculations have been performed (by David Dixon's group at the University of Alabama) to determine the GAs theoretically and to gain information on structures. Six standard (C-terminal -COOH) peptides were studied: triglycine (GGG), trialanine (AAA), trisarcosine (G′G′G′), tri-2-methylalanine (A′A′A′), glycylalanylglycine (GAG), and alanylglycylalanine (AGA). Three peptides were studied with C-termini that had been converted to a methyl ester: triglycine methyl ester (GGG-OMe), trialanine methyl ester (AAA-OMe), and glycylalanylglycine methyl ester (GAG-OMe). Other peptide methyl esters, trisarcosine methyl ester (G′G′G′-OMe), tri-2-methylalanine methyl ester (A′A′A′-OMe), and alanylglycylalanine methyl ester (AGA-OMe) did not produce abundant $[M - H]^-$ by ESI; thus their GAs could not be determined experimentally. In the absence of an acidic group such as the C-terminal carboxylic acid functionality, a peptide should preferentially deprotonate at the lowest energy site on the backbone. Amide nitrogens and alpha carbons are potential sites for deprotonation on the peptide backbone. G3(MP2) calculations by the Dixon research group show that the backbone amide nitrogens of the peptides in this research are the lowest energy sites of backbone deprotonation.

The collision-induced dissociation (CID) spectra of several protonated and deprotonated tripeptides with standard and methyl esterified C-termini were also acquired. Deprotonated methyl esters produce primarily $[M - H - MeOH]^-$ under CID condtions. The deprotonated peptides composed of non-standard amino acid residues (e.g. G′G′G′ and A′A′A′) yield typical CID fragmentation for alkyl based peptides, however, G′G′G′ produces higher abundances of peaks related to amide bond cleavage than observed for the other peptides. CID of protonated GGG-OMe and AAA-OMe produce enhanced $y_1''^+$ compared to GGG and AAA. G′G′G′ and G′G′G′-OMe produce an unusual internal ion not previously reported in the literature.

6.2 Introduction

Deprotonation of a peptide is generally accepted to take place at an acidic functional group such as a C-terminal -COOH or a glutamic acid or aspartic acid side chain (which is also a -COOH).[1, 2] While acidic groups are favored sites of deprotonation, there have been reports on deprotonation of neutral or even basic peptides by electrospray ionization (ESI), matrix-assisted laser desorption ionization (MALDI) and fast atom bombardment (FAB).[3-6] (Also discussed in Chapter 3) Therefore, typical mass spectrometry ionization techniques are capable of deprotonating a peptide somewhere along the backbone, such as at the amide nitrogen or alpha carbon. Deprotonation of a peptide at a position other than the C-terminus may have a significant effect on dissociation, since most dissociation is charge-directed.[7, 8] Exploration of alternate deprotonation sites for peptides may enhance the collective understanding of the mechanistic pathways of peptide dissociation in mass spectrometry. Determination of the gas-phase acidity (GA) for peptides that do not posess traditional acidic sites is important to understanding the energetic basis for deprotonation along the backbone. GA is defined as the

negative Gibbs free energy change for the deprotonation reaction shown in Reaction 6.1 (defined at 298 K):

$$M \rightarrow [M - H]^- + H^+ \qquad -\Delta G_{reaction} = GA \qquad 6.1$$

The GAs for 19 of the standard amino acids (not including glutamic and aspartic acids) were determined by Bowie and coworkers[9] using the kinetic method (which was discussed in Chapter 2, Section 2.4). Previous work in the Cassady group[2] investigated the GAs of glutamic acid, aspartic acid, and their amino acid amides. The GA determinations involving amino acids and (except for those of Cassady and coworkers[2]) focused on species possessing C-terminal carboxylic acid groups (-COOH); however, this provides an incomplete representation of amino acid residues in the context of a peptide backbone. When an amino acid residue is positioned at the C-terminus, the GAs of that amino acid can be of importance. When the residue is present in a position other than the C-terminus, the GA of that amino acid (which typically represents deprotonation at the C-terminal -COOH) becomes insignificant because the C-terminal of the amino acid does not exist in the residue. Thus, the GAs of the amino acid amides (which possess a $-CONH_2$ at the C-terminus rather than a -COOH) provide a more complete representation of the peptide backbone.

Deprotonation of amino acids (as discussed in Chapter 5) and peptides at sites other than the C-terminus is important. As mentioned in Chapter 3, Section 3.3, substance P amide does not have any acidic amino acid residues in the peptide sequence (in fact, the peptide sequence is quite basic, containing arginine and lysine) and has an amidated C-terminus. Substance P still produces abundant $[M - H]^-$ by both MALDI and ESI.[3, 6] As discussed in Chapter 5, tyrosine has two potential deprotonation sites, the phenolic -OH and the C-terminal -COOH. The results of

the GA experiments and theoretical calculations in Chapter 5 show that deprotonation at both sites of tyrosine have similar energies. The capability of phenylalanine amide (Phe-NH_2, discussed in Chapter 5) to deprotonate also shows that typical acidic sites are not necessary for deprotonation by ESI.

The dissociative behavior of small, alkyl-based peptides has been thoroughly studied by low- and high-energy CID. Much of the early work on high-energy CID involved production of ions by negative chemical ionization (nCI) or fast atom bombardment (FAB) (to produce $[M - H]^-$) or electron ionization (EI) (to produce M^-).[1, 4, 10-14] High-energy CID of small negatively-charged peptides produces abundant loss of CO_2 (forming a_n^-, n = length of peptide) from $[M - H]^-$, as well as abundant $''b_n^-$ and y_n^- ions. Low-energy CID of small, deprotonated peptides possessing alkyl side chains produces the same types of fragmentation, with a larger emphasis on the $''b_n^-$ and y_n^- ions.[15] Harrison[15] attributed the production of abundant a_3^- to a higher energy process, which rationalizes why these ions were less abundant in his low-energy CID experiments. Larger deprotonated peptides produce primarily c-type ions under CID conditions.[16]

The work discussed here focuses on a select group of model tripeptides composed of amino acids with alkyl or hydrogen side chains, as well as the methyl esters of these peptides. Hydrogens were removed at specific sites along the peptide backbone (and replaced with methyl groups) in order to obtain information about protonation site and its affect on acidity. Gas-phase acidities (GAs) were determined using ion/molecule reactions. Dissociative behavior was investigated using CID of the protonated, $[M + H]^+$,and deprotonated, $[M - H]^-$, species. Experimental GA results are reinforced by computations performed by the Dixon group at the University of Alabama.

6.3 Experimental

6.3.1. Mass spectrometry methods

All CID experiments were performed using a Bruker HCTultra PMT Discovery System equipped with ESI (Billerica, MA). Both deprotonated and protonated peptides were produced using ESI, and CID was performed on each species. Samples were prepared for analysis in ~2 μM concentrations in both 50:50:1 (V:V:V) ACN:H_2O:NH_4OH (to produce $[M - H]^-$) and 50:50:1 ACN:H2O:AcOH (to produce $[M +H]^+$). The ESI and CID experiments were performed as described in Chapter 2.

Ion/molecule reactions were performed in a Bruker BioApex 7T FT-ICR mass spectrometer (Billerica, MA). Samples were prepared 60 μM in 50:50:1 MeOH:H_2O:NH_4OH, then introduced to the Apollo API source (Bruker Daltonics, Billerica, MA) using a syringe pump (Cole Parmer, Vernon Hills, IL) set to deliver ~90 μL/hr. Electrospray ionization (ESI) employed a 3.5-4.0 kV potential to produce the deprotonated and protonated molecular ions of interest. The source pressure was ~10^{-7} mbar. Ions were allowed to accumulate in the hexapole for 700 ms before being transported to the ICR cell by electrostatic focusing. Deprotonated ions, $[M - H]^-$, were mass selected for isolation using correlated frequency ion ejection techniques[17] and then allowed to react with a reference compound that was introduced to the ICR cell through a leak valve at constant pressure. A pumping delay was set to allow ion/molecule reactions to proceed before detection.

Each of the ions selected for study were reacted with a series of reference compounds that have known GAs.[18] The ion gauge was calibrated as detailed in Chapter 2. Performing several sets of reactions using reference compounds with varying acidities allows for accurate bracketing to determine the experimental GA of the amino acid analogs. These pseudo-first

order reactions allow for determination of the experimental rate constant (k_{exp}) from a semi-logarithmic plot of the decreasing precursor ion intensity as a function of time. In cases where deprotonation was in competition with proton-bound dimer formation, k_{exp} was determined by fitting the experimental reaction data as discussed in Chapter 2 (Section 2.4).

The ratio of the experimental rate constant to the thermal capture rate constant[19, 20] produces a reaction efficiency (RE) that is used to establish the GA. A RE of 0.27 is used as a break point, to designate the point at which the reaction becomes exoergic (as discussed in Chapter 2).

6.3.2. Computational methods

The calculations by Michele Stover of the Dixon group were performed at the density functional theory (DFT) and correlated molecular orbital (MO) theory levels with the program Gaussian-03.[21] The geometries were initially optimized at the DFT level with the B3LYP exchange-correlation functional[22, 23] and the DZVP2 basis set.[24] Vibrational frequencies were calculated to show that the structures are minima and to provide zero point and thermal corrections to the enthalpy and entropies so that free energies could be calculated for direct comparison to experiment. The most stable conformers were determined by optimizing a range of structures. In previous work by the Dixon and Cassady groups on the GAs of amino acids[2, 25, 26] and organic acids[25] high level G3(MP2) correlated molecular orbital method[27] gave agreement for the acidities with the experimental values to within about ±1 kcal/mol. G3(MP2) has an additional advantage over DFT methods in terms of reliable predictions for these types of compounds because the correlated molecular orbital methods in G3(MP2) perform better in the

prediction of hydrogen bond energies as well as steric non-bonded interactions than do most widely-used DFT exchange-correlation functionals.

6.4 Results and discussion

Six model tripeptides were chosen for this experiment: GGG, AAA, GAG, AGA, G′G′G′, and A′A′A′. G′G′G′ is structurally similar to GGG, except that each of the amide nitrogens along the peptide backbone are methylated (and the N-terminal nitrogen has one methyl group and one hydrogen). A′A′A′ is similar to AAA, except that each of the alpha carbons along the peptide backbone has two methyl groups (i.e., no hydrogens present on any of the alpha carbons). The structures of each of these model peptides can be seen in Figure 6.1.

The methyl esters of each of these peptides were also studied and their structures can be seen in Figure 6.2. This means that the C-terminal carboxylic acid group (-COOH) was converted to a methyl ester group (-$COCH_3$ or -COMe). Studies using ESI and CID of some of the deprotonated peptide methyl esters (which will be discussed later) revealed that three of the peptide methyl esters were not suitable for ion/molecule reactions because of a very weak deprotonated ion, $[M - H]^-$, signal. Thus, AGA-OMe, G′G′G′-OMe, and A′A′A′-OMe (structures shown in Figure 6.3) were eliminated from the ion/molecule reaction study, but calculations were still performed to elucidate structures that may explain why these peptides could not be deprotonated by ESI.

(a) GGG:

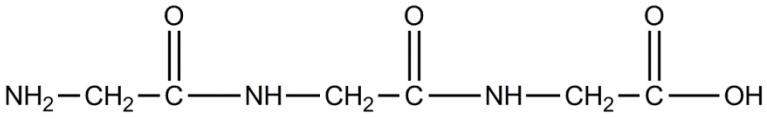

(b) AAA:

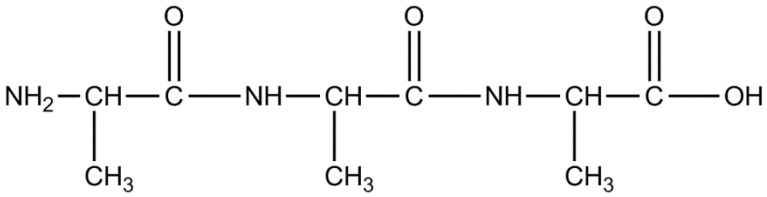

(c) GAG:

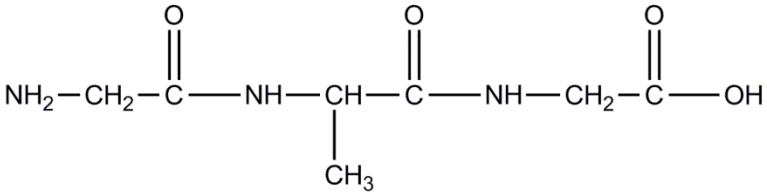

(d) AGA:

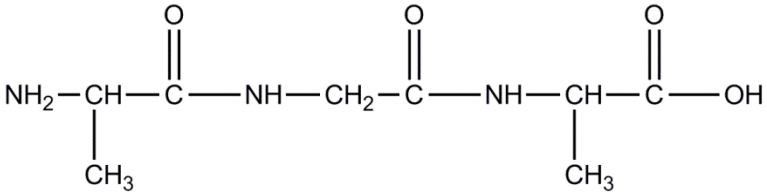

(e) G'G'G':

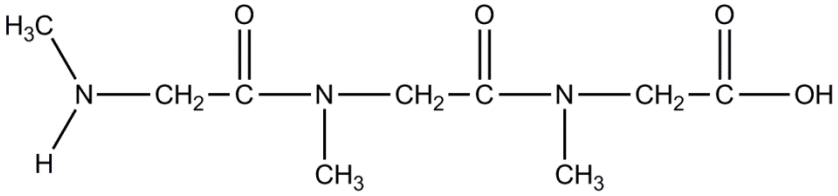

(f) A'A'A':

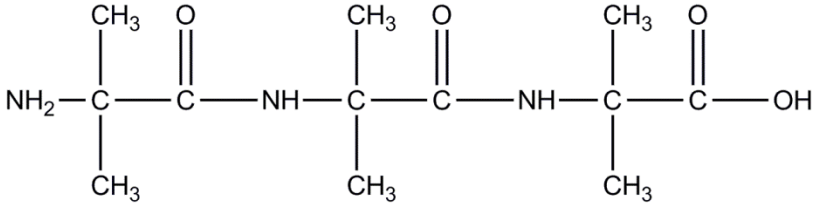

Figure 6.1 Structures of tripeptides (GGG, AAA, GAG, AGA, G′G′G′, and A′A′A′) used in this research.

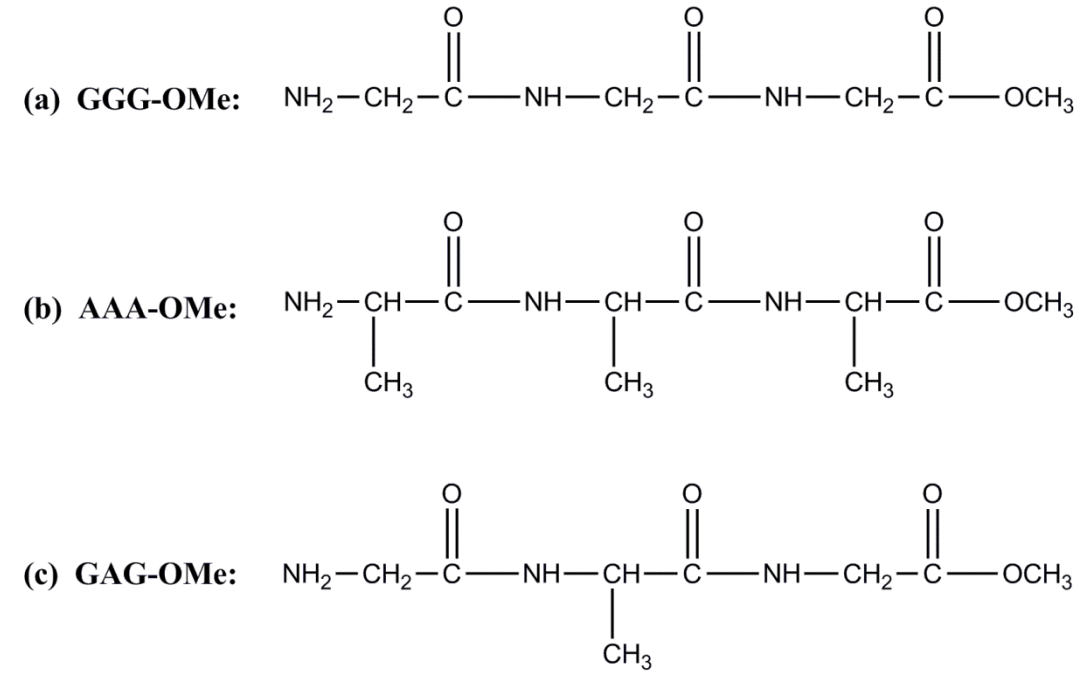

Figure 6.2. Structures of tripeptide methyl esters (GGG-OMe, AAA-OMe, and GAG-OMe) used in the CID and ion/molecule reaction study.

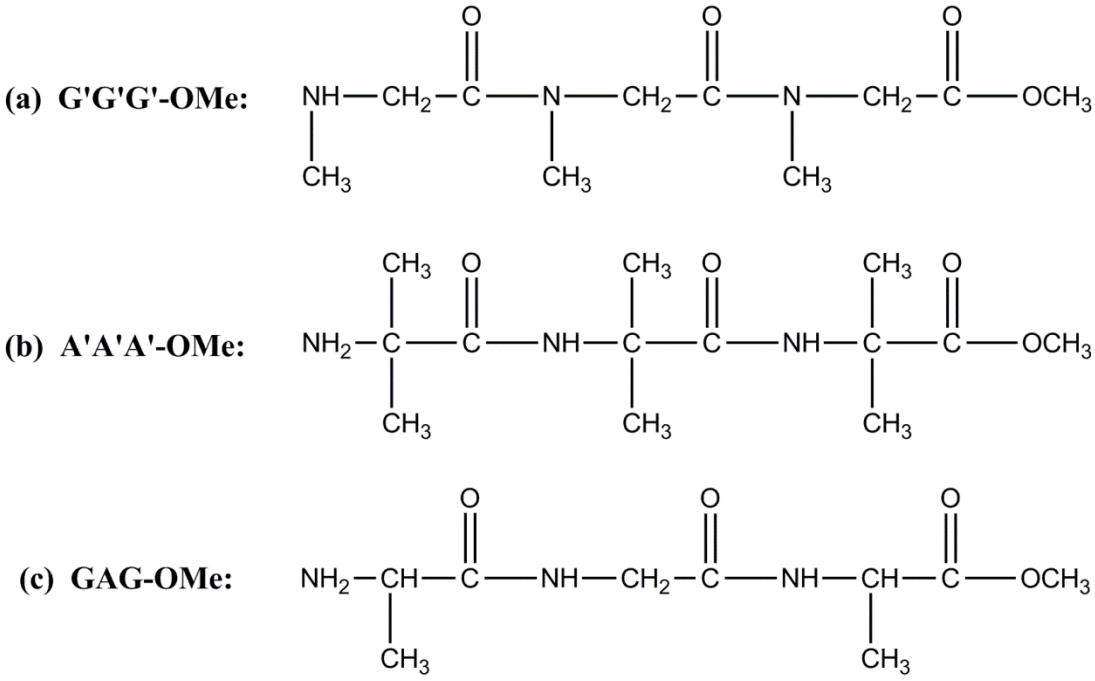

Figure 6.3. Structures of tripeptide methyl esters (G′G′G′-OMe, A′A′A′-OMe, and AGA-OMe) that did not produce sufficient $[M - H]^-$ for study by ion/molecule reactions but where studied by CID.

6.4.1 ESI of deprotonated tripeptides

ESI MS experiments were performed on the tripeptides and their methyl esters to determine the ease with which they deprotonate. Abundant $[M - H]^-$ is necessary for the ion/molecule reactions. The Bruker HCTultra PMT Discovery System QIT MS was used to perform ESI studies on GGG, AAA, G′G′G′, A′A′A′, and their respective methyl esters. The Bruker BioApex 7e FT-ICR MS was used to perform ESI studies on GAG, AGA, and their methyl esters. ESI studies on the Bruker BioApex were also performed on GGG, AAA, G′G′G′, A′A′A′, and their respective methyl esters to confirm the results from the ESI studies on the Bruker HCTultra prior to ion/molecule reactions. The two instruments have ESI sources with very similar designs.

Abundant $[M - H]^-$ was produced by all of the standard (C-terminal -COOH) tripeptides under ESI conditions. The peptide methyl esters produced much less abundant $[M - H]^-$, with the exception of AAA-OMe (this is discussed in Section 6.4.3). In negative ion mode ESI, the C-terminal -COOH is a charge site. Esterification of the C-terminus removes the acidic group from the peptides in this study; thus deprotonation must occur at a site other than the C-terminus.

Average intensities for $[M - H]^-$ ranged from 10,000 to 100,000 for GGG, AAA, G′G′G′, and A′A′A′. This is sufficient for performing CID experiments in the Bruker HCTultra. Much lower $[M - H]^-$ intensities were observed for GGG-OMe, G′G′G′-OMe, and A′A′A′-OMe. These methyl esters produced $[M - H]^-$ in average intensities ranging between 1,000 and 4,000, which is considerably lower than desired for CID. The dissociative behavior of these low intensity deprotonated methyl esters can still be studied by additional signal averaging. An interesting exception to the peptide methyl esters was AAA-OMe, which produced abundant $[M - H]^-$ in absolute intensities in the 250,000-300,000 range. These intensities were higher than observed

for the standard C-terminal -COOH peptides. AAA-OMe was also included in a previous study by Harrison[15] using deprotonated peptides with alkyl and hydrogen side chains. In that work, he reported the ability of AAA-OMe to deprotonate readily.

The results of the ESI experiments (using the Bruker BioApex FT-ICR) revealed that two of the methyl esters were not suitable for ion/molecule reactions. Very low ESI signals were observed for $[M - H]^-$ from G′G′G′-OMe and A′A′A′-OMe. Thus, these methyl esters were eliminated from the GA study. The other peptide methyl esters, GGG-OMe and AAA-OMe produced abundant $[M - H]^-$ for use in ion/molecule reactions. Methylation of the amide nitrogens and additional methyl groups present on the alpha carbons have a significant effect on the deprotonation of these methyl esters (when compared to GGG-OMe and AAA-OMe). These ESI results suggest that *both* the alpha carbon and amide nitrogen must be available sites of deprotonation when the C-terminus is an ester.

ESI studies on GAG, AGA and their methyl esters were performed on the Bruker BioApex 7e FT-ICR MS. Both of the standard C-terminal -COOH tripeptides produced abundant $[M - H]^-$ for ion/molecule reactions. GAG-OMe also produced acceptable intensities for use in ion/molecule reactions. AGA-OMe, however, did not produce an adequate amount of $[M - H]^-$ and had to be eliminated from the ion/molecule reaction study. The calculated lowest energy structures for neutral and deprotonated AGA-OMe can be seen in Figure 6.5(c) and 6.5(d). Neutral AGA-OMe has a structure nearly identical to the calculated lowest energy structure of neutral AGA. A similar hydrogen bonding pattern is present on both molecules. AGA-OMe has two isoenergetic structures for the deprotonated species, resulting from deprotonation at either of the backbone NH groups.

6.4.2 Interactions that prevent $[M - H]^-$ formation by ESI

Solvent interactions can potentially hinder deprotonation of a peptide. For instance, a low intensity of $[M - H]^-$ may be observed if the solvent is more acidic than the peptide. The reported GAs[18] for the components of the solvent system used in this research are as follows: methanol GA = 376.02 ± 0.62 kcal/mol and water GA = 383.74 ± 0.06 kcal/mol.[18] These GAs values are much higher (less acidic) than the calculated GAs of G′G′G′-OMe, A′A′A′-OMe, and AGA-OMe (which are discussed in Section 6.4.3). This means that these methyl esters are more acidic than their solvent system, and thus solvent acidity cannot be the cause for their inability to form abundant $[M - H]^-$.

Steric and conformational interactions within the neutral peptide are another viable reason for poor $[M - H]^-$ formation from G′G′G′-OMe and A′A′A′-OMe. Conformation is known to affect the ability of ESI to protonate and deprotonate peptides (i.e., the charge state distribution produced by ESI).[28-32] The additional methyl groups present on G′G′G′-OMe and A′A′A′-OMe could be severely limiting the access to the backbone deprotonation sites, thus limiting the production of $[M - H]^-$. Evidence of the importance of conformation and steric hindrance to deprotonation is provided by AGA-OMe, which produces relatively little $[M - H]^-$ by ESI. In contrast, AAA and GGG, which should have similar GAs (as discussed in Section 6.4.3), produce abundant $[M - H]^-$ by ESI.

6.4.3 Experimental and theoretical gas-phase acidities of tripeptide methyl esters

The GAs of the peptide methyl esters of GGG, AAA, and GAG were determined for the first time. Converting the C-terminal carboxylic acid group to a methyl ester removes an acidic

Table 6.1. Reaction efficiencies for the proton transfer reactions of deprotonated tripeptide methyl esters with reference compounds.

Reference Compound	GA (kcal/mol)[18]	Average Reaction Efficiency		
		GGG-OMe	GAG-OMe	AAA-OMe
phenol	342.3 ± 2	0.05 ± 0.01	0.02 ± 0.004	0.04 ± 0.02
acetic acid	341.1 ± 2	0.025 ± 0.002	0.02 ± 0.005	0.02 ± 0.001
formic acid	339.1 ± 2	0.11 ± 0.06	0.10 ± 0.04	0.09 ± 0.02
isovaleric acid	338.5 ± 2	0.23 ± 0.04 **BREAK**[a]	0.09 ± 0.04	0.05 ± 0.03
trimethylacetic acid	337.6 ± 2	0.31 ± 0.18	0.22 ± 0.15 **BREAK**	0.12 ± 0.02 **BREAK**
p-chlorophenol	336.2 ± 2	0.32 ± 0.01	0.41 ± 0.03	0.34 ± 0.01
3-trifluoromethyl phenol	332.4 ± 2	–[b]	1.02 ± 0.09	1.09 ± 0.08

[a] "BREAK" indicates the point where experimental GA was assigned.
[b] "–" indicates no experiment was performed

Table 6.2. Experimental and G3(MP2) theoretical GAs for peptide methyl esters.

Peptide	GA (kcal/mol)						
	Experimental	G3MP2					
		C-terminal $C_\alpha H$	C-terminal NH	Central $C_\alpha H$	Central NH	N-terminal $C_\alpha H$	N-terminus (NH_2)
GGG-OMe	338.1 ± 2.1	348.7	342.8	358.7	340.1	359.5	–[a]
AAA-OMe	336.7 ± 2.2	344.2	334.3	349.6	334.1	349.8	353.3
GAG-OMe	337.2 ± 2.1	350.6	342.4	360.2	339.8	360	–[a]
G′G′G′-OMe	N/A[b]	351.6	–[c]	358.3	–[c]	365.2	369.6
A′A′A′-OMe	N/A	–[c]	341.2	–[c]	326.2	–[c]	349.5
AGA-OMe	N/A	349.4	339.1	356.5	339.1	360.6	–[a]

[a] Attempts to deprotonate at this site resulted in a reversion back to deprotonation at the central NH.
[b] Experimental GA could not be determined by ion/molecule reactions because peptide could not be deprotonated by ESI.

site on a peptide, thus forcing deprotonation to occur at another site. Table 6.1 lists the reference compounds and respective reaction efficiencies for the deprotonation reactions with the methyl ester peptides. Using a reaction efficiency of 0.27 as the point to assign GA values,[33] the GAs of the peptide methyl esters were determined. Table 6.2 lists the experimental GAs of each of the peptide methyl esters and the G3(MP2) calculated GAs for each of the deprotonation sites that were explored. Figure 6.4 shows the lowest energy calculated structures for the neutral and deprotonated peptide methyl esters. Figure 6.5 shows the lowest energy structures for the neutral and deprotonated methyl esters that could not be deprotonated by ESI.

The GA of GGG-OMe was experimentally determined to be 338.1 ± 2.1 kcal/mol. G3(MP2) calculations show deprotonation of the amide nitrogens and the N-terminus to be very close in energy. The central amide nitrogen has a G3(MP2) calculated GA of 340.1 kcal/mol and the C-terminal amide nitrogen has a GA of 342.8 kcal/mol. Thus, GGG-OMe is likely deprotonating at one of these backbone nitrogen sites. The experimental and calculated GAs are within experimental error. The calculated lowest energy structures for the neutral and lowest energy anion of GGG-OMe are shown in Figure 6.4(a). Neutral GGG-OMe adopts a somewhat closed conformation. Hydrogen bonds are formed between the N-terminus and the C-terminal carbonyl, between the N-terminus and the N-terminal amide nitrogen, and between the C-terminal NH and the N-terminal carbonyl. Deprotonation occurs at the central NH of GGG-OMe and the resulting structure is more open than the neutral molecule. Hydrogen bonding is still observed between the C-terminal NH and the N-terminal carbonyl, and the N-terminus experiences hydrogen bonding to the central nitrogen (the site of deprotonation). Delocalization of the negative charge occurs over the central nitrogen and the adjacent carbonyl to form an amidate structure ($C(=O)N^- \leftrightarrow C(=N)=O^-$).

The experimental GA of AAA-OMe was determined to be 336.7 ± 2.1 kcal/mol. This is the most acidic peptide methyl ester in the study, which is consistent with inductive effects from the methyl groups of the alanine residues allowing enhanced stabilization of the negative charge. G3(MP2) calculations show that the central NH and the C-terminal NH are the most energetically favored sites of deprotonation for AAA-OMe, with GAs of 334.1 and 334.3 kcal/mol, respectively. The experimental GA is in good agreement with the theoretical results. The lowest energy calculated structures for neutral and central NH deprotonated AAA-OMe are shown in Figure 6.4(b). The neutral form of AAA-OMe adopts a very open confirmation with two hydrogen bonds, between the N-terminal carbonyl and the C-terminal NH and between the N-terminus and the central NH. Deprotonation of AAA-OMe at the central NH does not affect the structure greatly, as both hydrogen bonds are retained. These hydrogen bonds however are strengthened in the deprotonation process. The hydrogen bond between the central NH (N^- in deprotonated form) and between the N-terminus shortens from 2.43 to 2.17 Å from the neutral to deprotonated peptide. The hydrogen bond between the N-terminal carbonyl and the C-terminal NH shortens from 2.03 to 1.64 Å from the neutral to deprotonated peptide. The deprotonated methyl ester forms an amidate like that described for GGG-OMe.

GAG-OMe has an experimentally determined GA of 337.2 ± 2.1 kcal/mol. G3(MP2) calculations show that deprotonation at the central NH is the lowest energy site with a GA of 339.8 kcal/mol, and the C-terminal amide nitrogen is slightly less acidic at 342.4 kcal/mol. Each of these backbone nitrogens are energetically accessible sites of deprotonation for GAG-OMe, and are within the error of the experimentally determined GA. Calculated structures for neutral and central NH deprotonated GAG-OMe are shown in Figure 6.4(c). GAG-OMe adopts a somewhat closed neutral structure, very similar to the neutral structure of GGG-OMe. Hydrogen

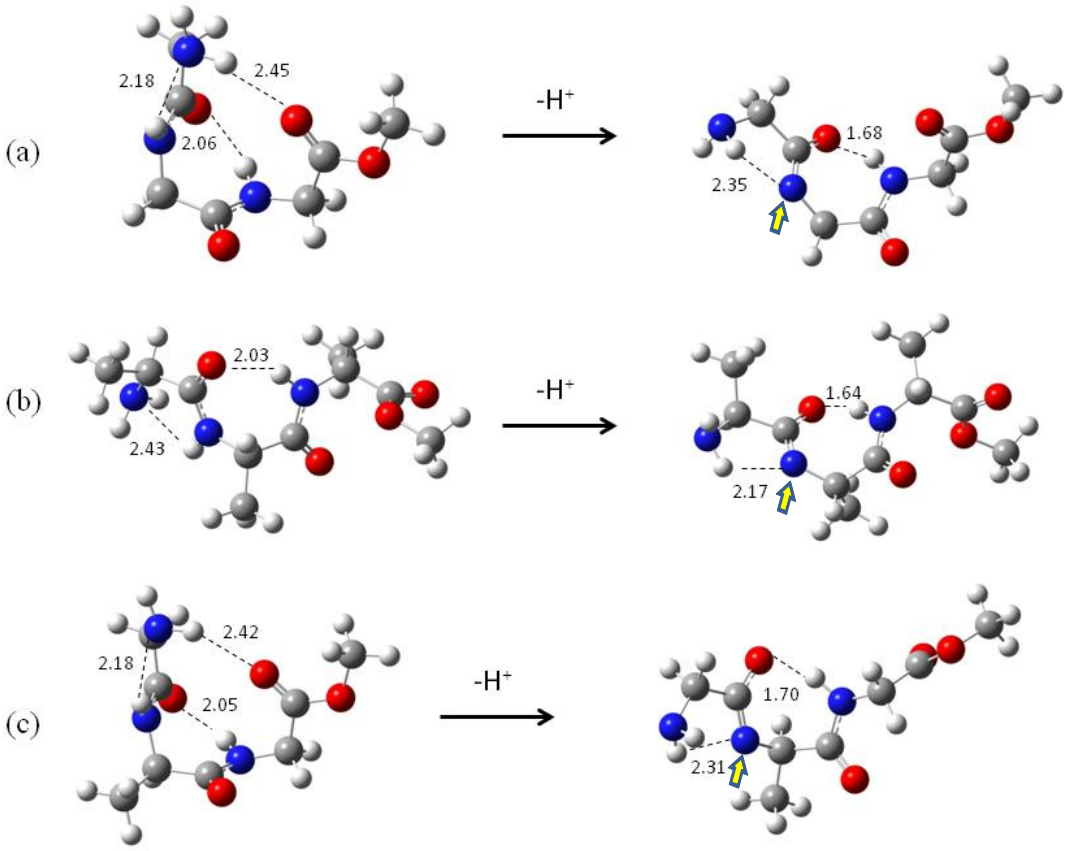

Figure 6.4. G3(MP2) calculated structures for neutral and deprotonated (a) GGG-OMe, (b) AAA-OMe, and (c) GAG-OMe. Arrows indicate the deprotonation site.

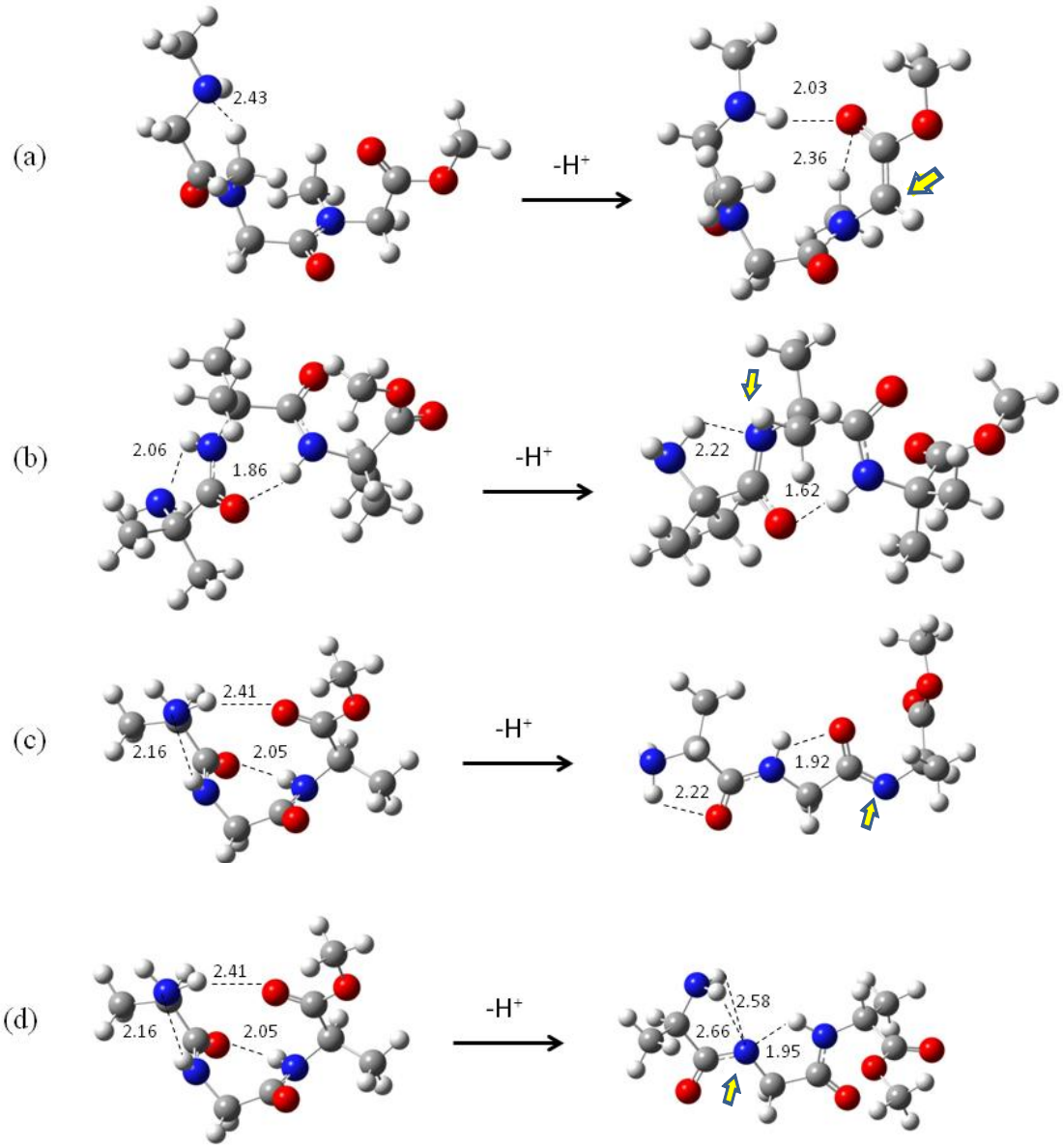

Figure 6.5. G3(MP2) calculated structures for neutral and deprotonated (a) G′G′G′-OMe, (b) A′A′A′-OMe, (c) AGA-OMe, and (d) AGA-OMe. AGA-OMe has two isoenergetic structures for the deprotonated species. Arrows indicate the deprotonation site.

bonding occurs between the N-terminus and the C-terminal carbonyl, between the N-terminus and the N-terminal amide nitrogen, and between the C-terminal NH and the N-terminal carbonyl. Deprotonation of GAG-OMe at the central NH results in a structure similar to that of deprotonated GGG-OMe. Hydrogen bonds between the C-terminal NH and the N-terminal carbonyl (shortened by 0.82 Å), and the N-terminus to the central nitrogen (site of deprotonation, bond lengthened by 0.13 Å) are retained. Delocalization of the negative charge across the central amide nitrogen and the adjacent carbonyl occurs to form an amidate structure like that described for GGG-OMe and AAA-OMe.

6.4.4 Experimental and theoretical gas-phase acidities of tripeptides

Table 6.3 lists the reference compounds and respective reaction efficiencies for the reactions with the tripeptides. Experimental GAs for each of the tripeptides are shown in Table 6.4 as well as the G3(MP2) calculated GAs for each of the possible deprotonation sites. The GAs of all of the tripeptides were bracketed between difluoroacetic acid and pentafluorophenol. All have very similar GAs within a small 1.2 kcal/mol range. The lowest-energy G3(MP2) calculated structures for the neutral and deprotonated peptides Figure 6.6.

The uncertainties for the experimental GAs listed in Tables 6.2 and 6.5 are assigned as half of the difference in literature GA between the two reference compounds at the break point. An additional 2 kcal/mol has been added to account for uncertainties associated with these literature values.[18] This results in a rather large uncertainty, but the resulting assigned uncertainties for the GAs of the peptides in this study would be abnormally low if the literature uncertainties were used directly to propogate the experimental uncertainty.

Table 6.3. Reaction efficiencies for the proton transfer reactions of deprotonated tripeptides with reference compounds.

Reference Compound	GA[a] (kcal/mol)	Average Reaction Efficiency					
		G′G′G′	GGG	A′A′A′	AAA	GAG	AGA
Trifluoropropionic acid	327.0 ± 1.1	0.08 ± 0.01	0.05 ± 0.01	0.04 ± 0.01	0.04 ± 0.00	0.05 ± 0.00	0.06 ± 0.05
Difluoroacetic acid	323.8 ± 2	0.07 ± 0.00	0.06 ± 0.02	0.04 ± 0.01	0.04 ± 0.01	0.06 ± 0.01	0.04 ± 0.01
		BREAK[b]	**BREAK**	**BREAK**	**BREAK**	**BREAK**	**BREAK**
Pentafluorophenol	320.7 ± 2	0.57 ± 0.02	0.45 ± 0.05	0.34 ± 0.02	0.48 ± 0.03	0.48 ± 0.02	0.43 ± 0.02
Trifluoroacetic acid	317.4 ± 2	0.72 ± 0.06	0.52 ± 0.06	0.55 ± 0.11	0.51 ± 0.08	0.53 ± 0.07	0.53 ± 0.09

[a] All reference compound GAs were obtained from reference [18].
[b] "BREAK" indicates the point where experimental GA was assigned.

Table 6.4. Experimental and G3(MP2) theoretical GAs for tripeptides.

Peptide	GA (kcal/mol)							
	Experimental	G3MP2						
		C-terminus (COOH)	C-terminal $C_\alpha H$	C-terminal NH	Central $C_\alpha H$	Central NH	N-terminal $C_\alpha H$	N-terminus (NH_2)
AAA-OH	322.2 ± 2.2	319.6	343.1	338.9	352.3	335.2	351.4	354.5
GAG-OH	322.3 ± 2.2	321.6	347.5	337.7	359.4	331.3	359.5	–[b]
AGA-OH	322.0 ± 2.2	318.4	346.0	338.2	355.8	338.8	359.7	–[b]
A′A′A′-OH	321.4 ± 2.2	322.1	–[a]	328.9	–[a]	330.4	–[a]	–[b]
G′G′G′-OH	322.6 ± 2.1	323.7	348.7	–[a]	356.4	–[a]	347.0	369.1
GGG-OH	322.1 ± 2.3	323.5	344.3	328.5	344.5	334.7	350.6	413.6

[a] This site does not exist in the peptide..
[b] Attempts to deprotonate at this site in the calculations resulted in a reversion back to deprotonation at the central NH.

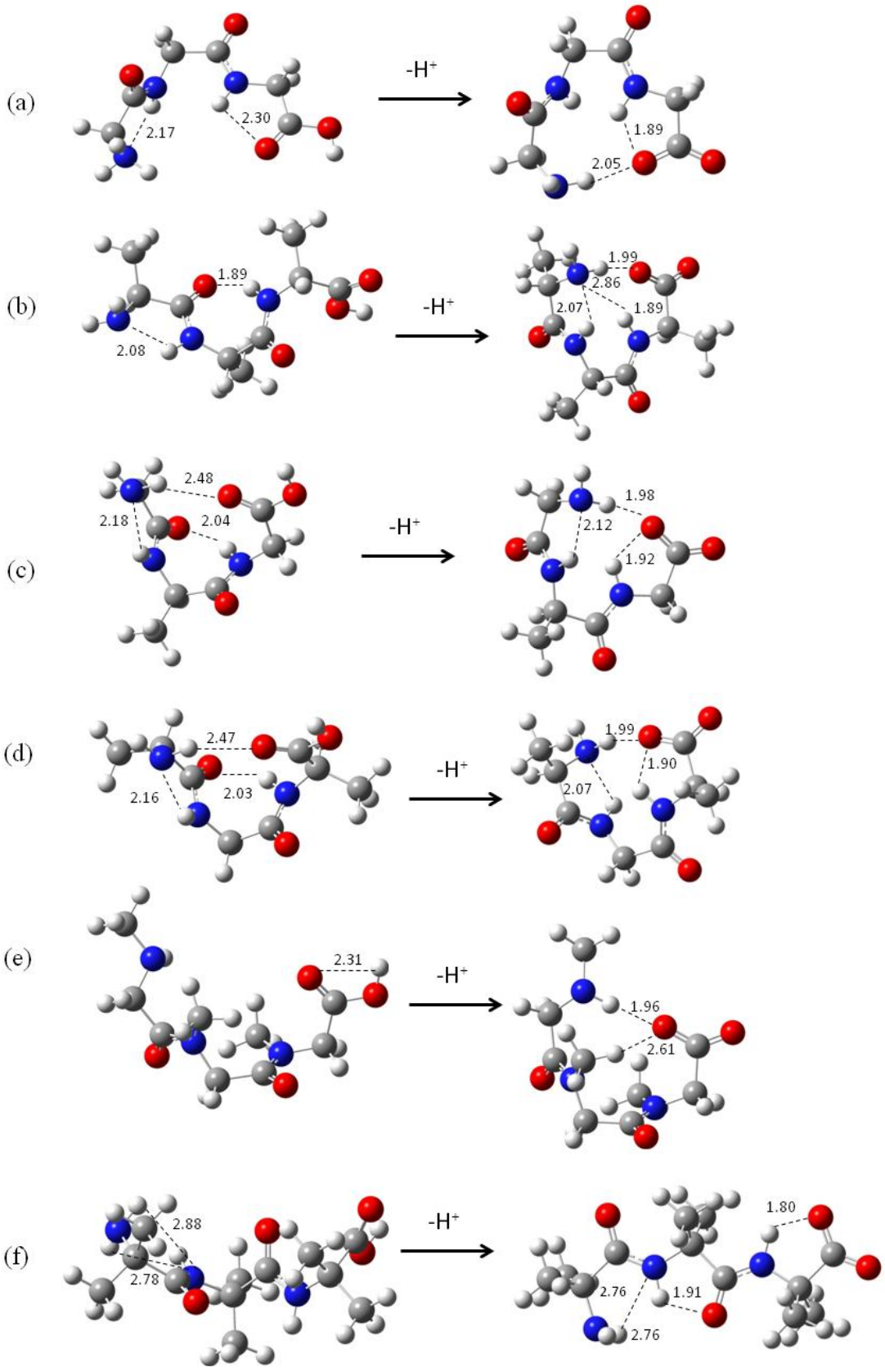

Figure 6.6: G3(MP2) calculated structures for neutral and deprotonated (a) GGG, (b) AAA, (c) GAG, (d) AGA, (e) G′G′G′, and (f) A′A′A′. Arrows indicate the deprotonation site.

Trisarcosine (G′G′G is the least acidic of the peptides (albeit only by 0.3 kcal/mol), both theoretically and experimentally. G′G′G′ has an experimental GA of 322.6 ± 2.1 kcal/mol. The most acidic site of G′G′G′ is the C-terminus with a calculated GA of 323.7 kcal/mol. This is 23 kcal/mol more acidic than the next most acidic site, the methylene carbon of the N-terminus. The methyl groups present on each of the nitrogens eliminate potential alternate deprotonation sites along the peptide backbone. As was seen from the theoretical results for the peptide methyl esters, the backbone amide nitrogens and the N-terminus are the likely sites for deprotonation when the C-terminus is not available. The lack of available amide hydrogens on the backbone may also be why G′G′G′-OMe did not produce a sufficient $[M - H]^-$ signal for ion/molecule reactions, since deprotonation at an alpha carbon (of G′G′G′) would require >23 kcal/mol more energy than deprotonation at the C-terminus. The calculated structures for the neutral and C-terminally deprotonated G′G′G′ are shown in Figure 6.6(e). Neutral G′G′G′ adopts a fairly open structure, and has only one hydrogen bonding interaction between the C-terminal carbonyl oxygen and OH. Deprotonated G′G′G′ has a much more compact structure than its neutral counterpart. Hydrogen bonding occurs between the C-terminal carbonyl oxygen and the N-terminus and between the C-terminal carbonyl oxygen and the central $N(CH_3)$.

GAG has an experimental GA of 322.3 ± 2.2 kcal/mol. The calculated GA for deprotonation of the C-terminus (the most acidic site) is 321.6 kcal/mol. The agreement between the experimental and calculated values is excellent. The lowest energy calculated structures for neutral and deprotonated GAG are shown in Figure 6.6(c). Neutral GAG adopts a closed structure, with three hydrogen bonding interactions. The C-terminal carbonyl oxygen forms a hydrogen bond with the N-terminus. The N-terminus also hydrogen bonds to the central NH and the N-terminal carbonyl oxygen forms a hydrogen bond with the C-terminal NH.

Deprotonated GAG retains the hydrogen bond between the C-terminal carbonyl and the N-terminus and the bond length decreases by 0.5 Å. The C-terminal carbonyl oxygen also forms a strong hydrogen bond with the C-terminal NH (which is not present in the neutral molecule) and the hydrogen bond between the N-terminus and the central NH is retained.

Trialanine has an experimental GA of 322.2 ± 2.2 kcal/mol. G3(MP2) calculations give a GA of 319.6 kcal/mol for deprotonation at the C-terminus. The lowest energy calculated structures for neutral and C-terminally deprotonated AAA are shown in Figure 6.6(b). Neutral AAA adopts an open structure, forming only two hydrogen bonds. The N-terminus forms a hydrogen bond with the central NH and the N-terminal carbonyl oxygen forms a hydrogen bond with the C-terminal NH. Deprotonated AAA has a much more compact structure than the neutral, with the N-terminus forming three hydrogen bonds to the C-terminal carbonyl oxygen and the central and C-terminal NHs. The C-terminal carbonyl oxygen also forms a hydrogen bond with the C-terminal NH. The experimental GA of AAA is about 2.6 kcal/mol higher than the calculated value. This is not a large deviation, especially given the experimental error and the complexity of the calculations.

The experimental GA of GGG is 322.1 ± 2.3 kcal/mol. The calculated GA for GGG is 323.5 kcal/mol, which involves deprotonation at the C-terminus. Interestingly, the C-terminal NH deprotonation site has a GA of 328.5 kcal/mol, a mere 5 kcal/mol less acidic (higher GA value) than the carboxylic acid group of the C-terminus. This site was also one of the potential deprotonation sites for GGG-OMe; however, it was not as acidic as the central amide nitrogen or the N-terminus. This is due to the very different gas-phase confirmations adopted by (and confirmed by calculated structures) GGG (Figure 6.6(a)) and GGG-OMe (Figure 6.4(a)). The lowest energy calculated structures for neutral and C-terminally deprotonated GGG are shown in

Figure 6.6(a). Neutral GGG forms a fairly open structure with two hydrogen bonds. The N-terminus forms a hydrogen bond to the central NH and the C-terminal carbonyl oxygen forms a hydrogen bond to the C-terminal NH. Deprotonated GGG slightly more compact than the neutral. The hydrogen bond between the C-terminal carbonyl oxygen is retained, and this carbonyl also forms a hydrogen bond to the N-terminus.

AGA has an experimental GA of 322.0 ± 2.0 kcal/mol. G3(MP2) calculations once again show the C-terminus as the most acidic site with a GA of 318.4 kcal/mol. Furthermore, the theoretical GA of AGA is the lowest (i.e. most acidic) value of the entire set of peptides in the study. This also brings back the issue of deprotonation for AGA-OMe. Each of the backbone amide and N-terminal nitrogens of AGA have reasonable calculated GAs, which means these values are very similar to the calculated GAs for deprotonation at analogous sites on GAG-OMe and the other methyl esters. The calculated structures for AGA-OMe (Figure 6.5(c) and (d)) do not show any conformational feature that could limit accessibility to the most acidic site of AGA-OMe and limit production of $[M - H]^-$ by ESI. Thus, the inability of ESI to deprotonate AGA-OMe is inexplicable. The lowest energy calculated structures for neutral and deprotonated AGA are shown in Figure 6.6(d). Neutral AGA adopts a somewhat open structure, with three hydrogen bonding interactions. The N-terminus forms two of these hydrogen bonds, one to the central NH and the other to the C-terminal carbonyl oxygen. The other hydrogen bond is formed between the N-terminal carbonyl oxygen and the C-terminal NH. Deprotonated AGA forms a more compact structure. The hydrogen bond between the N-terminus and the C-terminal carbonyl is retained, and the bond length is decreased by 0.48 Å. The hydrogen bond between the N-terminus and the central NH is retained, and the bond length is decreased only slightly

(0.09 Å). A new hydrogen bond is formed between the C-terminal carbonyl oxygen and the C-terminal NH.

A′A′A′ has an experimental GA of 321.4 ± 2.2 kcal/mol, making it the most acidic peptide studied. The calculated GA for the C-terminus of A′A′A′ is 320.9 kcal/mol. Interestingly, only 8.3 kcal/mol separates the GA of the C-terminus from the least acidic site on A′A′A′. When compared to the results from the peptide methyl esters, the backbone amide nitrogens are suitable sites for deprotonation. The calculated GA of A′A′A′-OMe is 326.2 kcal/mol, which corresponds to deprotonation at the central NH, which is consequently the most acidic site calculated for any of the peptide methyl esters. The lowest energy structure of neutral A′A′A′-OMe (Figure 6.6(b)), however, shows that the most acidic site is somewhat protected by the four adjacent methyl groups, which could explain why A′A′A′-OMe could not be deprotonated. The lowest energy calculated structures for the neutral and deprotonated forms of A′A′A′ are shown in Figure 6.6(f). Neutral A′A′A′ adopts an open conformation, as the additional methyl groups present on the alpha carbons increase the bulk of the peptide, limiting motion to other conformations. The N-terminus of neutral A′A′A′ has two hydrogen bonding interactions with the central NH group. Deprotonated A′A′A′ also adopts an open conformation, with more order to the structure. The C-terminal carbonyl oxygen forms a hydrogen bond with the C-terminal NH. The two hydrogen bonding interactions are retained between the N-terminus and the central NH. A hydrogen bond is also formed between the central NH and the central carbonyl oxygen.

6.4.5 CID of deprotonated tripeptides and methyl esters

CID was performed on $[M - H]^-$ produced from GGG, GGG-OMe, AAA, AAA-OMe, G′G′G′, G′G′G′-OMe, A′A′A′, and A′A′A′-OMe. The resulting spectra from each of the standard (C-terminal -COOH) peptides were compared to their respective peptide methyl esters. Spectra resulting from CID of GGG and GGG-OMe can be seen in Figure 6.7. The peptide methyl esters produced drastically different CID spectra than their C-terminal acid analogs. Charge site often dictates dissociation,[7, 34-37] and the C-terminal -COOH is the charge site for the standard peptides whereas the -COOMe of the methyl ester peptides is not a charge site. Also, the OMe ($-OCH_3$) of a deprotonated peptide methyl ester can participate in a rearrangement to eliminate methanol, while the O^- is a deprotonated peptide acid is not readily involved in a rearrangement to eliminate water.

GGG produces a_3^- as the base peak of the CID spectrum. This is in agreement with previous reports by Bowie and coworkers[5] and Kulik and Heerma.[11] Harrison[15] reported that a_3^- was an unstable product ion resulting in loss of the N-terminal amino acid residue. Deprotonated GGG-OMe produces a drastically different dissociation pattern. In fact, the only product ion produced is loss of methanol (MeOH) from the precursor ion. Loss of methanol from deprotonated peptide methyl esters has been previously reported [4, 38, 39] as a dominant CID pathway and is an indication that an intact methoxy group exists in the deprotonated peptide methyl ester ion.

CID of $[M - H]^-$ from AAA and AAA-OMe produce spectra that are shown in Figure 6.8. Trialanine produces abundant y_1^-, which is one of the most frequently observed CID products for alkyl-based small peptides.[15] Both $″b_2^-$ and a_3^- are also present in the CID spectrum of

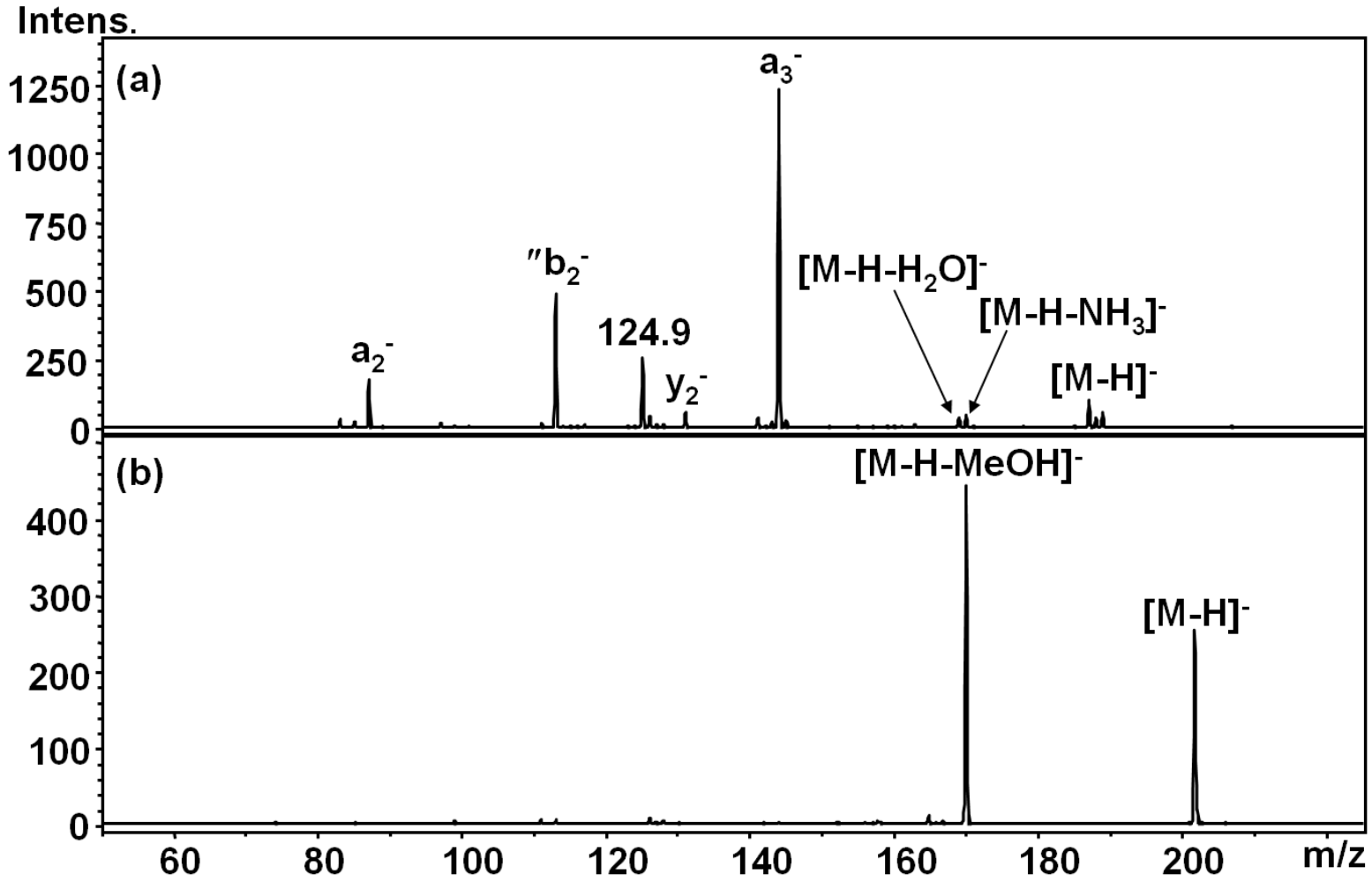

Figure 6.7. CID spectra of $[M - H]^-$ from (a) GGG and (b) GGG-OMe.

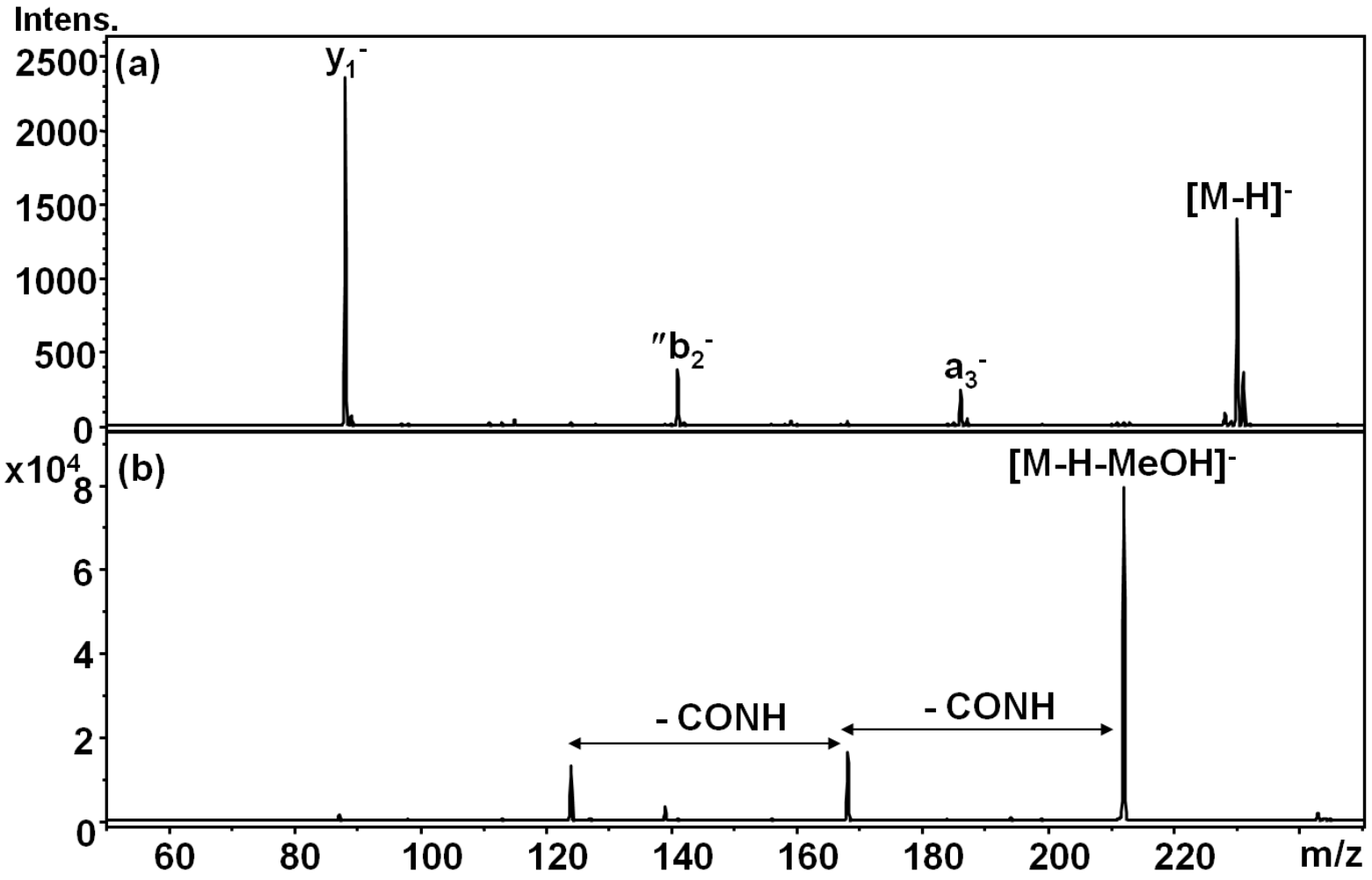

Figure 6.8. CID spectra of $[M - H]^-$ from (a) AAA and (b) AAA-OMe.

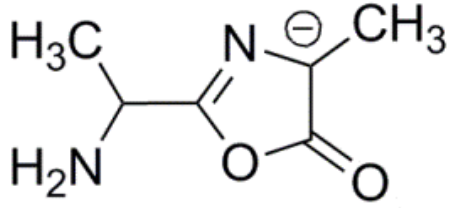

Figure 6.9. Oxazolone structure of b_2^- from AAA.

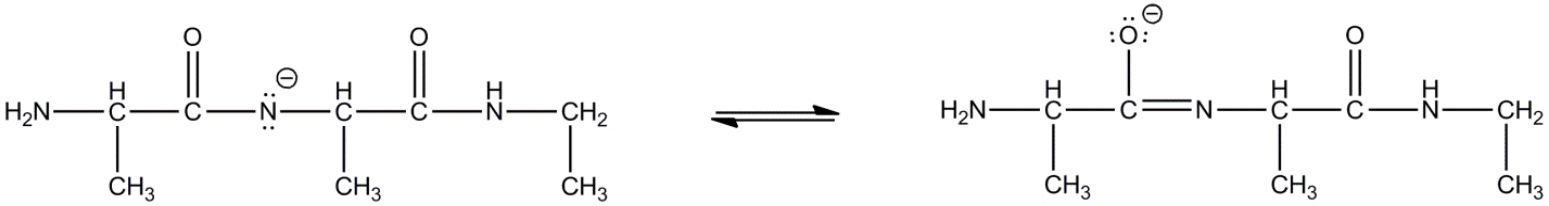

Figure 6.10. Amidate structure of a_3^- from AAA. (Adapted from Reference 40.)

deprotonated AAA. The $''b_2^-$ ion has been shown by infrared multiphoton dissociation (IRMPD) work by Oomens and coworkers[40] to have a deprotonated oxazolone structure (Figure 6.9). The a_3^- ion is loss of CO_2 from the precursor ion, and it has been reported that the structure of a_3^- from deprotonated trialanine is an amidate (Figure 6.10). CID of deprotonated AAA-OMe produces a more informative spectrum relative to the other peptide methyl esters. That is to say, AAA-OMe does more than just lose MeOH from the precursor ion. Two successive losses of CONH from $[M - H - MeOH]^-$ are observed at *m/z* 168 and *m/z* 124.

Figure 6.11 shows the CID spectra of $[M - H]^-$ from G′G′G′ and G′G′G-OMe. Dissociation of G′G′G′ (trisarcosine) has not been previously reported. The complimentary $''b_2^-$ /y_1^- pair are the most abundant product ions observed. In the CID spectrum of deprotonated GGG, a_3^- was observe as the base peak, $''b_2^-/y_1^-$ were observed as minor features. The $''b_2^-/y_1^-$ pair of ions result from cleaving the amide bond at the second G′ position. Formation of this ion pair in much greater abundance (when compared to GGG) suggests that the methyl groups present on the amide nitrogens weaken the amide bond. Figure 6.12 shows a proposed mechanism as for the formation of $''b_2^-$ and y_1^- from the deprotonated precursor. Harrison and coworkers[41] proposed a similar mechanism for the formation of these ions from deprotonated trialanine, except the deprotonated precursor ion had an amidate structure, meaning the charge does not reside at the alpha carbon where cleavage takes place (see Figure 6.10 for an example of this type of ion). The amidate structure has a resonance structure where the negative charge is either on the amide nitrogen or the adjacent carbonyl oxygen. Grzetic and Oomens[40] proposed a different mechanism for the formation of $''b_2^-$ from a_3^-. Also present are y_2^- and a_3^- and several neutral loss peaks. The work of Oomens and Steill[42] would suggest that the a_3^- ion is an amidate,

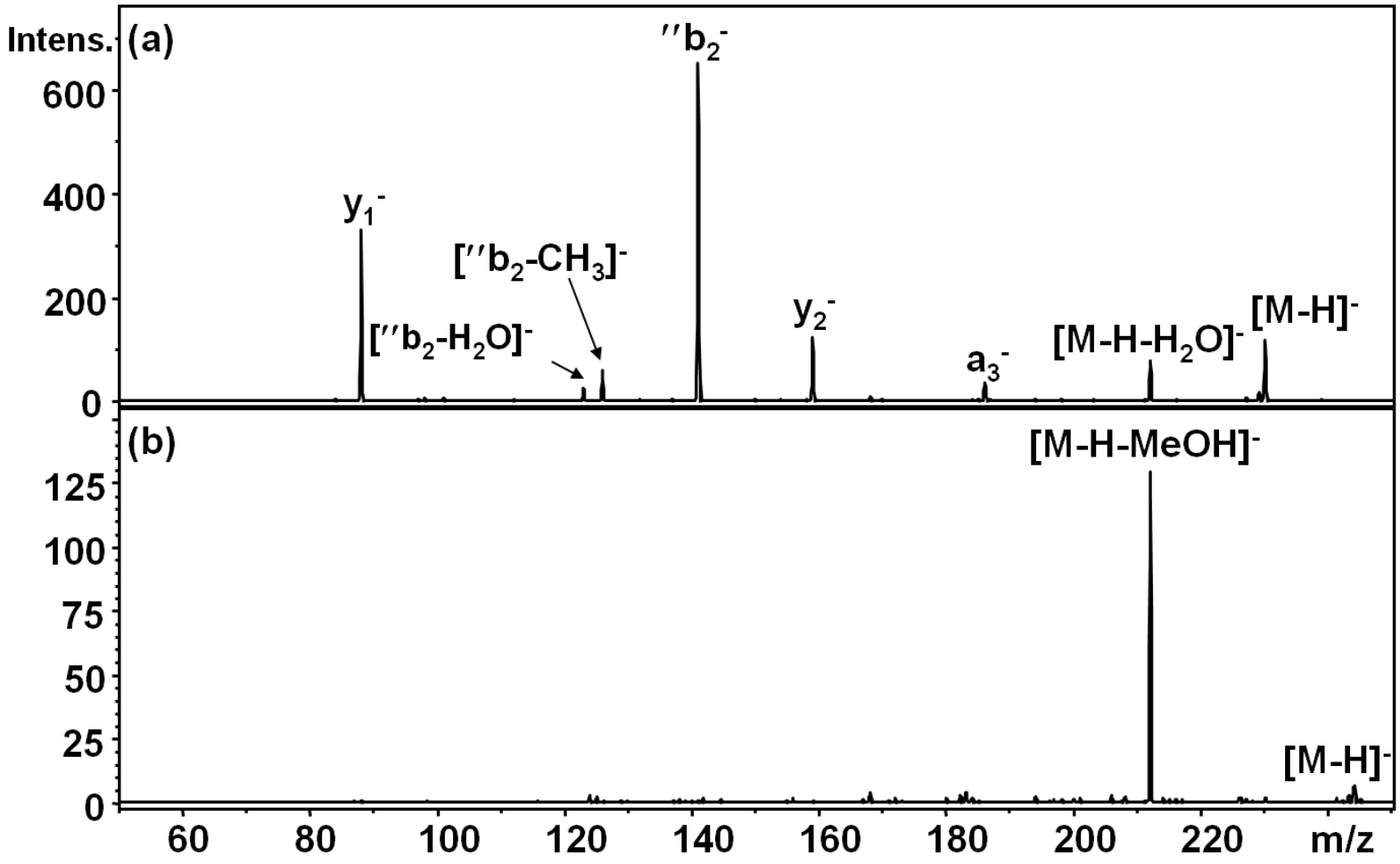

Figure 6.11. CID spectra of $[M - H]^-$ from (a) G′G′G′ and (b) G′G′G′-OMe.

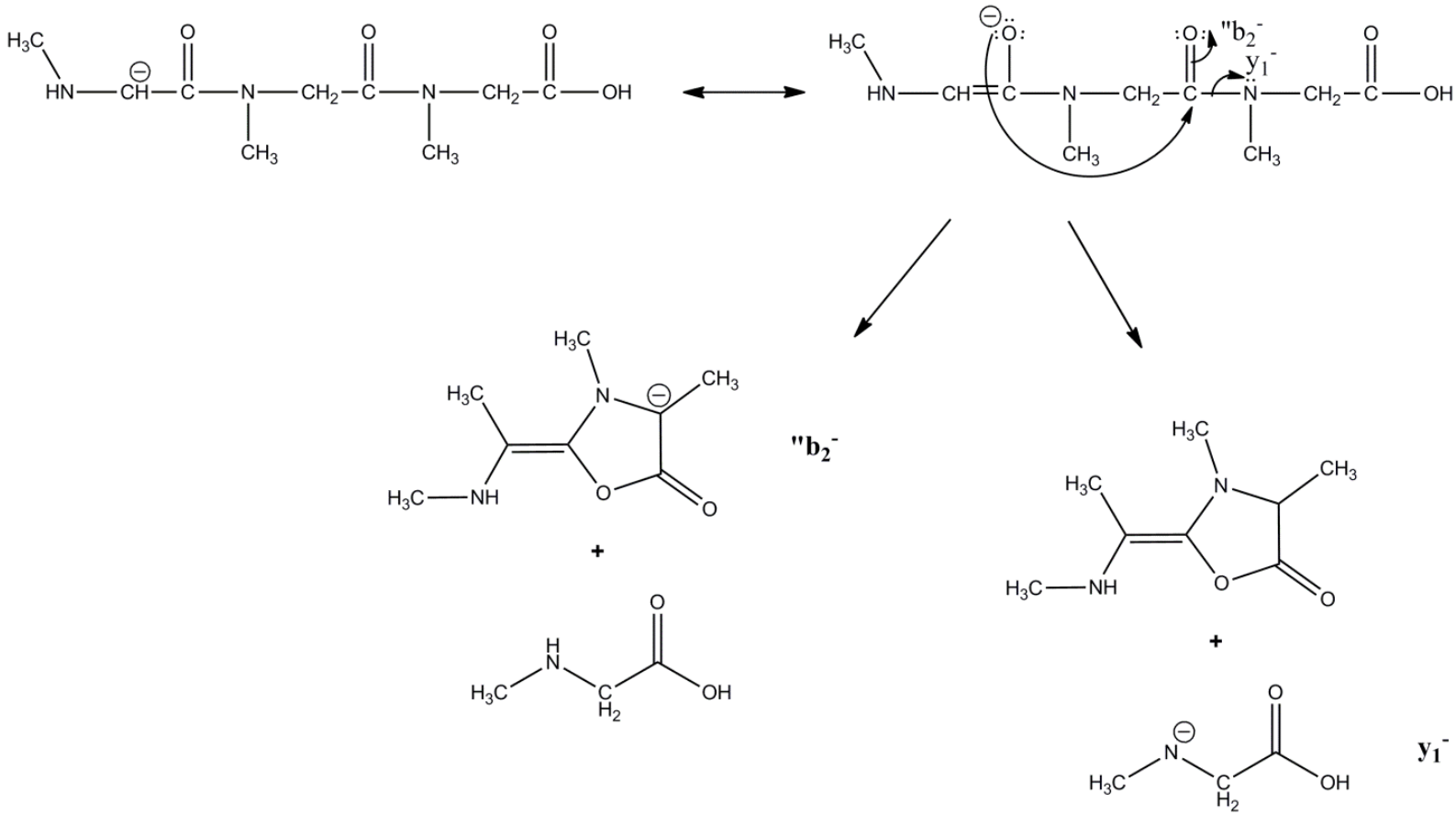

Figure 6.12. Mechanism for formation of b_2^- and y_1^- from G′G′G′.

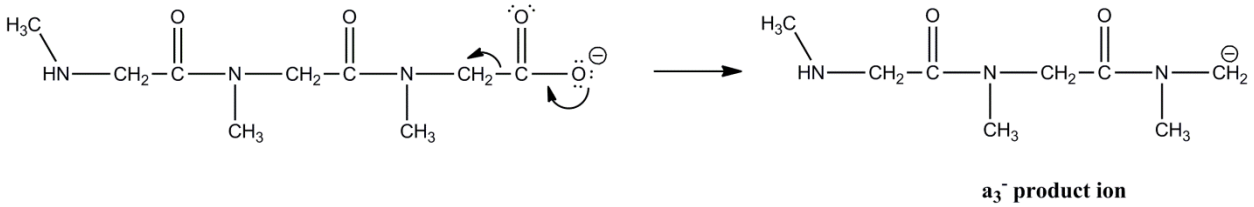

Figure 6.13. Mechanism for formation of a_3^- from G′G′G′.

however, the amide nitrogens of trisarcosine are blocked by methyl groups. Thus the structure of a_3^- cannot be the amidate and is likely a charge delocalized enolate structure (Figure 6.13). CID of G′G′G′-OMe produces only one peak, which corresponds to loss of MeOH from the precursor.

The CID spectra for deprotonated A′A′A′ and A′A′A′-OMe can be seen in Figure 6.14. Deprotonated A′A′A′ produces abundant y_1^- as the main fragmentation pathway. This is intriguing since the presence of two methyl groups on the backbone alpha carbons suggests that some fragmentation might be adjacent to an alpha carbon (because enhanced branching weakens C-C bonds). A proposed mechanism for the formation of y_1^- can be seen in Figure 6.15. Note that b_2^- is not an observed pathway for A′A′A′. CID of deprotonated A′A′A′ also produces a_3^- as a minor pathway as well as a few minor neutral loss peaks. The a_3^- product ion likely has an amidate structure similar to the one shown for trialanine in Figure 6.10. CID of deprotonated A′A′A′-OMe produces $[M - H - MeOH]^-$ as the only product ion.

6.4.6 CID of protonated tripeptides

CID of the protonated tripeptides were performed concurrently with the CID studies on deprotonated tripeptides, and it is in this context that this data is discussed. CID was performed

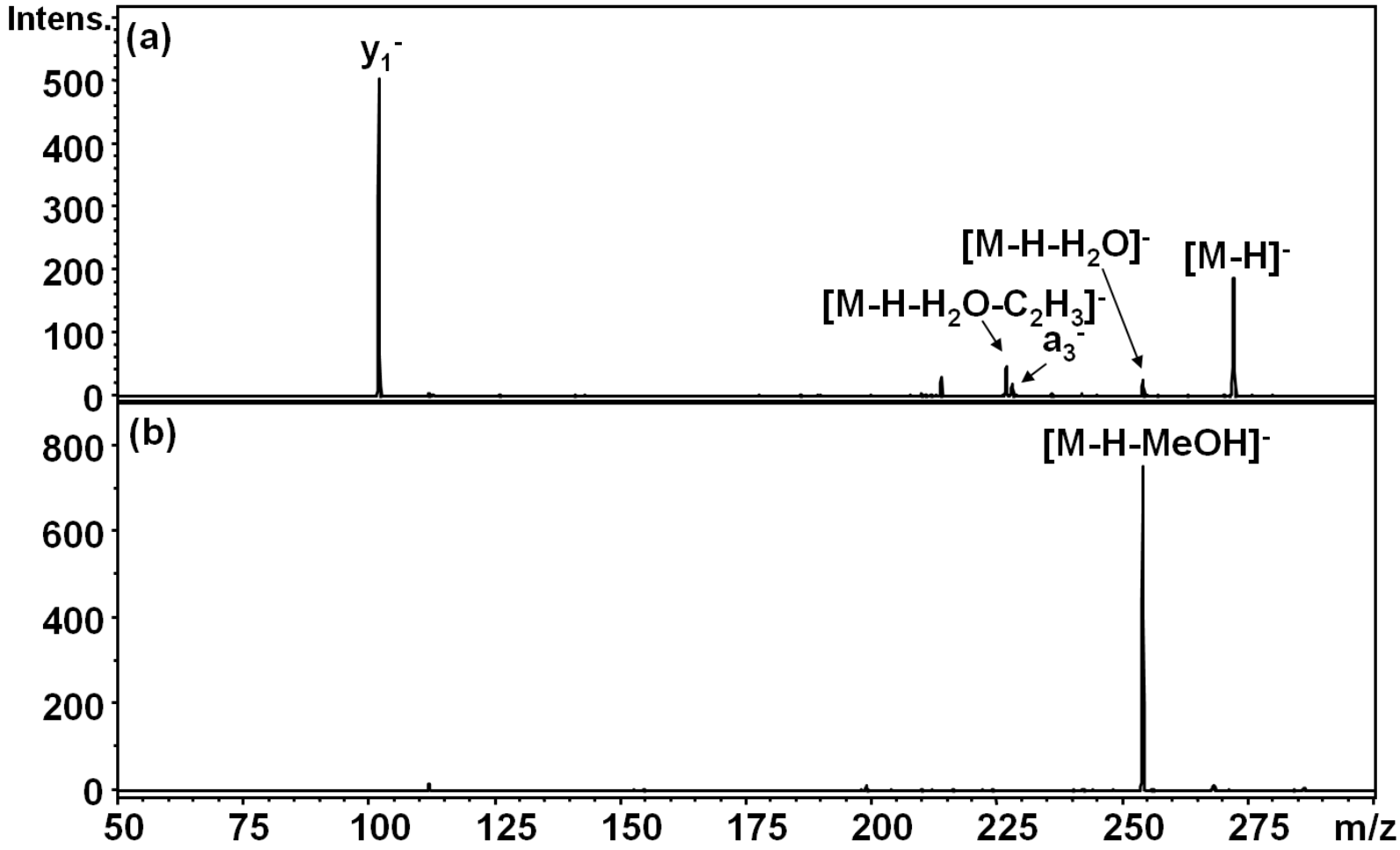

Figure 6.14. CID spectra of $[M - H]^-$ from (a) A′A′A′ and (b) A′A′A′-OMe.

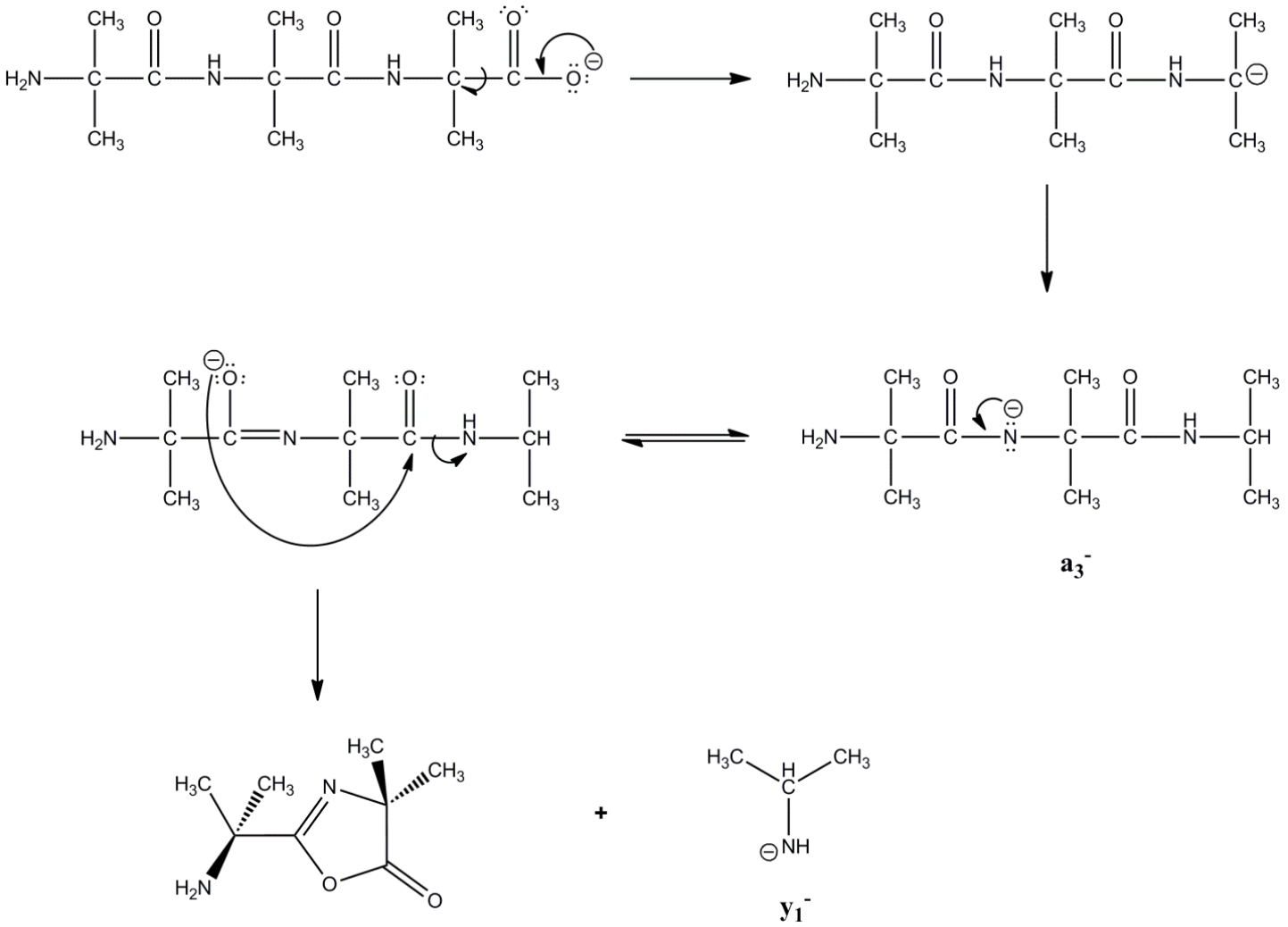

Figure 6.15. Mechanism for formation of y_1^- from A′A′A′.

on protonated GGG, AAA, G′G′G′, A′A′A′, and each of their respective peptide methyl esters. The results obtained from the standard peptides were compared to those from the peptide methyl esters. Several interesting differences appeared between the pairs.

Loss of MeOH from the precursor is minimal in the CID spectra of the protonated methyl esters, and differences between CID from the standard C-terminal acid peptides and from their methyl esters are minimial. In negative ion mode, a C-terminal -COOH group is a charge site but a -COMe is not. These C-terminal groups are not charge sites in the positive ion mode, explaining why there are fewer differences between the analogous tripeptides in the CID spectra.

The CID spectra for protonated GGG and GGG-OMe can be seen in Figure 6.16. GGG produces the expected CID spectrum, consisting of abundant b_2^+ as well as a_2^+ and $y_2''^+$. CID of GGG has been reported[43, 44] and exhibit the same dissociation pattern. GGG-OMe produces the same fragmentation with the addition of a very abundant $y_1''^+$ as the base peak. The $y_1''^+$ is the compliment to b_2^+, both are the result of cleaving the amide bond between Gly_2 and Gly_3.

CID of $[M + H]^+$ from protonated AAA and AAA-OMe can be seen in Figure 6.17. Fragmentation of protonated AAA produces abundant b_2^+ (base peak) and a_2^+, as well as a small amount of $y_2''^+$. AAA-OMe yields these ions as well, with the addition of abundant $y_1''^+$. Again, this $y_1''^+$ is the compliment to b_2^+, where both result from cleavage of the amide bond between Ala_2 and Ala_3.

The CID spectra for protonated G′G′G′ and G′G′G′-OMe can be seen in Figure 6.18.. Both G′G′G′ and G′G′G′-OMe produce abundant b_2^+, as well as $y_1''^+$ and $y_2''^+$. An unusual feature of these spectra is the presence of an atypical internal fragment, $c_2y_2^+$. This ion results from cleavage of the amide bond between G'_1 and G'_2 and cleaving the N–C_α bond of G'_3. MS^3 of this product (*m/z* 100) produces a single product ion at *m/z* 72 (loss of 28 Da from *m/z* 100).

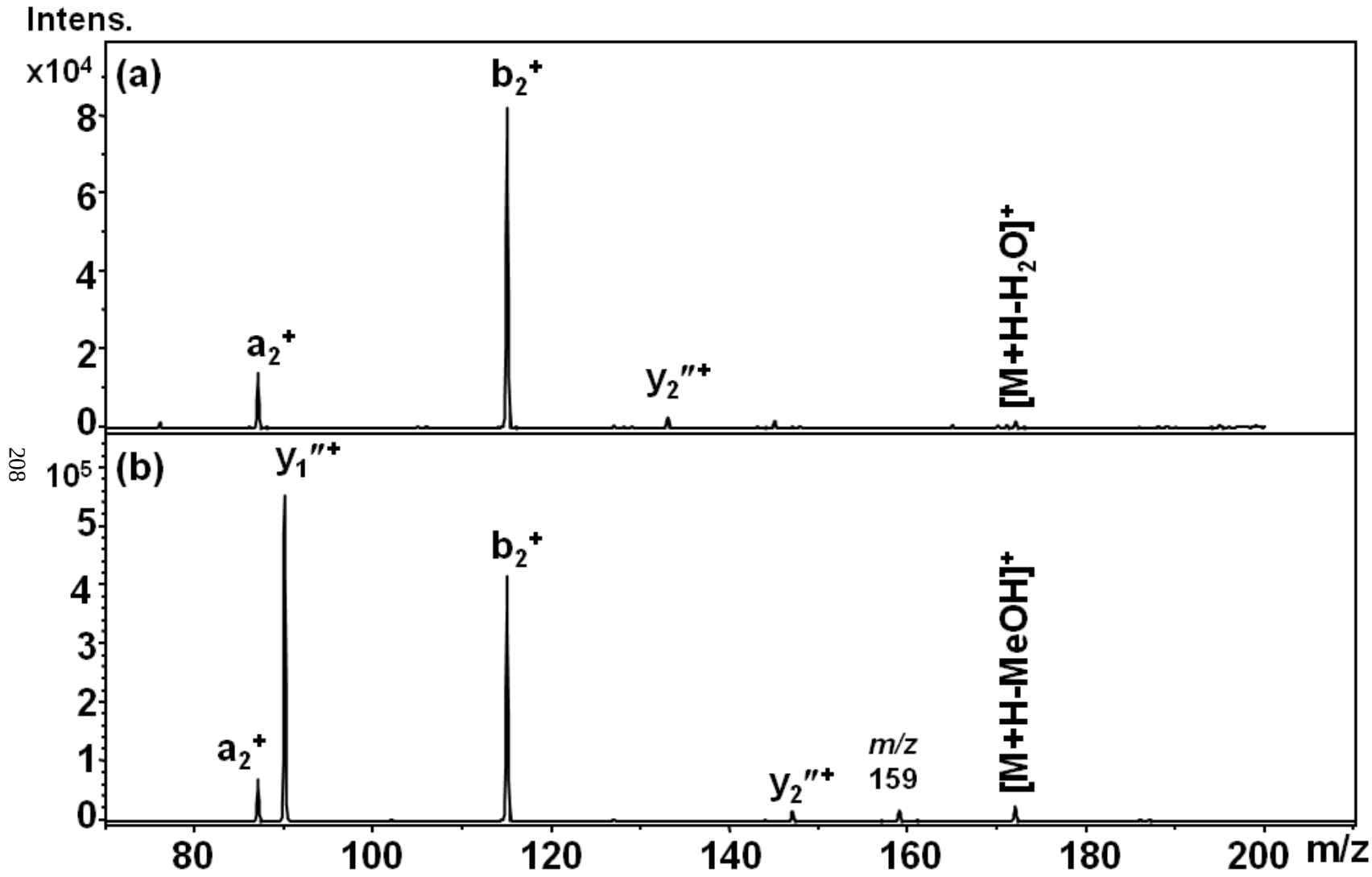

Figure 6.16. CID spectra of $[M + H]^+$ from (a) GGG and (b) GGG-OMe.

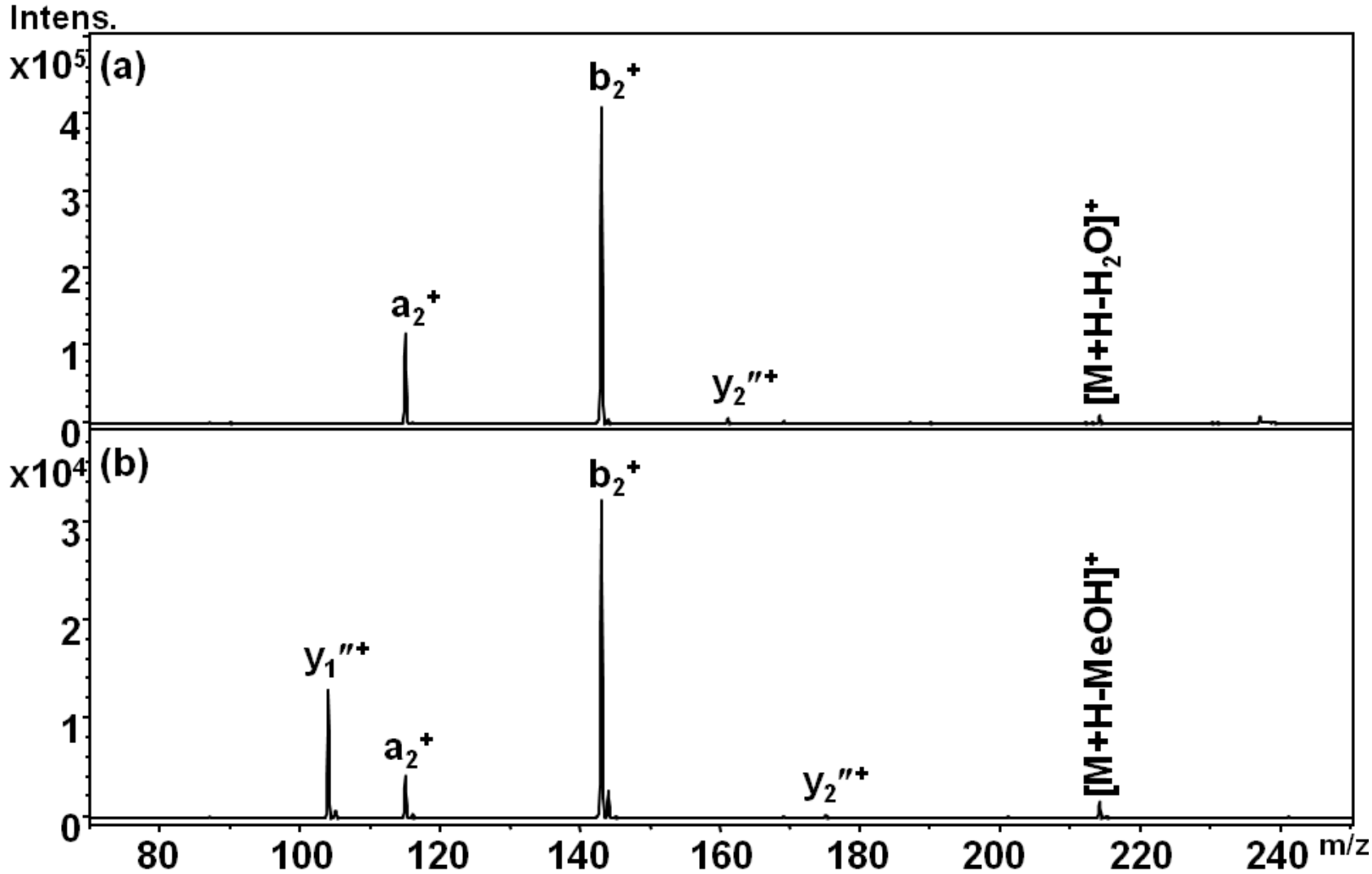

Figure 6.17. CID spectra of $[M + H]^+$ from (a) AAA and (b) AAA-OMe.

Loss of CO is typically attributed to a 28 Da loss, and given the availability of the CO on the c_2y_2 ion ($N(CH_3)CH_2CO$), this is a soft confirmation of this unusual c_2y_2 ion. Triglycine does not produce such an ion, which suggests that the additional methyl groups present on the nitrogens of G′G′G′ weaken the backbone amide and N–C_α bonds that adjoin the methylated nitrogen of G′, causing more facile fragmentation that is not typical of CID of protonated peptides.

Enhanced formation of b_n^+ ions occurs for CID of peptides possessing one internal N-methylated amino acid residue (meaning the residue is at a position other than the N-terminus). [45] Activation of the amide bond C-terminal to the N-methylated residue triggers this enhanced ion fomation. Kuzma et al.[46] reported increased b_n^+ formation in the CID of cyclosporins, which are cyclic peptides that possess several n-methylated amino acid residues in the peptide sequence. No unusual internal ions were reported, although consecutive n-methylated residues are present in the cyclic peptide sequences.[46] This suggests that the observation of the unusual c_2y_2 ion is related to cleavages of bonds on either side (amide or N–C_α) of the n-methylated residue is specific to small peptides composed of these types of residues. Small peptides composed of typical amino acid residues are reported to produce fragmentation different than that observed for larger peptides.[15, 16]

CID spectra for protonated A′A′A′ and A′A′A′-OMe can be seen in Figure 6.19. Fragmentation of protonated A′A′A′ produces abundant b_2^+ as the base peak. Also present are $y_1''^+$ and $y_2''^+$ as well as a_2^+ and less common a_1^+. CID of protonated A′A′A′-OMe produces the same fragmentation, however, in much lower intensity. Identical CID conditions were used, thus protonated A′A′A′-OMe likely has a very stable gas-phase structure that restricts fragmentation.

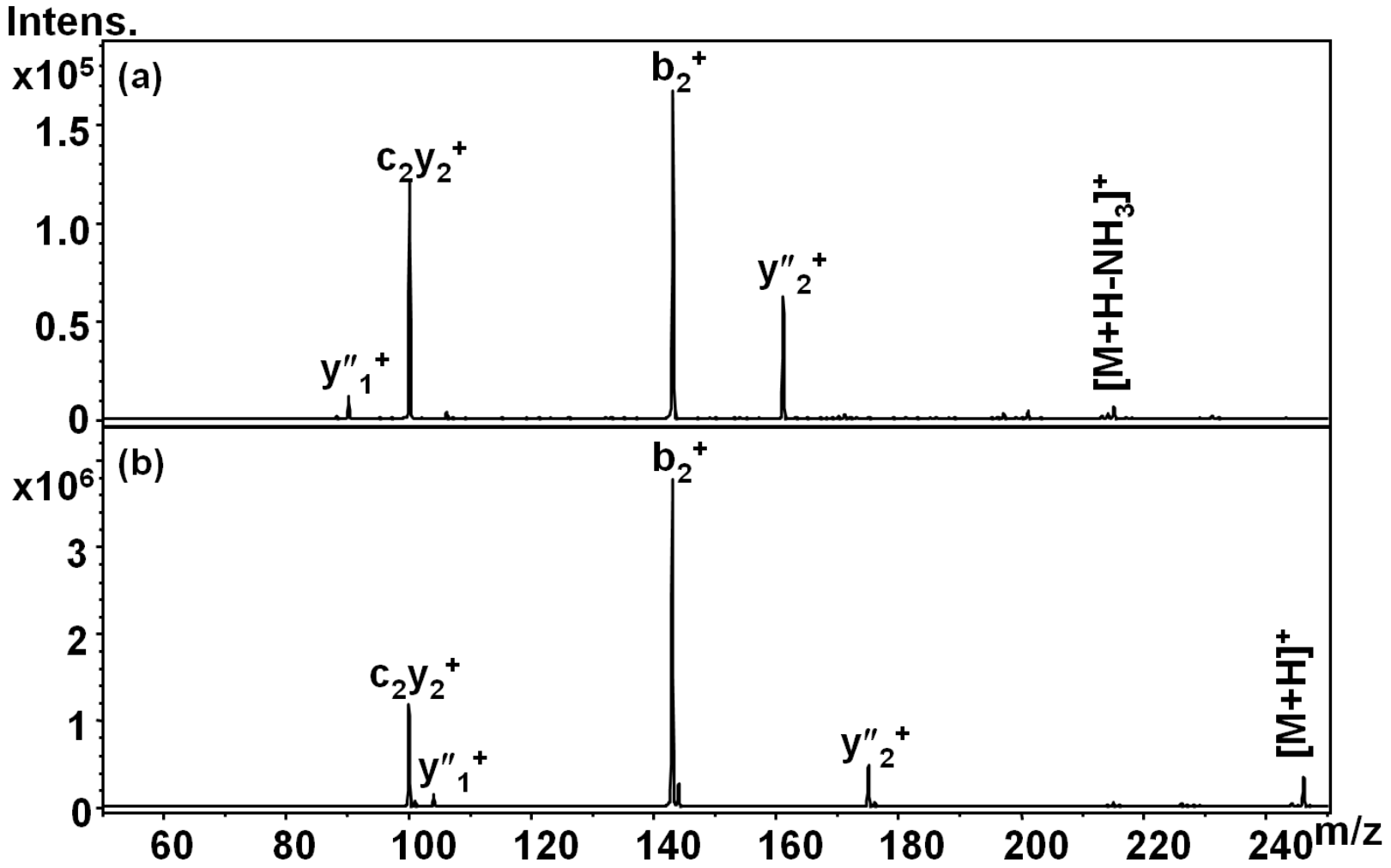

Figure 6.18. CID spectra of $[M + H]^+$ from (a) G′G′G′ and (b) G′G′G′-OMe.

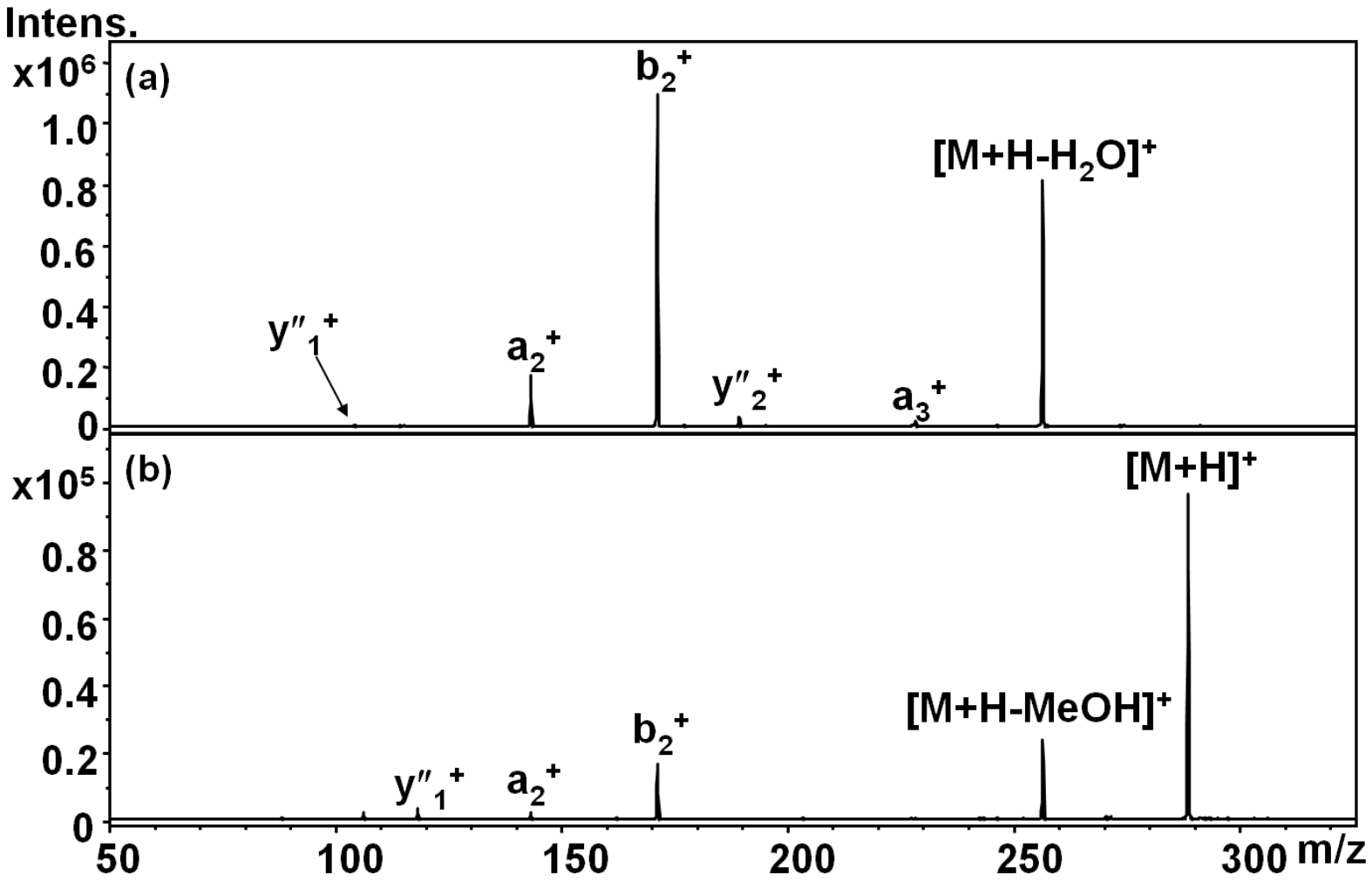

Figure 6.18. CID spectra of $[M + H]^+$ from (a) G′G′G′ and (b) G′G′G′-OMe.

6.5 Conclusions

The GAs of six tripeptides (GGG, AAA, GAG, AGA, G′G′G′, and A′A′A′) and three peptide methyl esters (GGG-OMe, AAA-OMe, and GAG-OMe) have been determined for the first time. Experimental and calculated GA values are in excellent agreement. The standard C-terminal acid (-COOH) peptides have very similar GAs, all falling within a 1.2 kcal/mol range. Deprotonation occurs at the C-terminus, as confirmed by computational results. The peptide methyl esters also have very close GA values, all falling within a 1.4 kcal/mol range. Due to the lack of a traditional acidic site (i.e. -COOH), deprotonation of the methyl esters must be occurring at one of the backbone sites of the peptide (e.g. backbone alpha carbon, backbone amide NH). Computations confirm that backbone deprotonation is possible and the central NH is the most energetically favorable site for backbone deprotonation.

The inability of ESI to deprotonate G′G′G′-OMe, A′A′A′-OMe, or AGA-OMe reveals that steric hindrance or conformation may hinder deprotonation of energetically favorable sites. For example, computations show that the central backbone NH of A′A′A′-OMe is the most acidic site of deprotonation for all of the peptide methyl esters, yet negligible $[M - H]^-$ formed by ESI. The calculated structure of neutral G′G′G′-OMe, however, did not show significant blockage of the acidic backbone alpha carbon sites. Availability of the backbone amide nitrogens is important to deprotonation by ESI, likely due to the $C(=O)N^- \leftrightarrow C(=N)=O^-$ resonance structure that forms. AGA-OMe is still somewhat of a mystery, given that the calculated structure of the neutral is very similar to AGA.

Dissociation by CID of the deprotonated peptides reveals the detrimental effect of methyl esterification on dissociation. Methyl esterified peptides produce little or no fragmentation, with the only major pathway being loss of MeOH from the precursor ion. This correlates with the

deprotonation site of the methyl esters being on the backbone as opposed to C-terminal deprotonation for the standard peptides (that consequently do not exhibit abundant water loss). Dissociation of the protonated peptides reveals the effect of backbone methylation. N-methylated G′G′G′ and G′G′G′-OMe produce a previously unreported internal c_2y_2 fragment related to the cleavage of amide and N–C_α bonds adjacent to the methylated nitrogens. Alpha carbon methylated peptides, A′A′A′ and A′A′A′-OMe produced cleavages similar to AAA and AAA-OMe (which does not posess the extra methyl groups on the alpha carbons), however, many were in reduced abundance. Protonated peptides and their methyl esters dissociate in an equivalent manner, with slightly varying ion intensities. The C-terminal carboxylic acid and methyl esters groups of these peptides are not charge sites in the positive ion mode, thus similar CID spectra are expected.

References

1. Marzluff, E. M.; Campbell, S.; Rogers, M. T.; Beauchamp, J. L. Low-energy dissociation pathways of small deprotonated peptides in the gas phase. *J. Am. Chem. Soc.* **1994**, *116*, 7787-7796.

2. Li, Z.; Matus, M. M.; Velazquez, H. A.; Dixon, D. A.; Cassady, C. J. Gas-phase acidities of aspartic acid, glutamic acid, and their amino acid amides. *Int. J. Mass Spectrom.* **2007**, *265*, 213-223.

3. Gao, J.; Cassady, C. J. Negative ion production from peptides and proteins by matrix-assisted laser desorption/ionization time-of-flight mass spectrometry. *Rapid Commun. Mass Spectrom.* **2008**, *22*, 4066-4072.

4. Bradford, A. M.; Waugh, R. J.; Bowie, J. H.; Vollmer, D. L.; Gross, M. L. Collision-induced dissociations of deprotonated dipeptide methyl esters containing H, alkyl or benzyl α side-chains. *Int. J. Mass Spectrom. Ion Processes* **1994**, *136*, 143-153.

5. Eckersley, M.; Bowie, J. H.; Hayes, R. N. Collision-induced dissociations of deprotonated peptides, dipeptides and tripeptides with hydrogen and alkyl a groups. An aid to structure determination. *Org. Mass Spectrom.* **1989**, *24*, 597-602.

6. Raftery, M. J.; Bowie, J. H. The collision-induced dissociations of deprotonated amides in the gas phase. *Int. J. Mass Spectrom. Ion Processes* **1988**, *85*, 167-186.

7. Wysocki, V. H.; Tsaprailis, G.; Smith, L. L.; Breci, L. A. Special feature: Commentary - Mobile and localized protons: a framework for understanding peptide dissociation. *J. Mass Spectrom.* **2000**, *35*, 1399-1406.

8. Summerfield, S.; Gaskell, S. Fragmentation efficiencies of peptide ions following low energy collisional activation. *Int. J. Mass Spectrom.* **1997**, *165*, 509-521.

9. O'Hair, R. A. J.; Bowie, J. H.; Gronert, S. Gas phase acidities of the alpha amino acids. *Int. J. Mass Spectrom.* **1992**, *117*, 23-36.

10. VanSetten, D.; Kulik, W.; Heerma, W. Isomeric tripeptides - A study on structure spectrum relationship. *Biomed. Environ. Mass Spectrom.* **1990**, *19*, 475-480.

11. Kulik, W.; Heerma, W. Fast atom bombardment tandem mass-spectrometry for amino-acid sequence determination in tripeptides. *Biomed. Environ. Mass Spectrom.* **1989**, *18*, 910-917.

12. Kulik, W.; Heerma, W. The determination of the amino-acid sequence in the fast atom bombardment mass-spectra of dipeptides. *Biomed. Environ. Mass Spectrom.* **1988**, *17*, 173-180.

13. Bradley, C. V.; Howe, I.; Beynon, J. H. Sequence-analysis of underivatized peptides by negative-ion chemical ionization and collision-induced dissociation. *Biomed. Mass Spectrom.* **1981**, *8*, 85-89.

14. Bradley, C. V.; Howe, I.; Beynon, J. H. Analysis of un-derivatized peptide mixtures by collision-induced dissociation of negative-ions. *J. Chem. Soc.* **1980**, *12*, 562-564.

15. Harrison, A. G. Sequence-specific fragmentation of deprotonated peptides containing H or alkyl side chains. *J. Am. Soc. Mass Spectrom.* **2001**, *12*, 1-13.

16. Pu, D. Mass spectrometric studies of peptide fragmentation and complexes of chromium (III) with acidic peptides. Ph.D. Dissertation, University of Alabama, Tuscaloosa, AL, 2007.

17. de Koning, L. J.; Nibbering, N. M. M.; van Orden, S. L.; Laukien, F. H. Mass selection of ions in a Fourier transform ion cyclotron resonance trap using correlated harmonic excitation fields (CHEF). *Int. J. Mass Spectrom.* **1997**, *165*, 209-219.

18. Bartmess, J. E. In *Negative Ion Energetics Data;* Linstrom, P. J., Mallard, W. G., Eds.; NIST Chemistry WebBook, NIST Standard Reference Database Number 69; National Institute of Standards and Technology: Gaithersburg MD, 20899, http://webbook.nist.gov, (retrieved August 2, 2011).

19. Su, T.; Chesnavich, W. J. Parametrization of the ion-polar molecule collision rate-constant by trajectory calculations. *J. Chem. Phys.* **1982**, *76*, 5183-5185.

20. Su, T. Trajectory Calculations of ion-polar molecule capture rate constants at low-temperatures. *J. Chem. Phys.* **1988**, *89*, 5355-5355.

21. Frisch, M. J.; Trucks, G. W.; Schlegel, H. B.; Scuseria, G. E.; Robb, M. A.; Cheeseman, J. R.; Scalmani, G.; Barone, V.; Mennucci, B.; Petersson, G. A.; Nakatsuji, H.; Caricato, M.; Li, X.; Hratchian, H. P.; Izmaylov, A. F.; Bloino, J.; Zheng, G.; Sonnenberg, J. L.; Hada, M.; Ehara, M.; Toyota, K.; Fukuda, R.; Hasegawa, J.; Ishida, M.; Nakajima, T.; Honda, Y.; Kitao, O.; Nakai, H.; Vreven, T.; Montgomery, J. A. J.; Peralta, J. E.; Ogliaro, F.; Bearpark, M.; Heyd, J. J.; Brothers, E.; Kudin, K. N.; Staroverov, V. N.; Keith, T.; Kobayshi, R.; Normand, J.; Raghavachari, K.; Rendell, A.; Burant, J. C.; Iyengar, S. S.; Tomasi, J.; Cossi, M.; Rega, N.; Millam, J. M.; Klene, M.; Knox, J. E.; Cross, J. B.; Bakken, V.; Adamo, C.; Jaramillo, J.; Gomperts, R.; Stratmann, R. E.; Yazyev, O.; Austin, A. J.; Cammi, R.; Pomelli, C.; Ochterski, J. W.; Martin, R. L.; Morokuna, K.; Zakrzewski, V. G.; Voth, G. A.; Salvador, P.; Dannenberg, J. J.; Dapprich, S.; Daniels, A. D.; Farkas, O.; Foresman, J. B.; Ortiz, J. V.; Cioslowshi, J.; Fox, D. J. Gaussian 09, Revision B.0. **2010**.

22. Becke, A. D. Density-functional thermochemistry. III. The role of exact exchange. *J. Chem. Phys.* **1993**, *98*, 5648-5652.

23. Lee, C.; Yang, W.; Parr, R. G. Development of the Colle-Salvetti correllation energy formula into a functional of the electron density. *Phys. Rev. B* **1988**, *37*, 785-789.

24. Godbout, N.; Salahub, D. R.; Andzelm, J.; Wimmer, E. Optimization of Gaussian-type basis sets for local spin density functional calculations. Part I. Boron through neon, optimization technique and validation. *Can. J. Chem.* **92**, *70*, 560-571.

25. Gutowski, K. E.; Dixon, D. A. Ab initio prediction of the gas- and solution-phase acidities of strong Brønsted acids: The calculation of pK_a values less than -10. *J. Phys. Chem. A* **2006**, *110*, 12044-12054.

26. Stover, M. L.; Jackson, V.; Matus, M.; Adams, M.; Cassady, C. J.; Dixon, D. A. Fundamental thermochemical properties of amino acids: Gas-phase and aqueous acidities and gas-phase heats of formation. *J. Phys. Chem. B* **2012**, *116*, 2905-2916.

27. Curtiss, L. A.; Redfern, P. C.; Raghavachari, K.; Rassolov, V.; Pople, J. A. Gaussian-3 theory using reduced Moller-Plesset order. *J. Chem. Phys.* **1999**, *110*, 4703-4709.

28. Hoaglund-Hyzer, C.; Counterman, A.; Clemmer, D. Anhydrous protein ions. *Chem. Rev.* **1999**, *99*, 3037-3079.

29. Price, W.; Schnier, P.; Williams, E. Tandem mass spectrometry of large biomolecule ions by blackbody infrared radiative dissociation. *Anal. Chem.* **1996**, *68*, 859-866.

30. Schier, P. D.; Gross, D. S.; Williams, E. R. On the maximum charge-state and proton-transfer reactivity of peptide and protein ions formed by electrospray-ionization. *J. Am. Soc. Mass Spectrom.* **1995**, *6*, 1086-1097.

31. Williams, E. Proton transfer reactivity of large multiply charged ions. *J. Mass Spectrom.* **1996**, *31*, 831-842.

32. Loo, R. R. O.; Smith, R. D. Proton-transfer reactions of multiply-charged peptide and protein cations and anions. *J. Mass Spectrom.* **1995**, *30*, 339-347.

33. Bouchoux, G.; Salpin, J. Y. Re-evaluated gas phase basicity and proton affinity data from the thermokinetic method. *Rapid Commun. Mass Spectrom.* **1999**, *13*, 932-936.

34. Paizs, B.; Suhai, S. Fragmentation pathways of protonated peptides. *Mass Spectrom. Rev.* **2005**, *24*, 508-548.

35. Loo, J. A.; Edmonds, C. G.; Smith, R. D. Tandem mass spectrometry of very large molecules. 2. Dissociation of multiply-charged proline containing proteins from electrospray ionization. *Anal. Chem.* **1993**, *65*, 425-438.

36. Tsaprailis, G.; Nair, H.; Somogyi, A.; Wysocki, V. H.; Zhong, W. Q.; Futrell, J. H.; Summerfield, S. G.; Gaskell, S. J. Influence of secondary structure on the fragmentation of protonated peptides. *J. Am. Chem. Soc.* **1999**, *121*, 5142-5154.

37. Tabb, D.; Huang, Y.; Wysocki, V.; Yates, J. Influence of basic residue content on fragment ion peak intensities in low-energy - collision-induced dissociation spectra of peptides. *Anal. Chem.* **2004**, *76*, 1243-1248.

38. Steinborner, S. T.; Bradford, A. M.; Waugh, R. J.; Bowie, J. H.; Vollmer, D. L.; Gross, M. L. Collision-induced dissociations of deprotonated dipeptide methyl esters containing serine or threonine. *Aust. J. Chem.* **1994**, *47*, 1851-1857.

39. Froelicher, S. W.; Lee, R. E.; Squires, R. R.; Freiser, B. S. Collision-induced dissociation of ester enolate ions using Fourier transform mass spectrometry. *Org. Mass Spectrom.* **1985**, *20*, 4-9.

40. Grzetic, J.; Oomens, J. Spectroscopic evidence for an oxazolone structure in anionic ***b***-type peptide fragments. *J. Am. Soc. Mass Spectrom.* **2012**, *23*, 290-300.

41. Harrison, A. G.; Siu, K. W. M.; El Aribi, H. Amide bond cleavage in deprotonated tripeptides: a newly discovered pathway to "b_2 ions. *Rapid Commun. Mass Spectrom.* **2003**, *17*, 869-875.

42. Oomens, J.; Steill, J. D. The structure of deprotonated tri-alanine and its a_3^- fragment anion by IR spectroscopy. *J. Am. Soc. Mass Spectrom.* **2010**, *21*, 698-706.

43. El Aribi, H.; Rodriquez, C. F.; Almeida, D. R. P.; Ling, Y.; Mak, W. W.; Hopkinson, A. C.; Siu, K. W. M. Elucidation of fragmentation mechanisms of protonated peptide ions and their products: A case study on glycylglycylglycine using density functional theory and threshold collision-induced dissociation. *J. Am. Chem. Soc.* **2003**, *125*, 9229-9236.

44. El Aribi, H.; Orlova, G.; Rodriquez, C. F.; Almeida, D. R. P.; Hopkinson, A. C.; Siu, K. W. M. Fragmentation mechanisms of product ions from protonated tripeptides. *J. Phys. Chem. B* **2004**, *108*, 18743-18749.

45. Vaisar, T.; Urban, J. Gas-phase fragmentation of protonated mono-N-methylated peptides. Analogy with solution-phase acid-catalyzed hydrolysis. *J. Mass Spectrom.* **1998**, *33*, 505-524.

46. Kuzma, M.; Jegorov, A.; Hesso, A.; Tornaeus, J.; Sedmera, P.; Havlicek, V. Role of amino acid N-methylation in cyclosporins on ring opening and fragmentation mechanisms during collisionally induced dissociation in an ion trap. *J. Mass Spectrom.* **2002**, *37*, 292-298.

CHAPTER 7: CONCLUSIONS AND FUTURE DIRECTIONS

The significance of the backbone and C-terminus to the mass spectrometry of peptides has been addressed using various contemporary mass spectrometry techniques. Several dissociative characteristics, unique to the identity of the C-terminal end group (-$CONH_2$ or -COOH), have been explored using collsion-induced dissociation (CID) and electron transfer dissociation (ETD). Experimental gas-phase acidities (GA) have been obtained for several amino acids, amino acid amides, tripeptides, and tripeptide methyl esters.

CID of deprotonated peptide acids and amides yielded fragmentation that was unique to each species. Theoretical results provided insight to the energetic reasoning for the formation of these dissociation products. To better understand the observed CID products, larger model peptides (composed of amino acids with alkyl or H- side chains) with C-terminal acid and amide endgroups may be useful to study.

CID of protonated peptide acids and amides as well as ETD of multiply-protonated peptide acid and amides provided conclusive evidence that the C-terminus is not a charge site in the positive ion mode. Regardless of C-terminal identity, the peptides generally produce comparable spectra. Thus, the C-terminus is not a good candidate for a distinguishing characteristic for peptide or protein identification in proteomic applications when using protonated (positive) ions.

The GAs of tyrosine, phenylalanine, and their amino acid amides yielded an interesting insight to the acidity of amino acid residues in the context of a peptide backbone. The amino

acid amides mimic the backbone by replacing the carboxylic acid functional group with an amide, to eliminate the -COOH as a potential deprotonation site. Investigation of other amino acids and their respective amides would be very useful to further understanding the deprotonation of peptides, and charge-directed dissociation mechanisms. Other amino acids that possess hydroxyl (-OH) side chain functionalities, such as serine (S) or threonine (T), would be particularly interesting to compare with tyrosine. The hydroxyl group on the side chains of these amino acids may be a viable location to deprotonate by ESI, even though they are not considered solution-phase acidic sites. Study of serine and threonine amide alongside the C-terminal acid form will also elucidate the behavior of these amino acids in peptides. Establishing the GAs of all of the amino acid amides (except those already studied in this dissertation, and also those previously reported by Cassady and coworkers[1]) would be particularly informative for understanding the dissociation of deprotonated peptides by CID, and may further support the findings in Chapter 3.

Deprotonation of tyrosine occurs at either the carboxylic acid or phenolic -OH. Both species (a fast and slow reacting species) were observed during bracketing ion/molecule reactions, and relative abundances of each were determined. Hexapole accumulation time was found to greatly affect the appearance of the faster reacting species of deprotonated tyrosine. The deprotonation reactions do not indicate which structure (carboxylate or phenoxide) is the fast reacting species and which is the slow reacting species. Ion/molecule reactions of deprotonated tyrosine with trimethylsilylazide ($TMSN_3$) should elucidate the identity of the ion species. Reactions of deprotonated tyrosine with $TMSN_3$ were reported by Kass and coworkers[2] as a method for directly distinguishing the relative abundance of phenoxide and carboxylate present based on reaction products that are unique to each deprotonated species. Though solvent

system was not found in this dissertation research to affect the relative abundances of each ion population, further investigation of solvent affects is warranted. Pure water would be an interesting solvent to try, as it was not investigated here or by Kass and coworkers.[2] The addition of NH_4OH or NaOH to the solvent system is typically done to assist in ion formation, but this solvent additive may also be affecting the observed ion populations. Investigation of solvent systems devoid of these additives should also be considered. In addition, the long and short hexapole accumulation times should be included with the additional experiments to further understand the role of accumulation in observed ion populations.

Backbone deprotonation of peptides has been demonstrated for the methyl esters of triglycine (GGG), trialanine (AAA), and glycylalanylglycine (GAG). The experimental GAs of these peptides are approximately 14 kcal/mol higher (less acidic) than the non-esterified peptide; however, deprotonation of these methyl esters by ESI occurs in great abundance. Methyl esters of trisarcosine (G′G′G′-OMe), tri-2-methylalanine (A′A′A′-OMe), and alanylglycylalanine (AGA-OMe) were unable to produce abundant $[M - H]^-$ by ESI, indicating that steric and conformational interactions are preventing facile deprotonation. Further investigation of these steric and conformational interactions would be interesting, perhaps by ion mobility mass spectrometry (IMS),[3-8] which analyzes ions based on their size and shape. Hydrogen-deuterium exchange (HDX) mass spectrometry could be performed using the Bruker BioApex 7e FT-ICR. HDX is very useful for investigating the conformation of a peptide based on ease of access for the deuterated reagent to exchange with hydrogens on heteroatoms of the peptide backbone.[9-12] This method would be particularly interesting to use for tri-2-methylalanine, since the calculated GA for deprotonation at the central NH is 326.2 kcal/mol which is similar to that of the other tripeptides, yet $[M - H]^-$ was not abundantly produced by ESI.

All of the research discussed in this dissertation answered questions regarding particular features of biomolecules and their relation to improving peptide identification using mass spectral techniques. Deprotonation sites were proven to be an important characteristic for understanding gas-phase dissociation. The deprotonation of tyrosine, phenylalanine, and their amino acid amides show that functional groups other than traditional acidic sites (i.e. C-terminal -COOH, or the glutamic acid or aspartic acid side chain -COOH) can be suitable sites of deprotonation in ESI. Deprotonation of GGG-OMe, AAA-OMe, and GAG-OMe showed that backbone amide nitrogens are acidic enough for deprotonation by ESI. The lack of $[M - H]^-$ formation by G′G′G′-OMe, A′A′A′-OMe, and AGA-OMe showed that conformation and/or steric hindrances within the neutral molecule may inhibit deprotonation by ESI.

Establishing valuable thermochemical information such as GA for amino acids, amides, peptides, and methyl esters will further enhance our understanding of gas-phase behavior. Benchmark data such as this can be extremely useful for the development of charge-directed dissociation mechanisms (of importance to peptide sequencing), and for determining the relationship of solution-phase ion structure to gas-phase structure.

References

1. Li, Z.; Matus, M. M.; Velazquez, H. A.; Dixon, D. A.; Cassady, C. J. Gas-phase acidities of aspartic acid, glutamic acid, and their amino acid amides. *Int. J. Mass Spectrom.* **2007**, *265*, 213-223.

2. Tian, Z.; Wang, X.; Wang, L.; Kass, S. R. Are carboxyl groups the most acidic sites in amino acids? Gas-phase acidities, photoelectron spectra, and computations on tyrosine, p-hydroxybenzoic acid, and their conjugate bases. *J. Am. Chem. Soc.* **2009**, *131*, 1174-1181.

3. Wu, C.; Siems, W.; Asbury, G.; Hill, H. Electrospray ionization high-resolution ion mobility spectrometry - Mass spectrometry. *Anal. Chem.* **1998**, *70*, 4929-4938.

4. Ruotolo, B. T.; Benesch, J. L. P.; Sandercock, A. M.; Hyung, S.; Robinson, C. V. Ion mobility-mass spectrometry analysis of large protein complexes. *Nat. Protocols* **2008**, *3*, 1139-1152.

5. McLean, J.; Ruotolo, B.; Gillig, K.; Russell, D. Ion mobility-mass spectrometry: a new paradigm for proteomics. *Int. J. Mass Spectrom.* **2005**, *240*, 301-315.

6. Knapman, T. W.; Berryman, J. T.; Campuzano, I.; Harris, S. A.; Ashcroft, A. E. Considerations in experimental and theoretical collision cross-section measurements of small molecules using travelling wave ion mobility spectrometry-mass spectrometry. *Int. J. Mass Spectrom.* **2010**, *298*, 17-23.

7. Kanu, A. B.; Dwivedi, P.; Tam, M.; Matz, L.; Hill, H. H., Jr. Ion mobility-mass spectrometry. *J. Mass Spectrom.* **2008**, *43*, 1-22.

8. Jung, J. E.; Pierson, N. A.; Marquardt, A.; Scheffner, M.; Przybylski, M.; Clemmer, D. E. Differentiation of compact and extended conformations of di-ubiquitin conjugates with lysine-specific isopeptide linkages by ion mobility-mass spectrometry. *J. Am. Soc. Mass Spectrom.* **2011**, *22*, 1463-1471.

9. Rozman, M.; Srzic, D.; Klasinc, L. Gas-phase interaction of protonated lysine with water. *Int. J. Mass Spectrom.* **2006**, *253*, 201-206.

10. Freitas, M.; Hendrickson, C.; Emmett, M.; Marshall, A. High-field Fourier transform ion cyclotron resonance mass spectrometry for simultaneous trapping and gas-phase hydrogen/deuterium exchange of peptide ions *J. Am. Soc. Mass Spectrom.* **1998**, *9*, 1012-1019.

11. Eyles, S.; Speir, J.; Kruppa, G.; Gierasch, L.; Kaltashov, I. Protein conformational stability probed by Fourier transform ion cyclotron resonance mass spectrometry. *J. Am. Chem. Soc.* **2000**, *122*, 495-500.

12. Campbell, S.; Rodgers, M.; Marzluff, E.; Beauchamp, J. Deuterium exchange reactions as a probe of biomolecule structure. Fundamental studies of cas phase H/D exchange reactions of protonated glycine oligomers with D_2O, CD_3OD, CD_3CO_2D, and ND_3. *J. Am. Chem. Soc.* **1995**, *117*, 12840-12854.